NOVEL RESIDUAL-BASED LARGE EDDY SIMULATION TURBULENCE MODELS FOR INCOMPRESSIBLE MAGNETOHYDRODYNAMICS

By

David Sondak

A Thesis Submitted to the Graduate

Faculty of Rensselaer Polytechnic Institute

in Partial Fulfillment of the

Requirements for the Degree of

DOCTOR OF PHILOSOPHY

Major Subject: AEROSPACE ENGINEERING

Approved by the
Examining Committee:

_____
Assad A. Oberai, Thesis Adviser

_____
Mark Shephard, Member

_____
John Shadid, Member

_____
Peter Fox, Member

_____
Fengyan Li, Member

_____
Onkar Sahni, Member

Rensselaer Polytechnic Institute
Troy, New York

July 2013
(For Graduation August 2013)

CONTENTS

LIST OF TABLES

LIST OF FIGURES

x

Nomenclature

Acronyms

BDF   backward difference formula

DNS   direct numerical simulation

FDM   finite difference method

EM   electromagnetic

FEM   finite element method

FFT   fast Fourier transform

GMRES generalized minimum residual

GLS   Galerkin least-squares

HD   hydrodynamics

HIT   homogeneous, isotropic turbulence

IK   Iroshnikov-Kraichnan phenomenology of MHD turbulence

K41   Kolmogorov's 1941 theory of turbulence

LBB   Ladyženskaja-Babuška-Brezzi

MHD   magnetohydrodynamics

MWR   method of weighted residuals

ODE   ordinary differential equation

PDE   partial differential equation

RK4   fourth order Runge-Kutta time-marching scheme

RANS Reynolds-averaged Navier-Stokes

SI   International System of Units

VMS variational multiscale

Numerical Quantities

A global finite element node number

C_I constant in diffusion-term of stabilization matrix

C_t constant in time-term of stabilization matrix

e_i i^{th} finite element

N_A global finite element shape function for global node A

N_a finite element shape function at element node a

N_b finite element shape function at element node b

y_A solution degree of freedom at global node A

Dimensionless Parameters

Ha   Hartmann number

Pr_m magnetic Prandtl number

Re   Reynolds number

Re_τ friction Reynolds number

Rm   magnetic Reynolds number

S   interaction parameter

y^+ wall units

Function Spaces

$H^1(\Omega)$ Sobelev space with 1 square integrable derivative on Ω

$H_0^1(\Omega)$ Sobelev space with 1 square integrable derivative on Ω and homogeneous, essential boundary conditions

$L_2(\Omega)$ Hilbert space of square integrable functions on Ω

$\mathcal{S}$ finite element space for trial solutions

$\mathcal{V}$ finite element space for weighting functions

$\mathcal{V}^h$ finite dimensional finite element space

$\mathcal{V}'$ infinite dimensional space of numerically unresolvable functions

Greek Symbols

$\boldsymbol{\delta}$ Kronecker-delta

δ_{ij} Kronecker-delta in index notation

δ_ν viscous length scale

Δt time step size

η electrical resistivity

ϵ_0 electrical permittivity

ϵ^{I} magnetic energy dissipation rate

ϵ^{T} total MHD energy dissipation rate

ϵ^{V} kinetic energy dissipation rate

Γ spatial boundary

Γ_g essential boundary

Γ_h Neumann boundary

λ magnetic diffusivity

λ_T eddy magnetic diffusivity

μ_0 magnetic permeability

μ fluid dynamic viscosity

ν kinematic viscosity

ν_T eddy viscosity

Ω spatial domain

$\overline{\Omega}$ spatial domain with boundaries

ϕ scalar potential

ρ fluid density

ρ_e electric charge density

σ electrical conductivity

θ growth correlation

Types of Models

DSEV dynamic Smagorinsky eddy viscosity

DSEVA alignment-based dynamic Smagorinsky model

EDQNM eddy damped quasi normal Markovian approximation

EV   eddy viscosity

ILES implicit large eddy simulation

LES   large eddy simulation

MM   mixed model

RBEV residual-based eddy viscosity

Mathematical Operators

$\langle\cdot\rangle$ averaging operation

$\nabla\times$ curl operator

$\nabla\cdot$ diverence operator

$\cdot$ vector dot product

$\frac{\mathrm{d}}{\mathrm{dt}}$ ordinary time derivative

∇ gradient operator

∇^{s} symmetric gradient operator

∇^{a} antisymmetric gradient operator

$\imath$ imaginary number $\sqrt{-1}$

∇^2 Laplacian operator

$\frac{\mathrm{D}}{\mathrm{Dt}}$ material derivative

$\frac{\partial}{\partial\mathrm{t}}$ partial derivative in time

$\oint(\cdot)\,\mathrm{d}\mathbf{k}$ Surface integral over spherical shells

$:$ tensor inner product

tr trace of a matrix

Scalars

r' unresolved artificial magnetic pressure

s' unresolved weighting functions for artificial magnetic pressure

$E(k)$ hydrodynamic, kinetic energy spectrum

$E^{\mathrm{V}}(k,t)$ velocity energy spectrum

f arbitrary scalar field used for illustrative purposes

f' arbitrary fluctuating scalar field used for illustrative purposes

$\overline{P}$ filtered total MHD pressure

$\overline{r}$ filtered artificial magnetic pressure

g arbitrary scalar field used for illustrative purposes

g' arbitrary fluctuating scalar field used for illustrative purposes

h mesh parameter

H^C cross helicity

H^{I} magnetic helicity

k wavenumber

K^{I} magnetic energy per unit mass

$k_{\perp}$ wavenumber perpendicular to background magnetic field

k_p wavenumber in $x - z$ plane

K^{T} total MHD energy per unit mass

K^{V} kinetic energy per unit mass

p fluid pressure

P_a^e total magnetic pressure degree of freedom on element e at node a

P^h numerical total MHD pressure on grid h

$\widehat{P}_{\mathbf{k}}$ Fourier coefficient of total MHD pressure at wavenumber $\mathbf{k}$

$\widehat{\mathfrak{P}}_{\mathbf{k}}$ dummy pressure in wavenumber space at wavenumber $\mathbf{k}$

P total MHD pressure, fluid plus magnetic

ψ scalar magnetic potential

q weighting function for velocity continuity equation

s_a^e total magnetic pressure weighting function on element e at node a

q^h numerical weighting function for total MHD pressure on on grid h

r artificial magnetic pressure

r_a^e artificial magnetic pressure degree of freedom on element e at node a

r^h numerical artificial magnetic pressure on grid h

$\widehat{r}_{\mathbf{k}}$ Fourier coefficient of artificial magnetic pressure at wavenumber $\mathbf{k}$

s weighting function for induction continuity equation

q_a^e artificial magnetic pressure weighting function freedom on element e at node a

s^h numerical weighting function for artificial magnetic pressure on grid h

$\tau_c^{\mathrm{I-}}$ $\nabla \cdot \mathbf{u}$-$\nabla \cdot \mathbf{B}$ stabilization parameter for MHD stabilization matrix

$\tau_c^{\mathrm{I+}}$ $\nabla \cdot \mathbf{B}$-$\nabla \cdot \mathbf{B}$ stabilization parameter for MHD stabilization matrix

τ^{C} diagonal components of the stabilization parameter for the magnetic field continuity equation

τ^{C} diagonal components of the stabilization parameter for the velocity continuity equation

$\tau_c^{\mathrm{V-}}$ $\nabla \cdot \mathbf{B}$-$\nabla \cdot \mathbf{u}$ stabilization parameter for MHD stabilization matrix

$\tau_c^{\mathrm{V+}}$ $\nabla \cdot \mathbf{u}$-$\nabla \cdot \mathbf{u}$ stabilization parameter for MHD stabilization matrix

τ^{I} diagonal components of the stabilization parameter for the induction equation

τ^{V} diagonal components of the stabilization parameter for the momentum equation

$\overline{u}$ filtered field

u^h numerical quantity

P' unresolved total MHD pressure field

w arbitrary weighting function

q' unresolved weighting functions for pressure

Roman Symbols

B_0 characteristic magnetic field

$\overline{C}$ universal RBEV constant

C_K Kolmogorov constant

$G(\mathbf{r}, \mathbf{x})$ filtering kernal

k^h cut-off wavenumber

L characteristic length

q_i electric charge of ith particle

Q total electric charge of fluid element

U characteristic velocity

u_τ friction velocity

Tensors

$\mathbf{F}$ electromagnetic flux tensor

$\mathbf{G}$ metric tensor

$\mathbf{T}$ fluid stress tensor

$\boldsymbol{\tau}$ stabilization parameter (matrix, tensor)

$\boldsymbol{\mathcal{T}}^{\mathrm{I}}$	induction subgrid stress tensor
$\boldsymbol{\tau}^{\mathrm{II}}$	induction-induction stabilization submatrix for MHD stabilization matrix
$\boldsymbol{\tau}^{\mathrm{IV}}$	induction-momentum stabilization submatrix for MHD stabilization matrix
$\boldsymbol{\mathcal{T}}^{\mathrm{V}}$	momentum subgrid stress tensor
$\boldsymbol{\tau}^{\mathrm{VI}}$	momentum-induction stabilization submatrix for MHD stabilization matrix
$\boldsymbol{\tau}^{\mathrm{VV}}$	momentum-momentum stabilization submatrix for MHD stabilization matrix

Vectors

$\mathbf{A}$	magnetic vector potential
$\mathbf{B}$	magnetic field, magnetic induction
$\mathbf{B}_A$	magnetic field in Alfvén velocity units
$\mathbf{B}_a^e$	magnetic field degree of freedom on element e at node a
$\mathbf{B}^h$	numerical magnetic field on grid h
$\widehat{\mathbf{B}}_{\mathbf{k}}$	Fourier coefficient of magnetic field at wavenumber $\mathbf{k}$
$\mathbf{B}'$	unresolved magnetic field
$\widehat{\mathbf{U}}$	Fourier coefficients of vector of trial solutions
$\widehat{\mathbf{W}}$	Fourier coefficients of vector of weighting functions
$\mathbf{c}$	vector of weighting functions for induction equation
$\mathbf{c}_a^e$	induction weighting function on element e at node a
$\mathbf{c}^h$	numerical weighting functions for induction equation on grid h
$\mathbf{c}'$	unresolved induction weighting functions
$\mathbf{c}_P$	a vector of model parameters

$\mathbf{c}_P^{\mathrm{I}}$ a vector of induction model parameters

$\mathbf{c}_P^{\mathrm{V}}$ a vector of momentum model parameters

$\mathbf{E}$ electric field

$\mathbf{e}_j$ unit vector in the j direction

$\mathbf{F}$ vector of force vectors

$\mathbf{f}$ arbitrary volumetric force vector

$\overline{\mathbf{B}}$ filtered magnetic field

$\mathbf{f}_{\mathrm{EM}}$ volumetric electromagnetic force

$\overline{\mathbf{f}^{\mathrm{I}}}$ filtered induction forcing

$\overline{\mathbf{f}^{\mathrm{V}}}$ filtered momentum forcing

$\mathbf{f}^{\mathrm{I}}$ magnetic forcing function

$\widehat{\mathbf{f}^{\mathrm{I}}}_{\mathbf{k}}$ Fourier coefficient of induction forcing function at wavenumber $\mathbf{k}$

$\widehat{\mathbf{f}}_{\mathbf{k}}$ dummy forcing in wavenumber space at wavenumber $\mathbf{k}$

$\mathbf{F}_{q_i}$ electric force on particle i with charge q

$\overline{\mathbf{u}}$ filtered velocity field

$\mathbf{f}^{\mathrm{V}}$ momentum forcing function

$\widehat{\mathbf{f}^{\mathrm{V}}}_{\mathbf{k}}$ Fourier coefficient of momentum forcing function at wavenumber $\mathbf{k}$

$\mathbf{j}$ electric current density

$\mathbf{j}^h$ numerical electric current density

$\mathbf{J}$ electric current

$\mathbf{K}_i,\ i=1,4$ parameters in the RK4 scheme

$\mathbf{n}$ unit outward normal to the boundary

$\mathbf{v}^n$ solution at time step n

$\boldsymbol{\mathcal{R}}$ MHD residual

$\boldsymbol{\mathcal{R}}^{\mathrm{I}}\left(\mathbf{U}^h\right)$ induction residual

$\boldsymbol{\mathcal{R}}^{\mathrm{V}}\left(\mathbf{U}^h\right)$ momentum residual

$\mathbf{U}$ vector of solution vectors

$\mathbf{u}$ velocity field

$\mathbf{u}_a^e$ velocity degree of freedom on element e at node a

$\mathbf{U}^h$ numerical vector of trial solutions on grid h

$\mathbf{u}^h$ numerical velocity field on grid h

$\widehat{\mathbf{u}}_{\mathbf{k}}$ Fourier coefficient of velocity field at wavenumber $\mathbf{k}$

$\mathbf{u}'$ unresolved velocity field

$\mathbf{v}$ arbitrary vector quantity used for illustrative purposes

$\mathbf{V}^h$ arbitrary numerical vector used for illustrative purposes

$\widehat{\mathbf{v}}_{\mathbf{k}}$ arbitrary Fourier coefficient at wavenumber $\mathbf{k}$

$\mathbf{V}'$ arbitrary numerically unresolved vector used for illustrative purposes

$\mathbf{v}_{q_i}$ velocity of particle i with charge q

$\mathbf{V}$ arbitrary vector quantity used for illustrative purposes

$\mathbf{W}$ vector of weighting functions

$\mathbf{w}$ vector of weighting functions for momentum equation

$\mathbf{w}_a^e$ momentum weighting function on element e at node a

$\mathbf{W}^h$ numerical vector of weighting functions on grid h

$\mathbf{w}^h$ numerical weighting functions for momentum equation on grid h

$\mathbf{w}'$ unresolved momentum weighting functions

$\mathbf{x}$ spatial coordinate in physical space

Other Symbols

$\mathfrak{d}$ dummy diffusion coefficient

$\mathcal{D}$ differential operator for Neumann boundary conditions

$(\xi,\ \eta,\ \zeta)$ element coordinates

$\mathbb{F}$ filtering operator

$(\cdot,\cdot)$ L_2 inner product

$\mathbb{I}$ identity operator

$\mathcal{L}$ MHD partial differential operator

ℓ_I induction mixing length

$\widehat{\mathcal{L}}$ linear differential operator in wavenumber space

ℓ_K Kolmogorov length-scale

ℓ_V momentum mixing length

$\mathcal{M}\left(\mathbf{W}^h,\mathbf{U}^h;h,\mathbf{c}_P\right)$ model term for MHD system inclusive of momentum and induction models

$\mathcal{M}_\mathrm{V}\left(\mathbf{w}^h,\mathbf{U}^h;h,\mathbf{c}_P^\mathrm{V}\right)$ induction model

$\mathcal{M}_\mathrm{I}\left(\mathbf{c}^h,\mathbf{U}^h;h,\mathbf{c}_P^\mathrm{I}\right)$ momentum model

$\mathcal{N}$ arbitrary nonlinear term

$\mathcal{N}^\mathrm{I}$ nonlinear term in the induction equation

$\boldsymbol{\mathcal{N}}_F^{\text{I}}$ filtered nonlinear term for induction equation

$\boldsymbol{\mathcal{N}}_h^{\text{I}}$ discretized nonlinear term in induction equation

$\widehat{\boldsymbol{\mathcal{N}}^{\text{I}}}$ induction nonlinear term in wavenumber space

$\widehat{\boldsymbol{\mathcal{N}}}$ arbitrary nonlinear term in wavenumber space

$\boldsymbol{\mathcal{N}}_F^{\text{V}}$ filtered nonlinear term for momentum equation

$\boldsymbol{\mathcal{N}}_h^{\text{V}}$ discretized nonlinear term in momentum equation

$\widehat{\boldsymbol{\mathcal{N}}^{\text{V}}}$ momentum nonlinear term in wavenumber space

$\mathcal{N}$ arbitrary scalar nonlinear term

$\boldsymbol{\mathcal{N}}^{\text{V}}$ nonlinear term in the momentum equation

$\varnothing$ empty set

$\boldsymbol{\mathcal{P}}$ spectral projection operator for nonlinear terms

$\mathcal{P}$ space-time boundary

P_{jlm} index notation of spectral projection operator for nonlinear terms

$\mathbb{P}'$ VMS fine scale projection operator

$\mathcal{P}_g$ space-time essential boundary

$\mathbb{P}^h$ VMS projection operator

$\mathcal{P}_h$ space-time Neumann boundary

$\boldsymbol{\mathcal{Q}}$ spectral projection operator for forcing terms

$\mathcal{Q}_{jl}$ index notation of spectral projection operator for forcing terms

$\mathcal{Q}$ space-time domain

$\overline{\mathcal{Q}}$ space-time domain with boundary

$\mathcal{T}_\mathrm{I}^\mathrm{C}$ energy transfer between resolved and unresolved scales

$\mathcal{T}_D$ subgrid dynamo term

$\mathcal{T}_\mathrm{I}^\mathrm{K}$ energy transfer between resolved scales

τ_{ℓ_K} Kolmogorov time-scale

$\mathcal{T}_\mathrm{I}^\mathrm{R}$ energy transfer between unresolved scales

u_{ℓ_K} Kolmogorov velocity-scale

ACKNOWLEDGMENTS

To my mentor Assad A. Oberai, I would like to express my deepest gratitude. His humility and kind patience have made all the difference in my development as a researcher and as a person. I am honored to have been given the chance to interact with and learn from him.

I have also been fortunate to have John N. Shadid as a mentor during the last year of my PhD research. He opened up his research group at Sandia, provided access to his group's well-written FEM code, and gave me considerable research guidance and perspective. Here again is a humble mentor that I feel lucky to have worked with. I would also like to thank John for telling me some of the secrets of the mountains of New Mexico.

The last three years of my dissertation research were generously funded through a graduate fellowship from the Department of Energy. This grant, the Department of Energy, Office of Science Graduate Fellowship, gave me considerable research freedom. I was able to travel to many conferences and gain exceptionally valuable experience networking, presenting, and discussing my research with experts from my field and interested scientists from outside my field. I also made valuable friendships with other fellows. I like to think we gave each other some perspective on graduate school. For my part, I am very thankful for this. I would especially like to mention Lauren Garrison, Carson Cook, and Micah Sheppard.

I would like to thank my committee members for the parts they each played during my time as a doctoral student: Mark Shephard for being an exceptional teacher of the finite element method and a diligent manager of SCOREC, Peter Fox for his kind support of and confidence in me, Fengyan Li for interesting mathematical discussions on diverse topics from functional analysis to the Vlasov equation, and Onkar Sahni for being a constant personal mentor since I first arrived at RPI.

The Drekar group at Sandia was instrumental in helping me implement the new models into the Drekar FEM code. Tom Smith in particular gave me access to several Sandia tools that ensured I did not have to reinvent the wheel on numerous occasions.

This work is dedicated to an idea and to everyone who taught me what it really means: Never Give Up.

ABSTRACT

The goal of this work was to develop, introduce, and test a promising computational paradigm for the development of turbulence models for incompressible magnetohydrodynamics (MHD). MHD governs the behavior of an electrically conducting fluid in the presence of an external electromagnetic (EM) field. The incompressible MHD model is used in many engineering and scientific disciplines from the development of nuclear fusion as a sustainable energy source to the study of space weather and solar physics. Many interesting MHD systems exhibit the phenomenon of turbulence which remains an elusive problem from all scientific perspectives. This work focuses on the computational perspective and proposes techniques that enable the study of systems involving MHD turbulence.

Direct numerical simulation (DNS) is not a feasible approach for studying MHD turbulence. In this work, turbulence models for incompressible MHD were developed from the variational multiscale (VMS) formulation wherein the solution fields were decomposed into resolved and unresolved components. The unresolved components were modeled with a term that is proportional to the residual of the resolved scales. Two additional MHD models were developed based off of the VMS formulation: a residual-based eddy viscosity (RBEV) model and a mixed model that partners the VMS formulation with the RBEV model. These models are endowed with several special numerical and physics features. Included in the numerical features is the internal numerical consistency of each of the models. Physically, the new models are able to capture desirable MHD physics such as the inverse cascade of magnetic energy and the subgrid dynamo effect.

The models were tested with a Fourier-spectral numerical method and the finite element method (FEM). The primary test problem was the Taylor-Green vortex. Results comparing the performance of the new models to DNS were obtained. The performance of the new models was compared to classic and cutting-edge dynamic Smagorinsky eddy viscosity (DSEV) models. The new models typically outperform the classical models.

CHAPTER 1
Introduction and Scope of Work

The field of magnetohydrodynamics (hereafter MHD) is a fascinatingly rich field of physics and applied mathematics that considers the behavior of an electrically conducting fluid in the presence of an external electromagnetic (EM) field. Although inspiring in its own right, MHD also has numerous engineering and science applications. These range from the pursuit of reliable energy sources such as nuclear fusion (Strauss 1976; Sovinec et al. 2003; Tang 2008; Dobran 2012) to understanding near-earth plasmas such as the solar wind (Podesta and Borovsky 2010) and more exotic astrophysical objects such as stars (Fox, Theobald, and Sofia 1991; Fox, Sofia, and Chan 1991; Brun, Miesch, and Toomre 2004), black holes (Takahashi et al. 1990), and the interstellar medium (Zweibel 1999). Virtually all of these areas experience the phenomenon of turbulence and the role turbulence places in engineering and science applications is certainly critical. This work focuses on a subsection of MHD called incompressible MHD and seeks to develop novel turbulence models for computational studies of various phenomena governed by the incompressible MHD model. The following sections include, in turn, reviews of MHD, fluid and MHD turbulence, and computational techniques. The chapter concludes by highlighting the primary contributions of this thesis and summarizing the organization of the remaining chapters.

1.1   Review of Magnetohydrodynamics

The field of MHD can be said to have started with Faraday although his researches may be more aptly considered the prehistory of MHD. For a nice account of his studies of electrically conducting fluids as well as his contributions to electrodynamics see (Davidson 2001, chap. 2). The birth of modern MHD came about with the discoveries of Hans Alfvén (Alfvén 1942, 1950). The present discussion will focus on the qualitative aspects of MHD. A more mathematical account will be presented in Chapter 2. For full accounts of MHD the reader can refer to a number

of sources, (Branover 1978; Davidson 2001; Biskamp 2003; Goedbloed and Poedts 2006; Goedbloed, Keppens, and Poedts 2010; Moreau 1990) and references therein. To initiate the discussion, the essential aspects of MHD are presented in Figure 1.1.
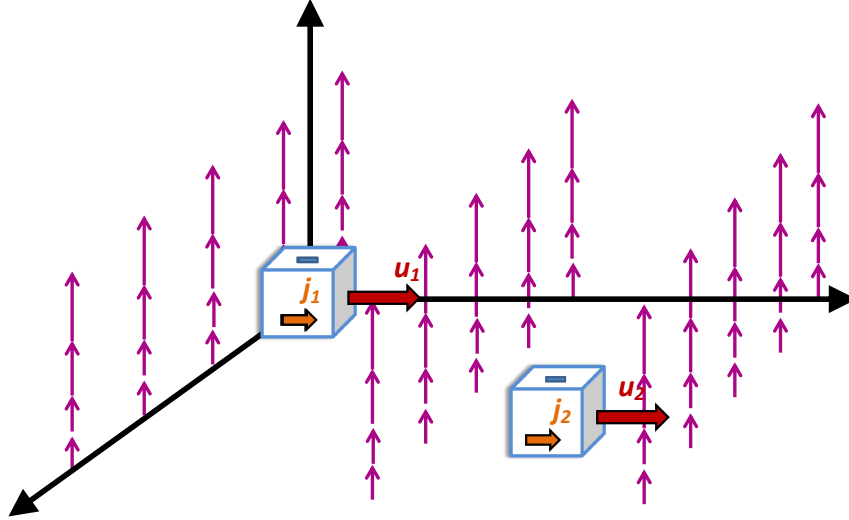
Figure 1.1: A fluid element carrying current j_1, moving in an EM field to the right with velocity u_1 feels a force that pushes it to a new location and modifies its current and velocity. This in turn creates an induced magnetic field that modifies the background EM field.

As previously mentioned, MHD is concerned with the behavior of fluids in the presence of an EM field. Of course, if the fluid does not conduct electricity, then it will not influence, nor will it be influenced by, the EM field. Although Faraday initiated the field of MHD, the mathematical formulation came later only after the discovery of Maxwell's equations. The dynamics of a fluid with density ρ are encapsulated by the momentum equation

$$\rho\frac{D\mathbf{u}}{Dt} = \nabla \cdot \mathbf{T} + \sum_i \mathbf{f}_i. \tag{1.1}$$

In this work, we will frequently refer to (1.1) as the Navier-Stokes equations although this is not quite accurate in a strict sense. Strictly speaking (1.1) reduces to the Navier-Stokes equations upon specifying a linear relationship between the stress tensor $\mathbf{T}$ and the fluid pressure and rate of strain. For more details on this, refer to

Appendix A.

For a very interesting account on the history of these equations see (Darrigol 2002). In (1.1) $D/Dt = \partial/\partial t + \mathbf{u} \cdot \nabla$ represents the total derivative of a field. In this case, the field of interest is the velocity field $\mathbf{u}$. This acceleration is influenced by the forces on the right hand side of (1.1) in the form of the stress tensor $\mathbf{T}$ and possible body forces $\mathbf{f}_i$. There are many possible body forces examples of which include gravity and the Coriolis force. We will concern ourselves with only one body force for the time-being. Because the fluid can conduct electricity, this body force, $\mathbf{f}$, is an electromagnetic force called the Laplace force which is the fluid-element counterpart to the Lorentz force. In the literature, the term Lorentz force is typically used in place of the Laplace force. An illustration of the effect of the Lorentz force on a fluid element is presented in Figure 1.1. The essential idea is that the fluid consists of current-carrying fluid elements. As the current flows in the external EM field the Lorentz force is generated which acts on the fluid elements. Interestingly, the fluid does not need to be in motion for the Lorentz force to be generated. Simply passing an electric current through a stationary fluid can generate the Lorentz force.

1.2   Review of Turbulence

This section provides an overview of the phenomenon of fluid turbulence, a scope of what the turbulence "problem" actually is, and finally discusses aspects of fluid and MHD turbulence. The phenomenon of fluid turbulence is fundamental to our natural world, yet it remains an exceptionally difficult problem. Presently, the turbulence problem is still intractable from the point of view of all three pillars of science: theory, computation, and experiments. Before proceeding with a qualitative description of the turbulence phenomenon, it is instructive to specify just what is meant by the turbulence "problem." The explanation of the turbulence problem here is not a universally accepted explanation, but is useful in explaining the fundamental difficulties. The turbulence problem is a two-headed beast: the basic tenets of the phenomenon remain unexplained and the methods for controlling and exploiting turbulence are still in their infancy.

The pillars of science each struggle with turbulence in their own way. The

theoretical pillar comes up against extreme mathematical difficulties associated with the fundamental fluid equations. Additionally, turbulence has turned out to not be amenable to physical intuition. The computational branch is unable to adequately represent all of the necessary details of a turbulent flow field and will continue to have difficulties for the foreseeable future. Experimentally, measurements of turbulent quantities to describe the flow field can only reach a certain resolution before the limits of measurement techniques are reached. Finally, all three pillars run up against the enormity of data involved in a turbulent flow field. The amount of information required to understand a given flow field is staggering.

To illustrate the concept of turbulence, one can conjure up a thought experiment. The main points of the thought experiment are illustrated in Figure 1.2.
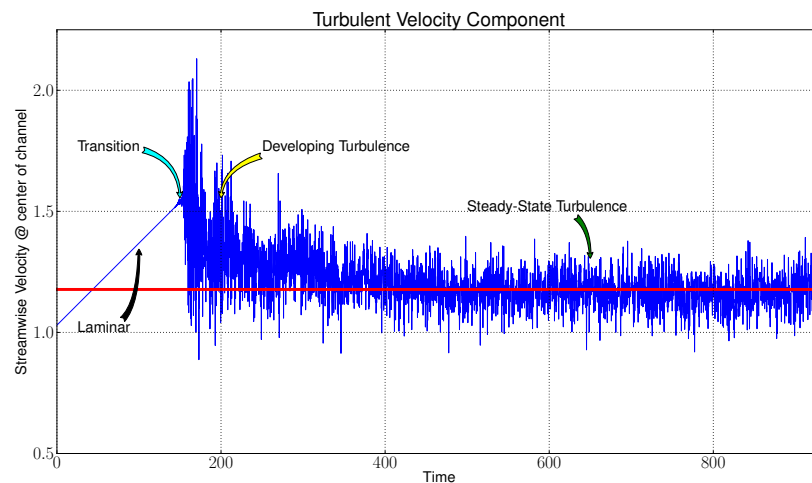
Figure 1.2: The anatomy of a turbulent flow field.

Suppose there exists a channel with a fluid flowing inside of it. Next, a probe is placed at a specific point within the channel and is able to measure the velocity field at the spatial point at each point in time. Initially, the flow field is laminar, meaning that it is devoid of velocity fluctuations and is smooth. However, once inside the channel, an external force (i.e. a pressure gradient) causes the fluid to experience an acceleration. What happens next is truly remarkable and not intuitive. For a time, the fluid continues its acceleration and remains smooth. Interestingly, after a finite time, small fluctuations in the flow field begin to occur. These fluctuations become larger until the flow becomes completely unstable and loses its smooth

character. The average velocity of the flow field at the point drops drastically and after a while a fascinating behavior occurs. The flow field is not smooth; indeed it is completely covered with fluctuations from one time-step to the next. However, the flow has reached a kind of equilibrium in which the applied external force and the forces within the fluid balance each other out. Additionally, a chaotic pattern emerges where the fluctuations are about a slowly varying periodic solution. Put another way, the flow field has a stationary equilibrium but not a simple periodic time dependence. Figure 1.2 presents the anatomy of this flow field. Next, more details on hydrodynamic (HD) and MHD turbulence are presented.

1.2.1 Hydrodynamic Turbulence

Humanity's first recorded acknowledgment of turbulence comes about in the 15$^{\text{th}}$ century ACE (after common era) with the great Leonardo da Vinci's observations and drawings. For a brief historical perspective see (Ecke 2005). However, it was roughly another four centuries before Osborne Reynolds first attempted to quantitatively study this phenomenon, first through experimental means (Reynolds 1883) and then through more mathematical considerations (Reynolds 1895). This was in the days when science had only two pillars (rather than the three today) in the form of theory and experiments. Reynolds was both an experimentalist and a theoretician. Indeed, his mathematical approach to turbulence theory dominated the field through the 20$^{\text{th}}$ century; first through theoretical pursuits and then adapted to tackle computational aspects of the problem. Two lasting contributions of Reynolds are acknowledged through the dimensionless Reynolds number and the Reynolds decomposition. The Reynolds number is an important number that characterizes the ratio of inertial to viscous forces. For a flow field with characteristic velocity U, characteristic length L, and kinematic viscosity ν the Reynolds number (Re) is,

$$\text{Re} = \frac{\text{inertial forces}}{\text{viscous forces}} = \frac{UL}{\nu}. \tag{1.2}$$

In his famous channel flow experiments, Reynolds determined a critical value for the Reynolds number at which the flow becomes turbulent.

Another approach that bears Reynolds's name is the Reynolds decomposition.

This approach centers around the idea that a turbulent flow field can be characterized by fluctuations about its average value. Thus, given a field quantity f that has an average $\langle f \rangle$ the Reynolds decomposition is

$$f = \langle f \rangle + f' \tag{1.3}$$

where f' represents fluctuations about the mean value. The central premise is that practical applications are really only concerned with the average effects of the flow field. The Reynolds Averaged Navier-Stokes (RANS) equations take this philosophy to heart. By solving the averaged momentum equation for the average field, one is able to determine the average flow field. Of course, the effects of the fluctuations do not disappear and are felt through the nonlinearities of the problem. This led to the well-known closure problem which remains unresolved to this day: What are the effects of the fluctuations on the average field? In fact, the closure problem is deeper than this. In actuality, one is concerned with the effects of the turbulent fluctuations on the large scale field.

A key observation of turbulence was that it increases the dissipation of a flow field. This led to the idea that turbulence might be characterized in part by a turbulent viscosity (see Schmitt 2007, for some history on this). That is, in the same way that momentum transfer between molecules gives rise to molecular viscosity, momentum transfer between turbulent eddies (the building blocks of a turbulent flow field) gives rise to a turbulent, or eddy, viscosity. This analogy was the first attempt at resolving the turbulence closure problem. However, it was still unknown just what the turbulent viscosity was. Prandtl (Prandtl 1925b; Tietjens 1934) introduced the idea of a turbulent mixing length which essentially characterized the length scale at which the turbulent eddies interact. Although useful, these analogies only went so far in explaining the turbulence phenomena.

The Richardson energy cascade represented another useful concept in turbulence (Richardson 2007). The idea is that the energy contained in the largest scales cascades to smaller and smaller scales until the scales containing the energy are at the dissipation length scale at which point the eddies are destroyed by viscosity. In this picture, energy is injected at the largest scales and reaches an equilibrium at

scales that are in between the large scales and the dissipation scales. Thus, energy does not accumulate in these scales; the eddies pass on exactly as much energy as is passed to them. This concept paved the way for Kolmogorov's 1941 theory of turbulence (K41) (Kolmogorov 1941a, 1941b, 1941c). . The basic idea of the Richardson cascade is depicted in Figure 1.3.
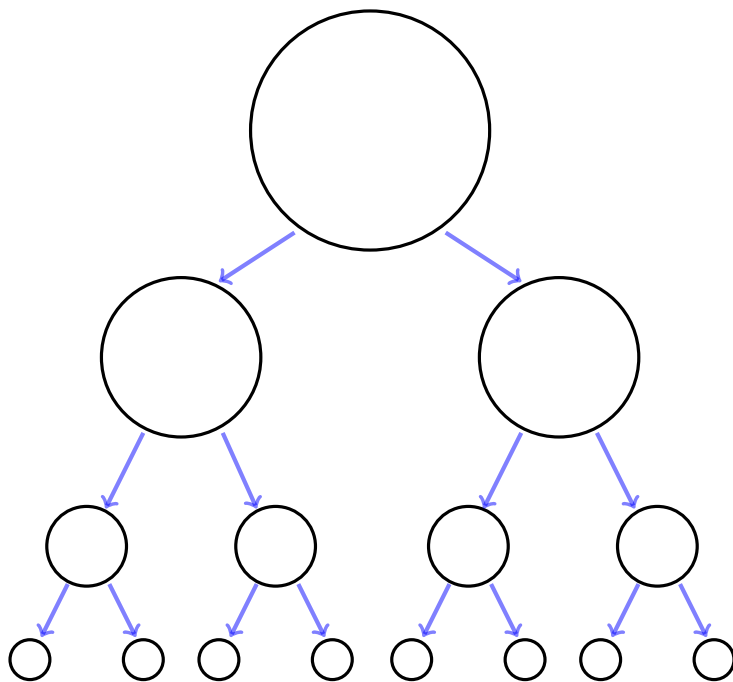
Figure 1.3: The Richardson energy cascade concept.

The K41 theory has served as a cornerstone of turbulence theory since its inception. There have been several modifications to this theory to account for phenomena such as local backscatter, intermittency, and inhomogeneous flows (see Waleffe 1997; Pope 2000; Biskamp 2003). However, in a real sense, the K41 theory represents the beginning of our understanding of turbulence. A more mathematical and deep treatment of this theory will be presented in Chapter 5. At this point, there are a few simple concepts that need to be introduced before explaining the basic idea. First of all, the kinetic energy in wavenumber space is called the energy spectrum and is denoted $E(k)$ where k is the wavenumber and has units of inverse length. The second concept concerns the wavenumber; by working in wavenumber space the scales of the problem are discretized. That is, the total energy of all structures that have a size of $1/k$ is contained in $E(k)$. The total energy of the

system is therefore obtained by summing up the energies in each wavenumber bin. A third concept is that of an inertial range. The inertial range is thought of as containing the scales that are in an energy equilibrium. That is, they are far enough away from the energy injection scales and from the energy dissipation scales that no net energy is added or taken away from them. They simply pass all of the energy that they receive on to the next scales of the flow.

The crux of the K41 theory is that in the inertial range the energy spectrum has a very particular form regardless of the type of flow field that is being considered. This is due to one of the hypotheses (to be introduced in Chapter 5) in the K41 phenomenology that postulates that the small scales of the flow field are universal in nature. Regardless of the situation in which turbulence arises, the small scales exhibit the same character. It is as if they forget where they come from and do not know where they are going. With this key assumption, the energy spectrum follows a power law behavior,

$$E\left(k\right) \sim k^{-5/3}. \tag{1.4}$$

This is illustrated in Figure 1.4 where $E\left(k\right)$ is plotted on a $\log - \log$ scale.
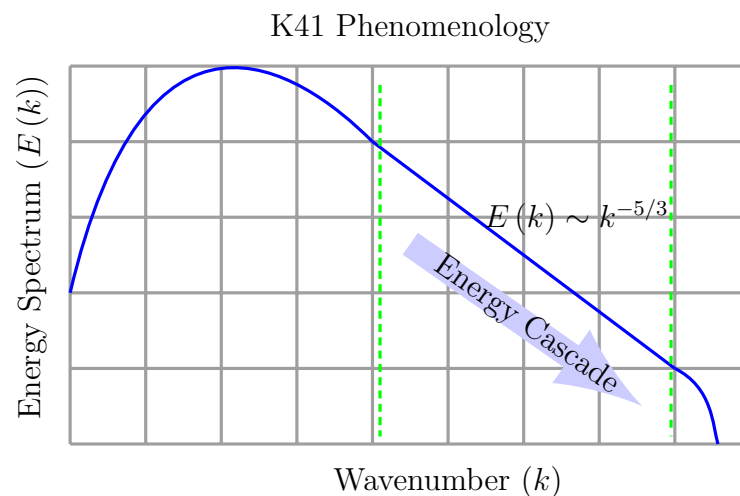
Figure 1.4: The Kolmogorov picture of turbulence.

Much of the history on the development of turbulence theory is encapsulated in famous books on the subject (Tennekes and Lumley 1972; Batchelor 1982; Frisch

1996; Pope 2000).

1.2.2 MHD Turbulence

The story of MHD turbulence is far shorter than that of pure HD turbulence. The topic of MHD turbulence is covered in detail in (Biskamp 2003). It can be said to have begun with (Iroshnikov 1963) and (R. H. Kraichnan 1965) wherein power law spectra for the total energy spectrum were determined to be $E(k) \sim k^{-3/2}$ in the presence of a strong background magnetic field. At the present time, there is still considerable debate as to the appropriate form of the energy spectrum for MHD turbulence (see Boldyrev 2006; Mininni 2010; Lee et al. 2010; Perez et al. 2012). Indeed, this concept is closely tied to the concept of the universality of turbulence in MHD (see Aluie and Eyink 2010; Pouquet 2012). Recall that the K41 phenomenology for HD turbulence rests on an assumption that the small scales of the flow field are universal regardless of the flow field. Because of the effects of the magnetic field (for example, it introduces an anisotropy into the flow field that is not present in HD flows) it is not clear whether or not a universal character exists in the inertial range for an MHD flow field. In the weak turbulence limit it was shown in (Galtier et al. 2000) that the total energy spectrum is $E(k) \sim k_{\perp}^{-2}$ where $k_{\perp}$ is the wavenumber perpendicular to the background magnetic field. Observations of turbulence in the solar wind indicate a K41 energy spectrum for the total energy as described in (Podesta, Roberts, and Goldstein 2007).

The debate on the universality of MHD turbulence is far from the only interesting aspect of MHD turbulence. A plethora of interesting phenomena exist ranging from fundamental physical studies to pure applications and everything in between. A strong magnetic field can have the effect of making the turbulence nearly two-dimensional. The effect of the inverse energy cascade is much more prominent in MHD turbulence than in HD turbulence. A topic of study in this area that has garnered much interest is the inverse cascade of magnetic helicity. The generation of the Earth's magnetic field is a fascinating topic in geophysics (Glatzmaier 2002). Geodynamo theory rests on the assumption (tentatively supported by experimental and numerical evidence (Kono and Roberts 2002)) that the liquid metal core of the

Earth is in a turbulent state. The turbulent velocity fluctuations pass energy to the large scale magnetic field thereby amplifying it and making life as we know it possible!

Before proceeding, we introduce some important dimensionless parameters in MHD. In addition to the fluid Reynolds number Re, these are the magnetic Reynolds number Rm, the interaction parameter S, magnetic Prandtl number Pr_m, and the Hartmann number Ha. The magnetic Reynolds number plays the same role as the HD Reynolds number. It measures the ratio of the advection of the magnetic field to the diffusion of the magnetic field. In introducing these parameters we consider a fluid with viscosity ν, density ρ, electrical conductivity σ, electrical resistivity $\eta = 1/\sigma$, and magnetic permeability μ_0. Furthermore, the magnetic diffusivity is defined as $\lambda = \eta/\mu_0$. The flow field has characteristic length L, characteristic velocity U, and characteristic magnetic field B_0. Then,

$$\text{Rm} = \mu_0 \sigma U L. \tag{1.5}$$

When $\text{Rm} \gg 1$ then the magnetic field is said to be "frozen" to the velocity field. The magnetic field lines are simply swept along by the velocity field. This situation is very common in astrophysical problems that have, quite literally, astronomical length scales. The interaction parameter measures the ratio of EM forces to inertial forces,

$$S = \frac{\text{EM forces}}{\text{Inertial forces}} = \frac{\sigma B_0^2 L}{\rho U}. \tag{1.6}$$

This parameter plays a role in the momentum equation and indicates the role of the Lorentz force. The magnetic Prandtl number is defined as the ratio of fluid viscosity to magnetic diffusivity,

$$Pr_m = \frac{\nu}{\lambda} = \frac{\text{Rm}}{\text{Re}}. \tag{1.7}$$

Flows that have very large or very small Pr_m are difficult to dissect because the velocity and magnetic fields act on very different scales. Finally, the Hartmann

number measures the ratio of EM forces to viscous forces,

$$\text{Ha} = \frac{\text{EM forces}}{\text{Viscous forces}} = B_0 L \sqrt{\frac{\sigma}{\rho\nu}}. \tag{1.8}$$

This parameter plays an important role in boundary layer MHD flows. Near the wall, viscous forces are strong. However, in MHD, the Lorentz force may also be quite strong in this region. A boundary layer that forms due to the Lorentz force is known as the Hartmann layer. We note that Ha can be written in terms of S and Re, $\text{Ha} = \sqrt{\text{SRe}}$

1.3 Review of Numerical Methods

This section provides an overview and motivation of numerical methods in fluid mechanics. It begins with a brief description of different numerical techniques. These include finite difference methods (Section 1.3.1), the finite element method (Section 1.3.2), and spectral methods (Section 1.3.3). As with almost all numerical methods, the goal is to reduce an ordinary differential equation (ODE) to a system of algebraic equations or a partial differential equation (PDE) to a system of ODEs. Following this introduction to numerical methods, a discussion on the state of numerical methods in fluid mechanics is provided in Section 1.3.4 with particular emphasis on the turbulence problem and a discussion of multiscale problems in general. This section also discusses the LES technique and introduces the variational multiscale (VMS) formulation.

1.3.1 The Finite Difference Method

The finite difference method (FDM) was the first numerical method. In fact, the concept of approximating differential equations with difference equations predates the advent of the modern digital computer. Indeed, Leonard Euler introduced finite difference techniques for approximating first order, linear ordinary differential equations. The basic idea behind finite difference techniques can be illustrated with a simple, one-dimensional example. Consider the following differential equation,

which is to be solved for $y(x)$,

$$\frac{\mathrm{d}y}{\mathrm{d}x} + y = 0. \tag{1.9}$$

On a computer, it is not feasible to solve for y at every value of x in the continuum. Thus, the concept of a numerical grid is introduced wherein one must solve for y at discrete values of x denoted by x_i where i is the ith grid point. In one dimension, a simple numerical grid may look like the one depicted in Figure 1.5.
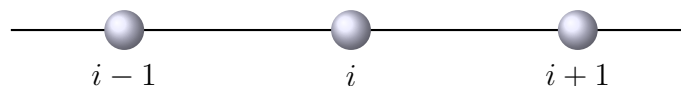
Figure 1.5: A simple numerical grid.

The finite difference method approximates the derivative with a difference. A simple example is

$$\frac{y_{i+1} - y_i}{x_{i+1} - x_i} + y_i = 0 \tag{1.10}$$

from which the solution at node $i + 1$ is

$$y_{i+1} = (1 - (x_{i+1} - x_i)) \, y_i. \tag{1.11}$$

This approach has been studied extremely extensively through the years (Thomas 1995). It can of course be applied to complicated, nonlinear PDEs like the Navier-Stokes equations. Error estimates have been obtained, convergence studies have been performed, and a plethora of various finite difference techniques have been proposed. Higher order techniques often provide better convergence and error properties but at the expense of more computational cost. In the example above, only the solution at the previous grid point must be stored. Higher order methods would expand this to include a wider stencil that could require the storage of other grid points such as the one at $i - 2$. It is also possible to define implicit finite difference schemes that require a matrix solve for subsequent grid points. Although implicit methods are considerably more expensive, they also have the potential to be un-

conditionally stable. We will not consider the finite difference method in any more depth.

1.3.2 The Finite Element Method

The finite element method (FEM) is a powerful numerical technique that found its first successes in the aerospace industry (Oden 1990; Meek 1996). Underlying this method is a beautiful mathematical theory. See (Hughes 2000) for an excellent introduction to the finite element method. Presently, we outline the classical finite element method in a quasi-qualitative way. There are two essential ideas underlying the numerical method: 1.) The concept of a finite element and 2.) Expansion of the numerical solution in a particular basis over the finite element. Together these ideas result in the finite element philosophy: *Approximate the solution over each finite element, assemble the element solutions into the global solution, and the result is an approximation of the desired solution.* Figure 1.6 illustrates the anatomy of a typical one-dimensional finite element mesh where e_i denotes the ith element and A is a global node number.
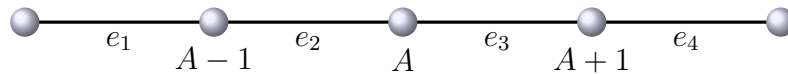
Figure 1.6: A representative, one-dimensional finite element mesh.

The solution is given as a linear combination of shape functions N_A which act as a set of basis functions for the numerical solution. Thus

$$y\left(x\right) \approx \sum_{A=1} y_A N_A \tag{1.12}$$

where y_A represents the solution at node A. A defining characteristic of the finite element method is the definition of the finite element basis functions as piecewise polynomials. Figure 1.7 presents the finite element mesh inclusive of piecewise linear basis functions. Critically, the basis functions are endowed with local support. This has important implications for computational cost. The basis functions could also be piecewise quadratic, cubic, etc. The numerical technique provides better solutions

as the order of the basis functions are increased. However, this comes with the price of increased computational cost.
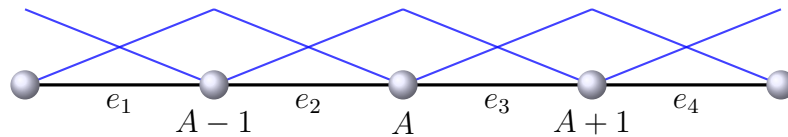
Figure 1.7: A finite element mesh with linear shape functions.

The FEM also differs from the FDM in that it uses as its starting point a variational statement and is part of the theory of the method of weighted residuals (MWR). To illustrate this, we consider the simple toy ODE (1.9). The MWR considers an integral equation over the problem domain $[x_1, \ x_2]$,

$$\int_{x_1}^{x_2} w \left(\frac{\mathrm{d}y}{\mathrm{d}x} + y \right) \ \mathrm{d}x = 0. \tag{1.13}$$

Thus, it enforces (1.9) in a weighted sense. The particular choice of weighting, w, results in different weighted-residual techniques. Intriguingly, the integral formulation resulting from the MWR is also a variational statement, although the absence of such a statement in physics does not preclude numerical methods built from the MWR. Thus, although no variational principle is known to exist for the incompressible MHD equations, it is still possible to build numerical methods out of the MWR. As a final note, we mention that working with an integral formulation of the problem also often permits a reduction of order of higher-order derivatives through integration by parts. This is extremely convenient because it relaxes continuity requirements on the finite element basis functions. Because of this property, the variational statement is frequently referred to as the weak form of the problem, weak referring to differentiability requirements on the basis functions and not to the ability of the statement itself. In subsequent sections, the finite element formulation of the incompressible MHD problem will be described in detail.

1.3.3 Spectral Methods

Spectral methods include some of the most celebrated techniques for analyzing ODEs and PDEs. One of the great strengths of these methods is that their

physical interpretation is intuitive. A spectral method decomposes a function into its constituent elements called its modes. From an analytical perspective, a suitably behaved function can be transformed into wavenumber space via the Fourier transform,

$$\widehat{f}(k) = \frac{1}{\sqrt{2\pi}} \int_{-\infty}^{\infty} f(x)\, e^{-ikx} \; \mathrm{d}x \tag{1.14}$$

A significant limitation of the Fourier-transform approach is that it works best for periodic functions. Therefore, if one wishes to solve a problem on a domain with a boundary for a non-periodic function, the Fourier-transform approach is not natural.

The numerical counterpart to the Fourier-transform is the Fourier-series. A Fourier-spectral numerical method expands the solution in terms for trigonometric basis functions as

$$f(x) \approx \sum_{-k}^{k} \widehat{f}(k)\, e^{ikx}. \tag{1.15}$$

Difficulties arise when analyzing nonlinear problems, as the Fourier transform does not offer any benefit in analyzing the nonlinear terms. Unfortunately, this results in additional computational cost for numerical methods. However, the fast Fourier transform (FFT) makes Fourier-spectral methods feasible and often the method of choice for their speed and ease of implementation. Despite these advantages over other numerical techniques, these methods suffer from a couple of disadvantages as well. In addition to the previously mentioned difficulties with non-periodic, bounded domains, spectral methods are also global and therefore require considerable inter-processor communication when implemented in a massively parallel framework.

As a final observation on these techniques, we wish to note that the Fourier-spectral method also falls under the purview of the MWR. Indeed, in subsequent sections, when deriving the incompressible MHD equations in wavenumber space, we begin from the same variational statement as used in the finite element method and simply change the basis functions from piecewise polynomials to trigonometric functions.

1.3.4 Numerics, Turbulence, and Multiscale Problems

Each numerical method described above has its own advantages and disadvantages. All numerical methods suffer the same fundamental difficulty when it comes to capturing the nature of the turbulence phenomenon: for the vast majority of problems, it is simply not possible to represent all of the scales involved in turbulence. A direct numerical simulation (DNS) is one in which the computational resolution is such that all the relevant scales of a problem are fully represented. Such a simulation would, in principle, be in good agreement with theory and experiment, limited only by the validity of the mathematical model being employed. Sadly, DNS is out a reach and will remain so for the foreseeable future.

To illustrate this, it is instructive to consider the relationship between the cost of performing a numerical simulation and the physics being considered. The cost of a DNS simulation is thought of in terms of how much resolution is required to resolve all of the scales. For example, a simulation that requires 100 timesteps and 10^6 spatial grid points is more expensive than a simulation that requires 50 timesteps and 100 grid points. Depending on the computational infrastructure available (i.e. computing power, memory, etc) this simulation cost has an actual financial cost. In the simplest case of HD turbulence it turns out that the computational cost is related to the Reynolds number as

$$\text{Cost} \sim 160\text{Re}^3. \tag{1.16}$$

The argument leading to this estimate is found in (Pope 2000, chap. 9). Most applications involving turbulence have very large values of Re. For example, around the fuselage of a Boeing 777 Re $\sim 10^8$! Such a simulation would require 5 years of dedicated, uninterrupted simulation time on a machine that has exaflop capabilities! Such a simulation is quite unimaginable. The situation is even more dire for MHD applications where the Reynolds numbers be even greater and an additional vector field comes into play.

It is not possible to refine the mesh enough so that all of the significant scales are captured by the numerical method when dealing with phenomena such as fluid turbulence. Such difficulties are characteristic of so-called multiscale problems. The

essential quality of a multiscale problem is that a range of scales interact with each other and that interactions among different scales are not negligible. Such problems are ubiquitous in nature. In fact, in order to develop more sophisticated models of the natural world, multiscale problems must be devised. Ultimately, we live in a multiscale world. Examples of this are everywhere, from chemical and biological processes, to economic laws, and of course within physics. As far as turbulence goes, the concept of an eddy is once again useful in illustrating the multiscale concept. The function of the smaller eddies is to accept energy from the larger eddies and to pass that energy on to ever smaller eddies. If a numerical simulation is able to represent eddies no smaller than a certain size, then the energy cascade cannot proceed to completion. Once the energy reaches eddies of a certain size, the energy can only accumulate because there is no physical mechanism by which the energy can be dissipated (aside from numerical dissipation which is not considered here).

Such observations led to the development of LES models in the turbulence community (Galperin 1993). LES models are the subject of this thesis and so will not be discussed in detail presently. The LES philosophy rests on the central tenet that the smallest scales of a flow field are universal and act in such a way that they dissipate energy. Thus, one needs only to capture the anisotropic dynamics of the large scales of the flow field which contain the most energy anyway. With this philosophy, it is therefore no longer necessary to numerically capture every detail of the flow field. A model that adds in extra dissipation is introduced into the numerical method. Ideally, this model provides the missing dissipation from the small scales that the numerical method is unable to capture. Considerable computational expense can be saved by performing an under-resolved simulation equipped with a model that seeks to capture the effect of the missing scales.

An important computational paradigm was introduced in (Hughes 1995; Hughes et al. 1998) and called the VMS formulation. This approach assumes scale separation and decomposes the solution field into resolved and unresolved scales,

$$f = f^h + f'. \tag{1.17}$$

Considerable detail will be provided on this technique in Chapter 2, Section 2.7.2

and Chapter 4. Indeed, it is the starting point for the development of the new turbulence models for MHD presented in this work. To illustrate the effect of this decomposition, consider the following quadratic nonlinearity,

$$\mathcal{N} = fg. \tag{1.18}$$

The VMS decomposition results in

$$\mathcal{N} = f^h g^h + f^h g' + f' g^h + f' g'. \tag{1.19}$$

Thus we see that the nonlinear term has three primary contributions,

1. Purely resolved scales, $f^h g^h$

2. Cross correlations between resolved and unresolved scales, $f^h g'$ and $f' g^h$

3. Correlations between purely unresolved scales, $f' g'$

Therefore, the VMS decomposition *induces* a model through subgrid correlations without invoking any *ad hoc* eddy viscosity principles.

Another important aspect of the VMS method is the development of suitable approximations for the subgrid solutions. Most of the turbulence modeling effort is confined to these approximations. Indeed, more sophisticated subgrid approximations lead to better VMS performance. A challenge in turbulence modeling is adequately representing the purely subgrid correlations as these are higher order subgrid correlations.

1.4 Primary Contributions

The content of the previous sections serve as motivation for the development of turbulence models in MHD. The current state of MHD turbulence modeling is reviewed in Section 1.4.1. Section 1.4.2 describes the primary contributions of this thesis.

1.4.1 Current State of MHD Turbulence Modeling

Turbulence modeling in MHD is still in its infancy. The extreme variation in physics and engineering applications makes the development of robust turbulence models particularly difficult. There is still no general consensus in the MHD turbulence community on the proper approach to take in developing turbulence models. One approach is to attempt to develop robust turbulence models that can be used in most, if not all, physics and engineering applications. In reality, of course, it is known that this goal will be exceptionally difficult to achieve. Indeed, even within the hydrodynamic turbulence modeling community, many variations of turbulence models exist for different applications. However, a unified approach could be very valuable even with tweaks to existing models for very specific applications being required. At the other end of the spectrum is the viewpoint that each application needs its own turbulence model. In MHD, this viewpoint is natural because of the wide range of physics that MHD encompasses. Solar physics differs from the physics of the solar wind which is in turn different than geodynamo physics which is vastly different from fusion physics. Could it really be the case the MHD phenomena are so vast that different models for each application must be developed?

Eddy viscosity (EV) models have been proposed for MHD by generalizing those for the hydrodynamic case (Theobald, Fox, and Sofia 1994). These models are a good starting point, but do not account for significant portions of the subgrid physics. For example, they do not allow for the possibility of backscatter or a subgrid dynamo effect wherein turbulent velocity fluctuations transfer energy to the resolved magnetic induction. Furthermore, it has been shown that the dynamic Smagorinsky EV (DSEV) model excessively damps out the effects of the dynamo effect in MHD (Haugen and Brandenburg 2006). Closures for the mean-field equations of MHD have been systematically worked out (Yoshizawa 1990) but these models are difficult to implement numerically. Newer models account for the coupled nature of the equations, permit the possibility of backscatter (Müller and Carati 2002), and are relatively straightforward to implement. These models depend on parameters that generally depend upon the flow field. Such parameters are determined on the fly during the computation with a dynamic procedure (Germano et al. 1991). The

dynamic procedure for determining the model coefficients can be cumbersome to implement, especially for flows with complicated geometries. In recent years, new eddy viscosity models have been proposed (Vreman 2004; John and Kindl 2008) that aim to eliminate the need for a dynamic procedure in the context of hydrodynamic turbulence. In MHD, work has been done for flows in which Rm is small compared to Re. One approach performs a DNS of the induction equation while using a subgrid LES model to represent the velocity field components that are smaller than the magnetic diffusion length (Ponty, Politano, and Pinton 2004). In yet another approach, the quasi-static approximation is used wherein the nonlinear terms in the magnetic induction equation are neglected (Knaepen and Moin 2004). Two point closure models in spectral space such as the eddy damped quasi normal Markovian approximation (EDQNM) (Orszag 1977; Biskamp 2003) have been generalized (Baerenzung et al. 2008b) and applied to MHD (Baerenzung et al. 2008a). Another popular closure model, the Lagrangian-averaged α model, introduces closure not through the diffusion terms but via the nonlinear terms (D Holm 1999; Montgomery and Pouquet 2002; Holm et al. 2005). This technique has also been applied to the MHD equations (D.D Holm 2002). Previous studies have been performed which apply stabilized finite elements to incompressible magnetohydrodynamics (Codina 2002; J. Shadid et al. 2010). Although useful in overcoming spurious oscillations in the solution and circumventing the Ladyženskaja-Babuška-Brezzi (LBB) condition (Hughes, Franca, and Hulbert 1989), stabilized finite elements only represent incomplete turbulence models.

Other numerical approaches for MHD involve using a hyperdiffusion operator ($\nabla^{2\alpha}$) in place of the usual Laplacian operator on the diffusion terms (Müller and Biskamp 2000; Biskamp 2003, see) and (Pope 2000, pg. 352). The hyperdiffusion approach is motivated mainly by numerical considerations; the goal is simply to smooth out the fields so that numerical computations become more feasible. Alternative approaches involve implicit LES models (ILES) in which no explicit turbulence model is included and numerical dissipation is used as a turbulence model that is inherent in the numerical method. For MHD see (Smolarkiewicz and Charbonneau 2013).

The length scales involved in many MHD turbulence problems are staggering.

MHD effects in the sun can range in scales from several thousand kilometers down to the molecular scale (Nelson et al. 2011, 2013). Furthermore, MHD effects often involve important anisotropic effects at the smallest scales. Inverse cascades of energy due to the interplay between the velocity and magnetic fields play an important role in many realms of MHD physics, see, for example (Zweibel and Yamada 2009). Classical Smagorinsky models are typically exclusively dissipative, which precludes such critical effects. Moreover, the velocity and magnetic scales can be vastly different (Ponty et al. 2005). Because of this, the inertial range of the velocity and magnetic fields may be at entirely different scales. How might a model be developed that saves computational time when the numerical simulation is only able to reach the inertial range of one of the fields?

Most of the numerical studies in MHD turbulence that we mentioned above were developed for astrophysical applications. We take some time now to review recent studies that have involved wall-bounded MHD flows. Specifically, we provide an overview of turbulent channel and duct flows. These types of flows are discussed in the texts by (Branover 1978; Moreau 1990; Müller and Bühler 2001). Such flow fields typically involve very small values for Pr_m. These flow fields are challenging to understand from both a numerical and experimental point of view. The configuration of a typical channel flow problem is such that a fluid is flowing within an imposed background magnetic field. This motion through the field generates the Lorentz force which affects the topology and dynamics of the velocity field. The situation for numerical methods is particularly dire. No DNS of these flow fields exists. A very small time step would be required in order to perform a meaningful simulation of such flows. Instead of a DNS of the full MHD equations, researchers implement the quasi-static MHD approximation (Branover 1978). This approach is valid for very small values of Rm and assumes that the magnetic field induced by the flow field is negligible compared to the applied background magnetic field. It is essentially a zero-th order approximation to the magnetic induction equation. The resulting system of equations to be solved is the momentum equation and a Poisson equation for the electric potential. The electric potential plays an important role in the Lorentz force of the momentum equation and only the applied magnetic field,

not the induced magnetic field, contributes to the Lorentz force.

The literature on DNS of the turbulent MHD channel or duct flow using the quasi-static approximation is rather extensive. In (Krasnov et al. 2004) the authors study the instability of the Hartmann layer in a channel flow. Later, in (Boeck, Krasnov, and Zienicke 2007), a study of turbulent MHD channel flow was performed for several values of Re and Ha. A follow up to this paper (Krasnov, Zikanov, and Boeck 2012) performed a systematic study of turbulent MHD duct flow. Another channel flow study in (S. Satake et al. 2006) used DNS of the quasi-static MHD equations to understand large scale turbulence structures at high Re. In (Chaudhary, Vanka, and Thomas 2010) another turbulent MHD duct flow was studied under the quasi-static assumption. All of these papers present useful benchmark results of turbulent statistics. They also demonstrate the various effects of the applied magnetic field on the velocity field. Each of the previously mentioned studies considers channels and ducts with perfectly electrically insulating walls. A slightly different simulation was performed in (S.i Satake et al. 2006) where the channel walls were electrically conducting. It was found that, compared to the perfectly insulating wall, a perfectly conducting wall leads to drag reduction near the wall.

LES of turbulent MHD channel and duct flow are not as common as the DNS. An early study was performed by (Shimomura 1991) where results were compared with experimental data. The new model proposed in that paper involved adding a magnetic damping factor to the classical turbulent eddy viscosity in the momentum equation. For a fluid that does not conduct electricity, the proposed model reduces to the standard HD eddy viscosity model. It was found that the new model performs better than the traditional DSEV model. A more recent study by (Kobayashi 2006) tested variants of the dynamic Smagorinsky model. Both of these studies used the quasi-static approximation.

We mention one study that has been performed for an MHD channel flow with $\mathrm{Pr_m} = 1$ for which the quasi-static approximation does not apply, (Hamba and Tsuchiya 2010). In this study the dynamic Smagorinsky model for MHD was used to study the cross-helicity dynamo effect in which the magnetic field is amplified through an inverse cascade of energy that takes place due to the cross helicity

mechanism. The authors were not able to perform a full DNS but did perform a substantial LES computation. They also note that the collection of turbulence statistics for the MHD flow takes considerably longer than for the pure HD case.

1.4.2 Contributions of this Thesis

The contribution of this work is to develop and introduce a promising computational paradigm into MHD turbulence modeling. Three new models are developed for the incompressible, resistive MHD equations (Sondak and Oberai 2012):

1. The pure variational multiscale formulation in which velocity, magnetic, and pressure fields are split into two scales: the resolved scales and the unresolved scales. The unresolved scales are assumed to be proportional to the residual of the unresolved scales. Such residual based models are desirable as they endow the numerical method with an inherent consistency. As the numerical grid is refined, the numerical solution approaches the exact solution. When this happens, the residual of the grid scales becomes smaller thereby forcing the contribution from the unresolved scales to be smaller. This makes physical and numerical sense since, when the numerical solution improves, it is able to capture more of the physics of the problem, thereby leaving fewer unresolved scales to be resolved. In this sense then, the turbulence model automatically vanishes when it is no longer needed.

2. A VMS inspired eddy viscosity model. This EV model, like most EV models, is proportional to a length scale times a velocity scale. The essential difference is that the velocity scale *is* the subgrid solution. The subgrid solution is approximated with the VMS representation for the subgrid scales. This new EV model is therefore termed the residual-based eddy viscosity (RBEV) model. Because of its dependence on the residual, it too is inherently dynamic. We postulate that the constant of proportionality in this model really is a true universal constant which circumvents the need for a dynamic procedure. The MHD version of this model has the momentum and induction EVs equivalent and proportional to the ratio of kinetic energy to total MHD energy. Such a formulation is described in detail in Chapter 4.

3. A mixed model (MM) combining the VMS formulation and the VMS inspired eddy viscosity model. This mixed model takes advantage of the strengths of the VMS and RBEV models. The resulting mixed model is a fully residual-based turbulence model that does not require any dynamic procedure in implementation.

These models bridge the gap between a purely computational turbulence modeling approach and a physics-based turbulence modeling approach. They are endowed with special properties that allow them to account for important MHD physics such as the inverse energy cascade while, at the same time, being easy to implement and possessing desirable computational properties such as their inherent dynamic nature. Although promising, these models do not attempt to address all of the current issues found in MHD turbulence modeling. Their flexibility does provide many opportunities to include essential MHD physics that has not been included in this first version of the models. In particular, taking into account the coupling of the momentum and induction equations in the models themselves may prove fruitful. We have obtained preliminary, promising results on this as discussed in Chapter 3. Furthermore, incorporating a dependence on Pr_m into the models may help address the severe scale discrepancies between the velocity and magnetic field in certain MHD problems.

The layout of the remainder of the dissertation will now be outlined. The stage for this work is set in Chapter 2 wherein notational conventions are introduced, the basic equations are derived and accompanying boundary conditions are introduced, and mathematical preliminaries are discussed. Furthermore, this chapter introduces in detail the numerical methods that are used to develop and test the new LES models. Chapter 3 is devoted to the stabilization parameter which is the central object in the theory of stabilized FEMs. It also plays a significant role in the development of the turbulence models presented in this work. Its origins and history are discussed and new contributions to its form for MHD are developed. Chapter 4 presents the bulk of the mathematical contribution of this thesis. Traditional turbulence models are introduced to put the new models into context. Following this, the new models are developed in detail and specialized to the finite element and Fourier spectral

methods. The performance of these new models is assessed in Chapter 5 through test problems on homogeneous, isotropic turbulence and turbulent MHD channel flow. Finally, Chapter 6 draws conclusions and speculates on extensions and future prospects for this work.

CHAPTER 2
Setting the Stage

In the following sections we put into mathematical language the discussion from Chapter 1. In Section 2.1 notational conventions are introduced. This is followed in Section 2.2 with a derivation of the incompressible magnetohydrodynamics equations. Appropriate boundary conditions are discussed in Section 2.4. Section 2.3 introduces the strong and weak formulations. The chapter concludes with Sections 2.6 and 2.7 which give an overview of the numerical techniques employed in this project and an introduction to the turbulence modeling approach that is taken, respectively.

2.1   Notational Considerations

2.1.1   Mathematical Conventions

Throughout this thesis scalars are denoted by a lowercase Roman letter such as f. Vectors are distinguished with a boldface, Roman letter such as $\mathbf{v}$ or $\mathbf{V}$. Tensors and matrices are denoted with boldface capital serif letters such as $\mathbf{T}$.

We briefly introduce notation for common operators from vector calculus that are used in this work. We suppose that we have a scalar $f \in \mathbb{C}$, vectors $\mathbf{v}$, $\mathbf{w} \in \mathbb{C}^n$ and tensors $\mathbf{S}$, $\mathbf{T} \in \mathbb{C}^{n \times m}$. We frequently employ index notation for which an overview is provided in Appendix C. Table 2.1 summarizes these operators in both tensor and index notation as they appear in this dissertation. Appendix C provides an overview of index notation. From time to time we will have cause to refer to the fact that a matrix can be decomposed into its symmetric and antisymmetric parts. In tensor notation this is

$$\mathbf{T} = \mathbf{S} + \mathbf{A} \tag{2.1}$$

where

$$\mathbf{S} = \frac{1}{2}\left(\mathbf{T} + \mathbf{T}^T\right) \tag{2.2}$$

$$\mathbf{A} = \frac{1}{2}\left(\mathbf{T} - \mathbf{T}^T\right) \tag{2.3}$$

and $\mathbf{T}^T$ denotes the transpose of a matrix. In index notation we write

$$\mathsf{T}_{ij} = \mathsf{T}_{(ij)} + \mathsf{T}_{[ij]} \tag{2.4}$$

where

$$\mathsf{T}_{(ij)} = \frac{1}{2}\left(\mathsf{T}_{ij} + \mathsf{T}_{ji}\right) \tag{2.5}$$

$$\mathsf{T}_{[ij]} = \frac{1}{2}\left(\mathsf{T}_{ij} - \mathsf{T}_{ji}\right). \tag{2.6}$$

We also introduce two modifications to the gradient operator called the symmetric and antisymmetric gradient operators. In tensor notation these are

$$\nabla^{\mathsf{s}}\mathbf{v} = \frac{1}{2}\left(\nabla\mathbf{v} + (\nabla\mathbf{v})^T\right) \quad \longrightarrow \quad \text{Symmetric gradient} \tag{2.7}$$

$$\nabla^{\mathsf{a}}\mathbf{v} = \frac{1}{2}\left(\nabla\mathbf{v} - (\nabla\mathbf{v})^T\right) \quad \longrightarrow \quad \text{Antisymmetric gradient.} \tag{2.8}$$

In index notation we have

$$v_{(i,j)} = \frac{1}{2}\left(v_{i,j} + v_{j,i}\right) \quad \longrightarrow \quad \text{Symmetric gradient} \tag{2.9}$$

$$v_{[i,j]} = \frac{1}{2}\left(v_{i,j} - v_{j,i}\right) \quad \longrightarrow \quad \text{Antisymmetric gradient.} \tag{2.10}$$

The magnitude of a vector $\mathbf{v}$ with components v_1, v_2, v_3 is given by

$$|\mathbf{v}| = \sqrt{v_1^2 + v_2^2 + v_3^2}. \tag{2.11}$$

Table 2.1: **A summary of the operators from vector calculus and their notation.**

Operator	Tensor Notation	Index Notation
Divergence	$\nabla \cdot \mathbf{v}$	$v_{j,j}$
	$\nabla \cdot \mathbf{T}$	$\mathsf{T}_{ij,j}$
Gradient	∇f	$f_{,j}$
	$\nabla \mathbf{v}$	$v_{i,j}$
Curl	$\nabla \times \mathbf{v}$	$\epsilon_{ijk} v_{j,k}$
Dot Product	$\mathbf{v} \cdot \mathbf{w}$	$v_j w_j$
Tensor Inner Product	$\mathsf{S} : \mathsf{T}$	$\mathsf{S}_{ij} \mathsf{T}_{ij}$
Outer Product (Diadic)	$\mathbf{v} \otimes \mathbf{w}$	$v_i w_j$

2.1.2 Physical Notational Conventions

The problem domain under consideration is given by $\Omega \subset \mathbb{R}^{n_{sd}}$ where n_{sd} denotes the number of spatial dimensions. In the present work we usually take $n_{sd} = 3$ although $n_{sd} = 2$ for some of the test problems in Chapter 3. The boundary of this domain is given by Γ. This concept is illustrated in Figure 2.1. The spatial
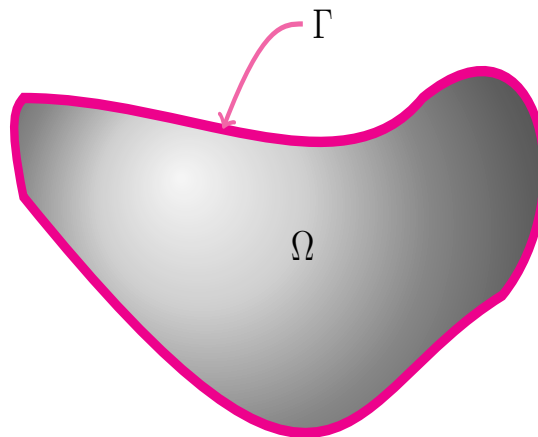
Figure 2.1: Illustration of a problem domain.

domain with its boundaries is denoted by

$$\overline{\Omega} = \Omega \cup \Gamma. \tag{2.12}$$

and the boundary of the domain is split into sections corresponding to essential and natural boundary conditions. Quantities involving essential boundary conditions are denoted by a subscript g while quantities related to natural boundary conditions are denoted by a subscript h. Thus,

$$\Gamma = \Gamma_g \cup \Gamma_h \tag{2.13}$$

where the essential and natural boundaries do not overlap, i.e.,

$$\Gamma_g \cap \Gamma_h = \varnothing. \tag{2.14}$$

For an account that is both intuitive and comprehensive see (Hughes 2000). The space-time domain is denoted by $\mathcal{Q}$ and is given as

$$\mathcal{Q} = \Omega \times \,]\,0, T\,[\tag{2.15}$$

where T is the final time in the temporal domain. Furthermore, the space-time boundary is

$$\mathcal{P} = \Gamma \times \,]\,0, T\,[\,. \tag{2.16}$$

The space-time domain with its space-time boundaries is denoted by

$$\overline{\mathcal{Q}} = \mathcal{Q} \cup \mathcal{P}. \tag{2.17}$$

Moreover,

$$\mathcal{P} = \mathcal{P}_g \cup \mathcal{P}_h \tag{2.18}$$

where

$$\mathcal{P}_g = \Gamma_g \times \,] \, 0, T \, [\tag{2.19}$$

and

$$\mathcal{P}_h = \Gamma_h \times \,] \, 0, T \, [\, . \tag{2.20}$$

The goal is to determine the configuration of the flow field on $\overline{\mathcal{Q}}$.

The coordinates under consideration are denoted $\mathbf{x}$ where $\mathbf{x} \in \Omega$ and

$$\mathbf{x} = \begin{bmatrix} x \\ y \\ z \end{bmatrix} = \begin{bmatrix} x_1 \\ x_2 \\ x_3 \end{bmatrix} . \tag{2.21}$$

A typical domain for each of the coordinate directions is

$$x \in [x_0, \ x_f] = \Omega_x \tag{2.22}$$

$$x \in [y_0, \ y_f] = \Omega_y \tag{2.23}$$

$$x \in [z_0, \ z_f] = \Omega_z \tag{2.24}$$

where a subscript 0 denotes the initial coordinate and a subscript f denotes the final coordinate.

2.1.3 Notation for Integral Forms

Our new models will be developed with the variational statement and will be written using the abstract mathematical notation of "forms." In particular, we will be working with integral forms. An example of an integral form is, given functions f and g,

$$\mathcal{A}(f, g) = \int_\Omega fg \ \mathrm{d}\Omega \tag{2.25}$$

where

$$\int_\Omega fg \ \mathrm{d}\Omega = \int_{\Omega_z} \int_{\Omega_y} \int_{\Omega_x} f\left(x,y,z\right) g\left(x,y,z\right) \ \mathrm{d}x \ \mathrm{d}y \ \mathrm{d}z. \qquad (2.26)$$

We will often use the notation $(\cdot, \cdot)$ to denote a single integral form and the notation $\mathcal{A}(\cdot, \cdot)$ to represent some combination of integral forms. For example,

$$\begin{aligned} \mathcal{A}\left(u, v\right) &= \int_\Omega fg \ \mathrm{d}\Omega + \int_\Omega f^2 \nabla^2 g \ \mathrm{d}\Omega \\ &= (f, g) + \left(f^2, \nabla^2 g\right). \end{aligned} \qquad (2.27)$$

If it is not clear from the context of the problem, we will denote the domain of the problem as a subscript after the parentheses. That is,

$$(f, g)_\Omega = \int_\Omega fg \ \mathrm{d}\Omega. \qquad (2.28)$$

Some properties of forms such as linearity, bilinearity, and symmetry are discussed in Appendix D. For a nice introduction to integral forms see (Hughes 2000).

2.2 Equations for Incompressible Magnetohydrodynamics

2.2.1 Comments on MHD Units

It is instructive to discuss MHD units before introducing the full MHD equations and the new turbulence models. In the engineering and fluid mechanics community, it is generally understood that the International System of Units (SI units) is used. Therefore, length scales are in meters (m), time is in seconds (s), and mass is in kilograms (kg). The force is a derived unit and is measured in Newtons (N). However, within the electromagnetics community, there is a large range of conventions for units. Certain fields prefer different conventions because the equations take on convenient forms when using different units. For a great summary of units in electromagnetism see (Jackson 1999, Appendix on Units and Dimensions). In the present work, we will work *almost* exclusively in SI units. All derivations, unless specifically stated otherwise, are performed in SI units. Therefore, the primary EM

quantities have the following dimensions,

$$\textbf{Current:} \longrightarrow \text{Units: Ampère} \longrightarrow \frac{\text{Charge}}{[s]} \longrightarrow [A] \qquad (2.29)$$

$$\textbf{Current\ \ density:} \longrightarrow \text{Units:} \longrightarrow \frac{[A]}{[m]^2} \qquad (2.30)$$

$$\textbf{Magnetic\ \ induction:} \longrightarrow \text{Units: Tesla} \longrightarrow \frac{[N]}{[A] \cdot [m]} \qquad (2.31)$$

$$\textbf{Magnetic permeability:} \longrightarrow \text{Units:} \ \longrightarrow \frac{[N]}{[A]^2}. \qquad (2.32)$$

One important exception in this work arises when the magnetic field is scaled to be in Alfvén velocity units. Thus $\mathbf{B}$ is replaced by $\sqrt{\mu_0 \rho}\,\mathbf{B}_A$. It is readily seen that $\mathbf{B}_A$ has the units of velocity. In this work, when the magnetic field is rescaled in this way, the subscript A will be left off but it will be made clear that the magnetic field actually has Alfvén velocity units.

2.2.2 A Derivation of the Incompressible MHD Equations

This section will present a formal derivation of the equations of incompressible MHD. Supplementary details on the present derivation can be found in (Davidson 2001; Biskamp 2003; Goedbloed and Poedts 2006). We adopt the continuum viewpoint here so that our starting point is the fluid equations augmented with an electromagnetic body force. A more rigorous derivation would begin from the Boltzmann kinetic equation which describes the evolution of distribution functions of particle species such as ions and electrons. By taking moments of the Boltzmann equation, and making appropriate simplifying assumptions, the incompressible MHD equations can be recovered. Details on this approach are given in (Goedbloed and Poedts 2006). The classic paper on this approach for MHD is (Braginskii 1965).

Magnetohydrodynamics is concerned with the behavior of an electrically conducting fluid in the presence of an EM field. The essential idea is understood by considering a fluid element immersed in a background EM field and which has the potential to carry an electric current. The electric forces on the charges in the fluid

element are given by

$$\mathbf{F}_{q_i} = q_i \left(\mathbf{E} + \mathbf{v}_{q_i} \times \mathbf{B} \right). \tag{2.33}$$

The ith particle has charge q_i and is traveling with a velocity $\mathbf{v}_{q_i}$. The electromagnetic field consists of the electric field $\mathbf{E}$ and the magnetic field $\mathbf{B}$. This force is commonly referred to as the Lorentz force. We are interested in the net effect of the forces on these individual charges. Therefore, summing over each charge in the fluid element gives

$$\sum \mathbf{F}_{q_i} = \sum q_i \mathbf{E} + \sum q_i \mathbf{v}_{q_i} \times \mathbf{B} \tag{2.34}$$

$$= Q\mathbf{E} + \mathbf{J} \times \mathbf{B} \tag{2.35}$$

where Q is the total charge in the fluid element (and therefore the charge *of* the fluid element) and $\mathbf{J}$ is the current carried within the fluid element. We shall be interested in the volumetric version of this force $\mathbf{f}$. Dividing by the volume of the fluid element gives

$$\mathbf{f}_{\text{EM}} = \rho_e \mathbf{E} + \mathbf{j} \times \mathbf{B}. \tag{2.36}$$

In (2.36) ρ_e is the charge density and $\mathbf{j}$ represents the current density. However, charge neutrality in a fluid implies that the net charge is negligible. Therefore, the version of the volumetric, electromagnetic force that a fluid element experiences is

$$\mathbf{f}_{\text{EM}} = \mathbf{j} \times \mathbf{B}. \tag{2.37}$$

To recap: an electrically conducting fluid element moving in a magnetic field experiences an external electromagnetic force. This force is given by (2.37). We now proceed to introduce the one-fluid, resistive MHD equations. Let us first consider the momentum equation from classical fluid dynamics.

$$\rho \frac{\partial \mathbf{u}}{\partial \text{t}} + \rho \mathbf{u} \cdot \nabla \mathbf{u} = \nabla \cdot \mathbf{T} + \mathbf{f}. \tag{2.38}$$

In (2.38) the velocity of the fluid element with density ρ is represented by $\mathbf{u}$. The stress tensor, $\mathbf{T}$, contains information about the normal and shearing stresses that the fluid element experiences. Finally, the possibility of an external, volumetric body force, denoted by $\mathbf{f}$, is included. For incompressible fluids this equation reduces to (see Appendix A)

$$\rho\frac{\partial \mathbf{u}}{\partial \mathrm{t}} + \rho\nabla \cdot (\mathbf{u} \otimes \mathbf{u}) = -\nabla p + \mu\nabla^2\mathbf{u} + \mathbf{f} \tag{2.39}$$

where p is the fluid pressure and μ is the fluid's dynamic viscosity. As already discussed, when considering electrically conducting fluids, the external body force is an electromagnetic one. Therefore, the momentum equation for incompressible MHD becomes

$$\rho\frac{\partial \mathbf{u}}{\partial \mathrm{t}} + \rho\nabla \cdot (\mathbf{u} \otimes \mathbf{u}) = -\nabla p + \mu\nabla^2\mathbf{u} + \mathbf{j} \times \mathbf{B}. \tag{2.40}$$

In order to determine the solution to (2.40) we must know the current density and the magnetic induction. The magnetic induction is determined from Maxwell's equations.

$$\nabla \times \mathbf{E} = -\frac{\partial \mathbf{B}}{\partial \mathrm{t}} \tag{2.41}$$

$$\nabla \times \mathbf{B} = \mu_0 \left(\mathbf{j} + \epsilon_0\frac{\partial \mathbf{E}}{\partial \mathrm{t}}\right) \tag{2.42}$$

$$\nabla \cdot \mathbf{B} = 0 \tag{2.43}$$

$$\nabla \cdot \mathbf{E} = \frac{\rho_e}{\epsilon_0} \tag{2.44}$$

where the only quantities that have not yet been introduced are the electrical permittivity ϵ_0 and the magnetic permeability μ_0 . A closure relation is required to specify the current density. The generalized Ohm's law suffices for this task,

$$\mathbf{j} = \sigma \left(\mathbf{E} + \mathbf{u} \times \mathbf{B}\right) \tag{2.45}$$

where σ is the electrical conductivity of the fluid. It is sufficient in MHD to neglect

the displacement current in Ampère's law (2.42). Thus,

$$\nabla \times \mathbf{B} = \mu_0 \mathbf{j}. \tag{2.46}$$

We wish to arrive at an equation only for the magnetic induction. To this end we seek to eliminate the curl of the electric field. From the generalized Ohm's law and after introducing the reciprocal of the electrical conductivity, the resistivity η, we have

$$\mathbf{E} = \frac{1}{\sigma}\mathbf{j} - \mathbf{u} \times \mathbf{B}$$

$$\Rightarrow \nabla \times \mathbf{E} = \nabla \times (\eta\mathbf{j}) - \nabla \times (\mathbf{u} \times \mathbf{B})$$

$$\Rightarrow \nabla \times \mathbf{E} = \nabla \times \left(\frac{\eta}{\mu_0}\nabla \times \mathbf{B}\right) - \nabla \times (\mathbf{u} \times \mathbf{B}).$$

Using this in the induction equation from Maxwell's equations (2.41) we arrive at an induction equation that is independent of the electric field.

$$\frac{\partial \mathbf{B}}{\partial t} - \nabla \times (\mathbf{u} \times \mathbf{B}) = -\nabla \times \left(\frac{\eta}{\mu_0}\nabla \times \mathbf{B}\right). \tag{2.47}$$

We will work with a different form of this equation. For a derivation of the new form of the equation please refer to Appendix E.1.

$$\frac{\partial \mathbf{B}}{\partial t} + \nabla \cdot (-\mathbf{u} \otimes \mathbf{B} + \mathbf{B} \otimes \mathbf{u}) = \nabla \cdot \left[\frac{\eta}{\mu_0}\left(\nabla\mathbf{B} - (\nabla\mathbf{B})^T\right)\right]. \tag{2.48}$$

If the material properties are constant then the induction equation becomes

$$\frac{\partial \mathbf{B}}{\partial t} + \nabla \cdot (-\mathbf{u} \otimes \mathbf{B} + \mathbf{B} \otimes \mathbf{u}) = \frac{\eta}{\mu_0}\nabla^2\mathbf{B}. \tag{2.49}$$

Finally, we call $\lambda = \eta/\mu_0$ the magnetic diffusivity.

Equipped with Maxwell's equations, and, more specifically, Ampère's law, we may now eliminate the current density from the electromagnetic force term in the

momentum equation. We find (see Appendix E.3.1) that

$$\mathbf{j} \times \mathbf{B} = \frac{1}{\mu_0} \nabla \cdot (\mathbf{B} \otimes \mathbf{B}) - \frac{1}{\mu_0} \nabla \left(\frac{1}{2} \mathbf{B} \cdot \mathbf{B} \right).$$ (2.50)

Thus, the momentum equation becomes

$$\rho \frac{\partial \mathbf{u}}{\partial t} + \rho \nabla \cdot (\mathbf{u} \otimes \mathbf{u}) = -\nabla p + \mu \nabla^2 \mathbf{u} + \frac{1}{\mu_0} \nabla \cdot (\mathbf{B} \otimes \mathbf{B}) - \frac{1}{\mu_0} \nabla \left(\frac{1}{2} \mathbf{B} \cdot \mathbf{B} \right).$$ (2.51)

This is written as

$$\frac{\partial \mathbf{u}}{\partial t} + \nabla \cdot \left(\mathbf{u} \otimes \mathbf{u} - \frac{1}{\mu_0 \rho} \mathbf{B} \otimes \mathbf{B} \right) = -\nabla P + \nu \nabla^2 \mathbf{u}.$$ (2.52)

In the above equation the pressure has been rewritten to include the magnetic pressure. The total MHD pressure is

$$P = \frac{1}{\rho} p + \frac{1}{2\mu_0 \rho} \mathbf{B} \cdot \mathbf{B}.$$ (2.53)

The incompressible MHD equations are therefore,

$$\frac{\partial \mathbf{u}}{\partial t} + \nabla \cdot \left(\mathbf{u} \otimes \mathbf{u} - \frac{1}{\mu_0 \rho} \mathbf{B} \otimes \mathbf{B} \right) = -\nabla P + \nu \nabla^2 \mathbf{u}$$ (2.54)

$$\nabla \cdot \mathbf{u} = 0$$ (2.55)

$$\frac{\partial \mathbf{B}}{\partial t} + \nabla \cdot (-\mathbf{u} \otimes \mathbf{B} + \mathbf{B} \otimes \mathbf{u}) = \lambda \nabla^2 \mathbf{B}$$ (2.56)

$$\nabla \cdot \mathbf{B} = 0$$ (2.57)

The final form of the MHD equations is written as

$$\boxed{\begin{aligned} \frac{\partial \mathbf{u}}{\partial t} + \nabla \cdot \boldsymbol{\mathcal{N}}^{\mathrm{V}} (\mathbf{u}, \mathbf{B}) &= -\nabla P + \nu \nabla^2 \mathbf{u} + \mathbf{f}^{\mathrm{V}} \\ \nabla \cdot \mathbf{u} &= 0 \\ \frac{\partial \mathbf{B}}{\partial t} + \nabla \cdot \boldsymbol{\mathcal{N}}^{\mathrm{I}} (\mathbf{u}, \mathbf{B}) &= \lambda \nabla^2 \mathbf{B} + \mathbf{f}^{\mathrm{I}} \\ \nabla \cdot \mathbf{B} &= 0 \end{aligned}}$$ (2.58)

where the nonlinear terms are given by

$$\boldsymbol{\mathcal{N}}^{\mathrm{V}}\left(\mathbf{u}, \mathbf{B}\right) = \mathbf{u} \otimes \mathbf{u} - \frac{1}{\mu_0 \rho} \mathbf{B} \otimes \mathbf{B} \tag{2.59}$$

$$\boldsymbol{\mathcal{N}}^{\mathrm{I}}\left(\mathbf{u}, \mathbf{B}\right) = -\mathbf{u} \otimes \mathbf{B} - \mathbf{B} \otimes \mathbf{u}. \tag{2.60}$$

Remarks:

- The following shorthand notation for the nonlinear terms will be used throughout

$$\boldsymbol{\mathcal{N}}^{\mathrm{V}} = \boldsymbol{\mathcal{N}}^{\mathrm{V}}\left(\mathbf{u}, \mathbf{B}\right) \tag{2.61}$$

$$\boldsymbol{\mathcal{N}}^{\mathrm{I}} = \boldsymbol{\mathcal{N}}^{\mathrm{I}}\left(\mathbf{u}, \mathbf{B}\right). \tag{2.62}$$

- In this work, an artificial magnetic pressure, r, will be included in the induction equation so that the induction equation becomes

$$\frac{\partial \mathbf{B}}{\partial \mathrm{t}} + \nabla \cdot \boldsymbol{\mathcal{N}}^{\mathrm{V}} = -\nabla r + \lambda \nabla^2 \mathbf{B} + \mathbf{f}^{\mathrm{I}}. \tag{2.63}$$

See (Codina and Hernández-Silva 2006) for an introduction to this approach. This pressure is not physical but plays a role in numerical methods. Its purpose is to act as a Lagrange multiplier for the induction equation so the solenoidal constraint on the magnetic induction is satisfied. This is the same role that the fluid pressure plays in the incompressible momentum equation. Boundary conditions will be selected so that the artificial magnetic pressure is zero if the divergence-free constraint on the magnetic induction is satisfied.

- The potential for external momentum and induction forcing functions ($\mathbf{f}^{\mathrm{V}}$ and $\mathbf{f}^{\mathrm{I}}$, respectively) has been included.

2.2.3 MHD Conservation Laws

At this point, it is useful to consider some properties of interest in MHD. Three of these properties are the total energy, cross helicity, and magnetic helicity. In the absence of dissipation and any sources (including those at the boundary)

these three quantities are conserved. In the following derivations, homogeneous, essential boundary conditions are assumed. The starting point is the ideal MHD equations,

$$\frac{\partial \mathbf{u}}{\partial t} + \nabla \cdot \boldsymbol{\mathcal{N}}^{\mathrm{V}} + \nabla P = 0 \tag{2.64}$$

$$\frac{\partial \mathbf{B}}{\partial t} + \nabla \cdot \boldsymbol{\mathcal{N}}^{\mathrm{I}} + \nabla r = 0. \tag{2.65}$$

Before proceeding with the actual derivations a few useful relationships are introduced. For solenoidal vector fields $\mathbf{v}$ and $\mathbf{w}$ with homogeneous essential boundary conditions,

$$\int_{\Omega} \mathbf{v} \cdot (\nabla \cdot (\mathbf{v} \otimes \mathbf{v})) \ \mathrm{d}\Omega = 0 \tag{2.66}$$

and

$$\int_{\Omega} \mathbf{v} \cdot (\nabla \cdot (\mathbf{v} \otimes \mathbf{w})) \ \mathrm{d}\Omega = 0. \tag{2.67}$$

For a scalar field f,

$$\int_{\Omega} \mathbf{v} \cdot \nabla f \ \mathrm{d}\Omega = 0. \tag{2.68}$$

These identities are proved in Appendix E.2.

2.2.4 Conservation of Total MHD Energy

The total energy is defined as

$$K^{\mathrm{T}} = K^{\mathrm{V}} + K^{\mathrm{I}}. \tag{2.69}$$

The kinetic energy per unit mass is

$$K^{\mathrm{V}} = \int_{\Omega} \frac{1}{2} \mathbf{u} \cdot \mathbf{u} \ \mathrm{d}\Omega \tag{2.70}$$

and the magnetic energy is

$$K^{\mathrm{I}} = \frac{1}{\mu_0 \rho} \int_\Omega \frac{1}{2} \mathbf{B} \cdot \mathbf{B} \ \mathrm{d}\Omega. \tag{2.71}$$

Taking the vector dot product of $\mathbf{u}$ with the momentum equation and integrating over the domain results in,

$$\underbrace{\int_\Omega \frac{\partial}{\partial t} \left(\frac{1}{2} \mathbf{u} \cdot \mathbf{u} \right) \ \mathrm{d}\Omega}_{I_1^{\mathrm{V}}} + \underbrace{\int_\Omega \mathbf{u} \cdot (\nabla \cdot (\mathbf{u} \otimes \mathbf{u})) \ \mathrm{d}\Omega}_{I_2^{\mathrm{V}}}$$

$$- \frac{1}{\mu_0 \rho} \underbrace{\int_\Omega \mathbf{u} \cdot (\nabla \cdot (\mathbf{B} \otimes \mathbf{B})) \ \mathrm{d}\Omega}_{I_3^{\mathrm{V}}} + \underbrace{\int_\Omega \mathbf{u} \cdot \nabla p \ \mathrm{d}\Omega}_{I_4^{\mathrm{V}}} = 0. \tag{2.72}$$

The first integral is written as

$$\begin{aligned} I_1^{\mathrm{V}} &= \frac{\mathrm{d}}{\mathrm{dt}} \int_\Omega \frac{1}{2} \mathbf{u} \cdot \mathbf{u} \ \mathrm{d}\Omega \\ &= \frac{\mathrm{d}K^{\mathrm{V}}}{\mathrm{dt}}. \end{aligned} \tag{2.73}$$

The second integral is zero by (2.66). The third integral becomes

$$\begin{aligned} \int_\Omega \mathbf{u} \cdot (\nabla \cdot (\mathbf{B} \otimes \mathbf{B})) \ \mathrm{d}\Omega &= \int_\Gamma \mathbf{u} \cdot (\mathbf{B} \otimes \mathbf{B}) \cdot \mathbf{n} \ \mathrm{d}\Gamma - \int_\Omega \mathbf{B} \cdot (\nabla \cdot (\mathbf{u} \otimes \mathbf{B})) \ \mathrm{d}\Omega \\ &= - \int_\Omega \mathbf{B} \cdot (\nabla \cdot (\mathbf{u} \otimes \mathbf{B})) \ \mathrm{d}\Omega. \end{aligned} \tag{2.74}$$

The fourth integral vanishes by (2.68). Thus,

$$\frac{\mathrm{d}K^{\mathrm{V}}}{\mathrm{dt}} = \frac{1}{\mu_0 \rho} \int_\Omega \mathbf{B} \cdot (\nabla \cdot (\mathbf{u} \otimes \mathbf{B})) \ \mathrm{d}\Omega. \tag{2.75}$$

The magnetic energy equation is obtained by taking the vector dot product of $\mathbf{B}$ with the ideal induction equation multiplied by $1/\left(\mu_0\rho\right)$. This gives

$$\frac{1}{\mu_0\rho}\underbrace{\int_\Omega \frac{\partial}{\partial t}\left(\frac{1}{2}\mathbf{B}\cdot\mathbf{B}\right)\ \mathrm{d}\Omega}_{I_1^{\mathrm{I}}} - \frac{1}{\mu_0\rho}\underbrace{\int_\Omega \mathbf{B}\cdot\left(\nabla\cdot\left(\mathbf{u}\otimes\mathbf{B}\right)\right)\ \mathrm{d}\Omega}_{I_2^{\mathrm{I}}}$$

$$+\frac{1}{\mu_0\rho}\underbrace{\int_\Omega \mathbf{B}\cdot\left(\nabla\cdot\left(\mathbf{B}\otimes\mathbf{u}\right)\right)\ \mathrm{d}\Omega}_{I_3^{\mathrm{I}}} + \frac{1}{\mu_0\rho}\underbrace{\int_\Omega \mathbf{B}\cdot\nabla r\ \mathrm{d}\Omega}_{I_4^{\mathrm{I}}} = 0. \qquad (2.76)$$

The first integral gives the rate of change of magnetic energy,

$$\frac{1}{\mu_0\rho}I_1^{\mathrm{I}} = \frac{\mathrm{d}K^{\mathrm{I}}}{\mathrm{d}t} \qquad (2.77)$$

and the third and fourth integrals vanish by (2.67) and (2.68), respectively. The second integral is not changed. Now, adding the two energy equations together gives

$$\frac{\mathrm{d}K^{\mathrm{V}}}{\mathrm{d}t} + \frac{\mathrm{d}K^{\mathrm{I}}}{\mathrm{d}t} =$$
$$-\frac{1}{\mu_0\rho}\int_\Omega \mathbf{B}\cdot\left(\nabla\cdot\left(\mathbf{u}\otimes\mathbf{B}\right)\right)\ \mathrm{d}\Omega + \frac{1}{\mu_0\rho}\int_\Omega \mathbf{B}\cdot\left(\nabla\cdot\left(\mathbf{u}\otimes\mathbf{B}\right)\right)\ \mathrm{d}\Omega. \qquad (2.78)$$

The right hand side is zero and the final result is conservation of total energy

$$\frac{\mathrm{d}K^{\mathrm{T}}}{\mathrm{d}t} = 0. \qquad (2.79)$$

2.2.5 Conservation of Cross Helicity

The cross helicity is defined as

$$H^C = \int_\Omega \frac{1}{\sqrt{\mu_0\rho}}\mathbf{u}\cdot\mathbf{B}\ \mathrm{d}\Omega. \qquad (2.80)$$

To obtain the conservation law for the cross-helicity the vector dot-product of the magnetic induction with the ideal momentum equation is taken and the vector dot product of the velocity with the ideal induction equation is taken. Performing this

operation on the momentum equation and integrating over the domain yields

$$
\underbrace{\int_\Omega \mathbf{B} \cdot \frac{\partial \mathbf{u}}{\partial t} \; \mathrm{d}\Omega}_{I_1^\mathrm{V}} + \underbrace{\int_\Omega \mathbf{B} \cdot (\nabla \cdot (\mathbf{u} \otimes \mathbf{u})) \; \mathrm{d}\Omega}_{I_2^\mathrm{V}}
$$

$$
- \frac{1}{\mu_0 \rho} \underbrace{\int_\Omega \mathbf{B} \cdot (\nabla \cdot (\mathbf{B} \otimes \mathbf{B})) \; \mathrm{d}\Omega}_{I_3^\mathrm{V}} + \underbrace{\int_\Omega \mathbf{B} \cdot \nabla P \; \mathrm{d}\Omega}_{I_4^\mathrm{V}} = 0. \qquad (2.81)
$$

Integrals I_3^V and I_4^V are zero by (2.66) and (2.68), respectively. Integral I_2^V is rewritten,

$$
\int_\Omega \mathbf{B} \cdot (\nabla \cdot (\mathbf{u} \otimes \mathbf{u})) \; \mathrm{d}\Omega = \int_\Gamma \mathbf{B} \cdot (\mathbf{u} \otimes \mathbf{u}) \cdot \mathbf{n} \; \mathrm{d}\Gamma - \int_\Omega \mathbf{u} \cdot (\nabla \cdot (\mathbf{B} \otimes \mathbf{u})) \; \mathrm{d}\Omega
$$

$$
= - \int_\Omega \mathbf{u} \cdot (\nabla \cdot (\mathbf{B} \otimes \mathbf{u})) \; \mathrm{d}\Omega. \qquad (2.82)
$$

Thus, the momentum equation becomes,

$$
\int_\Omega \mathbf{B} \cdot \frac{\partial \mathbf{u}}{\partial t} \; \mathrm{d}\Omega = \int_\Omega \mathbf{u} \cdot (\nabla \cdot (\mathbf{B} \otimes \mathbf{u})) \; \mathrm{d}\Omega. \qquad (2.83)
$$

Turning now to the induction equation yields

$$
\underbrace{\int_\Omega \mathbf{u} \cdot \frac{\partial \mathbf{B}}{\partial t} \; \mathrm{d}\Omega}_{I_1^\mathrm{I}} - \underbrace{\int_\Omega \mathbf{u} \cdot (\nabla \cdot (\mathbf{u} \otimes \mathbf{B})) \; \mathrm{d}\Omega}_{I_2^\mathrm{I}} \qquad (2.84)
$$

$$
+ \underbrace{\int_\Omega \mathbf{u} \cdot (\nabla \cdot (\mathbf{B} \otimes \mathbf{u})) \; \mathrm{d}\Omega}_{I_3^\mathrm{I}} + \underbrace{\int_\Omega \mathbf{u} \cdot \nabla r \; \mathrm{d}\Omega}_{I_4^\mathrm{I}} = 0. \qquad (2.85)
$$

Integrals I_2^I and I_4^I are zero by (2.67) and (2.68), respectively. The induction equation is therefore

$$
\int_\Omega \mathbf{u} \cdot \frac{\partial \mathbf{B}}{\partial t} \; \mathrm{d}\Omega = - \int_\Omega \mathbf{u} \cdot (\nabla \cdot (\mathbf{B} \otimes \mathbf{u})) \; \mathrm{d}\Omega. \qquad (2.86)
$$

Multiplying the resulting induction equation by $1/(\sqrt{\mu_0\rho})$ and adding the resulting momentum and induction equations results in

$$\int_\Omega \mathbf{B} \cdot \frac{\partial \mathbf{u}}{\partial t}\, \mathrm{d}\Omega + \frac{1}{\sqrt{\mu_0\rho}} \int_\Omega \mathbf{u} \cdot \frac{\partial \mathbf{B}}{\partial t}\, \mathrm{d}\Omega = 0 \tag{2.87}$$

$$\Rightarrow \frac{1}{\sqrt{\mu_0\rho}} \int_\Omega \frac{\partial \left(\mathbf{u} \cdot \mathbf{B}\right)}{\partial t}\, \mathrm{d}\Omega = 0 \tag{2.88}$$

$$\Rightarrow \frac{\mathrm{d}}{\mathrm{dt}} \int_\Omega \frac{1}{\sqrt{\mu_0\rho}} \mathbf{u} \cdot \mathbf{B}\, \mathrm{d}\Omega. \tag{2.89}$$

Therefore,

$$\frac{\mathrm{d}H^C}{\mathrm{dt}} = 0. \tag{2.90}$$

2.2.6 Conservation of Magnetic Helicity

The magnetic helicity is

$$H^{\mathrm{I}} = \int_\Omega \mathbf{A} \cdot \mathbf{B}\, \mathrm{d}\Omega \tag{2.91}$$

where the magnetic vector potential $\mathbf{A}$ is

$$\mathbf{B} = \nabla \times \mathbf{A}. \tag{2.92}$$

To derive this final conservation law, the momentum equation no longer plays a role. The two equations of interest are the magnetic induction equation (in curl form) and the evolution equation for the magnetic vector potential. The reason the curl form of the induction equation is used is that the magnetic vector potential is related to the magnetic induction through the curl operator. The curl form of the ideal magnetic induction equation is

$$\frac{\partial \mathbf{B}}{\partial t} + \nabla \times (\mathbf{u} \times \mathbf{B}) = 0. \tag{2.93}$$

To arrive at the equation for the magnetic vector potential, the curl form of the magnetic induction equation is "uncurled". Thus,

$$\frac{\partial \mathbf{A}}{\partial t} + \mathbf{u} \times \mathbf{B} = \nabla \phi \tag{2.94}$$

where ϕ is a scalar potential. Presently, the scalar potential is just a mathematical artifact as it will not contribute to the conservation law. Next, the vector dot product of (2.94) and $\mathbf{B}$ is taken and the result is integrated over the domain.

$$\underbrace{\int_\Omega \mathbf{B} \cdot \frac{\partial \mathbf{A}}{\partial t} \ d\Omega}_{I_1^A} + \underbrace{\int_\Omega \mathbf{B} \cdot (\mathbf{u} \times \mathbf{B}) \ d\Omega}_{I_2^A} = \underbrace{\int_\Omega \mathbf{B} \cdot \nabla \phi \ d\Omega}_{I_3^A} . \tag{2.95}$$

Integral I_3^A vanishes as a consequence of (2.68). The second integral becomes

$$\begin{aligned}
\int_\Omega \mathbf{B} \cdot (\mathbf{u} \times \mathbf{B}) \ d\Omega &= \int_\Omega (\nabla \times \mathbf{A}) \cdot (\mathbf{u} \times \mathbf{B}) \ d\Omega \\
&= \int_\Gamma (\mathbf{u} \times \mathbf{B}) \cdot (\mathbf{n} \times \mathbf{A}) \ d\Gamma - \int_\Omega \mathbf{A} \cdot \nabla \times (\mathbf{u} \times \mathbf{B}) \ d\Omega \\
&= - \int_\Omega \mathbf{A} \cdot \nabla \times (\mathbf{u} \times \mathbf{B}) \ d\Omega. \tag{2.96}
\end{aligned}$$

Refer to Appendix E.2.1 for more details on the origin of (2.96). Taking the vector dot product of the induction equation and $\mathbf{A}$ gives

$$\int_\Omega \mathbf{A} \cdot \frac{\partial \mathbf{B}}{\partial t} \ d\Omega + \int_\Omega \mathbf{A} \cdot \nabla \times (\mathbf{u} \times \mathbf{B}) \ d\Omega = 0. \tag{2.97}$$

Adding together (2.96) and (2.97) gives

$$\begin{aligned}
&\int_\Omega \mathbf{B} \cdot \frac{\partial \mathbf{A}}{\partial t} \ d\Omega + \int_\Omega \mathbf{A} \cdot \frac{\partial \mathbf{B}}{\partial t} \ d\Omega = 0 \\
&\Rightarrow \int_\Omega \frac{\partial (\mathbf{A} \cdot \mathbf{B})}{\partial t} \ d\Omega = 0 \\
&\Rightarrow \frac{d}{dt} \int_\Omega \mathbf{A} \cdot \mathbf{B} \ d\Omega = 0. \tag{2.98}
\end{aligned}$$

Therefore,

$$\frac{dH^{I}}{dt} = 0. \tag{2.99}$$

The conservation laws are summarized as

$$\frac{dK^{T}}{dt} = 0 \tag{2.100}$$

$$\frac{dH^{C}}{dt} = 0 \tag{2.101}$$

$$\frac{dH^{I}}{dt} = 0. \tag{2.102}$$

2.2.7 Dynamic Alignment

There is a tendency for the velocity and magnetic fields to align in MHD. To demonstrate this, the behavior of the total energy and the cross helicity are considered. In MHD, in the absence of sources, it is typical that the total energy decreases whereas the cross helicity remains approximately constant. This leads to the variational problem: Minimize the functional J where

$$J = K^{T} + \gamma H^{C}. \tag{2.103}$$

The total energy and cross helicity are given by the functionals,

$$K^{T} = \frac{1}{2} \int_{\Omega} \left(\mathbf{u} \cdot \mathbf{u} + \frac{1}{\mu_0 \rho} \mathbf{B} \cdot \mathbf{B} \right) \, d\Omega \tag{2.104}$$

$$H^{C} = \int_{\Omega} \frac{1}{\sqrt{\mu_0 \rho}} \mathbf{u} \cdot \mathbf{B} \, d\Omega. \tag{2.105}$$

To minimize the functional J, we consider the variational derivative,

$$\left. \frac{dJ}{d\epsilon} \right|_{\epsilon=0} = 0. \tag{2.106}$$

To find the minima consider arbitrary small variations about this minima and set the corresponding variations in J to zero.

$$
\begin{aligned}
\left.\frac{\mathrm{d}J}{\mathrm{d}\epsilon}\right|_{\epsilon=0} &= \frac{\mathrm{d}}{\mathrm{d}\epsilon}\left\{\frac{1}{2}\int_\Omega\left[(\mathbf{u}+\epsilon\delta\mathbf{u})\cdot(\mathbf{u}+\epsilon\delta\mathbf{u})+\frac{1}{\mu_0\rho}(\mathbf{B}+\epsilon\delta\mathbf{B})\cdot(\mathbf{B}+\epsilon\delta\mathbf{B})\right]\ \mathrm{d}\Omega\right. \\
&\qquad\left.\left.+\gamma\int_\Omega(\mathbf{u}+\epsilon\delta\mathbf{u})\cdot\frac{1}{\sqrt{\mu_0\rho}}(\mathbf{B}+\epsilon\delta\mathbf{B})\ \mathrm{d}\Omega\right\}\right|_{\epsilon=0} \\
&= \int_\Omega\left(\mathbf{u}\cdot\delta\mathbf{u}+\frac{1}{\mu_0\rho}\mathbf{B}\cdot\delta\mathbf{B}+\gamma\frac{1}{\sqrt{\mu_0\rho}}\mathbf{u}\cdot\delta\mathbf{B}+\gamma\frac{1}{\sqrt{\mu_0\rho}}\mathbf{B}\cdot\delta\mathbf{u}\right)\ \mathrm{d}\Omega = 0
\end{aligned}
$$

$$(2.107)$$

$$
\Rightarrow \int_\Omega\left(\mathbf{u}+\gamma\frac{1}{\sqrt{\mu_0\rho}}\mathbf{B}\right)\cdot\delta\mathbf{u}\ \mathrm{d}\Omega = -\int_\Omega\left(\frac{1}{\mu_0\rho}\mathbf{B}+\gamma\frac{1}{\sqrt{\mu_0\rho}}\mathbf{u}\right)\cdot\delta\mathbf{B}\ \mathrm{d}\Omega.
$$

$$(2.108)$$

Because of the arbitrariness of the variations, the resulting system of equations is

$$\mathbf{u}+\gamma\frac{1}{\sqrt{\mu_0\rho}}\mathbf{B}=0 \tag{2.109}$$

$$\frac{1}{\mu_0\rho}\mathbf{B}+\gamma\frac{1}{\sqrt{\mu_0\rho}}\mathbf{u}=0 \tag{2.110}$$

from which

$$\frac{1}{\mu_0\rho}\left(1-\gamma^2\right)\mathbf{B}=0 \tag{2.111}$$

$$\Rightarrow \gamma = \pm 1. \tag{2.112}$$

The interpretation is therefore that the velocity and magnetic fields align,

$$\mathbf{u}=\pm\frac{1}{\sqrt{\mu_0\rho}}\mathbf{B}. \tag{2.113}$$

This observation is even more remarkable in Alfvén velocity units,

$$\mathbf{u}=\pm\mathbf{B}_A \tag{2.114}$$

2.3 Strong and Weak Formulations

Precise statements of the strong and weak forms of the problem are presented next. The strong form of the problem is: *Given body forces* $\mathbf{f}^V : \mathcal{Q} \to \mathbb{R}^{n_{sd}}$ *and* $\mathbf{f}^I : \mathcal{Q} \to \mathbb{R}^{n_{sd}}$, *find* $\mathbf{u} : \overline{\mathcal{Q}} \to \mathbb{R}^{n_{sd}}$, $\mathbf{B} : \overline{\mathcal{Q}} \to \mathbb{R}^{n_{sd}}$, $r : \overline{\mathcal{Q}} \to \mathbb{R}^{n_{sd}}$, $P : \mathcal{Q} \to \mathbb{R}$ *such that*

$$\frac{\partial \mathbf{u}}{\partial t} + \nabla \cdot \boldsymbol{\mathcal{N}}^V + \nabla P - \nu \nabla^2 \mathbf{u} = \mathbf{f}^V \text{ on } \mathcal{Q} \tag{2.115}$$

$$\nabla \cdot \mathbf{u} = 0 \text{ on } \mathcal{Q} \tag{2.116}$$

$$\frac{\partial \mathbf{B}}{\partial t} + \nabla \cdot \boldsymbol{\mathcal{N}}^I + \nabla r - \lambda \nabla^2 \mathbf{B} = \mathbf{f}^I \text{ on } \mathcal{Q} \tag{2.117}$$

$$\nabla \cdot \mathbf{B} = 0 \text{ on } \mathcal{Q} \tag{2.118}$$

with boundary conditions

$$\mathbf{u} = \mathbf{g}^V \text{ on } \mathcal{P}_g \qquad \mathcal{D}\mathbf{u} = \mathbf{h}^V \text{ on } \mathcal{P}_h \tag{2.119}$$

$$\mathbf{B} = \mathbf{g}^I \text{ on } \mathcal{P}_g \qquad \mathcal{D}\mathbf{B} = \mathbf{h}^I \text{ on } \mathcal{P}_h \tag{2.120}$$

$$\int_\Omega P \, \mathrm{d}\Omega = 0 \tag{2.121}$$

$$r = 0 \text{ on } \mathcal{P}. \tag{2.122}$$

In (2.119) and (2.120) the Neumann boundary conditions involve the differential operator $\mathcal{D}$ which will be specified in Section 2.4 when the particular boundary conditions for the problems consider in this work are presented. The system of partial differential equations (2.115) - (2.118) can be written very concisely as

$$\boldsymbol{\mathcal{L}}\mathbf{U} = \mathbf{F}. \tag{2.123}$$

In (2.123), the goal is to solve for the vector of solutions $\mathbf{U}$. In essence this means inverting the differential operator $\mathcal{L}$. For incompressible MHD we have,

$$\mathbf{U} = \begin{bmatrix} \mathbf{u} \\ p \\ \mathbf{B} \\ r \end{bmatrix}, \qquad \mathbf{F} = \begin{bmatrix} \mathbf{f}^{\mathrm{V}} \\ 0 \\ \mathbf{f}^{\mathrm{I}} \\ 0 \end{bmatrix}. \tag{2.124}$$

Thus, at least formally, the solution is given by

$$\mathbf{U} = \mathcal{L}^{-1}\mathbf{F}. \tag{2.125}$$

Next, the variational form of the incompressible MHD equations is introduced. To this end, it is entirely acceptable algebraically to multiply both sides of the equation by a weighting function $\mathbf{W}$ followed by integrating both sides of the equation over the domain of interest. That is,

$$\int_{\Omega} \mathbf{W} \cdot \mathcal{L}\mathbf{U} \, \mathrm{d}\Omega = \int_{\Omega} \mathbf{W} \cdot \mathbf{F} \, \mathrm{d}\Omega. \tag{2.126}$$

This is the MWR for a vector system of equations where the residual is,

$$\mathcal{R}\left(\mathbf{U}\right) = \mathcal{L}\mathbf{U} - \mathbf{F}. \tag{2.127}$$

Recall from Chapter 1 that the MWR forces the residual of the PDE to be zero in a weighted sense. The choice of weighting functions $\mathbf{W}$ specifies the way that the residual is forced to zero. For instance, one might select $\mathbf{W}$ to be Dirac-delta functions whereby the residual will become zero at specific points. For incompressible MHD the vector of weighting functions is given as

$$\mathbf{W} = \begin{bmatrix} \mathbf{w} \\ q \\ \mathbf{c} \\ s \end{bmatrix} \tag{2.128}$$

where $\mathbf{w}$ is the vector of weighting functions for the momentum equation, q is the weighting function for the velocity field incompressibility constraint, $\mathbf{c}$ is the vector of weighting functions for the induction equation, and s is the weighting function for the solenoidal magnetic field equation.

From an analytical standpoint, this integration is only permissible if the functions are suitably behaved over the problem domain. The concept of functions spaces is now briefly introduced to define "suitably behaved." A function space refers to a collection of functions that have certain traits in common. The basic function spaces considered in this work are

$$H^1 (\Omega) = \left\{ \mathbf{v} \left| \int_\Omega (\mathbf{v} \cdot \mathbf{v} + \nabla \mathbf{v} : \nabla \mathbf{v}) \ \mathrm{d}\Omega < \infty \right. \right\} \tag{2.129}$$

$$H_0^1 (\Omega) = \left\{ \mathbf{v} \left| \int_\Omega (\mathbf{v} \cdot \mathbf{v} + \nabla \mathbf{v} : \nabla \mathbf{v}) \ \mathrm{d}\Omega < \infty \text{ and } \mathbf{v} = \mathbf{0} \text{ on } \Gamma_g \right. \right\} \tag{2.130}$$

$$L_2 (\Omega) = \left\{ \mathbf{v} \left| \int_\Omega (\mathbf{v} \cdot \mathbf{v}) \ \mathrm{d}\Omega < \infty \right. \right\}. \tag{2.131}$$

The particular function spaces used in the present work are built from these basic function spaces. For example, a function space $\boldsymbol{\mathcal{V}}$ is defined as

$$\boldsymbol{\mathcal{V}} = \left\{ \mathbf{v} \left| \mathbf{v} \in H_0^1 (\Omega) \right. \right\}. \tag{2.132}$$

An example of another function space is

$$\boldsymbol{\mathcal{S}} = \left\{ \mathbf{v} \left| \mathbf{v} \in H^1 (\Omega), \quad \mathbf{v} = \mathbf{g} \text{ on } \Gamma_g \right. \right\}. \tag{2.133}$$

Remarks:

The particular definition of the function space depends on the boundary conditions of the problem being considered. The specific definitions of the function spaces will be introduced with the problems that are considered. MHD boundary conditions are introduced in Section 2.4.

With these function spaces, the variational statement becomes: *Find* $\mathbf{U} \in \boldsymbol{\mathcal{S}}$ *such*

that $\forall\ \mathbf{W} \in \boldsymbol{\mathcal{V}}$

$$\int_\Omega \mathbf{W} \cdot \boldsymbol{\mathcal{L}}\mathbf{U}\ \mathrm{d}\Omega = \int_\Omega \mathbf{W} \cdot \mathbf{F}\ \mathrm{d}\Omega. \tag{2.134}$$

For incompressible MHD, the variational formulation is written as: *Find* $\mathbf{U} \in \boldsymbol{\mathcal{S}}$ *such that* $\forall\ \mathbf{W} \in \boldsymbol{\mathcal{V}}$

$$\mathcal{A}_T\left(\mathbf{W},\mathbf{U}\right) = \mathcal{A}_T^{\mathrm{V}}\left(\mathbf{W},\mathbf{U}\right) + \mathcal{A}_T^{\mathrm{I}}\left(\mathbf{W},\mathbf{U}\right) = \left(\mathbf{w},\mathbf{f}^{\mathrm{V}}\right) + \left(\mathbf{c},\mathbf{f}^{\mathrm{I}}\right). \tag{2.135}$$

In (2.135)

$$\begin{aligned}
\mathcal{A}_T^{\mathrm{V}}\left(\mathbf{W},\mathbf{U}\right) = {} & \left(\mathbf{w},\frac{\partial\mathbf{u}}{\partial\mathrm{t}}\right) - \left(\nabla\mathbf{w},\boldsymbol{\mathcal{N}}^{\mathrm{V}}\right) + \left(\mathbf{w},\boldsymbol{\mathcal{N}}^{\mathrm{V}}\cdot\mathbf{n}\right)_\Gamma \\
& - \left(\nabla\cdot\mathbf{w},P\right) + \left(\mathbf{w},P\mathbf{n}\right)_\Gamma + \left(\nabla^{\mathrm{s}}\mathbf{w},2\nu\nabla^{\mathrm{s}}\mathbf{u}\right) \\
& - \left(\nabla^{\mathrm{s}}\mathbf{w},2\nu\nabla^{\mathrm{s}}\mathbf{u}\cdot\mathbf{n}\right)_\Gamma - \left(\nabla q,\mathbf{u}\right) + \left(q,\mathbf{u}\cdot\mathbf{n}\right)_\Gamma
\end{aligned} \tag{2.136}$$

and

$$\begin{aligned}
\mathcal{A}_T^{\mathrm{I}}\left(\mathbf{W},\mathbf{U}\right) = {} & \left(\mathbf{c},\frac{\partial\mathbf{B}}{\partial\mathrm{t}}\right) - \left(\nabla\mathbf{c},\boldsymbol{\mathcal{N}}^{\mathrm{I}}\right) + \left(\mathbf{c},\boldsymbol{\mathcal{N}}^{\mathrm{I}}\cdot\mathbf{n}\right)_\Gamma \\
& - \left(\nabla\cdot\mathbf{c},r\right) + \left(\mathbf{c},r\mathbf{n}\right)_\Gamma + \left(\nabla^{\mathrm{a}}\mathbf{c},2\lambda\nabla^{\mathrm{a}}\mathbf{B}\right) \\
& - \left(\mathbf{c},2\lambda\nabla^{\mathrm{a}}\mathbf{B}\cdot\mathbf{n}\right)_\Gamma - \left(\nabla s,\mathbf{B}\right) + \left(s,\mathbf{B}\cdot\mathbf{n}\right)_\Gamma
\end{aligned} \tag{2.137}$$

where $\mathbf{n}$ is the unit outward normal to the boundary Γ. These forms comprise terms in the domain and on the boundary. They could be decomposed as

$$\mathcal{A}_T^{\mathrm{V,I}}\left(\mathbf{W},\mathbf{U}\right) = \mathcal{A}^{\mathrm{V,I}}\left(\mathbf{W},\mathbf{U}\right) + \mathcal{A}_B^{\mathrm{V,I}}\left(\mathbf{W},\mathbf{U}\right) \tag{2.138}$$

where $\mathcal{A}^{\mathrm{V,I}}\left(\mathbf{W},\mathbf{U}\right)$ contains terms that are in the domain and $\mathcal{A}_B^{\mathrm{V,I}}\left(\mathbf{W},\mathbf{U}\right)$ contains terms that are only on the boundary. This decomposition will be used in Section 2.4 when appropriate boundary conditions are introduced. The symmetric gradient operator (∇^{s}) and antisymmetric gradient operator (∇^{a}) are the result of the incompressibility of the fields and some algebraic manipulations. For an incom-

pressible vector field $\mathbf{v}$ and weighting function $\mathbf{w}$,

$$
\begin{aligned}
\left(\mathbf{w}, \nabla^2 \mathbf{v}\right) &= \left(\mathbf{w}, \nabla \cdot \left(\nabla \mathbf{v} + (\nabla \mathbf{v})^T\right)\right) \quad \longrightarrow \text{Since } \nabla \cdot \left((\nabla \mathbf{u})^T\right) = 0 \\
&= -\left(\nabla \mathbf{w}, \left(\nabla \mathbf{v} + (\nabla \mathbf{v})^T\right)\right) + \left(\mathbf{w}, \left(\nabla \mathbf{v} + (\nabla \mathbf{v})^T\right) \cdot \mathbf{n}\right)_\Gamma \\
&= -2 \left(\nabla \mathbf{w}, \frac{1}{2}\left(\nabla \mathbf{v} + (\nabla \mathbf{v})^T\right)\right) + 2 \left(\mathbf{w}, \frac{1}{2}\left(\nabla \mathbf{v} + (\nabla \mathbf{v})^T\right) \cdot \mathbf{n}\right)_\Gamma \\
&= -2 \left(\nabla^s \mathbf{w}, \nabla^s \mathbf{u}\right) + \left(\mathbf{w}, \nabla^s \mathbf{u} \cdot \mathbf{n}\right)_\Gamma
\end{aligned}
\tag{2.139}
$$

where the final step is the result of the fact that the inner product of a symmetric and antisymmetric tensor is zero. Note also that incompressibility ensures that

$$
\left(\mathbf{w}, \nabla^2 \mathbf{v}\right) = \left(\mathbf{w}, \nabla \cdot \left(\nabla \mathbf{v} - (\nabla \mathbf{v})^T\right)\right)
\tag{2.140}
$$

which is useful in establishing the analogous result for the induction equation.

2.4   Boundary Conditions for Incompressible MHD

This section describes the boundary conditions that are used for the problems that were used to test the new turbulence models. The first boundary conditions described are periodic boundary conditions. The second type of boundary conditions that are described are those that apply to a channel of finite thickness and finite electrical conductivity. In this work, we consider problems that use periodic boundary conditions and problems that have perfectly electrically conducting, no-slip walls.

The weighting functions $\mathbf{W}$ are selected so that they vanish on boundaries that have essential boundary conditions. Because of this, only Neumann boundary terms contribute to the variational statement. The variational statement is therefore: *Find* $\mathbf{U} \in \mathcal{V}$ *such that* $\forall \, \mathbf{W} \in \mathcal{V}$

$$
\mathcal{A}^{\mathrm{V}}\left(\mathbf{W}, \mathbf{U}\right) + \mathcal{A}^{\mathrm{I}}\left(\mathbf{W}, \mathbf{U}\right) = \left(\mathbf{w}, \mathbf{f}^{\mathrm{V}}\right) + \left(\mathbf{c}, \mathbf{f}^{\mathrm{I}}\right) - \mathcal{A}^{\mathrm{V}}_{\Gamma_h}\left(\mathbf{W}, \mathbf{U}\right) - \mathcal{A}^{\mathrm{I}}_{\Gamma_h}\left(\mathbf{W}, \mathbf{U}\right).
\tag{2.141}
$$

Note that $\mathbf{U}$, $\mathbf{W} \in \mathcal{V}$. This is because the space $\mathcal{V}$ is such that the solution $\mathbf{U} = 0$ on boundaries with essential boundary conditions. This implies that $\mathbf{U}$ will be

solved for only within the domain and it's values at the essential boundaries will be reconstructed from given boundary data. A more precise notational convention would have differentiated between $\mathbf{U} \in \mathcal{S}$ and $\mathbf{U} \in \mathcal{V}$. However, this distinction was not deemed necessary as everywhere in this dissertation $\mathbf{U}$ is understood to be the solution on the domain Ω.

We will see that with both sets of boundary conditions (periodic and perfectly electrically conducting walls) the variational statement reduces to: *Find* $\mathbf{U} \in \mathcal{V}$ *such that* $\forall$ $\mathbf{W} \in \mathcal{V}$

$$\mathcal{A}^{\mathrm{V}}\left(\mathbf{W}, \mathbf{U}\right) + \mathcal{A}^{\mathrm{I}}\left(\mathbf{W}, \mathbf{U}\right) = \left(\mathbf{w}, \mathbf{f}^{\mathrm{V}}\right) + \left(\mathbf{c}, \mathbf{f}^{\mathrm{I}}\right). \tag{2.142}$$

2.4.1 Periodic Boundary Conditions

The function spaces with periodic boundary conditions are

$$\mathcal{S} = \mathcal{V} = \left\{ \mathbf{W} \;\middle|\; \mathbf{W} = [\mathbf{w}, \; q, \; \mathbf{c}, \; s]^T \text{ s.t.} \right.$$
$$\mathbf{w}, \; \mathbf{c} \; \in H^1\left(\Omega\right), \; q, \; s \in L_2\left(\Omega\right),$$
$$\left. \mathbf{W}\left(\mathbf{y}, \mathrm{t}\right) = \mathbf{W}\left(\mathbf{x}, \mathrm{t}\right) \right\}. \tag{2.143}$$

The periodic domain is $\Omega = [-\pi, \pi]^3$ and

$$\mathbf{y} = \mathbf{x} + 2\pi\mathbf{e}_j \tag{2.144}$$

where $\mathbf{e}_j$ is the unit vector in the j direction; i.e. it has the value of one in the jth slot and zeros elsewhere. Furthermore, $\mathbf{x}$ is understood to be on one of the three faces of the cube denoted $\Gamma_j\left(-\pi\right)$ where $j = 1, 2, 3$. As an example, consider the face $\Gamma_3\left(-\pi\right)$. On this face, $\mathbf{x} = [x_1, \; x_2, \; -\pi]^T$. Then

$$\begin{bmatrix} y_1 \\ y_2 \\ y_3 \end{bmatrix} = \begin{bmatrix} x_1 \\ x_2 \\ -\pi \end{bmatrix} + 2\pi \begin{bmatrix} 0 \\ 0 \\ 1 \end{bmatrix} = \begin{bmatrix} x_1 \\ x_2 \\ \pi \end{bmatrix}. \tag{2.145}$$

This example is illustrated in Figure 2.2. The boundary terms for these boundary conditions are considered next. The boundary terms for the momentum equation are

$$\left(\mathbf{w}, \boldsymbol{\mathcal{N}}^{\mathrm{V}} \cdot \mathbf{n}\right)_{\Gamma} + (\mathbf{w}, P\mathbf{n})_{\Gamma} - (\mathbf{w}, 2\nu \nabla^{\mathrm{s}} \mathbf{u} \cdot \mathbf{n})_{\Gamma} + (q, \mathbf{u} \cdot \mathbf{n})_{\Gamma}. \tag{2.146}$$

The explicit dependence on each surface of the boundary terms is encapsulated with the expression,

$$\sum_{i=1}^{3} \left[\sum_{j=1}^{2} (-1)^{j} \left(\left(\mathbf{w}, \boldsymbol{\mathcal{N}}^{\mathrm{V}} \cdot \mathbf{e}_i\right)_{\Gamma_i} + (\mathbf{w}, P\mathbf{e}_i)_{\Gamma_i} - (\mathbf{w}, 2\nu \nabla^{\mathrm{s}} \mathbf{u} \cdot \mathbf{e}_i)_{\Gamma_i} + (q, \mathbf{u} \cdot \mathbf{e}_i)_{\Gamma_i} \right) \right].$$

$$\tag{2.147}$$

For algebraic simplicity, the pressure term will be considered,

$$\begin{aligned}
\sum_{i=1}^{3} \sum_{j=1}^{2} (-1)^{j} (\mathbf{w}, P\mathbf{e}_i)_{\Gamma_i} = &- (\mathbf{w}, P\mathbf{e}_1)_{\Gamma_1} + (\mathbf{w}, P\mathbf{e}_1)_{\Gamma_1} \\
&- (\mathbf{w}, P\mathbf{e}_2)_{\Gamma_2} + (\mathbf{w}, P\mathbf{e}_2)_{\Gamma_2} \\
&- (\mathbf{w}, P\mathbf{e}_3)_{\Gamma_3} + (\mathbf{w}, P\mathbf{e}_3)_{\Gamma_3} \\
= &\, 0. \tag{2.148}
\end{aligned}$$
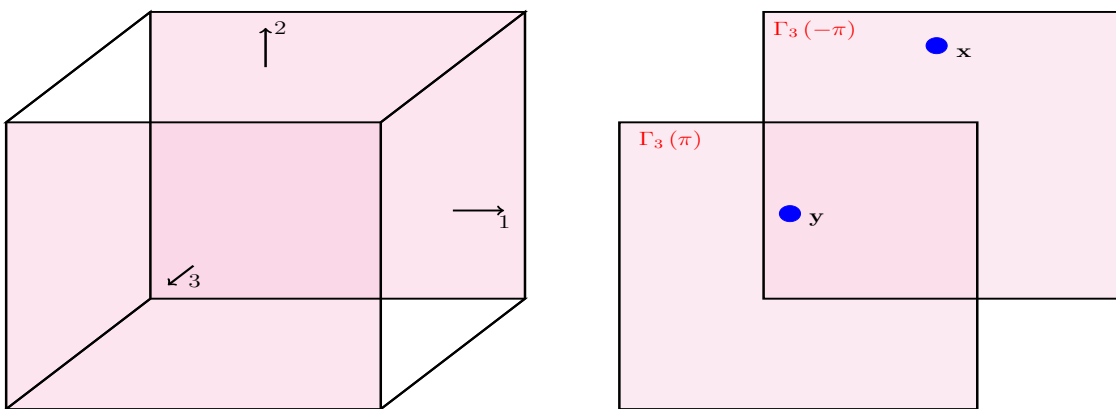
Figure 2.2: Illustration of periodic boundary conditions for a cubic geometry.

Thus, the boundary term for the pressure does not play a role. The other boundary terms are similar including those in the induction equation. Therefore, for this geometry and numerical method, the boundary terms do not contribute.

2.4.2   General Duct Boundary Conditions

The configuration considered in this section is a general wall-bounded domain with finite wall thickness and electrically conducting walls. This domain is referred to as a duct. The configuration is illustrated in Figure 2.3. The turbulence models were tested for a special case of the duct geometry, namely a channel flow with perfectly electrically conducting boundaries. The rest of this section is devoted to a discussion on the general, MHD boundary conditions for the duct.

To begin, the possible boundary conditions for Maxwell's equations are presented. These are (see Jackson 1999)

$$\mathbf{n} \cdot (\mathbf{B}_1 - \mathbf{B}_2) = 0 \tag{2.149}$$

$$\mathbf{n} \times (\mathbf{E}_1 - \mathbf{E}_2) = \mathbf{0} \tag{2.150}$$

where the subscripts refer to the region in which the fields reside. Region 1 represents the domain in which the problem is being solved and Region 2 represents the boundary region. We proceed to derive general MHD boundary conditions at a wall in terms of the magnetic induction. Note that (2.149) is already in terms of the desired field and simply provides a condition for the normal components of the magnetic field at the boundary.
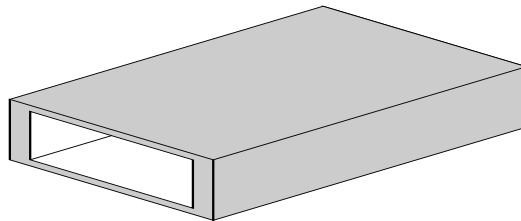
Figure 2.3: Illustration of a geometrical configuration consisting of a flow field bounded by electrically conducting walls, with constant, finite thickness.

We wish to put (2.150) in terms of the magnetic induction. Using Ohm's law

$$\mathbf{E} = \frac{1}{\sigma}\mathbf{j} - \mathbf{u} \times \mathbf{B} \tag{2.151}$$

in (2.150) yields

$$\mathbf{n} \times \left[\frac{1}{\sigma_1}\mathbf{j}_1 - \mathbf{u}_1 \times \mathbf{B}_1\right] = \mathbf{n} \times \left[\frac{1}{\sigma_2}\mathbf{j}_2 - \mathbf{u}_2 \times \mathbf{B}_2\right]. \tag{2.152}$$

The term with the velocity in (2.152) is rewritten as (see Appendix E.3.2),

$$-\mathbf{n} \times (\mathbf{u}_1 \times \mathbf{B}_1) = (-\mathbf{u}_1 \otimes \mathbf{B}_1 + \mathbf{B}_1 \otimes \mathbf{u}_1) \cdot \mathbf{n}.$$

With Ampère's law, the terms with the current density in (2.152) become

$$\mathbf{n} \times \frac{1}{\sigma\mu_0}\nabla \times \mathbf{B}. \tag{2.153}$$

Given two vectors $\mathbf{v}$ and $\mathbf{w}$ (see Appendix E.3.3), we have that

$$\mathbf{v} \times (\nabla \times \mathbf{w}) = -2\left[\nabla\mathbf{w} - (\nabla\mathbf{w})^{\mathrm{T}}\right] \cdot \mathbf{v}.$$

Therefore, the term with the current density is written as:

$$\frac{1}{\sigma_1\mu_1}\left[\nabla\mathbf{B}_1^{\mathrm{b}} - \left(\nabla\mathbf{B}_1^{\mathrm{b}}\right)^{\mathrm{T}}\right] \cdot \mathbf{n}. \tag{2.154}$$

The boundary conditions become

$$\left[-\mathbf{u}_1 \otimes \mathbf{B}_1 + \mathbf{B}_1 \otimes \mathbf{u}_1 + \frac{1}{\mu_1\sigma_1}\left(\nabla\mathbf{B}_1 - (\nabla\mathbf{B}_1)^{\mathrm{T}}\right)\right] \cdot \mathbf{n} =$$
$$\left[-\mathbf{u}_2 \otimes \mathbf{B}_2 + \mathbf{B}_2 \otimes \mathbf{u}_2 + \frac{1}{\mu_2\sigma_2}\left(\nabla\mathbf{B}_2 - (\nabla\mathbf{B}_2)^{\mathrm{T}}\right)\right] \cdot \mathbf{n}$$

which can be written as

$$\boxed{\mathbf{F}_1 \cdot \mathbf{n} = \mathbf{F}_2 \cdot \mathbf{n}.} \tag{2.155}$$

In words (2.155) states that the electromagnetic flux is continuous across the wall of the channel. Mathematically it provides boundary conditions for the tangential components of the magnetic induction. This boundary condition represents Neumann boundary conditions for the tangential components of the magnetic induction.

2.4.3 Channel Flow Boundary Conditions

This section considers the channel flow geometry depicted in Figure 2.4. Periodic boundary conditions are specified in the streamwise and spanwise directions. Homogeneous, essential boundary conditions for the velocity field are specified at the walls. Thus, the term $\mathcal{A}_{\Gamma_h}^{\mathrm{V}}(\mathbf{W}, \mathbf{U})$ in (2.141) does not contribute. We will work on specializing (2.155) to the walls of the channel. The following discussion focuses on two limits of (2.155): perfectly electrically insulating walls and perfectly electrically conducting walls. Note that the outward normals at the top and bottom surfaces are

$$
\mathbf{n}^t = \begin{bmatrix} 0 \\ 1 \\ 0 \end{bmatrix} \quad \text{and} \quad \mathbf{n}^b = \begin{bmatrix} 0 \\ -1 \\ 0 \end{bmatrix} . \tag{2.156}
$$
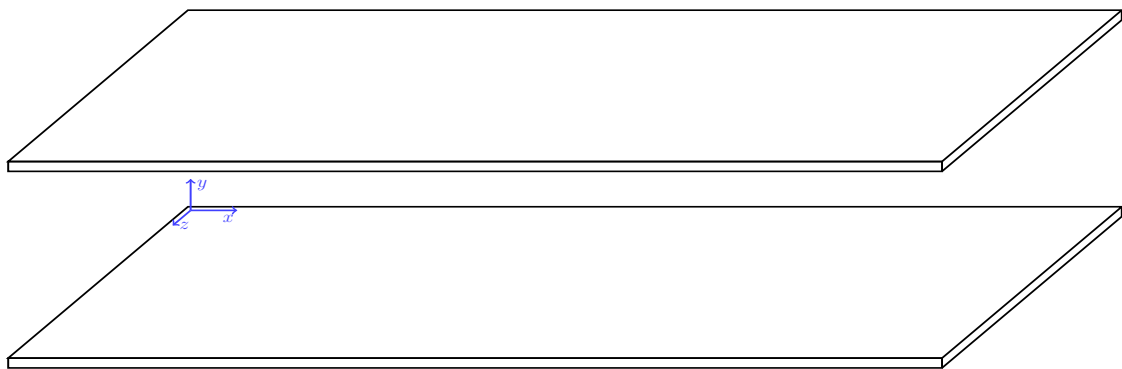
Figure 2.4: The three-dimensional channel geometry.

We refer to quantities inside of the boundary with a superscript (2) and quantities within the fluid with a superscript (1) in the following discussions.

2.4.4 Boundary Conditions: Perfectly Insulating Walls

In this case, the expression (2.155) is not particularly useful because the ratio $\sigma_1/\sigma_2 \to \infty$. We derive boundary conditions for a perfectly insulating wall using some physical intuition and requiring that the tangential components of the magnetic field are continuous at the wall. The bottom surface of the channel is shown in Figure 2.5 below with outward pointing normal $\mathbf{n}$.
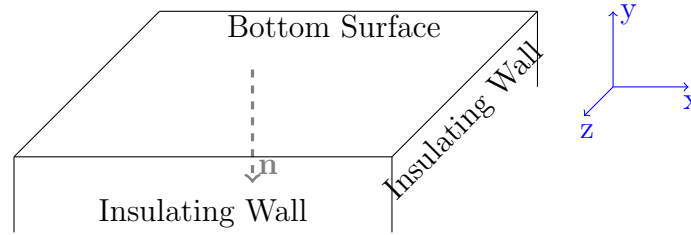
Figure 2.5: Bottom surface of the channel.

There is no current in the insulating wall and so

$$\mathbf{j}^{(2)} = \mathbf{0}. \tag{2.157}$$

Ampére's law states that

$$\nabla \times \mathbf{B} = \mu_0 \mathbf{j}. \tag{2.158}$$

At the insulating boundary then

$$\nabla \times \mathbf{B}^{(2)} = 0 \tag{2.159}$$

$$\Rightarrow \mathbf{B}^{(2)} = -\nabla\psi \tag{2.160}$$

where ψ is a scalar magnetic potential. Of course, we still have the continuity equation for the magnetic field,

$$\nabla \cdot \mathbf{B}^{(2)} = 0. \tag{2.161}$$

Therefore, in the insulating wall we have that

$$\nabla \cdot \mathbf{B}^{(2)} = -\nabla^2 \psi = 0. \tag{2.162}$$

Now, the boundary conditions at the wall interface are

$$\mathbf{B}^{(1)} \cdot \mathbf{n} = \mathbf{B}^{(2)} \cdot \mathbf{n} \tag{2.163}$$

where $\mathbf{n}$ is the outward pointing normal to the wall. Thus we have

$$\mathbf{B}^{(1)} \cdot \mathbf{n} = -\nabla \psi \cdot \mathbf{n} \tag{2.164}$$

at the boundary. At the bottom wall we have $\mathbf{n} = [0, \ -1, \ 0]^{T}$. Thus,

$$\left. \frac{\partial \psi}{\partial y} \right|_{y=y_B} = B_y^{(1)}(x, y_B, z) \tag{2.165}$$

The previous procedure results in a PDE for the magnetic potential at the bottom surface.

$$\nabla^2 \psi = 0, \quad y < y_B \tag{2.166}$$

$$\left. \frac{\partial \psi}{\partial y} \right|_{y=y_B} = B_y^{(1)}(x, y_B, z) \tag{2.167}$$

$$\lim_{y \to -\infty} \psi(x, y, z) < \infty, \quad y < y_B \tag{2.168}$$

There is a corresponding problem for the top surface. The only difference is that for the top surface we have $y > 0$ and $\mathbf{n} = [0, \ 1, \ 0]^{T}$. We will perform the analysis for the bottom surface here. At the end, the solution for the top surface will also be presented but its derivation will not be shown because it is straightforward. Proceeding with the problem for the bottom surface and taking a Fourier transform

in x and z gives

$$\frac{\mathrm{d}}{\mathrm{d}y}\widehat{\psi}\left(k_x, y, k_z\right) - k_p^2\widehat{\psi}\left(k_x, y, k_z\right) = 0, \quad y < y_B \tag{2.169}$$

$$\frac{\mathrm{d}}{\mathrm{d}y}\widehat{\psi}\left(k_x, y_B, k_z\right) = \widehat{B_y^{(1)}}\left(k_x, y_B, k_z\right) \tag{2.170}$$

where

$$k_p^2 = k_x^2 + k_z^2. \tag{2.171}$$

The solution to (2.169) is

$$\widehat{\psi}\left(k_x, y, k_z\right) = c_1 e^{k_p y} + c_2 e^{-k_p y}, \quad y < y_B. \tag{2.172}$$

Applying (2.168) in Fourier space requires $c_2 \to 0$. Thus

$$\widehat{\psi}\left(k_x, y, k_z\right) = c_1 e^{k_p y}, \quad y < y_B. \tag{2.173}$$

Using (2.170) yields

$$c_1 = \frac{1}{k_p}\widehat{B_y^{(1)}}\left(k_x, y_B, k_z\right) e^{-k_p y_B}. \tag{2.174}$$

Therefore the solution in wavenumber space is

$$\widehat{\psi}_B\left(k_x, y, k_z\right) = \frac{1}{k_p}\widehat{B_y^{(1)}}\left(k_x, y_B, k_z\right) e^{k_p(y - y_B)}, \ y \leq y_B \tag{2.175}$$

$$\widehat{\psi}_T\left(k_x, y, k_z\right) = \frac{1}{k_p}\widehat{B_y^{(1)}}\left(k_x, y_T, k_z\right) e^{k_p(y_T - y)}, \ y \geq y_T. \tag{2.176}$$

Of course, we are only interested in the potential at the surfaces. At these surfaces the magnetic potentials are

$$\widehat{\psi}_B\left(k_x, y_B, k_z\right) = \frac{1}{k_p}\widehat{B_y^{(1)}}\left(k_x, y_B, k_z\right) \tag{2.177}$$

$$\widehat{\psi}_T\left(k_x, y_T, k_z\right) = \frac{1}{k_p}\widehat{B_y^{(1)}}\left(k_x, y_T, k_z\right) \tag{2.178}$$

With (2.177) and (2.178) the tangential components of the magnetic field can be determined in the wall. We have

$$\widehat{B_x^{(1)}} = \widehat{B_x^{(2)}} = -\imath \frac{k_x}{k_p} \widehat{B_y^{(1)}} \left(k_x, y_B, k_z\right) \tag{2.179}$$

$$\widehat{B_z^{(1)}} = \widehat{B_z^{(2)}} = -\imath \frac{k_z}{k_p} \widehat{B_y^{(1)}} \left(k_x, y_B, k_z\right). \tag{2.180}$$

We conclude this section with an overview on how these boundary conditions could be implemented.

1. Start with an initial guess for the boundary conditions.

2. Solve the MHD equations at one time step.

3. Update the wall-normal boundary condition for B_y with the value of B_y at the first grid point from the wall. Call this $B_y^{(1)}$.

4. Transform $B_y^{(1)}$ to wavenumber space.

5. Use (2.179) and (2.180) to determine $\widehat{B_x^{(1)}}$ and $\widehat{B_z^{(1)}}$.

6. Transform back into physical space to get $B_x^{(1)}$ and $B_z^{(1)}$.

7. Update the tangential boundary conditions with $B_x^{(1)}$ and $B_z^{(1)}$.

8. Move onto the next time-step and solve the MHD equations. Repeat the same procedure after each time-step.

We note that this implementation of the electrically insulating boundary conditions interprets the boundary conditions for the magnetic field as essential boundary conditions. Thus, the term $\mathcal{A}_{\Gamma_h}^{\mathrm{I}} \left(\mathbf{W}, \mathbf{U}\right)$ in (2.141) does not contribute.

2.4.5 Perfectly Conducting Walls

We begin by considering the boundary condition on the normal components of the magnetic induction. The electric field inside a perfect conductor vanishes, i.e. $\mathbf{E}^{(2)} = 0$. This can be reasoned by recognizing that an electric field is the force field required to move an electric charge. Of course, in a perfect conductor

no force is required to move the charges and so the electric field is zero. The logic that follows in determining the normal components of the magnetic induction is borrowed from (Haus and Melcher 1989). If an unsteady magnetic field exists inside the perfect conductor then, by Faraday's law, we have

$$\nabla \times \mathbf{E}^{(2)} \neq 0. \tag{2.181}$$

But $\mathbf{E}^{(2)} = 0$ inside a perfect conductor. Thus, we cannot have a magnetic field within the perfect conductor and so the boundary condition for the normal component of the magnetic induction becomes

$$\mathbf{B}^{(1)} \cdot \mathbf{n} = 0. \tag{2.182}$$

Next we consider the boundary condition for the tangential components. The assumption of a perfect conductor implies $\sigma_1/\sigma_2 \to 0$. Then (2.155) becomes

$$\left[\nabla \mathbf{B}^{(1)} - \left(\nabla \mathbf{B}^{(1)} \right)^T \right] \cdot \mathbf{n} = 0. \tag{2.183}$$

We note that this represents a homogeneous Neumann boundary condition for the tangential components of the magnetic field. Because of this fact the term $\mathcal{A}^{\mathrm{I}}_{\Gamma_h} (\mathbf{W}, \mathbf{U})$ in (2.141) once again does not contribute.

2.5   Final Variational Statement

We now present the variational statement for the incompressible MHD equations that is used in this work. We note that regardless of the boundary conditions discussed in Section 2.4 the variational form of the problem is the same and only

the functions spaces differ. The variational statement is

> *Find* $\mathbf{U} \in \mathcal{V}$ *such that* $\forall \ \mathbf{W} \in \mathcal{V}$
>
> $$\mathcal{A}^{\mathrm{V}}\left(\mathbf{W}, \mathbf{U}\right) + \mathcal{A}^{\mathrm{I}}\left(\mathbf{W}, \mathbf{U}\right) = \left(\mathbf{w}, \mathbf{f}^{\mathrm{V}}\right) + \left(\mathbf{c}, \mathbf{f}^{\mathrm{I}}\right)$$
>
> *where* $\qquad\qquad\qquad\qquad\qquad\qquad\qquad\qquad\qquad$ (2.184)
>
> $$\mathcal{A}^{\mathrm{V}}\left(\mathbf{W}, \mathbf{U}\right) = \left(\mathbf{w}, \tfrac{\partial \mathbf{u}}{\partial \mathrm{t}}\right) - \left(\nabla\mathbf{w}, \boldsymbol{\mathcal{N}}^{\mathrm{V}}\right) - \left(\nabla \cdot \mathbf{w}, P\right) + \left(\nabla^{\mathrm{s}}\mathbf{w}, 2\nu\nabla^{\mathrm{s}}\mathbf{u}\right)$$
>
> $$\mathcal{A}^{\mathrm{I}}\left(\mathbf{W}, \mathbf{U}\right) = \left(\mathbf{c}, \tfrac{\partial \mathbf{B}}{\partial \mathrm{t}}\right) - \left(\nabla\mathbf{c}, \boldsymbol{\mathcal{N}}^{\mathrm{I}}\right) - \left(\nabla \cdot \mathbf{c}, r\right) + \left(\nabla^{\mathrm{a}}\mathbf{c}, 2\lambda\nabla^{\mathrm{a}}\mathbf{B}\right).$$

2.5.1 Function Spaces for Periodic Boundary Conditions

The function spaces for periodic boundary conditions are,

$$\mathcal{V} = \left\{\mathbf{W} \ \middle| \ \mathbf{W} = [\mathbf{w}, \ q, \ \mathbf{c}, \ s]^{T} \ \text{s.t.}\right.$$
$$\mathbf{w}, \ \mathbf{c} \ \in H^{1}\left(\Omega\right), \ q, \ s \in L_{2}\left(\Omega\right),$$
$$\left.\mathbf{W}\left(\mathbf{y}, \mathrm{t}\right) = \mathbf{W}\left(\mathbf{x}, \mathrm{t}\right)\right\}. \qquad (2.185)$$

The periodic domain is $\Omega = \left[-\pi, \pi\right]^{3}$ and

$$\mathbf{y} = \mathbf{x} + 2\pi\mathbf{e}_{j} \qquad\qquad (2.186)$$

where $\mathbf{e}_{j}$ is the unit vector in the j direction. Furthermore, $\mathbf{x}$ is understood to be on one of the three faces of the cube denoted $\Gamma_{j}\left(-\pi\right)$ where $j = 1, 2, 3$.

2.5.2 Function Spaces for Perfectly Conducting Walls

The relevant notation for the boundaries of a channel is similar to that for the periodic box. Periodic faces are denoted by Γ_{1} and Γ_{3} where Γ_{1} has unit normal $\mathbf{n} = \mathbf{e}_{1}$ and Γ_{3} has unit normal $\mathbf{n} = \mathbf{e}_{3}$. The surface $\Gamma_{1}\left(x_{1}^{0}\right)$ denotes the $y - z$ plane at which the flow enters the channel and the surface $\Gamma_{1}\left(x_{1}^{f}\right)$ is the $y - z$ plane at which the flow leaves the channel. The channel domain is $\Omega = \left[x_{1}^{0}, \ x_{1}^{f}\right] \times \left[x_{2}^{0}, \ x_{2}^{f}\right] \times \left[x_{3}^{0}, \ x_{3}^{f}\right]$. As a final note on notation, we clarify the meaning of the constant $c_{s_{j}}$ in

the definition of the function spaces below. When $j = 1$ this notation refers to a factor of π in the streamwise direction. Likewise, when $j = 3$, the notation refers to a factor in the spanwise direction. When the results are presented in Chapter 5 the specific simulation domain will be introduced. The function spaces are,

$$
\begin{aligned}
\mathcal{V} = \Big\{ \\
& \mathbf{W} \;\Big|\; \mathbf{W} = [\mathbf{w},\ q,\ \mathbf{c},\ s]^T \ \text{s.t.} \\
& \mathbf{w},\ \mathbf{c} \ \in\ H^1\left(\Omega\right),\quad q,\ s,\ \in\ L_2\left(\Omega\right), \\
& \mathbf{w}\left(\Gamma_j\left(x_j^0\right) + c_{\mathrm{s}_j}\pi\mathbf{e}_j, t\right) = \mathbf{w}\left(\Gamma_j\left(x_j^0\right), t\right) = 0, \\
& \mathbf{c}\left(\Gamma_j\left(x_j^0\right) + c_{\mathrm{s}_j}\pi\mathbf{e}_j, t\right) = \mathbf{c}\left(\Gamma_j\left(x_j^0\right), t\right) = 0, \\
& \mathbf{w}\left(\Gamma_2\left(y_2^0\right), t\right) = \mathbf{w}\left(\Gamma_2\left(y_2^f\right), t\right) = 0, \\
& c_2\left(\Gamma_2\left(x_2^0\right), t\right) = c_2\left(\Gamma_2\left(y_2^f\right), t\right) = 0 \\
& \Big\}.
\end{aligned}
\tag{2.187}
$$

From here on, these boundary conditions will be assumed when writing the variational statement and therefore the base variational statement is (2.184).

2.6 Numerical Methods

The jumping off point for all numerical methods is to consider a discretized version of the equations that are to be solved. In the present work, numerical solution fields are designated with a superscript h where h represents the "mesh parameter." The mesh parameter typically denotes the size of an element when working with finite elements or the grid spacing when working with finite differences.

We wish to call attention to a difference in vernacular between the present work and many other LES studies. In most of the literature on LES the following progression occurs:

1. Filter out the high-frequency components of the analytical solution. The fil-

tered field $\overline{u}$ is still defined everywhere on the continuum.

$$u = \overline{u} + u' \tag{2.188}$$

2. Numerically solve for the filtered quantity

$$\overline{u}^h \approx \overline{u} \tag{2.189}$$

3. For notational simplicity, the numerical quantity is denoted by u^h.

In contract to this, the approach that we take proceeds directly from the analytical solution to the numerical solution. Thus, we do not introduce the concept of a filtered, or smoothed, quantity.

The numerical methods considered here are based off of discretizations of the MWR. One particular class of test problems uses trigonometric basis functions to represent the numerical solution while the other uses linear polynomial basis functions to represent the solution. The first class corresponds to Fourier-spectral method while the second class corresponds to the FEM with linear finite elements. Via analogy with the finite element method, the spectral method is conceptually thought of as a FEM that has the entire domain as a single finite element and uses trigonometric basis functions.

The idea of nested, conforming function spaces is now briefly introduced. As motivated in Chapter 1, it is not possible to solve the full variational statement on a computer simply because of a lack of computational resources (i.e. finite processing time and memory). A numerical method introduces the idea of obtaining an approximate solution at a finite number of points in the domain. As a result, the full solution in all of its richness is not available. The functions that are available are a subset of all functions in a given function space. This subset is denoted $\boldsymbol{\mathcal{V}}^h$. A conforming subspace has the property,

$$\boldsymbol{\mathcal{V}}^h \subset \boldsymbol{\mathcal{V}}. \tag{2.190}$$

At this point, we also introduce the infinite-dimensional complementary space $\boldsymbol{\mathcal{V}}'$. This space completes $\boldsymbol{\mathcal{V}}^h$,

$$\boldsymbol{\mathcal{V}} = \boldsymbol{\mathcal{V}}^h \oplus \boldsymbol{\mathcal{V}}'. \tag{2.191}$$

The discretized version of the variational formulation for incompressible MHD is: *Find* $\mathbf{U}^h \in \boldsymbol{\mathcal{V}}^h \subset \boldsymbol{\mathcal{V}}$ *such that* $\forall \ \mathbf{W}^h \in \boldsymbol{\mathcal{V}}^h \subset \boldsymbol{\mathcal{V}}$

$$\mathcal{A}\left(\mathbf{W}^h, \mathbf{U}^h\right) = \mathcal{A}^{\mathrm{V}}\left(\mathbf{W}^h, \mathbf{U}^h\right) + \mathcal{A}^{\mathrm{I}}\left(\mathbf{W}^h, \mathbf{U}^h\right) = \left(\mathbf{w}^h, \mathbf{f}^{\mathrm{V}}\right) + \left(\mathbf{c}^h, \mathbf{f}^{\mathrm{I}}\right). \tag{2.192}$$

In (2.192)

$$\begin{aligned}
\mathcal{A}^{\mathrm{V}}\left(\mathbf{W}^h, \mathbf{U}^h\right) = {} & \left(\mathbf{w}^h, \frac{\partial \mathbf{u}^h}{\partial \mathrm{t}}\right) - \left(\nabla \mathbf{w}^h, \boldsymbol{\mathcal{N}}^{\mathrm{V}}\left(\mathbf{u}^h, \mathbf{B}^h\right)\right) \\
& - \left(\nabla \cdot \mathbf{w}^h, P^h\right) + \left(\nabla^{\mathrm{s}} \mathbf{w}^h, 2\nu \nabla^{\mathrm{s}} \mathbf{u}^h\right) \\
& - \left(\nabla q^h, \mathbf{u}^h\right)
\end{aligned} \tag{2.193}$$

and

$$\begin{aligned}
\mathcal{A}^{\mathrm{I}}\left(\mathbf{W}^h, \mathbf{U}^h\right) = {} & \left(\mathbf{c}^h, \frac{\partial \mathbf{B}^h}{\partial \mathrm{t}}\right) - \left(\nabla \mathbf{c}^h, \boldsymbol{\mathcal{N}}^{\mathrm{I}}\left(\mathbf{u}^h, \mathbf{B}^h\right)\right) \\
& - \left(\nabla \cdot \mathbf{c}^h, r^h\right) + \left(\nabla^{\mathrm{a}} \mathbf{c}^h, 2\lambda \nabla^{\mathrm{a}} \mathbf{B}^h\right) \\
& - \left(\nabla s^h, \mathbf{B}^h\right).
\end{aligned} \tag{2.194}$$

<u>Remarks:</u>

In subsequent sections we use the following simplified notation for the discretized nonlinear terms:

$$\boldsymbol{\mathcal{N}}_h^{\mathrm{V}} = \boldsymbol{\mathcal{N}}^{\mathrm{V}}\left(\mathbf{u}^h, \mathbf{B}^h\right) \tag{2.195}$$

$$\boldsymbol{\mathcal{N}}_h^{\mathrm{I}} = \boldsymbol{\mathcal{N}}^{\mathrm{I}}\left(\mathbf{u}^h, \mathbf{B}^h\right). \tag{2.196}$$

2.6.1 Fourier-Spectral Method

The particular basis functions selected here are trigonometric basis functions and lead to the so-called Fourier-spectral methods. See (Gottlieb and Orszag 1987) for details on this approach for hydrodynamics. Our numerical implementation follows the ideas developed therein. We have,

$$\mathbf{W}^h = \sum_{\mathbf{q}} \widehat{\mathbf{W}}\left(\mathbf{q}\right) e^{-\imath \mathbf{q}\cdot\mathbf{x}} \tag{2.197}$$

and

$$\mathbf{U}^h = \sum_{\mathbf{k}} \widehat{\mathbf{U}}\left(\mathbf{k}\right) e^{\imath \mathbf{k}\cdot\mathbf{x}} \tag{2.198}$$

where $\imath = \sqrt{-1}$.

<u>Remarks</u>:

- $\mathbf{q}$ and $\mathbf{k}$ are called the wavevectors of the solution. We also use the term wavenumber although strictly speaking the wavenumber is the magnitude of the wavevector.

- $\widehat{\mathbf{W}}$ and $\widehat{\mathbf{U}}$ are the Fourier coefficients.

- The basis functions for the weighting functions are the complex conjugate of the basis functions for the solution.

- The following simplified notation is adopted for a vector field $\widehat{\mathbf{v}}\left(\mathbf{k}\right)$ in wavenumber space,

$$\widehat{\mathbf{v}}\left(\mathbf{k}\right) = \widehat{\mathbf{v}}_{\mathbf{k}}. \tag{2.199}$$

- The wavenumbers have the units of $[L^{-1}]$

Next, the selected trigonometric basis functions are substituted into the variational form for the incompressible MHD equations (2.192)-(2.194). Indeed, the

resulting system of equations are the incompressible MHD equations in wavenumber space. Thus, this choice of basis functions amounts to taking a Fourier transform of the MHD equations. Numerical techniques applied to this system of equations are referred to as Fourier-spectral methods. The detailed derivation of the resulting ODEs is presented in Appendix F. The resulting system is

$$\frac{\mathrm{d}\widehat{\mathbf{u}}_{\mathbf{k}}}{\mathrm{dt}} + \imath\widehat{\boldsymbol{\mathcal{N}}^{\mathrm{V}}} \cdot \mathbf{k} + \imath\mathbf{k}\widehat{P}_{\mathbf{k}} + |\mathbf{k}|^2\widehat{\mathbf{u}}_{\mathbf{k}} = \widehat{\mathbf{f}^{\mathrm{V}}}_{\mathbf{k}} \tag{2.200}$$

$$\imath\mathbf{k} \cdot \widehat{\mathbf{u}}_{\mathbf{k}} = 0 \tag{2.201}$$

$$\frac{\mathrm{d}\widehat{\mathbf{B}}_{\mathbf{k}}}{\mathrm{dt}} + \imath\widehat{\boldsymbol{\mathcal{N}}^{\mathrm{I}}} \cdot \mathbf{k} + \imath\mathbf{k}\widehat{r}_{\mathbf{k}} + |\mathbf{k}|^2\widehat{\mathbf{B}}_{\mathbf{k}} = \widehat{\mathbf{f}^{\mathrm{I}}}_{\mathbf{k}} \tag{2.202}$$

$$\imath\mathbf{k} \cdot \widehat{\mathbf{B}}_{\mathbf{k}} = 0. \tag{2.203}$$

In (2.200) and (2.202) the nonlinear terms are

$$\widehat{\boldsymbol{\mathcal{N}}^{\mathrm{V}}} = \sum_{\mathbf{l}} \left(\widehat{\mathbf{u}}\,(\mathbf{l}) \otimes \widehat{\mathbf{u}}\,(\mathbf{k} - \mathbf{l}) - \widehat{\mathbf{B}}\,(\mathbf{l}) \otimes \widehat{\mathbf{B}}\,(\mathbf{k} - \mathbf{l}) \right) \tag{2.204}$$

and

$$\widehat{\boldsymbol{\mathcal{N}}^{\mathrm{I}}} = \sum_{\mathbf{l}} \left(-\widehat{\mathbf{u}}\,(\mathbf{l}) \otimes \widehat{\mathbf{B}}\,(\mathbf{k} - \mathbf{l}) + \widehat{\mathbf{B}}\,(\mathbf{l}) \otimes \widehat{\mathbf{u}}\,(\mathbf{k} - \mathbf{l}) \right). \tag{2.205}$$

Remarks:

- Notationally, the nonlinear terms are understood to be evaluated at wavenumber $\mathbf{k}$. Thus

$$\widehat{\boldsymbol{\mathcal{N}}^{\mathrm{V}}} = \widehat{\boldsymbol{\mathcal{N}}^{\mathrm{V}}_{\mathbf{k}}} \tag{2.206}$$

$$\widehat{\boldsymbol{\mathcal{N}}^{\mathrm{I}}} = \widehat{\boldsymbol{\mathcal{N}}^{\mathrm{I}}_{\mathbf{k}}} \tag{2.207}$$

$$\widehat{\boldsymbol{\mathcal{N}}} = \widehat{\boldsymbol{\mathcal{N}}_{\mathbf{k}}}. \tag{2.208}$$

  This notational dependency is implied in all subsequent chapters involving the equations in wavenumber space.

- In practical numerical applications, the nonlinear terms are not actually com-

puted directly in wavenumber space as suggested by (2.204) and (2.205).

- The nonlinear terms are computed as follows (see Gottlieb and Orszag 1987, sec. 10),

    1. Take an inverse FFT of the solutions

    2. Compute the nonlinear terms in physical space by performing the appropriate multiplications

    3. Take an FFT of the nonlinear terms to transfer them back into wavenumber space

- Because not all of the computations are carried out in wavenumber space, this method is not a true spectral method and is therefore referred to as a pseudospectral method.

The momentum and induction equation can be written in the same form using a dummy pressure $\widehat{\mathfrak{P}}_{\mathbf{k}}$, diffusion coefficient $\mathfrak{d}$, and vector field $\widehat{\mathbf{v}}_{\mathbf{k}}$,

$$\widehat{\mathcal{L}}\widehat{\mathbf{v}}_{\mathbf{k}} + i\widehat{\mathcal{N}} \cdot \mathbf{k} + i\mathbf{k}\widehat{\mathfrak{P}}_{\mathbf{k}} = \widehat{\mathfrak{f}}_{\mathbf{k}} \tag{2.209}$$

where

$$\widehat{\mathcal{L}} = \frac{\mathrm{d}}{\mathrm{dt}} + \mathfrak{d}|\mathbf{k}|^2. \tag{2.210}$$

Taking the divergence of (2.209), which amounts to multiplying by $i\mathbf{k}$, permits an explicit formula for the pressure,

$$\widehat{\mathfrak{P}}_{\mathbf{k}} = -\frac{1}{|\mathbf{k}|^2} \left(\mathbf{k} \otimes \mathbf{k} : \widehat{\mathcal{N}} + i\mathbf{k} \cdot \widehat{\mathfrak{f}}_{\mathbf{k}} \right). \tag{2.211}$$

Using (2.211) in (2.209) yields,

$$\mathcal{L}\widehat{\mathbf{v}}_{\mathbf{k}} = -\mathcal{P}\widehat{\mathcal{N}} + \mathcal{Q}\widehat{\mathfrak{f}}_{\mathbf{k}} \tag{2.212}$$

where

$$\boldsymbol{\mathcal{P}} = \imath \left(\boldsymbol{\delta} - \frac{\mathbf{k} \otimes \mathbf{k}}{|\mathbf{k}^2|} \right) \otimes \mathbf{k} \tag{2.213}$$

$$\boldsymbol{\mathcal{Q}} = \boldsymbol{\delta} - \frac{\mathbf{k} \otimes \mathbf{k}}{|\mathbf{k}|^2}. \tag{2.214}$$

Remarks:

In index notation the projection operators corresponding to equation j are given as

$$\mathcal{P}_{jlm} = \imath \left(\delta_{jl} - \frac{k_j k_l}{|\mathbf{k}|^2} \right) k_m$$

and

$$\mathcal{Q}_{jl} = \delta_{jl} - \frac{k_j k_l}{|\mathbf{k}|^2}.$$

It can be shown, however, that in the absence of the external body force, the artificial magnetic pressure $\widehat{r}_{\mathbf{k}}$ is identically zero in wavenumber space. This is readily demonstrated using index notation.

$$\begin{aligned}
\widehat{r}_{\mathbf{k}} &= -\frac{1}{|\mathbf{k}|^2} k_i k_j \widehat{\mathcal{N}^{\mathrm{I}}}_{ij} \\
&= -\frac{1}{|\mathbf{k}|^2} k_i k_j \left(-\widehat{u_i B_j} + \widehat{B_i u_j} \right) \\
&= -\frac{1}{|\mathbf{k}|^2} \left(-k_i k_j \widehat{u_i B_j} + k_i k_j \widehat{B_i u_j} \right) \\
&= -\frac{1}{|\mathbf{k}|^2} \left(-k_i k_j \widehat{u_i B_j} + k_j k_i \widehat{B_j u_i} \right) \\
&= 0.
\end{aligned}$$

Hence,

$$\boldsymbol{\mathcal{P}}\widehat{\boldsymbol{\mathcal{N}}^{\mathrm{I}}} = \widehat{\boldsymbol{\mathcal{N}}^{\mathrm{I}}} \cdot \mathbf{k}. \tag{2.215}$$

The final set of equations is

$$
\boxed{
\begin{aligned}
\frac{\partial \widehat{\mathbf{u}}_{\mathbf{k}}(t)}{\partial t} + \nu |\mathbf{k}|^2 \widehat{\mathbf{u}}_{\mathbf{k}} &= \mathcal{Q}\widehat{\mathbf{f}^{\mathrm{V}}}_{\mathbf{k}} - \mathcal{P}\widehat{\mathcal{N}^{\mathrm{V}}} \\
\frac{\partial \widehat{\mathbf{B}}_{\mathbf{k}}(t)}{\partial t} + \lambda |\mathbf{k}|^2 \widehat{\mathbf{B}}_{\mathbf{k}} &= \mathcal{Q}\widehat{\mathbf{f}^{\mathrm{I}}}_{\mathbf{k}} - \widehat{\mathcal{N}^{\mathrm{I}}} \cdot \mathbf{k}
\end{aligned}
}
\tag{2.216}
$$

The classic fourth order Runge-Kutta (RK4) numerical integration scheme is used to update the solution at each time step. For equations of the form

$$
\frac{\mathrm{d}\widehat{\mathbf{U}}_{\mathbf{k}}}{\mathrm{d}t} = \mathbf{f}\left(\widehat{\mathbf{U}}_{\mathbf{k}}, t\right)
\tag{2.217}
$$

the Runge-Kutta scheme is given by (see (Zwillinger 2003) for a reference)

$$
\widehat{\mathbf{U}}^{n+1} = \widehat{\mathbf{U}}^n + \frac{\Delta t}{6}\left[\mathbf{K}_1 + 2\mathbf{K}_2 + 2\mathbf{K}_3 + \mathbf{K}_4\right]
\tag{2.218}
$$

where Δt is the time-step size and n is the value of the field at the current time step. In Equation (2.218),

$$
\mathbf{K}_1 = \mathbf{f}\left(\widehat{\mathbf{U}}^n, t^n\right)
\tag{2.219}
$$

$$
\mathbf{K}_2 = \mathbf{f}\left(\widehat{\mathbf{U}}^n + \frac{\Delta t}{2}\mathbf{K}_1, t^n + \frac{\Delta t}{2}\right)
\tag{2.220}
$$

$$
\mathbf{K}_3 = \mathbf{f}\left(\widehat{\mathbf{U}}^n + \frac{\Delta t}{2}\mathbf{K}_2, t^n + \frac{\Delta t}{2}\right)
\tag{2.221}
$$

$$
\mathbf{K}_4 = \mathbf{f}\left(\widehat{\mathbf{U}}^n + \Delta t\mathbf{K}_3, t^{n+1}\right).
\tag{2.222}
$$

It is possible to get (2.212) into the same form as (2.217) by multiplying (2.212) by $e^{\partial |\mathbf{k}|^2 t}$ and introducing a new variable

$$
\widehat{\mathbf{y}}_{\mathbf{k}} = \widehat{\mathbf{v}}_{\mathbf{k}} e^{\partial |\mathbf{k}|^2 t}.
\tag{2.223}
$$

Thus

$$
\frac{\mathrm{d}\widehat{\mathbf{y}}_{\mathbf{k}}}{\mathrm{d}t} = \left(\mathcal{Q}\widehat{\mathbf{f}}_{\mathbf{k}} - \mathcal{P}\widehat{\mathcal{N}}\right) e^{\partial |\mathbf{k}|^2 t}.
\tag{2.224}
$$

Therefore,

$$\widehat{\mathbf{v}}_{\mathbf{k}}^{n+1} = \widehat{\mathbf{v}}_{\mathbf{k}}^{n} e^{-\eth |\mathbf{k}|^2 \Delta t} + \frac{\Delta t}{6} \left[\mathbf{K}_1 e^{-\eth |\mathbf{k}|^2 \Delta t} + 2\mathbf{K}_2 e^{-\eth |\mathbf{k}|^2 \frac{\Delta t}{2}} + 2\mathbf{K}_3 e^{-\eth |\mathbf{k}|^2 \frac{\Delta t}{2}} + \mathbf{K}_4 \right]$$

$$(2.225)$$

where $\mathbf{K}_i$, $i = 1, 4$ have already been defined in (2.219)- (2.222).

2.6.2 Finite Element Method

The element point of view (rather than the global point of view) is taken in detailing the finite element approach to incompressible MHD. The details of this approach are presented in (Hughes 2000). Working from the element point of view rather than a global point of view is especially convenient for practical implementations of a finite element code. The solutions are expanded over an element domain with n_{np} nodal points as

$$\mathbf{u}^h = \sum_{a=1}^{n_{\mathrm{np}}} N_a \mathbf{u}_a^e, \qquad P^h = \sum_{a=1}^{n_{\mathrm{np}}} N_a P_a^e \qquad (2.226)$$

$$\mathbf{B}^h = \sum_{a=1}^{n_{\mathrm{np}}} N_a \mathbf{B}_a^e, \qquad r^h = \sum_{a=1}^{n_{\mathrm{np}}} N_a r_a^e \qquad (2.227)$$

and the weighting functions are expanded as

$$\mathbf{w}^h = \sum_{b=1}^{n_{\mathrm{np}}} N_b \mathbf{w}_b^e, \qquad q^h = \sum_{b=1}^{n_{\mathrm{np}}} N_b P_b^e \qquad (2.228)$$

$$\mathbf{c}^h = \sum_{b=1}^{n_{\mathrm{np}}} N_b \mathbf{B}_b^e, \qquad s^h = \sum_{b=1}^{n_{\mathrm{np}}} N_b s_b^e \qquad (2.229)$$

where the shape functions are denoted by $N_a = N_a(\xi, \eta, \zeta)$. The superscript e on the nodal values implies that the respective quantities belong to element e. The coordinates of the element in the physical domain, (x, y, z), are related to the coordinates

of the element in the parent domain, (ξ, η, ζ), via the isoparametric mapping,

$$x\left(\xi, \eta, \zeta\right) = \sum_{i=1}^{n_{\mathrm{np}}} N_a\left(\xi, \eta, \zeta\right) x_a^e \qquad (2.230)$$

$$y\left(\xi, \eta, \zeta\right) = \sum_{i=1}^{n_{\mathrm{np}}} N_a\left(\xi, \eta, \zeta\right) y_a^e \qquad (2.231)$$

$$z\left(\xi, \eta, \zeta\right) = \sum_{i=1}^{n_{\mathrm{np}}} N_a\left(\xi, \eta, \zeta\right) z_a^e. \qquad (2.232)$$

The present work uses trilinear, hexahedral finite elements. An example of such an element along with its node numbering and coordinates is given in Figure 2.6. The shape functions for these elements are

$$N_a = \frac{1}{8}\left(1 + \xi_a\xi\right)\left(1 + \eta_a\eta\right)\left(1 + \zeta_a\zeta\right) \qquad (2.233)$$

where ξ_a, η_a, and ζ_a are the values of the coordinates at element node "a".

Remarks:

The shape functions are piecewise continuous across element boundaries. Therefore the solution is globally C^0 continuous. The variational statement is linearized before substituting the expressions for the solutions and the weighting functions. It is then integrated in time to arrive at a system of algebraic equations that need to be solved at each time step. Once the linearization is complete, and the basis functions are substituted into the linearized variational statement, a matrix system for each element is obtained,

$$\mathbf{A}^e\mathbf{d}^e = \mathbf{f}^e. \qquad (2.234)$$

In order to obtain the global solution, the element matrices and degrees of freedom must be assembled into a global matrix, $\mathbf{A}$ and global degree of freedom vector $\mathbf{d}$. This is done with the finite element assembly operator as detailed in (Hughes 2000). Once the global system is formed one must solve the linear matrix problem

$$\mathbf{A}\mathbf{d} = \mathbf{f}. \qquad (2.235)$$
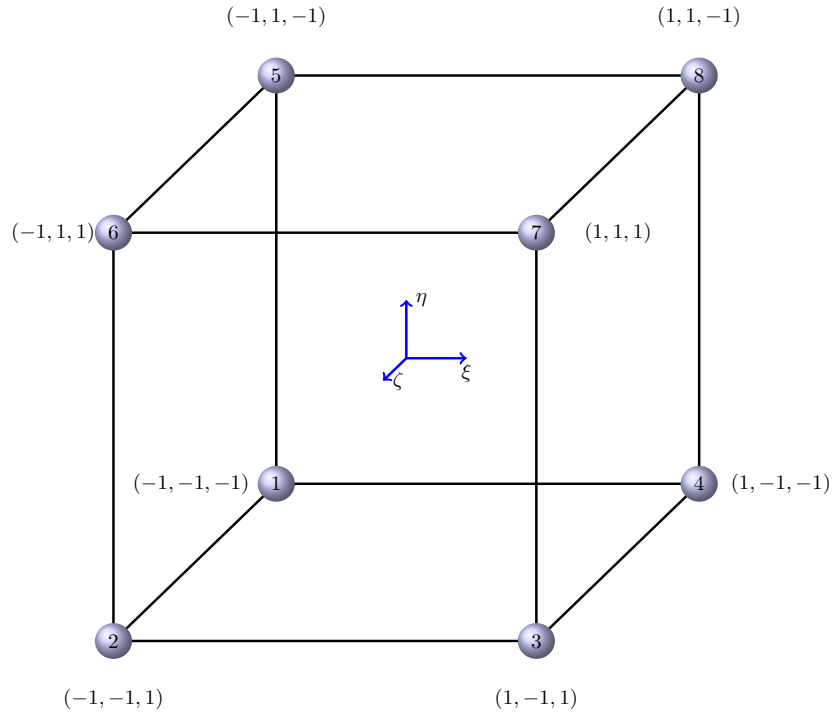
Figure 2.6: A trilinear, hexahedral element.

Note that an iterative technique is used to converge to the solution of the non-linear problem. Typically either Newton's method or a variant thereof is employed. A matrix system must be solved at each nonlinear iteration regardless of the non-linear solution technique that is used. A very popular iterative linear solver is the generalized minimum residual (GMRES) solver. For details on this approach refer to (Trefethen and Bau III 1997). Finally, we note that the time-integration scheme used for the finite element simulations is a 3rd order backward difference formula (BDF) method. The finite element code that was used to perform the simulations in this work was developed at Sandia National Labs and is called Drekar. For details on the numerical method and Drekar refer to (J. Shadid et al. 2010; J. N. Shadid et al. 2010; Cyr, Shadid, and Tuminaro 2012; Pawlowski, Phipps, and Salinger 2012; Pawlowski et al. 2012).

2.7 Turbulence Modeling: Large Eddy Simulation

This section initiates the discussion on LES. The first part reviews classical LES techniques such as the filtering operation. This part works with the strong formulation. The second part provides an overview of the VMS formulation and its role in turbulence modeling and LES.

2.7.1 Classical Approach

The classical approach to large eddy simulation requires the introduction of a filtering operator denoted by $\mathbb{F}$. The filtered velocity and magnetic induction are written as

$$\mathbb{F}\mathbf{u}\left(\mathbf{x}, t\right) = \int G\left(\mathbf{r}, \mathbf{x}\right) \mathbf{u}\left(\mathbf{x} - \mathbf{r}, t\right) \ d\mathbf{r} \tag{2.236}$$

$$\mathbb{F}\mathbf{B}\left(\mathbf{x}, t\right) = \int G\left(\mathbf{r}, \mathbf{x}\right) \mathbf{B}\left(\mathbf{x} - \mathbf{r}, t\right) \ d\mathbf{r} \tag{2.237}$$

where $G\left(\mathbf{r}, \mathbf{x}\right)$ is a filtering kernel. For more background on the design of an appropriate filter, the reader is referred to (Pope 2000). The goal is now to solve for the filtered fields rather than the exact field in order to make numerical simulations possible.

Remarks:

- The filtered fields still have values at all points in space. That is, they are not discrete. The filtering operation removes the high frequencies from the solution thereby making numerical computations more feasible.

- In the following description, the filtered field will be written as

$$\bar{\mathbf{u}} = \mathbb{F}\mathbf{u}\left(\mathbf{x}, t\right) \tag{2.238}$$

$$\overline{\mathbf{B}} = \mathbb{F}\mathbf{B}\left(\mathbf{x}, t\right). \tag{2.239}$$

Next, the filter is applied to the incompressible MHD equations. For specific details, refer to Appendix B. The application of the filter to the momentum equation yields

$$\frac{\partial \overline{\mathbf{u}}}{\partial t} + \nabla \cdot \left(\boldsymbol{\mathcal{N}}_F^{\mathrm{V}} + \boldsymbol{\mathcal{T}}^{\mathrm{V}} \right) = -\nabla \overline{P} + \nu \nabla^2 \overline{\mathbf{u}} + \overline{\mathbf{f}^{\mathrm{V}}} \tag{2.240}$$

where the nonlinear term of the filtered fields is

$$\boldsymbol{\mathcal{N}}_F^{\mathrm{V}} = \overline{\mathbf{u}} \otimes \overline{\mathbf{u}} - \frac{1}{\mu_0 \rho} \overline{\mathbf{B}} \otimes \overline{\mathbf{B}} \tag{2.241}$$

and the subgrid stress tensor for the momentum equation is

$$\boldsymbol{\mathcal{T}}^{\mathrm{V}} = \overline{(\mathbf{u} \otimes \mathbf{u})} - \frac{1}{\mu_0 \rho} \overline{(\mathbf{B} \otimes \mathbf{B})} - \left(\overline{\mathbf{u}} \otimes \overline{\mathbf{u}} - \frac{1}{\mu_0 \rho} \overline{\mathbf{B}} \otimes \overline{\mathbf{B}} \right). \tag{2.242}$$

Remarks:
- The filter is assumed to commute with spatial and temporal differentiation.

It is this term, $\boldsymbol{\mathcal{T}}^{\mathrm{V}}$, that turbulence modeling efforts have focused on for decades. To see where the term "subgrid stress tensor" originates, it is instructive to write the equations as

$$\frac{\partial \overline{\mathbf{u}}}{\partial t} + \nabla \cdot \boldsymbol{\mathcal{N}}_F^{\mathrm{V}} = \nabla \overline{P} + \nabla \cdot \left(\nu \nabla^{\mathrm{s}} \overline{\mathbf{u}} - \boldsymbol{\mathcal{T}}^{\mathrm{V}} \right) + \overline{\mathbf{f}^{\mathrm{V}}}. \tag{2.243}$$

Therefore, it becomes apparent that the new term is subjected to the divergence operator in the same way that the viscous stress tensor is. In Chapter 4 this observation will be used to motivate decades of work on modeling the effects of the subgrid stress tensor. Similarly, the filtered magnetic induction equation is,

$$\frac{\partial \overline{\mathbf{B}}}{\partial t} + \nabla \cdot \left(\boldsymbol{\mathcal{N}}_F^{\mathrm{I}} + \boldsymbol{\mathcal{T}}^{\mathrm{I}} \right) = -\nabla \overline{r} + \lambda \nabla^2 \overline{\mathbf{B}} + \overline{\mathbf{f}^{\mathrm{I}}} \tag{2.244}$$

where the filtered nonlinear term is

$$\boldsymbol{\mathcal{N}}_F^{\mathrm{I}} = -\overline{\mathbf{u}} \otimes \overline{\mathbf{B}} + \overline{\mathbf{B}} \otimes \overline{\mathbf{u}} \tag{2.245}$$

and the subgrid stress tensor for the induction equation is

$$\boldsymbol{\mathcal{T}}^{\mathrm{I}} = -\overline{(\mathbf{u} \otimes \mathbf{B})} + \overline{(\mathbf{B} \otimes \mathbf{u})} - \left(-\overline{\mathbf{u}} \otimes \overline{\mathbf{B}} + \overline{\mathbf{B}} \otimes \overline{\mathbf{u}}\right). \tag{2.246}$$

An analog to (2.243) exists for the induction equation as well.

$$\frac{\partial \overline{\mathbf{B}}}{\partial \mathrm{t}} + \nabla \cdot \boldsymbol{\mathcal{N}}_F^{\mathrm{I}} = \nabla \overline{r} + \nabla \cdot \left(\lambda \nabla^{\mathrm{a}} \overline{\mathbf{B}} - \boldsymbol{\mathcal{T}}^{\mathrm{I}}\right) + \overline{\mathbf{f}^{\mathrm{I}}}. \tag{2.247}$$

2.7.2 Variational Multiscale Formulation

This section will introduce the variational multiscale formulation in a relatively abstract setting. For details on the development of this approach see (Hughes 1995; Hughes et al. 1998; Bazilevs et al. 2007). A semi-linear weak form will be assumed, the exact form of which is not known. However, the form is linear in its first argument and nonlinear in its second argument. The VMS approach will be taken in Chapter 4 with the goal of developing large eddy simulation models for incompressible MHD. For now, consider the problem: *Find* $\mathbf{U} \in \boldsymbol{\mathcal{V}}$ *s.t.* $\forall \mathbf{W} \in \boldsymbol{\mathcal{V}}$

$$\mathcal{A}\left(\mathbf{W}, \mathbf{U}\right) = \left(\mathbf{W}, \mathbf{F}\right) \quad \forall \mathbf{W} \in \boldsymbol{\mathcal{V}}. \tag{2.248}$$

We have already discussed at length the infeasibility of solving (2.248) analytically and via a naive numerical approach. The VMS approach seeks an *optimal* solution in a finite dimensional space $\boldsymbol{\mathcal{V}}^h$. With this in mind, a projection operator $\mathbb{P}^h$ is introduced that restricts a function $\mathbf{V}$ to the finite dimensional space.

$$\mathbf{V}^h = \mathbb{P}^h \mathbf{V}, \quad \mathbf{V}^h \in \boldsymbol{\mathcal{V}}^h. \tag{2.249}$$

Moreover, the projection operator is selected so that when it is applied to the analytical solution $\mathbf{U}$ the resulting finite dimensional solution $\mathbf{U}^h$ represents an *optimal* finite dimensional solution. The term "optimal" here depends on the person performing the simulation.

Remarks:

- Selection of the projection operator represents a paradigm in computational

physics. This is because, in principle, the projection operator is selected so as to define an *optimal* numerical solution. The user determines what is meant by optimal. Examples include a projection operator that results in nodally exact solutions or one that minimizes some type of error.

- Application of the projection operator to the analytical solution results in discrete resolved scales. This is contrary to the classical LES approach wherein the filtering operation results in a smooth solution that is defined at every point in the domain.

Once a projection operator has been selected the function decomposition becomes unique. Thus, for any function $\mathbf{V}$ we have

$$\mathbf{V} = \mathbf{V}^h + \mathbf{V}'. \tag{2.250}$$

Furthermore,

$$\begin{aligned}
\mathbf{V}' &= \mathbf{V} - \mathbf{V}^h \\
&= \mathbf{V} - \mathbb{P}^h \mathbf{V} \\
&= \left(\mathbb{I} - \mathbb{P}^h \right) \mathbf{V} \\
&= \mathbb{P}' \mathbf{V}
\end{aligned}$$

where $\mathbb{P}'$ is called the fine scale projector and $\mathbb{I}$ is the identity operator. Note that

$$\mathbf{U}^h \in \boldsymbol{\mathcal{V}}^h, \quad \mathbf{U}' \in \boldsymbol{\mathcal{V}}' \tag{2.251}$$

$$\mathbf{W}^h \in \boldsymbol{\mathcal{V}}^h, \quad \mathbf{W}' \in \boldsymbol{\mathcal{V}}'. \tag{2.252}$$

The decomposition (2.250) is used in (2.248). Exploiting the linearity of the first slot in the variational statement results in the following two problems: *Find* $\mathbf{U}^h \in \boldsymbol{\mathcal{V}}^h$ *s.t.* $\forall\, \mathbf{W}^h \in \boldsymbol{\mathcal{V}}^h$

$$\mathcal{A}\left(\mathbf{W}^h, \mathbf{U}^h + \mathbf{U}' \right) = \left(\mathbf{W}^h, \mathbf{F} \right) \tag{2.253}$$

and: *Find* $\mathbf{U}' \in \mathcal{V}'$ *s.t.* $\forall\, \mathbf{W}' \in \mathcal{V}'$

$$\mathcal{A}\left(\mathbf{W}', \mathbf{U}^h + \mathbf{U}'\right) = \left(\mathbf{W}', \mathbf{F}\right). \tag{2.254}$$

The goal is to solve (2.253) for the resolved scales, $\mathbf{U}^h$. However, it is obvious that the resolved scales depend on the subgrid solutions. The solution of (2.254) is as difficult to obtain as the original system of PDEs. It is reasonable to seek an approximation to the subgrid scales that hinges on their self-similarity and universality. The details of a particular approximation to the subgrid scales are presented in (Bazilevs et al. 2007). A related, but slightly different approach is described in (Wang and Oberai 2010b). Both approximations seek a first order approximation to the fine scales via an asymptotic series. However, the approximation in (Bazilevs et al. 2007) is not consistently first order in that contributions from higher order terms are present. It turns out that keeping the higher-order terms does not offer any benefit to the numerical method (Wang and Oberai 2010b). The present exposition follows that in (Wang and Oberai 2010b). The first step is to subtract $\mathcal{A}\left(\mathbf{W}', \mathbf{U}^h\right)$ from (2.254). After an integration by parts on the right hand side the result is

$$\mathcal{A}\left(\mathbf{W}', \mathbf{U}^h + \mathbf{U}'\right) - \mathcal{A}\left(\mathbf{W}', \mathbf{U}^h\right) = -\left(\mathbf{W}', \mathcal{L}\mathbf{U}^h - \mathbf{F}\right). \tag{2.255}$$

Next, assume an asymptotic expansion for $\mathbf{U}'$ in terms of a small parameter $\epsilon = \left\|\mathcal{L}\mathbf{U}^h - \mathbf{F}\right\|$ such that

$$\mathbf{U}' = \sum_{i=0}^{\infty} \epsilon^i \mathbf{U}^{(i)}. \tag{2.256}$$

Note that

$$\mathcal{L}\mathbf{U}^h - \mathbf{F} = \epsilon \frac{\mathcal{L}\mathbf{U}^h - \mathbf{F}}{\left\|\mathcal{L}\mathbf{U}^h - \mathbf{F}\right\|}. \tag{2.257}$$

Following the usual asymptotic series approach, terms of the same order are equated.
$\underline{i = 0}$

$$\mathcal{A}\left(\mathbf{W}', \mathbf{U}^h + \mathbf{U}^{(0)}\right) - \mathcal{A}\left(\mathbf{W}', \mathbf{U}^h\right) = 0. \tag{2.258}$$

A solution to this problem is $\mathbf{U}^{(0)} = \mathbf{0}$.

<u>$i = 1$</u>

$$\begin{aligned}
&\mathcal{A}\left(\mathbf{W}', \mathbf{U}^h\right) \\
&+\epsilon\left[\left(\mathbf{w}', \frac{\partial \mathbf{u}^{(1)}}{\partial t}\right) - \left(\nabla \cdot \mathbf{w}', P^{(1)}\right) + \left(\nabla^{\mathrm{s}}\mathbf{w}', 2\nu\nabla^{\mathrm{s}}\mathbf{u}^{(1)}\right)\right. \\
&\qquad\left. - \left(\nabla\mathbf{w}', \mathbf{u}^{(1)} \otimes \mathbf{u}^h + \mathbf{u}^h \otimes \mathbf{u}^{(1)} - \frac{1}{\mu_0\rho}\left[\mathbf{B}^{(1)} \otimes \mathbf{B}^h + \mathbf{B}^h \otimes \mathbf{B}^{(1)}\right]\right)\right] \\
&+\epsilon^2\left(\nabla\mathbf{w}', -\left(\mathbf{u}^{(1)} \otimes \mathbf{u}^{(1)} - \frac{1}{\mu_0\rho}\left[\mathbf{B}^{(1)} \otimes \mathbf{B}^{(1)}\right]\right)\right) \\
&+\epsilon\left[\left(\mathbf{c}', \frac{\partial \mathbf{B}^{(1)}}{\partial t}\right) - \left(\nabla \cdot \mathbf{c}', r^{(1)}\right) + \left(\nabla^{\mathrm{a}}\mathbf{c}', 2\lambda\nabla^{\mathrm{a}}\mathbf{B}^{(1)}\right)\right. \\
&\qquad\left. - \left(\nabla\mathbf{c}', -\left[\mathbf{u}^h \otimes \mathbf{B}^{(1)} + \mathbf{u}^{(1)} \otimes \mathbf{B}^{(h)}\right] + \mathbf{B}^h \otimes \mathbf{u}^{(1)} + \mathbf{B}^{(1)} \otimes \mathbf{u}^{(h)}\right)\right] \\
&+\epsilon^2\left(\nabla\mathbf{c}', -\left(-\mathbf{u}^{(1)} \otimes \mathbf{B}^{(1)} + \mathbf{B}^{(1)} \otimes \mathbf{u}^{(1)}\right)\right) \\
&+\epsilon\left[\left(q', \nabla \cdot \mathbf{u}^{(1)}\right) + \left(s', \nabla \cdot \mathbf{B}^{(1)}\right)\right] \\
&-\mathcal{A}\left(\mathbf{W}', \mathbf{U}^h\right) = -\epsilon\left(\mathbf{W}', \frac{\boldsymbol{\mathcal{L}}\mathbf{U}^h - \mathbf{F}}{\|\boldsymbol{\mathcal{L}}\mathbf{U}^h - \mathbf{F}\|}\right).
\end{aligned} \tag{2.259}$$

Matching ϵ^1 terms yields

$$\mathcal{A}_1\left(\mathbf{W}', \epsilon\mathbf{U}^{(1)}; \mathbf{U}^h\right) = -\left(\mathbf{W}', \boldsymbol{\mathcal{L}}\mathbf{U}^h - \mathbf{F}\right). \tag{2.260}$$

It is straightforward to verify that $\mathcal{A}_1\left(\cdot, \epsilon\mathbf{U}^{(1)}; \mathbf{U}^h\right)$ is the linearization of $\mathcal{A}\left(\cdot, \cdot\right)$ about $\mathbf{U}^h$ in the direction of $\mathbf{U}'$,

$$\mathcal{A}_1\left(\cdot, \epsilon\mathbf{U}^{(1)}; \mathbf{U}^h\right) = \left.\frac{\mathrm{d}}{\mathrm{d}\epsilon}\mathcal{A}\left(\cdot, \mathbf{U}^h + \epsilon\mathbf{U}'\right)\right|_{\epsilon=0}. \tag{2.261}$$

At this point, (2.254) has been written in terms of the coarse scale residual, the fine scales have been approximated with an asymptotic series, and only terms up to first order in the small parameter have been retained. Introducing an inverse differential

operator (I_D) on (2.260) allows the solution for $\epsilon \mathbf{U}^{(1)}$ to be obtained as

$$\epsilon \mathbf{U}^{(1)} = -I_D \left(\mathcal{L} \mathbf{U}^h - \mathbf{F} \right). \tag{2.262}$$

Of course, I_D is not known and in practice an algebraic approximation to this inverse differential operator (denoted by $\boldsymbol{\tau}$) is employed. Thus,

$$\mathbf{U}' \approx \epsilon \mathbf{U}^{(1)} \approx -\mathbb{P}' \boldsymbol{\tau} \mathbb{P}'^T \left(\mathcal{L} \mathbf{U}^h - \mathbf{F} \right). \tag{2.263}$$

Note that the fine-scale projection operator $\mathbb{P}'$ has been used to constrain the subgrid solution to the subgrid space. Historically $\boldsymbol{\tau}$ is called the stabilization parameter. Considerable effort in the literature has been dedicated to finding suitable definitions for the stabilization parameter (see Shakib, Hughes, and Johan 1991; Hughes 1995; Codina 2002; Codina et al. 2007; Hughes and Sangalli 2008) and references therein). The form of $\boldsymbol{\tau}$ used in this work will be presented in subsequent sections (see Chapter 5, Sections 5.1 and 5.2). Chapter 3 is dedicated to a discussion of the stabilization parameter. The final statement of the first order variational multiscale formulation is: *Find* $\mathbf{U}^h \in \boldsymbol{\mathcal{V}}^h$ *s.t.* $\forall\, \mathbf{W}^h \in \boldsymbol{\mathcal{V}}^h$

$$\mathcal{A} \left(\mathbf{W}^h, \mathbf{U}^h \right) + \mathcal{A}_1 \left(\mathbf{W}^h, \epsilon \mathbf{U}^{(1)}; \mathbf{U}^h \right) = \left(\mathbf{W}^h, \mathbf{F} \right) \tag{2.264}$$

with $\mathbf{U}'$ given by (2.263). If the solution decomposition was not consistently first order then the VMS statement would be: *Find* $\mathbf{U}^h \in \boldsymbol{\mathcal{V}}^h$ *s.t.* $\forall\, \mathbf{W}^h \in \boldsymbol{\mathcal{V}}^h$

$$\mathcal{A} \left(\mathbf{W}^h, \mathbf{U}^h + \mathbf{U}' \right) = \left(\mathbf{W}', \mathbf{F} \right) \tag{2.265}$$

with the subgrid solution still given by the first order approximation (2.263). This is the form of the VMS formulation that is studied in (Bazilevs et al. 2007). It has been shown (see Wang and Oberai 2010b, 2010a) that the second order terms in (2.265) with (2.263) do not impact the solution. Thus, it is reasonable to use the consistent first order VMS formulation (2.264).

Remarks:

- In the VMS formulation there is no need to introduce the concept of the subgrid stress tensor.

- Modeling efforts are confined to approximations of the subgrid solutions.

- The better the approximation to the subgrid scales, the better the numerical solution.

- In this work, we will not make a notational distinction between (2.264) and (2.265) as their performance is the same.

The exact form of the VMS applied to incompressible MHD will be presented in Chapter 4, Section 4.2.

CHAPTER 3
Stabilization Parameter

The stabilization parameter $\boldsymbol{\tau}$ plays a critical role in the development of VMS-based turbulence models. This chapter provides details on this important parameter and the role that it plays in MHD turbulence models. We further develop this parameter for the incompressible MHD. This development includes the derivation of new forms for $\boldsymbol{\tau}$ for MHD. It must be noted, however, that this chapter does not strictly follow the theme of this dissertation in that it considers an *incomplete* turbulence model and does not focus on the development of new turbulence models. Furthermore, the results derived and presented in this chapter are not used in subsequent chapters although prospects for their use in the new turbulence models are discussed.

We begin this chapter with a classical stabilized finite element method called the Galerkin-least squares (GLS) method (see Hughes, Franca, and Hulbert 1989). This stabilized FEM can be thought of as an incomplete turbulence model. That is, a complete turbulence model includes all of the terms from the VMS formulation. Here only one term in addition to the Galerkin terms is considered.

The GLS formulation is: *Find* $\mathbf{U}^h \in \boldsymbol{\mathcal{V}}^h$ *s.t.* $\forall\, \mathbf{W}^h \in \boldsymbol{\mathcal{V}}^h$

$$\mathcal{A}\left(\mathbf{W}^h, \mathbf{U}^h\right) + \left(\boldsymbol{\mathcal{L}}\mathbf{W}^h, \boldsymbol{\tau}\boldsymbol{\mathcal{R}}\mathbf{U}^h\right)_{\Omega'} = \left(\mathbf{w}^h, \mathbf{f}^{\mathrm{V}}\right) + \left(\mathbf{c}^h, \mathbf{f}^{\mathrm{I}}\right). \tag{3.1}$$

The notation $(u, v)_{\Omega'}$ represents

$$(u, v)_{\Omega'} = \sum_e \int_{\Omega^e} uv \ \mathrm{d}\Omega^e \tag{3.2}$$

where e represents an element and Ω^e an element domain. Stabilized FEMs were introduced to combat difficulties arising with traditional finite elements such as the development of spurious oscillations in advection-dominated problems. They also arose in response to the inf-sup condition which poses a restriction on the finite element spaces that can be used for the velocity and pressure solutions. Specifically, the velocity and pressure functions spaces cannot use the same finite element inter-

polations. Using stabilized finite element methods, one is able to circumvent this issue and use equal order finite elements for the velocity and pressure solutions (see Hughes, Franca, and Balestra 1986). Figure 3.1 demonstrates the central problem with advection-dominated flow fields.
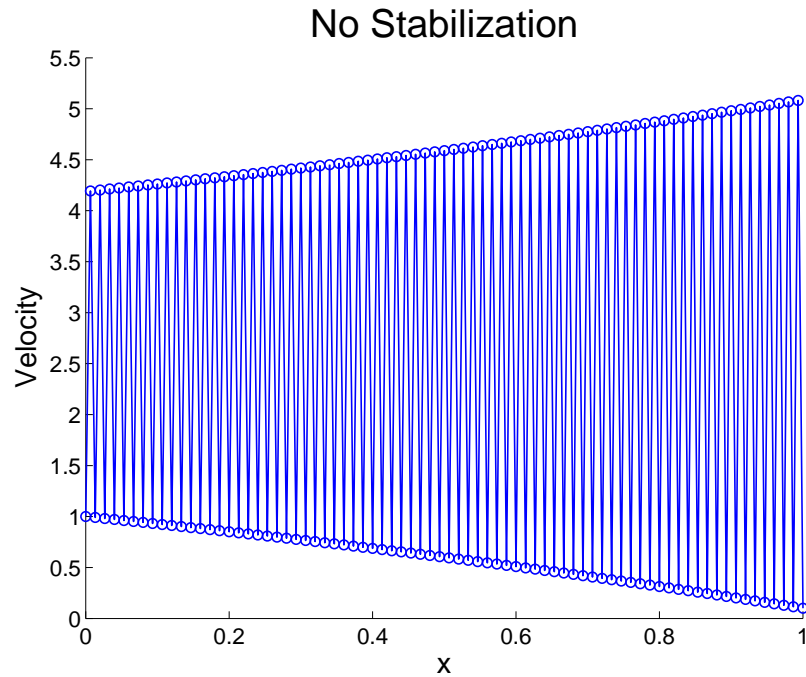
Figure 3.1: A simulation of the Burgers MHD equations without any stabilization. The numerical solution exhibits severe spurious oscillations .

These spurious oscillations are overcome by using the GLS stabilization technique. Figure 3.2 presents the solution to the same problem using the GLS stabilization technique.

A heuristic derivation of the stabilization parameter is presented in Section 3.1 wherein the finite element weighting functions are enhanced through an artificial diffusivity. The form of this artificial diffusivity is motivated through finite difference methods. A discussion on the deeper meaning of the stabilization parameter follows this derivation along with the presentation of more sophisticated results on the subject. Section 3.2 discusses a general multidimensional version of the stabilization parameter.

In Section 3.3, a new stabilization parameter is derived for the incompressible

MHD equations. The derivation is done in steps: first the purely advective, one-dimensional case is considered in Section 3.3.1. Encouraging results are presented. Then in Section 3.3.2, a generalization to multiple dimensions is presented.
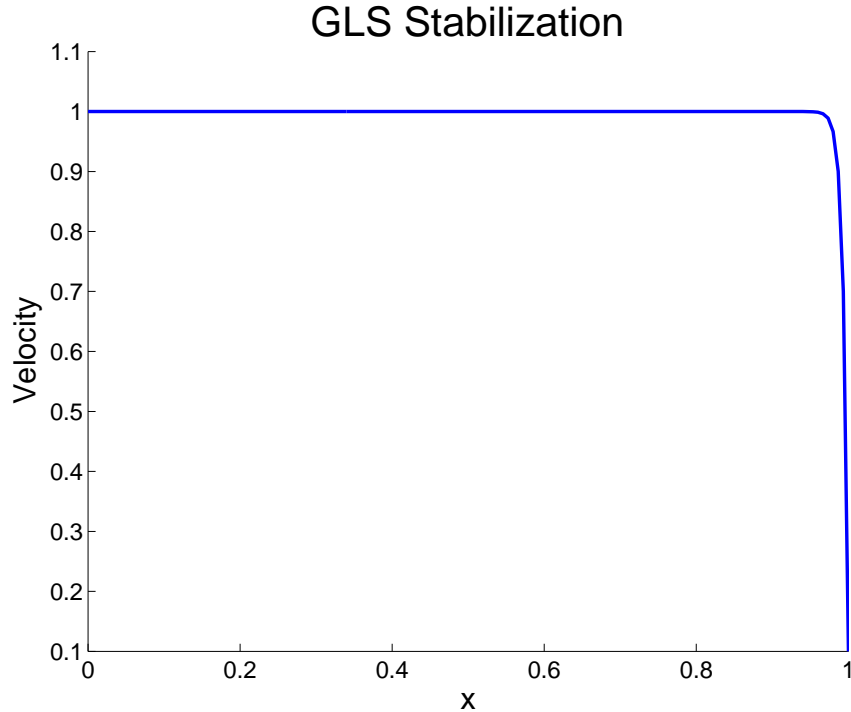
Figure 3.2: A simulation of the Burgers MHD equations with GLS stabilization.

Next, diffusive effects are included and results are presented for a two-dimensional problem. Finally, in Section 3.3.3, the one-dimensional Burgers MHD equations (see (3.41)- (3.42) below) are considered and the exact expression for a new stabilization parameter that includes both advective and diffusive effects is presented. All of the new stabilization parameters are derived with steady versions of the MHD equations.

3.1   Origins

A heuristic derivation of the stabilization parameter was presented in (Hughes et al. 1994). This derivation provides the basic idea behind the stabilization parame-

ter. To begin, the linear, one-dimensional advection diffusion equation is considered.

$$au_{,x} - \nu u_{,xx} = 0. \tag{3.3}$$

In (3.3) a is the advection coefficient, ν is the diffusion coefficient, and u represents a field that is advected and diffuses. Classically, discretization schemes such as the finite difference method considered a modified advection diffusion equation where ν is replaced by an effective diffusivity $\nu \to \nu + \nu_T$, ν_T being an artificial diffusivity. This is motivated by considerable experience in advection-dominated problems wherein the numerical solution develops unrealistic solutions such as spurious oscillations. In the FEM, the artificial diffusivity is introduced by enhancing the weighting function space with the weighting functions p. Thus, to find the variational form, the strong form is multiplied by $w + p$. This leads to stabilized finite element methods. Indeed, the stabilization parameter gets its name because it was first introduced in this context.

<u>Remarks:</u>

Note that the enhancing finite element functions p are *not* the same as the fluid pressure. The fluid pressure does not make an appearance in this chapter.

The problem statement is: *Find $u^h \in \mathcal{V}^h$ s.t. $\forall\, w^h, p^h \in \mathcal{V}^h$*

$$-\left(aw_{,x}^h, u^h\right) + \left(p^h, \left(au_{,x}^h - \nu u_{,xx}^h\right)\right) + \nu\left(w_{,x}^h, u_{,x}^h\right) = 0. \tag{3.4}$$

The weighting function p^h is selected such that $p^h \propto aw_{,x}^h$. Such a choice corresponds to an upwinding scheme. The proportionality of p^h to $aw_{,x}^h$ is through the stabilization parameter τ.

$$p^h = \tau aw_{,x}^h. \tag{3.5}$$

Simple dimensional arguments indicate that τ should have the units of time. A time-scale can be obtained by combining the artificial diffusion ν_T with the advection scale

$|a|$. That is

$$\tau = \frac{\nu_T}{|a|^2}.$$ (3.6)

The present goal is to determine an exact expression for ν_T which will result in an expression for the stabilization parameter. To this end, consider a central difference approximation to (3.3).

$$a\frac{u_{A+1} - u_{A-1}}{2h} - \nu_T \frac{u_{A+1} - 2u_A + u_{A-1}}{h^2} = 0$$ (3.7)

where u_A represents the solution at node A and h is the grid spacing. It is not too difficult to show that the solution is

$$u_A = c_1 + c_2 \left(\frac{1 + \frac{ah}{2\nu_T}}{1 - \frac{ah}{2\nu_T}} \right)^A.$$ (3.8)

The analytical solution to (3.3) is

$$u(x) = c_3 + c_4 e^{\mathrm{Pe}\frac{x}{L}}$$ (3.9)

where $\mathrm{Pe} = ah/\nu$ is the Péclet number. Assuming that the solutions should be equal at the nodes yields,

$$\frac{1 + \frac{ah}{2\nu_T}}{1 - \frac{ah}{2\nu_T}} = e^{\mathrm{Pe}\frac{x}{L}}.$$ (3.10)

This results in,

$$\frac{1}{\frac{1}{\alpha} + \tilde{\xi}} = \tanh \alpha$$

$$\Rightarrow \tilde{\xi} = \coth \alpha - \frac{1}{\alpha}$$ (3.11)

with

$$\tilde{\xi} = \frac{2\nu_T}{ah}, \quad \alpha = \frac{ah}{2\nu}, \quad \tilde{\alpha} = \frac{ah}{2\nu_T}.$$ (3.12)

Thus from (3.11)

$$\nu_T = \frac{ah}{2} \left(\coth \alpha - \frac{1}{\alpha} \right).$$
(3.13)

Therefore, the stabilization parameter is

$$\tau = \frac{h}{2a} \left(\coth \alpha - \frac{1}{\alpha} \right).$$
(3.14)

To summarize, an exact form for the stabilization parameter was derived based on analogies with artificial diffusion approaches in finite differences. Indeed, the stabilization parameter is reasoned to derive from an enhancement of the finite element weighting functions. Dimensional arguments led to the observation that the stabilization parameter is actually a time-scale. A convenient time-scale can be selected based on diffusion and velocity scales. From experience with artificial diffusion methods, the diffusion scale in the stabilization parameter is taken to be the artificial diffusion. An expression for the artificial diffusion was obtained when considering the artificial diffusion approach on a 2nd order centered finite difference scheme. This expression was found by equating the exact solution for the advection diffusion equation to the numerical solution at the nodes.

More sophisticated and revealing expressions for the stabilization parameter exist. In (Hughes 1995) stabilized finite element methods are connected to the variational multiscale formulation. In doing so, a profound result concerning the stabilization parameter was discovered. This is namely that the stabilization parameter is an element-wise average of the fine-scale Green's function, G'. The fine-scale Green's function is found by considering the relevant PDE over a single element. The resulting expression for the stabilization parameter is

$$\tau = \frac{1}{\text{meas}\,(\Omega^e)} \int_{\Omega_y} \int_{\Omega_x} G'\,(x, y) \; \mathrm{d}\Omega_x \; \mathrm{d}\Omega_y.$$
(3.15)

Using this expression for the one-dimensional, linear advection diffusion case, the analytical "coth" expression for τ (3.14) was recovered.

In (Hughes and Sangalli 2008) a detailed study of the fine-scale Green's func-

tion was performed in which it was related to the coarse-scale Green's function through projection operators selected for the VMS method. Again, explicit expressions for the stabilization parameter are derived. In particular, closed form expressions for τ for linear, quadratic, and cubic elements were presented for the one-dimensional case.

The stabilization parameter in multiple dimensions does not have an analytical expression. What is more, in multiple dimensions (or for systems of equations) the stabilization parameter is a matrix of scalar stabilization parameters. Depending on the coupling of the equations under consideration, it may be desirable to use a non-diagonal matrix stabilization parameter. Once again, however, it is exceptionally difficult, in general, to derive a parameter matrix that is fully populated. Indeed, in the pure hydrodynamic case, a diagonal stabilization matrix is used,

$$\boldsymbol{\tau} = \begin{bmatrix} \tau^{\mathrm{V}} & 0 & 0 & 0 \\ 0 & \tau^{\mathrm{V}} & 0 & 0 \\ 0 & 0 & \tau^{\mathrm{V}} & 0 \\ 0 & 0 & 0 & \tau^{\mathrm{C}} \end{bmatrix} \tag{3.16}$$
$$= \mathrm{diag}\left(\tau^{\mathrm{V}}, \ \tau^{\mathrm{C}}\right).$$

The most widely employed expression for the stabilization parameter in fluid dynamics stems from asymptotic scaling arguments presented in (Shakib, Hughes, and Johan 1991) where

$$\tau^{\mathrm{V}} = \frac{1}{\sqrt{\left(\frac{2C_t}{\Delta t}\right)^2 + \mathbf{u} \cdot \mathbf{G}\mathbf{u} + C_I \nu^2 \mathbf{G} : \mathbf{G}}} \tag{3.17}$$

$$\tau^{\mathrm{C}} = \frac{1}{8C_t \mathrm{tr}\left(\mathbf{G}\right)} \tag{3.18}$$

and $\mathbf{G}$ is the metric tensor which is given by

$$\mathbf{G} = \nabla\boldsymbol{\xi} \cdot \nabla\boldsymbol{\xi} \tag{3.19}$$

where

$$\nabla \boldsymbol{\xi} = \frac{\partial \xi_k}{\partial x_i}. \tag{3.20}$$

In (3.20) ξ_i represents coordinates in the element space and x_i represents coordinates in physical space. Note also that (3.17) contains some constants which were shown in (Liu 2012) to greatly influence the outcome of simulations. Thus, they must be selected carefully. Finally, it is observed that (3.17) includes the effects of time-scales.

An expression for the diagonal elements of the stabilization matrix for the steady MHD equations was provided by (Codina and Hernández-Silva 2006) as

$$\boldsymbol{\tau} = \operatorname{diag}\left(\tau_1, \ \tau_1, \ \tau_1, \ \tau_2, \ \tau_3, \ \tau_3, \ \tau_3, \ \tau_4\right) \tag{3.21}$$

with

$$\tau_1 = \left(c_1 \frac{|\mathbf{u}|}{h} + c_2 \frac{1}{\mathrm{Re}h^2} + c_3 \frac{\mathrm{S}|\mathbf{B}|}{h}\right)^{-1} \tag{3.22}$$

$$\tau_2 = c_4 \frac{h^2}{\tau_1} \tag{3.23}$$

$$\tau_3 = \frac{1}{\mathrm{S}} \left(c_1 \frac{|\mathbf{B}|}{h} + c_2 \frac{1}{\mathrm{Rm}h^2}\right)^{-1} \tag{3.24}$$

$$\tau_4 = c_4 \frac{h^2}{\mathrm{S}^2 \tau_3}. \tag{3.25}$$

3.2   Multi-dimensional, advective-diffusive systems

One dimensional advective diffusive systems permit an analytical expression for the stabilization parameter if they can be diagonalized. The diagonalized system results in a system of uncoupled equations for which the stabilization parameter can be written for each equation. The multidimensional case is similar; if it could be diagonalized then an expression for the stabilization parameter is known. To begin, consider a multi-dimensional, advection-diffusion system of the form

$$- \left(\mathbf{W}_{,i}, \mathbf{A}_i \mathbf{U}\right) + \left(\boldsymbol{\mathcal{L}}\mathbf{W}, \boldsymbol{\tau}\boldsymbol{\mathcal{L}}\mathbf{U}\right) + \left(\mathbf{W}_{,i}, \mathbf{D}_{ij}\mathbf{U}_{,j}\right) = \left(\mathbf{W}, \mathbf{F}\right). \tag{3.26}$$

In (3.26) the coefficient matrices $\mathbf{A}_i$ and $\mathbf{D}_i$ are of size $n_{\mathrm{sd}}n_{\mathrm{eq}} \times n_{\mathrm{eq}}$ and $n_{\mathrm{sd}}n_{\mathrm{eq}} \times n_{\mathrm{sd}}n_{\mathrm{eq}}$, respectively. Thus, in the present derivation, the ith index refers to the ith submatrix. Similarly, the ij position in the diffusion matrix refers to the submatrix that populates the ij position in the diffusion matrix. The goal is to diagonalize (3.26). To this end, consider the following transformations,

$$\mathbf{U} = \mathbf{L}^{-T}\mathbf{V}, \ \ \mathbf{W} = \mathbf{L}^{-T}\mathbf{Z}, \ \text{and} \ \mathbf{F} = \mathbf{L}^{-T}\widehat{\mathbf{F}}. \tag{3.27}$$

The transformation matrix $\mathbf{L}$ is the Cholesky factorization of the diffusion matrix $\mathbf{D}_{ij}$,

$$\mathbf{D}_{ij} = \left(\mathbf{L}\mathbf{L}^T\right)_{ij}. \tag{3.28}$$

A useful identity that will be exploited later is

$$\mathbf{L}^{-1}\mathbf{D}_{ij}\mathbf{L}^{-T} = \mathbf{I}_{ij} \tag{3.29}$$

where $\mathbf{L}^{-T}$ is the transpose of the inverse of $\mathbf{L}$. We note that (3.29) is true when $\mathbf{D}$ is a diagonal matrix. When $\mathbf{D}$ is diagonal we have $\left(\mathbf{L}^{-1}\right)^T = \left(\mathbf{L}^T\right)^{-1}$. Introducing (3.27) into (3.26) turns the diffusion matrix into the identity matrix.

$$
\begin{aligned}
& -\left(\mathbf{L}^{-T}\mathbf{Z}_{,i}, \mathbf{A}_i\mathbf{L}^{-T}\mathbf{V}\right) + \left(\mathcal{L}\mathbf{L}^{-T}\mathbf{Z}, \tau\left[\mathcal{L}\mathbf{L}^{-T}\mathbf{V} - \mathbf{L}^{-T}\widehat{\mathbf{F}}\right]\right) \\
& \quad + \left(\mathbf{L}^{-T}\mathbf{Z}_{,i}, \mathbf{D}_{ij}\mathbf{L}^{-T}\mathbf{V}_{,j}\right) = \left(\mathbf{L}^{-T}\mathbf{Z}, \mathbf{L}^{-T}\widehat{\mathbf{F}}\right) \\
& \Rightarrow -\left(\mathbf{Z}_{,i}, \mathbf{L}^{-1}\mathbf{A}_i\mathbf{L}^{-T}\mathbf{V}\right) + \left(\mathcal{L}\mathbf{Z}, \mathbf{L}^{-1}\tau\mathbf{L}^{-T}\left[\mathcal{L}\mathbf{V} - \widehat{\mathbf{F}}\right]\right) \\
& \quad + \left(\mathbf{Z}_{,i}, \mathbf{L}^{-1}\mathbf{D}_{ij}\mathbf{L}^{-T}\mathbf{V}_{,j}\right) = \left(\mathbf{Z}, \mathbf{L}^{-1}\mathbf{L}^{-T}\widehat{\mathbf{F}}\right) \\
& \Rightarrow -\left(\mathbf{Z}_{,i}, \widehat{\mathbf{A}}_i\mathbf{V}\right) + \left(\mathcal{L}\mathbf{Z}, \widehat{\tau}\left[\mathcal{L}\mathbf{V} - \widehat{\mathbf{F}}\right]\right) - \left(\mathbf{Z}_{,i}, \mathbf{I}_{ij}\mathbf{V}_{,j}\right) = \left(\mathbf{Z}, \mathbf{L}^{-1}\mathbf{L}^{-T}\widehat{\mathbf{F}}\right). \tag{3.30}
\end{aligned}
$$

In (3.30) two new matrices play a role,

$$\widehat{\mathbf{A}}_i = \mathbf{L}^{-1}\mathbf{A}_i\mathbf{L}^{-T} \tag{3.31}$$

and

$$\widehat{\boldsymbol{\tau}} = \mathbf{L}^{-1}\boldsymbol{\tau}\mathbf{L}^{-T}. \tag{3.32}$$

The system is still non-diagonal because of the advection matrix $\widehat{\mathbf{A}}_i$. However, a matrix can be diagonalized by its eigenvectors. Hence, the transformations

$$\mathbf{V} = \boldsymbol{\Upsilon}\mathbf{X}, \ \mathbf{Z} = \boldsymbol{\Upsilon}\mathbf{Y}, \ \text{and} \ \widehat{\mathbf{F}} = \boldsymbol{\Upsilon}\widetilde{\mathbf{F}} \tag{3.33}$$

are considered where $\boldsymbol{\Upsilon}$ is a matrix of the eigenvectors of $\widehat{\mathbf{A}}$ and which has been orthonormalized so that

$$\boldsymbol{\Upsilon}^{-1} = \boldsymbol{\Upsilon}^{T}. \tag{3.34}$$

Substituting this into (3.30) yields,

$$
\begin{aligned}
& -\left(\boldsymbol{\Upsilon}\mathbf{Y}_{,i}, \widehat{\mathbf{A}}_i \boldsymbol{\Upsilon}\mathbf{X}\right) + \left(\mathcal{L}\boldsymbol{\Upsilon}\mathbf{Y}, \widehat{\boldsymbol{\tau}}\left[\mathcal{L}\boldsymbol{\Upsilon}\mathbf{X} - \boldsymbol{\Upsilon}\widetilde{\mathbf{F}}\right]\right) \\
& \qquad + (\boldsymbol{\Upsilon}\mathbf{Y}_{,i}, \mathbf{I}_{ij}\boldsymbol{\Upsilon}\mathbf{X}_{,j}) = \left(\boldsymbol{\Upsilon}\mathbf{Y}, \mathbf{L}^{-1}\mathbf{L}^{-T}\boldsymbol{\Upsilon}\widetilde{\mathbf{F}}\right) \\
\Rightarrow & -\left(\mathbf{Y}_{,i}, \boldsymbol{\Upsilon}^{T}\widehat{\mathbf{A}}_i \boldsymbol{\Upsilon}\mathbf{X}\right) + \left(\mathcal{L}\mathbf{Y}, \boldsymbol{\Upsilon}^{T}\widehat{\boldsymbol{\tau}}\boldsymbol{\Upsilon}\left[\mathcal{L}\mathbf{X} - \widetilde{\mathbf{F}}\right]\right) \\
& \qquad + \left(\mathbf{Y}_{,i}, \boldsymbol{\Upsilon}^{T}\mathbf{I}_{ij}\boldsymbol{\Upsilon}\mathbf{X}_{,j}\right) = \left(\mathbf{Y}, \boldsymbol{\Upsilon}^{T}\mathbf{L}^{-1}\mathbf{L}^{-T}\boldsymbol{\Upsilon}\widetilde{\mathbf{F}}\right) \\
\Rightarrow & -(\mathbf{Y}_{,i}, \boldsymbol{\Lambda}_{,i}\mathbf{X}) + \left(\mathcal{L}\mathbf{Y}, \boldsymbol{\tau}^{d}\left[\mathcal{L}\mathbf{X} - \widetilde{\mathbf{F}}\right]\right) \\
& \qquad + (\mathbf{Y}_{,i}, \mathbf{I}_{ij}\mathbf{X}_{,j}) = \left(\mathbf{Y}, \boldsymbol{\Upsilon}^{T}\mathbf{L}^{-1}\mathbf{L}^{-T}\boldsymbol{\Upsilon}\widetilde{\mathbf{F}}\right). \tag{3.35}
\end{aligned}
$$

In (3.35) $\boldsymbol{\Lambda}_i$ is a diagonal matrix of the eigenvalues of $\widehat{\mathbf{A}}_i$ and

$$
\begin{aligned}
\boldsymbol{\tau}^{d} &= \boldsymbol{\Upsilon}^{T}\widehat{\boldsymbol{\tau}}\boldsymbol{\Upsilon} \\
&= \boldsymbol{\Upsilon}^{T}\mathbf{L}^{-1}\boldsymbol{\tau}\mathbf{L}^{-T}\boldsymbol{\Upsilon}. \tag{3.36}
\end{aligned}
$$

It follows from (3.36) that

$$\boldsymbol{\tau} = \mathbf{L}\boldsymbol{\Upsilon}\boldsymbol{\tau}^{d}\boldsymbol{\Upsilon}^{T}\mathbf{L}^{T}. \tag{3.37}$$

Finally, $\boldsymbol{\tau}^d$ designates a diagonal matrix. This form is reasoned by the fact that the system of equations to be solved for $\mathbf{X}$ is fully decoupled. Therefore, each equation has its own stabilization parameter and is not influenced by the stabilization of the other equations. These results will be used in Section 3.3 to derive non-diagonal stabilization matrices for MHD.

3.3   Stabilization for MHD Equations

Determination of the stabilization matrix is not a trivial matter. Much research has gone into this area with expressions for the stabilization parameter being guided by numerical error analysis and asymptotic arguments. See (Shakib, Hughes, and Johan 1991; Hughes 1995; Hughes et al. 1998; Codina 2002; Codina and Hernández-Silva 2006; Codina et al. 2007; Hughes and Sangalli 2008) and references therein for the development of the parameter. The essential points of this operator are as follows

1. It is an algebraic approximation to $\boldsymbol{\mathcal{L}}^{-1}$.

2. It is related to the fine scale Green's function.

3. Specifically, it is the average value over a finite element of the fine-scale Green's function.

4. It is a matrix operator.

In general, the stabilization matrix will be a full matrix of dimension n $\times$ n where n $=$ $n_{sd} \times n_{eq, \, v} + n_{eq,s}$ and a subscript v denotes a vector equation and a subscript s denotes a scalar equation. For incompressible MHD $n_{eq,v} = 2$, $n_{sd} = 3$, and $n_{eq,s} = 2$. Hence, the stabilization matrix will have dimension 8×8. In the literature the stabilization matrix is typically assumed to be diagonal for simplicity. Indeed, the present work uses a diagonal implementation of the stabilization parameter. However, an attempt to develop a non-diagonal stabilization parameter was undertaken. The new stabilization parameter for MHD did not exhibit any significant improvement over conventional diagonal representations of the parameter.

There is some evidence that suggests that a non-diagonal parameter may be beneficial for some problems; particularly those with radically large and small magnetic Prandtl numbers. Further work in this area will shed some light on this question. The non-diagonal stabilization parameter for MHD developed here has the form

$$
\boldsymbol{\tau} = \begin{bmatrix} \boldsymbol{\tau}^{\mathrm{VV}} & \mathbf{0} & \boldsymbol{\tau}^{\mathrm{VI}} & \mathbf{0} \\ \mathbf{0}^T & \tau_c^{\mathrm{V}+} & \mathbf{0}^T & \tau_c^{\mathrm{I}-} \\ \boldsymbol{\tau}^{\mathrm{IV}} & \mathbf{0} & \boldsymbol{\tau}^{\mathrm{II}} & 0 \\ \mathbf{0}^T & \tau_c^{\mathrm{V}-} & 0 & \tau_c^{\mathrm{I}+} \end{bmatrix}.
\tag{3.38}
$$

In (3.38) the submatrices $\boldsymbol{\tau}^{\mathrm{VV}}$, $\boldsymbol{\tau}^{\mathrm{II}}$, $\boldsymbol{\tau}^{\mathrm{VI}}$, and $\boldsymbol{\tau}^{\mathrm{IV}}$ are diagonal while τ_c^+ and τ_c^- are scalars. The boldface zero indicates the zero vector. In the results shown in Chapters 4 and 5 the stabilization matrix is diagonal and so

$$
\boldsymbol{\tau}^{\mathrm{VI}} = \boldsymbol{\tau}^{\mathrm{IV}} = \mathbf{0}
\tag{3.39}
$$

and

$$
\tau_c^{\mathrm{V},\mathrm{I}-} = 0.
\tag{3.40}
$$

In the following sections, in addition to the full MHD equations, a one-dimensional version of the steady MHD equations is considered. This system is known as the steady Burgers MHD equations and is given by

$$
uu_{,x} - BB_{,x} - \nu u_{,xx} = 0
\tag{3.41}
$$

$$
-Bu_{,x} + uB_{,x} - \lambda B_{,xx} = 0.
\tag{3.42}
$$

The new stabilization parameter will first be developed in stages:

1. Stage 1: Development based on the Burgers MHD system without viscous or magnetic diffusion

2. Stage 2: Generalization of the analysis from Stage 1 to the multi-dimensional

MHD system

3. Stage 3: Development based on the full Burgers MHD equations accounting for diffusion of the fields

3.3.1   Case 1: Pure Advection

In the absence of fluid and magnetic diffusion and external forcing the Burgers MHD equations reduce to

$$uu_{,x} - BB_{,x} = 0 \tag{3.43}$$

$$-Bu_{,x} + uB_{,x} = 0. \tag{3.44}$$

In matrix form this is

$$\mathbf{A}\mathbf{U}_{,x} = \mathbf{0} \tag{3.45}$$

with

$$\mathbf{A} = \begin{bmatrix} u & -B \\ -B & u \end{bmatrix}. \tag{3.46}$$

The eigenvalues of $\mathbf{A}$ are

$$r_1 = u - B, \ r_2 = u + B. \tag{3.47}$$

These are recognized as the Elsässer variables $z^+ = r_2$, $z^- = r_1$. The corresponding eigenvector matrix (after orthonormalization) is

$$\mathbf{\Upsilon} = \frac{1}{\sqrt{2}} \begin{bmatrix} 1 & 1 \\ 1 & -1 \end{bmatrix}. \tag{3.48}$$

The diagonalized system is therefore,

$$\mathbf{\Lambda}\mathbf{V}_{,x} = \mathbf{0} \tag{3.49}$$

where

$$\boldsymbol{\Lambda} = \begin{bmatrix} z^- & 0 \\ 0 & z^+ \end{bmatrix} \tag{3.50}$$

and

$$\mathbf{V} = \begin{bmatrix} z^+ \\ z^- \end{bmatrix}. \tag{3.51}$$

The GLS method applied to this system is

$$- \left(\mathbf{Z}, \boldsymbol{\Lambda}\mathbf{V} \right) + \left(\mathcal{L}\mathbf{Z}, \boldsymbol{\Upsilon}^T \boldsymbol{\tau} \boldsymbol{\Upsilon} \mathcal{L}\mathbf{V} \right) = 0. \tag{3.52}$$

As in Section 3.2, the stabilization parameter for the diagonalized system is required to be a diagonal matrix. In the advection-dominated case it takes the form

$$\boldsymbol{\tau}^d = \mathrm{diag}\left(\tau_1, \ \tau_2 \right) \tag{3.53}$$

with

$$\tau_1 = \frac{h}{2|z^-|}, \quad \tau_2 = \frac{h}{2|z^+|}. \tag{3.54}$$

Transforming the diagonal stabilization matrix back to the original variables results in

$$\boldsymbol{\tau} = \frac{1}{2} \begin{bmatrix} \tau_1 + \tau_2 & \tau_1 - \tau_2, \\ \tau_1 - \tau_2 & \tau_1 + \tau_2 \end{bmatrix}. \tag{3.55}$$

A simulation of the Burgers MHD equations (3.43)- (3.44) was performed for Re $\to$ ∞ and Rm $\to$ ∞. The boundary conditions were essential boundary conditions wherein both the velocity and magnetic fields were pinned at the boundaries. A diagonal and non-diagonal representation of the stabilization parameters were both used and the results were compared. The results of are shown in Figures 3.3 and 3.4.
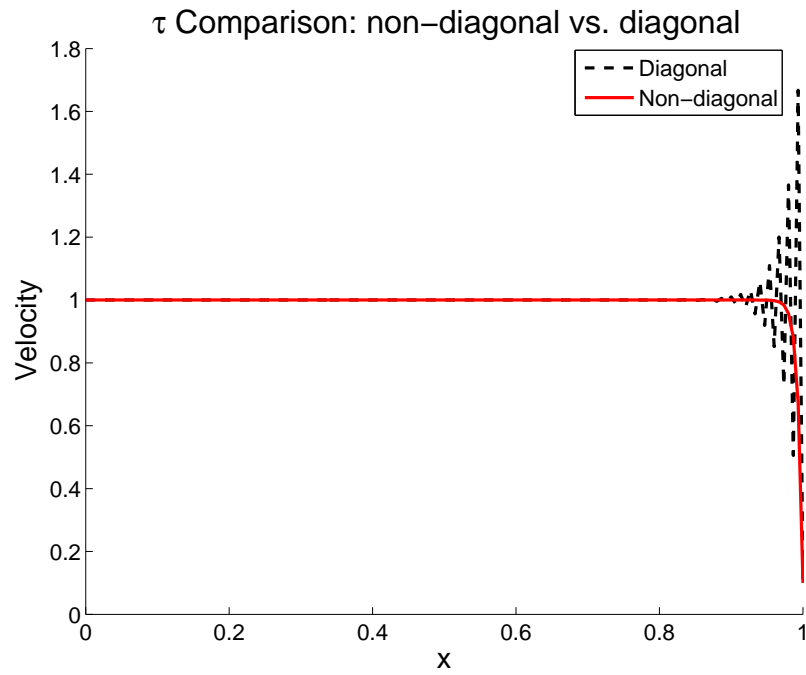
Figure 3.3: The velocity field from Burgers MHD for large Re obtained using diagonal and non-diagonal stabilization matrices.
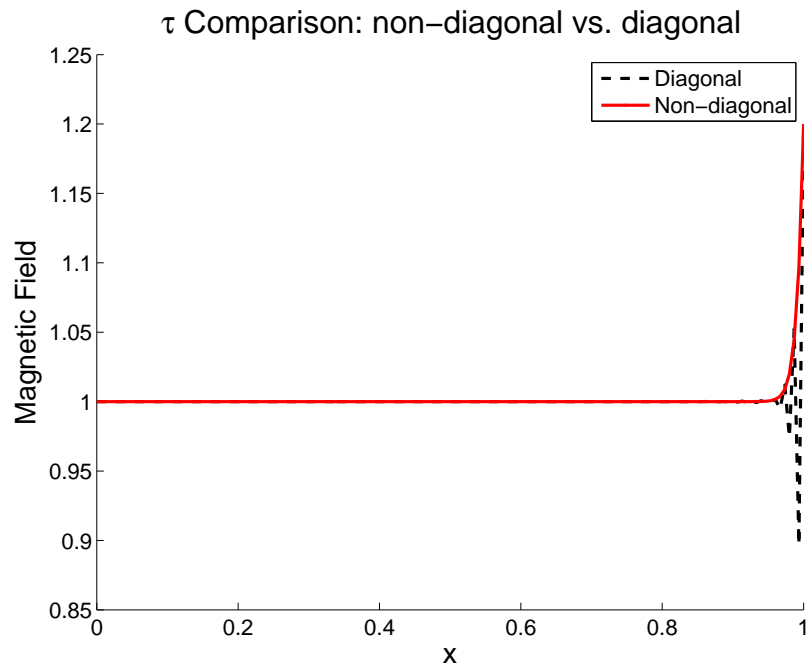
Figure 3.4: The magnetic field from Burgers MHD for large Re obtained using diagonal and non-diagonal stabilization matrices.

The non-diagonal stabilization parameter outperforms the diagonal stabilization parameter. This behavior can be understood by considering the physics of the problem. For such high values of Re and Rm the two equations are strongly coupled. The diagonal version of the stabilization parameter neglects this crucial fact. These results are promising. Further tests on the new stabilization parameter require a generalization to multiple dimensions.

An expression for the purely advective multidimensional case can be derived via an analogous procedure. The orthonormalized transformation matrix from primitive variables to Elsässer variables is

$$\boldsymbol{\Upsilon} = \frac{1}{\sqrt{2}} \boldsymbol{\Psi} \tag{3.56}$$

where $\boldsymbol{\Psi}$ is the Elsässer transformation matrix,

$$\boldsymbol{\Psi} = \begin{bmatrix} \mathbf{I} & \mathbf{0} & \mathbf{I} & \mathbf{0} \\ \mathbf{0}^T & 1 & \mathbf{0}^T & 1 \\ \mathbf{I} & \mathbf{0} & -\mathbf{I} & \mathbf{0} \\ \mathbf{0}^T & 1 & \mathbf{0}^T & -1 \end{bmatrix}. \tag{3.57}$$

Thus, the expression for the non-diagonal stabilization matrix is

$$\boldsymbol{\tau} = \begin{bmatrix} \frac{1}{2}\left(\tau_1 + \tau_3\right)\mathbf{I} & \mathbf{0} & \frac{1}{2}\left(\tau_1 - \tau_3\right)\mathbf{I} & \mathbf{0} \\ \mathbf{0}^T & \frac{1}{2}\left(\tau_2 + \tau_4\right) & \mathbf{0}^T & \frac{1}{2}\left(\tau_2 - \tau_4\right) \\ \frac{1}{2}\left(\tau_1 - \tau_3\right)\mathbf{I} & \mathbf{0} & \frac{1}{2}\left(\tau_1 + \tau_3\right)\mathbf{I} & \mathbf{0} \\ \mathbf{0}^T & \frac{1}{2}\left(\tau_2 - \tau_4\right) & \mathbf{0}^T & \frac{1}{2}\left(\tau_2 + \tau_4\right) \end{bmatrix} \tag{3.58}$$

with

$$\tau_1 = \frac{h}{2|\mathbf{z}^-|} \tag{3.59}$$

$$\tau_2 = h|\mathbf{z}^-| \tag{3.60}$$

$$\tau_3 = \frac{h}{2|\mathbf{z}^+|} \tag{3.61}$$

$$\tau_4 = h|\mathbf{z}^+|. \tag{3.62}$$

3.3.2 Case 2: Adding in Diffusion

The transformations suggested in the previous section will not, in general, diagonalize the full MHD system. This significantly complicates matters when dealing with systems that involve both advection and diffusion. Applying the Elsässer transformation to the full MHD equations results in the following diffusion matrix,

$$
\mathbf{D} = \begin{bmatrix}
\frac{1}{2}\left(\nu + \lambda\right)\mathbf{I} & \mathbf{0} & \frac{1}{2}\left(\nu - \lambda\right)\mathbf{I} & \mathbf{0} \\
\mathbf{0}^T & 0 & \mathbf{0}^T & 0 \\
\frac{1}{2}\left(\nu - \lambda\right)\mathbf{I} & \mathbf{0} & \frac{1}{2}\left(\nu + \lambda\right)\mathbf{I} & \mathbf{0} \\
\mathbf{0}^T & 0 & \mathbf{0}^T & 0
\end{bmatrix}. \tag{3.63}
$$

Note that when the magnetic Prandtl number ($\mathrm{Pr}_\mathrm{m} = \nu/\lambda$) is unity the diffusion matrix is still diagonal. Therefore, (3.58) is still valid but with different definitions of the diagonal stabilization parameters. Building off of work on the stabilization parameter for the Navier-Stokes equations (see (3.17) and (Shakib, Hughes, and Johan 1991)), the diagonal stabilization parameters are

$$
\tau_1 = \frac{1}{\sqrt{\mathbf{z}^- \cdot \mathbf{G}\mathbf{z}^- + C_I\left(\lambda + \nu\right)^2 \mathbf{G} : \mathbf{G}}} \tag{3.64}
$$

$$
\tau_2 = \frac{1}{8\mathrm{tr}\left(\mathbf{G}\right)\tau_1} \tag{3.65}
$$

$$
\tau_3 = \frac{1}{\sqrt{\mathbf{z}^+ \cdot \mathbf{G}\mathbf{z}^+ + C_I\left(\lambda + \nu\right)^2 \mathbf{G} : \mathbf{G}}} \tag{3.66}
$$

$$
\tau_4 = \frac{1}{8\mathrm{tr}\left(\mathbf{G}\right)\tau_3}. \tag{3.67}
$$

We have tested this version of the non-diagonal stabilization parameter on the two-dimensional Hartmann flow problem. This problem involves the steady, two dimensional flow of an electrically conducting fluid in the presence of a uniform, background magnetic field in the wall-normal direction. The test case involved no-slip, impermeable boundary conditions with perfectly insulating walls. Thus, $u_x = u_y = 0$ at the top and bottom surfaces and the magnetic induction is $B_x = 0$

at the boundaries while $B_y = B_0$ at the boundaries. The solution to this problem is

$$u_x\left(y\right) = u_0\left(1 - \frac{\cosh\left(\text{Ha}y\right)}{\cosh\left(\text{Ha}\right)}\right) \tag{3.68}$$

$$B_x\left(y\right) = \frac{B_0 u_0}{\lambda}\frac{\tanh\left(Ha\right)}{\text{Ha}}\left(-y + \frac{\sinh\left(\text{Ha}y\right)}{\sinh\left(\text{Ha}\right)}\right). \tag{3.69}$$

In (3.68) and (3.69) y is the dimensionless wall-normal coordinate scaled by the channel half-width h. The results of the simulation are presented in Figures 3.5 and 3.6.
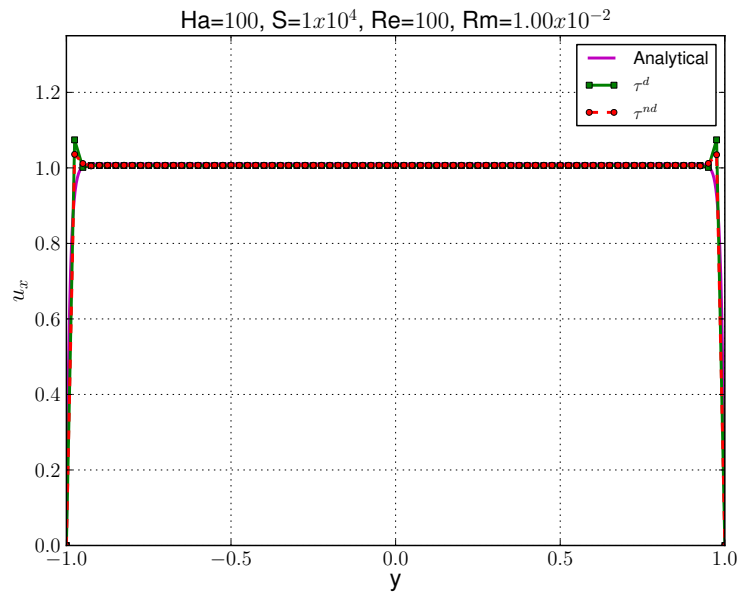
Figure 3.5: **The velocity field in the Hartmann problem. A comparison between the analytical solution and the simulations using diagonal and non-diagonal versions of the stabilization parameter.**

This simulation was performed at a relatively moderate value of Re which may be the reason that the stabilization matrices perform similarly. For this problem, it is also possible to show that for $\text{Pr}_\text{m} = 1$ the non-diagonal and diagonal stabilization matrices are the same; that is, the non-diagonal entries of the new stabilization parameter are zero. A simulation of decaying homogeneous, isotropic turbulence was also performed using a pseudospectral code but once again the results from the

simulations with different stabilization matrices were very similar indicating that there is no real advantage to the new non-diagonal stabilization matrix.
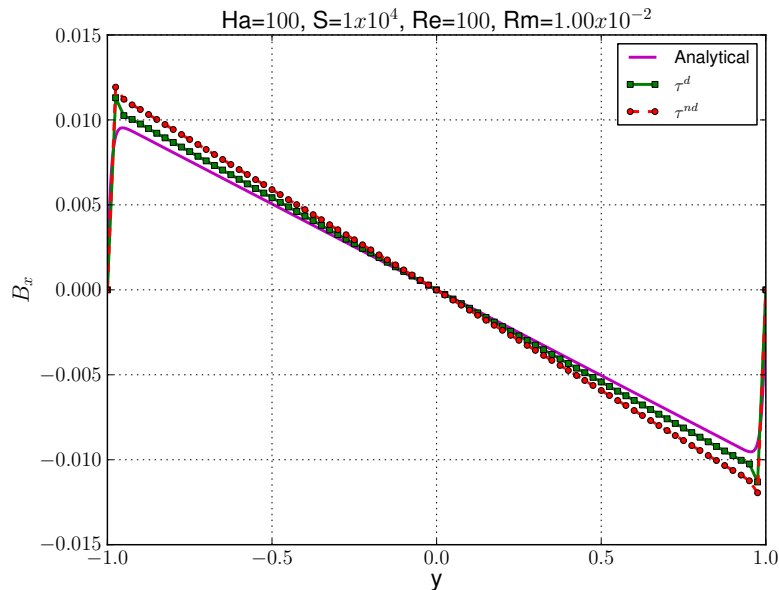
Figure 3.6: The magnetic field in the Hartmann problem. A comparison between the analytical solution and the simulations using diagonal and non-diagonal versions of the stabilization parameter is made.

With this in mind, it is instructive to consider the behavior of the non-diagonal stabilization matrix in various parameter limits. The arguments presented here are somewhat heuristic and should be placed on a firmer mathematical or numerical foundation. The contributions from the non-diagonal stabilization matrix to the momentum and induction equations are

$$\boldsymbol{\tau}^{\mathrm{VV}}\boldsymbol{\mathcal{R}}^{\mathrm{V}} + \boldsymbol{\tau}^{\mathrm{VI}}\boldsymbol{\mathcal{R}}^{\mathrm{I}} \quad \longrightarrow \quad \text{momentum equation contribution} \qquad (3.70)$$

$$\boldsymbol{\tau}^{\mathrm{IV}}\boldsymbol{\mathcal{R}}^{\mathrm{V}} + \boldsymbol{\tau}^{\mathrm{II}}\boldsymbol{\mathcal{R}}^{\mathrm{I}} \quad \longrightarrow \quad \text{induction equation contribution.} \qquad (3.71)$$

The momentum and induction residuals are most active when the numerical method is not able to capture all of the scales of the solutions, i.e. when $\mathrm{Re} \to \infty$ or $\mathrm{Rm} \to \infty$ or when both Reynolds numbers are very large simultaneously. When both fields exhibit turbulent behavior we can expect both residuals to play a role in the numerical

formulation. In the absence of the off-diagonal contributions from the stabilization matrix, only the momentum or induction residual will be active in their corresponding equations. A systematic study that demonstrates this behavior would consider a high Reynolds number flow field where both Reynolds numbers are large. A good starting point would be $\mathrm{Pr_m} = 1$. A quantitative analysis of the magnitude of the off diagonal terms of the stabilization matrix compared to the diagonal components would indicate the relative importance of the cross coupling of the residuals in the momentum and induction equations. We have begun such a study and results are pending. Also of interest is the effect of $\mathrm{Pr_m} \neq 1$. Such a situation may cause the momentum residual to be active in both equations while the induction residual is very small. Without a non-diagonal formulation the contribution to the induction equation from the momentum residual would go unnoticed.

3.3.3 Towards a Genuine Stabilization Parameter for MHD

A systematic diagonalization of the Burgers MHD system will be carried out in this section thereby leading to an expression for the non-diagonal stabilization parameter that is specific to MHD. The Burgers MHD equations have the advective diffusive form,

$$
\underbrace{\begin{bmatrix} u & -B \\ -B & u \end{bmatrix}}_{\mathbf{A}} \begin{bmatrix} u \\ B \end{bmatrix}_{,x} - \underbrace{\begin{bmatrix} \nu & 0 \\ 0 & \lambda \end{bmatrix}}_{\mathbf{D}} \begin{bmatrix} u \\ B \end{bmatrix}_{,xx} = \begin{bmatrix} 0 \\ 0 \end{bmatrix}. \tag{3.72}
$$

The GLS weak-form for this equation is

$$
-\left(\mathbf{W}_{,x}, \mathbf{A}\mathbf{U}\right) + \left(\boldsymbol{\mathcal{L}}\mathbf{W}, \boldsymbol{\tau}\boldsymbol{\mathcal{L}}\mathbf{U}\right) + \left(\mathbf{W}_{,x}, \mathbf{D}\mathbf{U}_{,x}\right) = 0 \tag{3.73}
$$

where

$$
\boldsymbol{\tau} = \begin{bmatrix} \tau^{\mathrm{VV}} & \tau^{\mathrm{VI}} \\ \tau^{\mathrm{IV}} & \tau^{\mathrm{II}} \end{bmatrix} \tag{3.74}
$$

and $\mathbf{W} = [w, \ c]^T$ is a vector of weighting functions. The Cholesky factorization of the diffusion matrix is

$$\mathbf{L} = \begin{bmatrix} \sqrt{\nu} & 0 \\ 0 & \sqrt{\lambda} \end{bmatrix}. \tag{3.75}$$

Applying to this equation the transformation given in (3.27) results in

$$-\left(\mathbf{Z}_{,x}, \widehat{\mathbf{A}}\mathbf{V}\right) + (\mathcal{L}\mathbf{Z}, \widehat{\tau}\mathcal{L}\mathbf{V}) + (\mathbf{Z}_{,x}, \mathbf{V}_{,x}) = 0 \tag{3.76}$$

where

$$\widehat{\mathbf{A}} = \begin{bmatrix} \frac{u}{\nu} & -\frac{B}{\sqrt{\nu\lambda}} \\ -\frac{B}{\sqrt{\nu\lambda}} & \frac{u}{\lambda} \end{bmatrix}. \tag{3.77}$$

The eigenvalues of $\widehat{\mathbf{A}}$ are

$$r_1 = r_f + r_b, \quad r_2 = r_f - r_b \tag{3.78}$$

where

$$r_f = \frac{u}{2\nu\lambda} \left(\frac{\text{Pr}_{\text{m}}^2 \lambda + \nu}{\text{Pr}_{\text{m}}} \right), \tag{3.79}$$

$$r_b = \frac{u}{2\lambda \text{Pr}_{\text{m}}} \sqrt{\text{Pr}_{\text{m}}^2 - 2\left(1 - \frac{2B^2}{u^2}\right)\text{Pr}_{\text{m}} + 1} \tag{3.80}$$

The corresponding eigenvector matrix is

$$\Upsilon = \begin{bmatrix} \frac{u-\lambda r_1}{B} & \frac{\text{Pr}_{\text{m}} P}{B\ell} \\ \sqrt{\text{Pr}_{\text{m}}} & -\frac{(u-\lambda r_1)P}{\ell} \end{bmatrix} \tag{3.81}$$

with

$$P = \frac{2\lambda r_b}{\left(u - \lambda r_1\right)^2 + \mathrm{Pr_m}} \tag{3.82}$$

and

$$\ell = P^2 \left[\left(\frac{\mathrm{Pr_m}}{B}\right)^2 + \left(u - \lambda r_1\right)^2\right]. \tag{3.83}$$

Finally, the expression for the stabilization matrix is,

$$\tau^{\mathrm{VV}} = \frac{\nu \tau_1}{B^2}\left(u - \lambda r_1\right)^2 + \frac{\nu \tau_2}{B^2}\left(\frac{\mathrm{Pr_m} P}{\ell}\right)^2 \tag{3.84}$$

$$\tau^{\mathrm{VI}} = \frac{\sqrt{\nu \lambda \mathrm{Pr_m}}\,\tau_1}{B}\left(u - \lambda r_1\right) - \frac{\sqrt{\nu \lambda \mathrm{Pr_m^2}}}{B}\left(u - \lambda r_1\right)\left(\frac{P}{\ell}\right)^2 \tag{3.85}$$

$$\tau^{\mathrm{IV}} = \frac{\sqrt{\nu \lambda \mathrm{Pr_m}}\,\tau_2}{B} - \frac{\sqrt{\nu \lambda \mathrm{Pr_m^2}}}{B}\left(u - \lambda r_1\right)\left(\frac{P}{\ell}\right)^2 \tag{3.86}$$

$$\tau^{\mathrm{II}} = \tau_1 \lambda \mathrm{Pr_m} + \tau_2 \lambda \left(\frac{P\left(u - \lambda r_1\right)^2}{\ell}\right). \tag{3.87}$$

This version of the stabilization parameter has not yet been implemented and tested. However, a few observations can be made based on the form of the components of the stabilization matrix. First of all, the dependence on $\mathrm{Pr_m}$ is a desirable property as it helps account for situations when one field dominates over the other. Such a situation arises frequently in MHD systems such as channel flow simulations of a liquid metal or astrophysical simulations of stars. A drawback of this model may be that it is somewhat cumbersome to implement. Numerical tests will help to highlight the feasibility of this expression.

CHAPTER 4
New Contributions to MHD Turbulence Modeling

This chapter presents the major contributions of this work. Section 4.1 seeks to place the new models in context and to this end provides an overview of the classical eddy viscosity approach to turbulence modeling. Section 4.2 presents new LES models derived from the VMS formulation. Following this a new type of EV model is introduced in Section 4.3. The chapter closes with Section 4.4 by presenting a mixed model (MM) that seeks to encompass the strengths of both the VMS-derived models and the new eddy viscosity model.

4.1 Classical Eddy Viscosity Models

This section introduces the eddy viscosity concept. The numerical approximation to the filtered equations in Section 2.7.1 written in a variational form is

$$\mathcal{A}\left(\mathbf{W}^h, \mathbf{U}^h\right) - \left(\nabla \mathbf{w}^h, \boldsymbol{\mathfrak{T}}^{\mathrm{V}}\right) - \left(\nabla \mathbf{c}^h, \boldsymbol{\mathfrak{T}}^{\mathrm{I}}\right) = \left(\mathbf{w}^h, \mathbf{f}^{\mathrm{V}}\right) + \left(\mathbf{c}^h, \mathbf{f}^{\mathrm{I}}\right). \qquad (4.1)$$

In practice, this problem is replaced by

$$\mathcal{A}\left(\mathbf{W}^h, \mathbf{U}^h\right) + \mathcal{M}\left(\mathbf{W}^h, \mathbf{U}^h; h, \mathbf{c}_P\right) = \left(\mathbf{w}^h, \mathbf{f}^{\mathrm{V}}\right) + \left(\mathbf{c}^h, \mathbf{f}^{\mathrm{I}}\right) \qquad (4.2)$$

where

$$\mathcal{M}\left(\mathbf{W}^h, \mathbf{U}^h; h, \mathbf{c}_P\right) = \mathcal{M}_{\mathrm{V}}\left(\mathbf{w}^h, \mathbf{U}^h; h, \mathbf{c}_P^{\mathrm{V}}\right) + \mathcal{M}_{\mathrm{I}}\left(\mathbf{c}^h, \mathbf{U}^h; h, \mathbf{c}_P^{\mathrm{I}}\right) \qquad (4.3)$$

is a model that approximates the terms with the subgrid stress tensors and $\mathbf{c}_P^{\mathrm{V,I}}$ represent model parameters for the momentum and induction equation, respectively. The central structures that are modeled are the subgrid stress tensors $\boldsymbol{\mathfrak{T}}^{\mathrm{V}}$ and $\boldsymbol{\mathfrak{T}}^{\mathrm{I}}$.

The subgrid stress tensor in the momentum equation has a long and rich history.

Remarks:

(4.1) was stated to be the numerical approximation to the filtered equations. However, if a projection operator was applied to the MHD equations and a numerical solution was used to approximate the solution to the projected fields, the notation would be the same as in (4.1).

Boussinesq was the first to propose a turbulent eddy viscosity as a mechanism for turbulent transport (see Schmitt 2007, for some history). This concept was made via analogy with the concept of classical molecular viscosity μ which characterizes the amount of momentum that is transported between neighboring fluid elements. The idea of the turbulent eddy viscosity essentially considers a fluid eddy as a basic fluid structure with momentum transported between eddies in a turbulent flow field. Although this idea has limited use in developing a phenomenological theory of turbulence, it has enjoyed immense popularity in the numerical community. In this section, an overview of the turbulent eddy diffusivity idea applied to MHD is discussed.

Remarks:

The turbulent viscosity is not a property of the fluid but a property of the flow field.

The goal behind the eddy diffusivity is to relate the subgrid stress tensor to characteristic properties of the flow field such as the velocity field and the magnetic induction. In the case of numerical simulations, the characteristic properties of the flow field are the computed numerical quantities. Through analogy with the traditional stress tensor the subgrid stress tensor is approximated as

$$\boldsymbol{\mathcal{T}}^{\mathrm{V}} \approx -2\nu_T \nabla^{\mathrm{s}} \mathbf{u}^h \tag{4.4}$$

The induction equation induces a turbulent magnetic diffusivity, λ_T which results in a subgrid stress tensor of

$$\boldsymbol{\mathcal{T}}^{\mathrm{I}} \approx -2\lambda_T \nabla^{\mathrm{a}} \mathbf{B}^h. \tag{4.5}$$

From an analytical and numerical standpoint modeling the subgrid stress tensor with a turbulent eddy viscosity model is very convenient. This is because the form of the equations is essentially unchanged and therefore no new mathematical operators are introduced into the equations and the numerical implementation is straightforward.

Remarks:

Sophisticated subgrid stress tensor closures were derived by (Yoshizawa 1990) for the Reynolds averaged MHD equations. However, these models are unwieldy to implement from a numerical standpoint.

Remarks:

The diffusivities are represented as scalars. In general, the diffusivities are matrices. However, for an isotropic fluid the diffusivities are scalar quantities.

This is not the whole story, however. In order to close the equations, expressions for the turbulent diffusivities are still required. One of the first closure models for fluid dynamics was provided by (Prandtl 1925a). In this model, the turbulent eddy viscosity is proportional to a characteristic velocity scale via the mixing length, ℓ_{V}. A modern version of this hypothesis is presented in (Pope 2000):

$$\mu_T \approx \rho \ell_{\mathrm{V}}^2 \left| 2\nabla^s \mathbf{u}^h \right|. \tag{4.6}$$

Similarly, in (Theobald, Fox, and Sofia 1994) the turbulent magnetic diffusivity satisfies an equation similar to,

$$\lambda_T \approx \ell_{\mathrm{I}}^2 \left| \sqrt{\frac{\mu_0}{\rho}} \mathbf{j}^h \right|. \tag{4.7}$$

Remarks:

- The expression for the turbulent magnetic diffusivity can be found via analogy with the Drude model for resistivity in electrodynamics. This is done in Section 4.3.1.

- In the expression for the turbulent viscosity μ_T we use the notation

$$|\mathbf{A}| = \sqrt{\mathbf{A} : \mathbf{A}} \tag{4.8}$$

for the matrix $\mathbf{A}$.

To complete the closure, an expression for the mixing length is needed. The Smagorinsky mixing length was proposed by (Smagorinsky 1963). It postulates that the mixing length is proportional to the filter width. Typically, the filter width is equal to the spacing between the grid points, h. Thus,

$$\ell_V \approx \sqrt{C_S^V}\, h, \tag{4.9}$$

$$\ell_I \approx \sqrt{C_S^I}\, h. \tag{4.10}$$

The classical closure models for the incompressible MHD equations are therefore,

$$\boldsymbol{\mathcal{T}}^V \approx -2C_S^V h^2 \left| 2\nabla^s \mathbf{u}^h \right| \nabla^s \mathbf{u}^h \tag{4.11}$$

$$\boldsymbol{\mathcal{T}}^I \approx -2C_S^I h^2 \left| \sqrt{\frac{\mu_0}{\rho}}\, \mathbf{j}^h \right| \nabla^a \mathbf{B}^h. \tag{4.12}$$

The coefficients of proportionality are called the Smagorinsky coefficients. Ideally, they would be constant but experience has shown that this is not at all the case. There are also instances in which these coefficients are negative. Such cases correspond to the phenomenon of backscatter. Using (4.11) and (4.12) in (4.1) results in the variational form,

$$\mathcal{A}\left(\mathbf{W}^h, \mathbf{U}^h\right) + \left(\nabla \mathbf{w}^h, 2C_S^V h^2 \left| 2\nabla^s \mathbf{u}^h \right| \nabla^s \mathbf{u}^h\right)$$
$$+ \left(\nabla \mathbf{c}^h, 2C_S^I h^2 \left| \sqrt{\frac{\mu_0}{\rho}}\, \mathbf{j}^h \right| \nabla^a \mathbf{B}^h\right) = \left(\mathbf{w}^h, \mathbf{f}^V\right) + \left(\mathbf{c}^h, \mathbf{f}^I\right). \tag{4.13}$$

Note that in (4.13) the model terms are given by,

$$\mathcal{M}_V\left(\mathbf{w}^h, \mathbf{U}^h; h, \mathbf{c}_P^V\right) = \left(\nabla \mathbf{w}^h, 2C_S^V\left(h\right) \left| 2\nabla^s \mathbf{u}^h \right| \nabla^s \mathbf{u}^h\right) \tag{4.14}$$

$$\mathcal{M}_I\left(\mathbf{c}^h, \mathbf{U}^h; h, \mathbf{c}_P^I\right) = \left(\nabla \mathbf{c}^h, 2C_S^I\left(h\right) \left| \sqrt{\frac{\mu_0}{\rho}}\, \mathbf{j}^h \right| \nabla^a \mathbf{B}^h\right) \tag{4.15}$$

where the original Smagorinsky coefficients have been replaced by the mesh-dependent Smagorinsky coefficients,

$$C_S^V h^2 \longrightarrow C_S^V (h) \tag{4.16}$$

$$C_S^I h^2 \longrightarrow C_S^I (h) . \tag{4.17}$$

The only thing left to do is to determine the Smagorinsky coefficients C_S^V and C_S^I. In general this is not a trivial task and considerable work over the years has focused on determining their correct value. Treating the Smagorinsky coefficients as universal constants would require them be tuned for every simulation that is performed. This is a highly ineffective and undesirable way to operate. An inspired way of determining the Smagorinsky coefficients during a simulation was introduced by (Germano et al. 1991) and is referred to as the Germano identity. Using the Germano identity with Smagorinsky's mixing length results in the dynamic Smagorinsky EV (DSEV) model. The variational counterpart to the Germano identity was introduced in (Oberai and Wanderer 2005). In the next section, the variational Germano identity will be used to determine the Smagorinsky coefficients for MHD.

4.1.1 Variational Germano Identity for MHD

The Germano identity is a relationship between the scales of a problem. This relationship has a physical basis in turbulence due to the self-similarity of the small scales (i.e. the scales that are to be modeled). A brief summary of the Germano identity is now presented.

1. Consider the problem on two grids, h and H, where $H > h$ and the solution is desired on the $h-$grid.

2. **Assume that the form of the model is the same on each grid.** This assumption is critical and is attributed to the self-similarity of turbulence at small scales.

3. Project the $h-$grid problem onto the $H-$grid.

4. Subtracting the projected $h-$grid problem from the original $H-$grid problem gives constraints on a model parameter.

The following discussion is a specialization of the more general theory worked out by (Oberai and Wanderer 2005). To put these points into mathematical language a hierarchy of nested function spaces is introduced such that $\mathcal{V}^H \subset \mathcal{V}^h \subset \mathcal{V}$. The variational statement on the $h-$grid is: *Find* $\mathbf{U}^h \in \mathcal{V}^h$ *s.t.* $\forall\ \mathbf{W}^h \in \mathcal{V}^h$

$$\mathcal{A}\left(\mathbf{W}^h, \mathbf{U}^h\right) + \mathcal{M}\left(\mathbf{W}^h, \mathbf{U}^h; h, \mathbf{c}_P\right) = \left(\mathbf{w}^h, \mathbf{f}^V\right) + \left(\mathbf{c}^h, \mathbf{f}^I\right) \tag{4.18}$$

and the corresponding problem on the $H-$ grid is: *Find* $\mathbf{U}^H \in \mathcal{V}^H$ *s.t.* $\forall\ \mathbf{W}^H \in \mathcal{V}^H$

$$\mathcal{A}\left(\mathbf{W}^H, \mathbf{U}^H\right) + \mathcal{M}\left(\mathbf{W}^H, \mathbf{U}^H; H, \mathbf{c}_P\right) = \left(\mathbf{w}^H, \mathbf{f}^V\right) + \left(\mathbf{c}^H, \mathbf{f}^I\right). \tag{4.19}$$

Due to the fact that the weighting functions are arbitrary, and because of the nested function spaces, it is permissible to choose $\mathbf{W}^h = \mathbf{W}^H$. Making this substitution corresponds to projecting the $h-$grid equation to the $H-$grid. At this point, the two equations are subtracted to arrive at the variational form of the Germano identity.

$$\mathcal{M}\left(\mathbf{W}^H, \mathbf{U}^H; H, \mathbf{c}_P\right) - \mathcal{M}\left(\mathbf{W}^h, \mathbf{U}^h; h, \mathbf{c}_P\right)$$
$$= -\left(\mathcal{A}\left(\mathbf{W}^H, \mathbf{U}^H\right) - \mathcal{A}\left(\mathbf{W}^h, \mathbf{U}^h\right)\right). \tag{4.20}$$

If it assumed that the numerical solutions on both scales, h and H, are optimal then $\mathbf{U}^h = \mathbb{P}^h \mathbf{U}$ and $\mathbf{U}^H = \mathbb{P}^H \mathbf{U}$. Further assuming that $\mathbb{P}^H \mathbb{P}^h = \mathbb{P}^H$ it is possible to write $\mathbf{U}^H = \mathbb{P}^H \mathbf{U}^h$ in (4.20). The result is then a set of equations that involve only the numerical solution $\mathbf{U}^h$, and its projection $\mathbb{P}^H$. This can be used to determine the unknown parameters $\mathbf{c}_P$.

This procedure is further specialized to the MHD equations below. It is assumed that the mesh parameters are related via,

$$H = \alpha h, \quad \alpha \in \mathbb{Z}, \quad \alpha > 1. \tag{4.21}$$

This allows $C_S^{\mathrm{V,I}}(H)$ to be written in terms of $C_S^{\mathrm{V,I}}(h)$,

$$C_S^{\mathrm{V,I}}(H) = \alpha^2 C_S^{\mathrm{V,I}}(h). \tag{4.22}$$

Before proceeding, it is noted that the Smagorinsky coefficients find themselves in different equations (i.e. C_S^{V} is multiplying $\mathbf{w}^h$ while C_S^{I} is multiplying $\mathbf{c}^h$). With this in mind, and exploiting the arbitrariness of the weighting functions, the two Smagorinsky coefficients are determined separately. C_S^{V} is determined first by choosing $\mathbf{W}^h = \left[\mathbf{w}^h,\, q^h,\, 0,\, 0\right]^T$ which allows the focus to be solely on the momentum equation. Then,

$$\left(\mathbf{w}^h, \frac{\partial \mathbf{u}^h}{\partial \mathrm{t}}\right) - \left(\nabla \mathbf{w}^h, \mathcal{N}_h^{\mathrm{V}}\right) + 2C_S^V(h)\left(\nabla^{\mathrm{s}}\mathbf{w}^h, \left|2\nabla^{\mathrm{s}}\mathbf{u}^h\right|\nabla^{\mathrm{s}}\mathbf{u}^h\right)$$
$$- \left(\nabla \cdot \mathbf{w}^h, P^h\right) + \nu\left(\nabla^{\mathrm{s}}\mathbf{w}^h, \nabla^{\mathrm{s}}\mathbf{u}^h\right) - \left(\nabla q^h, \mathbf{u}^h\right) = 0. \tag{4.23}$$

On the H grid,

$$\left(\mathbf{w}^H, \frac{\partial \mathbf{u}^H}{\partial \mathrm{t}}\right) - \left(\nabla \mathbf{w}^H, \mathcal{N}_H^{\mathrm{V}}\right) + 2\alpha^2 C_S^V(h)\left(\nabla^{\mathrm{s}}\mathbf{w}^H, \left|2\nabla^{\mathrm{s}}\mathbf{u}^H\right|\nabla^{\mathrm{s}}\mathbf{u}^H\right)$$
$$- \left(\nabla \cdot \mathbf{w}^H, P^H\right) + \nu\left(\nabla^{\mathrm{s}}\mathbf{w}^H, \nabla^{\mathrm{s}}\mathbf{u}^H\right) - \left(\nabla q^H, \mathbf{u}^H\right) = 0. \tag{4.24}$$

Choosing $\mathbf{W}^h = \mathbf{W}^H$ and subtracting the h equation from the H equation results in

$$- \left(\nabla \mathbf{w}^H, \mathcal{N}_H^{\mathrm{V}} - \mathcal{N}_h^{\mathrm{V}}\right) - 2C_S^V(h)\times$$
$$\left[-\alpha^2\left(\nabla^{\mathrm{s}}\mathbf{w}^H, \left|2\nabla^{\mathrm{s}}\mathbf{u}^H\right|\nabla^{\mathrm{s}}\mathbf{u}^H\right) + \left(\nabla^{\mathrm{s}}\mathbf{w}^H, \left|2\nabla^{\mathrm{s}}\mathbf{u}^h\right|\nabla^{\mathrm{s}}\mathbf{u}^h\right)\right] = 0.$$

Note that the linear terms vanish. This is demonstrated on the pressure term,

$$- \left(\nabla \cdot \mathbf{w}^H, P^H\right) + \left(\nabla \cdot \mathbf{w}^H, P^h\right) = -\left(\nabla \cdot \mathbf{w}^H, \left(P^H - P^h\right)\right)$$
$$= -\left(\nabla \cdot \mathbf{w}^H, \mathbb{P}'_H P^h\right)$$
$$= 0$$

where $\mathbb{P}'_H$ is the projection onto the subgrid scales corresponding to the $H-$grid. The last line follows because $\mathbb{P}'_H$ does not live on the $H-$grid while $\mathbf{w}^H$ lives only on the $H-$grid. Hence, they are orthogonal and therefore their inner product is zero. The other linear terms are similar.

Remarks:

The nonlinear terms do not cancel due to the multiplications that occur within them. Because of these multiplications, information from the $H-$grid can cascade to scales represented by the $h-$grid and their difference is not guaranteed to be solely on the subgrid scales corresponding to the $H-$grid.

Solving for $C_S^V(h)$ gives

$$\boxed{C_S^V(h) = \frac{1}{2}\frac{\left(\nabla\mathbf{w}^H,\mathcal{N}_H^V\right) - \left(\nabla\mathbf{w}^H,\mathcal{N}_h^V\right)}{\alpha^2\left(\nabla^s\mathbf{w}^H,|2\nabla^s\mathbf{u}^H|\nabla^s\mathbf{u}^H\right) - \left(\nabla^s\mathbf{w}^H,|2\nabla^s\mathbf{u}^h|\nabla^s\mathbf{u}^h\right)}.} \tag{4.25}$$

Now the same analysis is performed by choosing $\mathbf{W}^h = \begin{bmatrix}0, & 0, & \mathbf{c}^h, & s^h\end{bmatrix}^T$ which allows the determination of C_S^I. This leads to

$$\left(\mathbf{c}^h, \frac{\partial\mathbf{B}^h}{\partial t}\right) - \left(\nabla\mathbf{c}^h, \mathcal{N}_h^I\right) + 2C_S^I(h)\left(\nabla^a\mathbf{c}^h, \left|\sqrt{\frac{\mu_0}{\rho}}\mathbf{j}^h\right|\nabla^a\mathbf{B}^h\right)$$

$$- \left(\nabla\cdot\mathbf{c}^h, r^h\right) + \lambda\left(\nabla^a\mathbf{c}^h, \nabla^a\mathbf{B}^h\right) - \left(\nabla s^h, \mathbf{B}^h\right) = 0.$$

On the H grid,

$$\left(\mathbf{c}^H, \frac{\partial\mathbf{B}^H}{\partial t}\right) - \left(\nabla\mathbf{c}^H, \mathcal{N}_H^I\right) + 2\alpha^2 C_S^I(H)\left(\nabla^a\mathbf{c}^H, \left|\sqrt{\frac{\mu_0}{\rho}}\mathbf{j}^H\right|\nabla^a\mathbf{B}^H\right)$$

$$- \left(\nabla\cdot\mathbf{c}^H, r^H\right) + \lambda\left(\nabla^a\mathbf{c}^H, \nabla^a\mathbf{B}^H\right) - \left(\nabla s^H, \mathbf{B}^H\right) = 0.$$

The equations on different grids are subtracted to give

$$- \left(\nabla\mathbf{c}^H, \mathcal{N}_H^I - \mathcal{N}_h^I\right) + \left(\nabla\mathbf{c}^H, \mathcal{N}_h^I\right) - 2C_S^I(h)\times$$

$$\left[-\alpha^2\left(\nabla^a\mathbf{c}^H, \left|\sqrt{\frac{\mu_0}{\rho}}\mathbf{j}^H\right|\nabla^a\mathbf{B}^H\right) + \left(\nabla^a\mathbf{c}^H, \left|\sqrt{\frac{\mu_0}{\rho}}\mathbf{j}^h\right|\nabla^a\mathbf{B}^h\right)\right].$$

Solving for $C_S^{\mathrm{I}}(h)$ yields

$$C_S^{\mathrm{I}}(h) = \frac{1}{2} \frac{\left(\nabla \mathbf{c}^H, \boldsymbol{\mathcal{N}}_H^{\mathrm{I}}\right) - \left(\nabla \mathbf{c}^H, \boldsymbol{\mathcal{N}}_h^{\mathrm{I}}\right)}{\alpha^2 \left(\nabla^{\mathsf{a}} \mathbf{c}^H, \left|\sqrt{\frac{\mu_0}{\rho}} \mathbf{j}^H\right| \nabla^{\mathsf{a}} \mathbf{B}^H\right) - \left(\nabla^{\mathsf{a}} \mathbf{c}^H, \left|\sqrt{\frac{\mu_0}{\rho}} \mathbf{j}^h\right| \nabla^{\mathsf{a}} \mathbf{B}^h\right)}. \tag{4.26}$$

4.1.2 Alignment-based Dynamic Smagorinsky Model

This section concludes by introducing a new type of Smagorinsky model that was developed specifically for MHD in (Müller and Carati 2002). The goal of this model is to circumvent the issue that classical EV models preclude inverse cascades of energy. It is especially desirable to have a model that can account for this behavior since the inverse energy cascade is important in MHD. The model for the eddy viscosities that was introduced is:

$$\nu_T = C_S^{\mathrm{V}} h^2 \sqrt{\mathrm{abs}\left(\nabla^{\mathsf{s}} \mathbf{u}^h : \frac{1}{\sqrt{\mu_0 \rho}} \nabla^{\mathsf{s}} \mathbf{B}^h\right)} \tag{4.27}$$

$$\lambda_T = C_S^{\mathrm{I}} h^2 \mathrm{sgn}\left(\mathbf{j}^h \cdot \boldsymbol{\omega}^h\right) \sqrt{\mathrm{abs}\left(\sqrt{\frac{\mu_0}{\rho}} \mathbf{j}^h \cdot \boldsymbol{\omega}^h\right)} \tag{4.28}$$

where $\mathrm{sgn}\,(\cdot)$ gives the sign of its argument, $\mathrm{abs}\,(\cdot)$ gives the absolute value of its argument, and $\boldsymbol{\omega}^h = \nabla \times \mathbf{u}^h$ is the fluid vorticity. This model was derived by considering the dissipation in the cross-helicity equation. The dissipation associated with the terms from the momentum equation is proportional to the tensor inner product of the symmetric gradients of the velocity and magnetic fields. The cross helicity dissipation due to the terms in the induction equation is proportional to the vector dot product of the current density and fluid vorticity fields. We refer to this model as the alignment-based dynamic Smagorinsky (DSEVA) model. The reason for this terminology emanates from the magnetic diffusivity in (4.28). The turbulent magnetic diffusivity is largest when the current density and vorticity are aligned. This model also has the potential to act as an energy source. The model has been designed so that when the fields are aligned it acts as an energy sink and when the fields are anti-aligned it acts as an energy source. This is consistent with the local MHD physics. The local cross-helicity dissipation dictates the direction of

energy transfer. The sgn function in (4.28) accounts for the sign of the cross helicity dissipation due to the induction equation.

4.2 Variational Multiscale Formulation for MHD

The VMS formulation is now specialized to incompressible MHD. The general idea of the VMS formulation was introduced in Section 2.7.2. For MHD the fields are decomposed as

$$\mathbf{u} = \mathbf{u}^h + \mathbf{u}', \qquad P = P^h + P' \tag{4.29}$$

$$\mathbf{B} = \mathbf{B}^h + \mathbf{B}', \qquad r = r^h + r' \tag{4.30}$$

and the weighting functions as

$$\mathbf{w} = \mathbf{w}^h + \mathbf{w}', \qquad q = q^h + q' \tag{4.31}$$

$$\mathbf{c} = \mathbf{c}^h + \mathbf{c}', \qquad s = s^h + s'. \tag{4.32}$$

Introducing this decomposition into the variational form (2.184) results in

$$
\begin{aligned}
\mathcal{A}^{\mathrm{V}}\left(\mathbf{W}^h, \mathbf{U}^h\right) &- \left(\nabla \mathbf{w}^h, \boldsymbol{\mathcal{N}}_C^{\mathrm{V}} + \boldsymbol{\mathcal{N}}_R^{\mathrm{V}}\right) - \left(\nabla \cdot \mathbf{w}^h, P'\right) \\
&+ \left(\nabla^{\mathrm{s}} \mathbf{w}^h, 2\nu \nabla^{\mathrm{s}} \mathbf{u}'\right) - \left(\nabla q^h, \mathbf{u}'\right) \\
+\mathcal{A}^{\mathrm{V}}\left(\mathbf{W}', \mathbf{U}^h\right) &- \left(\nabla \mathbf{w}', \boldsymbol{\mathcal{N}}_C^{\mathrm{V}} + \boldsymbol{\mathcal{N}}_R^{\mathrm{V}}\right) - \left(\nabla \cdot \mathbf{w}', P'\right) \\
&+ \left(\nabla^{\mathrm{s}} \mathbf{w}', 2\nu \nabla^{\mathrm{s}} \mathbf{u}'\right) - \left(\nabla q', \mathbf{u}'\right) \\
+\mathcal{A}^{\mathrm{I}}\left(\mathbf{W}^h, \mathbf{U}^h\right) &- \left(\nabla \mathbf{c}^h, \boldsymbol{\mathcal{N}}_C^{\mathrm{I}} + \boldsymbol{\mathcal{N}}_R^{\mathrm{I}}\right) - \left(\nabla \cdot \mathbf{c}^h, r'\right) \\
&+ \left(\nabla^{\mathrm{a}} \mathbf{c}^h, 2\lambda \nabla^{\mathrm{a}} \mathbf{B}'\right) - \left(\nabla s^h, \mathbf{B}'\right) \\
+\mathcal{A}^{\mathrm{I}}\left(\mathbf{W}', \mathbf{U}^h\right) &- \left(\nabla \mathbf{c}', \boldsymbol{\mathcal{N}}_C^{\mathrm{I}}\right) - \left(\nabla \cdot \mathbf{c}', r'\right) \\
&+ \left(\nabla^{\mathrm{a}} \mathbf{c}', 2\lambda \nabla^{\mathrm{a}} \mathbf{B}'\right) - \left(\nabla s', \mathbf{B}'\right) \\
= \left(\mathbf{w}^h, \mathbf{f}^{\mathrm{V}}\right) &+ \left(\mathbf{c}^h, \mathbf{f}^{\mathrm{I}}\right) + \left(\mathbf{w}', \mathbf{f}^{\mathrm{V}}\right) + \left(\mathbf{c}', \mathbf{f}^{\mathrm{I}}\right).
\end{aligned}
\tag{4.33}
$$

In (4.33) the cross stresses for the momentum and induction equation are defined respectively as

$$\boldsymbol{\mathcal{N}}_C^{\mathrm{V}} = \boldsymbol{\mathcal{N}}_C^{\mathrm{V}}\left(\mathbf{U}^h, \mathbf{U}'\right) = \left(\mathbf{u}^h \otimes \mathbf{u}' + \mathbf{u}' \otimes \mathbf{u}^h\right) - \frac{1}{\mu_0 \rho}\left(\mathbf{B}^h \otimes \mathbf{B}' + \mathbf{B}' \otimes \mathbf{B}^h\right) \quad (4.34)$$

$$\boldsymbol{\mathcal{N}}_C^{\mathrm{I}} = \boldsymbol{\mathcal{N}}_C^{\mathrm{I}}\left(\mathbf{U}^h, \mathbf{U}'\right) = -\left(\mathbf{u}^h \otimes \mathbf{B}' + \mathbf{B}' \otimes \mathbf{u}^h\right) + \left(\mathbf{B}^h \otimes \mathbf{u}' + \mathbf{u}' \otimes \mathbf{B}^h\right) \quad (4.35)$$

while

$$\boldsymbol{\mathcal{N}}_R^{\mathrm{V}} = \boldsymbol{\mathcal{N}}_R^{\mathrm{V}}\left(\mathbf{U}^h, \mathbf{U}'\right) = \left(\mathbf{u}' \otimes \mathbf{u}'\right) - \frac{1}{\mu_0 \rho}\left(\mathbf{B}' \otimes \mathbf{B}'\right) \quad (4.36)$$

$$\boldsymbol{\mathcal{N}}_R^{\mathrm{I}} = \boldsymbol{\mathcal{N}}_R^{\mathrm{I}}\left(\mathbf{U}^h, \mathbf{U}'\right) = -\left(\mathbf{u}' \otimes \mathbf{B}'\right) + \left(\mathbf{B}' \otimes \mathbf{u}'\right) \quad (4.37)$$

define the Reynolds stress contributions to the momentum and induction equations respectively. The term "Reynolds stresses" is a relic from classical turbulence modeling vernacular. In fact, these terms are not strictly Reynolds stresses because they are not the result of the Reynolds-averaged approach. We refer to these terms as Reynolds stresses and subgrid correlations interchangeably in this work. The form (4.33) actually represents two problems on two different scales. Thus, the two variational statements are: *Find* $\mathbf{U}^h \in \boldsymbol{\mathcal{V}}^h$ *s.t.* $\forall \, \mathbf{W}^h \in \boldsymbol{\mathcal{V}}^h$

$$\begin{aligned}
\mathcal{A}^{\mathrm{V}}\left(\mathbf{W}^h, \mathbf{U}^h\right) &- \left(\nabla \mathbf{w}^h, \boldsymbol{\mathcal{N}}_C^{\mathrm{V}} + \boldsymbol{\mathcal{N}}_R^{\mathrm{V}}\right) - \left(\nabla \cdot \mathbf{w}^h, P'\right) \\
&+ \left(\nabla^{\mathrm{s}} \mathbf{w}^h, 2\nu \nabla^{\mathrm{s}} \mathbf{u}'\right) - \left(\nabla q^h, \mathbf{u}'\right) \\
+\mathcal{A}^{\mathrm{I}}\left(\mathbf{W}^h, \mathbf{U}^h\right) &- \left(\nabla \mathbf{c}^h, \boldsymbol{\mathcal{N}}_C^{\mathrm{I}} + \boldsymbol{\mathcal{N}}_R^{\mathrm{I}}\right) - \left(\nabla \cdot \mathbf{c}^h, r'\right) \\
&+ \left(\nabla^{\mathrm{a}} \mathbf{c}^h, 2\lambda \nabla^{\mathrm{a}} \mathbf{B}'\right) - \left(\nabla s^h, \mathbf{B}'\right) \\
= \left(\mathbf{w}^h, \mathbf{f}^{\mathrm{V}}\right) &+ \left(\mathbf{c}^h, \mathbf{f}^{\mathrm{I}}\right)
\end{aligned} \quad (4.38)$$

and *Find* $\mathbf{U}' \in \boldsymbol{\mathcal{V}}'$ *s.t.* $\forall \mathbf{W}' \in \boldsymbol{\mathcal{V}}'$

$$\mathcal{A}^{\mathrm{V}}\left(\mathbf{W}', \mathbf{U}^h\right) - \left(\nabla\mathbf{w}', \boldsymbol{\mathcal{N}}_C^{\mathrm{V}} + \boldsymbol{\mathcal{N}}_R^{\mathrm{V}}\right) - \left(\nabla \cdot \mathbf{w}', P'\right)$$
$$+ \left(\nabla^{\mathrm{s}}\mathbf{w}', 2\nu\nabla^{\mathrm{s}}\mathbf{u}'\right) - \left(\nabla q', \mathbf{u}'\right)$$
$$+ \mathcal{A}^{\mathrm{I}}\left(\mathbf{W}', \mathbf{U}^h\right) - \left(\nabla\mathbf{c}', \boldsymbol{\mathcal{N}}_C^{\mathrm{I}} + \boldsymbol{\mathcal{N}}_R^{\mathrm{I}}\right) - \left(\nabla \cdot \mathbf{c}', r'\right)$$
$$+ \left(\nabla^{\mathsf{a}}\mathbf{c}', 2\lambda\nabla^{\mathsf{a}}\mathbf{B}'\right) - \left(\nabla s', \mathbf{B}'\right)$$
$$= \left(\mathbf{w}', \mathbf{f}^{\mathrm{V}}\right) + \left(\mathbf{c}', \mathbf{f}^{\mathrm{I}}\right). \tag{4.39}$$

The solution to (4.39) is approximated by (2.263) as

$$\begin{bmatrix} \mathbf{u}' \\ P' \\ \mathbf{B}' \\ r' \end{bmatrix} \approx -\mathbb{P}'\boldsymbol{\tau}\mathbb{P}'^T \begin{bmatrix} \boldsymbol{\mathcal{R}}^{\mathrm{V}}\left(\mathbf{U}^h\right) \\ \nabla \cdot \mathbf{u}^h \\ \boldsymbol{\mathcal{R}}^{\mathrm{I}}\left(\mathbf{U}^h\right) \\ \nabla \cdot \mathbf{B}^h \end{bmatrix} \tag{4.40}$$

where

$$\boldsymbol{\mathcal{R}}^{\mathrm{V}}\left(\mathbf{U}^h\right) = \frac{\partial \mathbf{u}^h}{\partial \mathsf{t}} + \nabla \cdot \boldsymbol{\mathcal{N}}^{\mathrm{V}}\left(\mathbf{u}^h, \mathbf{B}^h\right) + \nabla P^h - \nu\nabla^2\mathbf{u}^h - \mathbf{f}^{\mathrm{V}} \tag{4.41}$$

$$\boldsymbol{\mathcal{R}}^{\mathrm{I}}\left(\mathbf{U}^h\right) = \frac{\partial \mathbf{B}^h}{\partial \mathsf{t}} + \nabla \cdot \boldsymbol{\mathcal{N}}^{\mathrm{I}}\left(\mathbf{u}^h, \mathbf{B}^h\right) + \nabla r^h - \lambda\nabla^2\mathbf{B}^h - \mathbf{f}^{\mathrm{I}}. \tag{4.42}$$

For an extensive discussion on the parameter $\boldsymbol{\tau}$ and its design for MHD refer to Chapter 3. Presently, we take

$$\boldsymbol{\tau} = \begin{bmatrix} \boldsymbol{\tau}^{\mathrm{VV}} & \mathbf{0} & \mathbf{0} & 0 \\ \mathbf{0}^T & \tau_c^{\mathrm{V}} & \mathbf{0}^T & 0 \\ \mathbf{0} & \mathbf{0} & \boldsymbol{\tau}^{\mathrm{II}} & 0 \\ \mathbf{0}^T & 0 & \mathbf{0}^T & \tau_c^{\mathrm{V}} \end{bmatrix}. \tag{4.43}$$

$$\boldsymbol{\tau}^{\mathrm{VV}} = \mathrm{diag}\left(\tau^{\mathrm{V}}\right) \tag{4.44}$$

$$\boldsymbol{\tau}^{\mathrm{II}} = \mathrm{diag}\left(\tau^{\mathrm{I}}\right). \tag{4.45}$$

The specific forms of the entries of the diagonal stabilization matrix will be provided in Sections 4.2.1 and 4.2.2 specialized to the particular Fourier spectral and finite element methods, respectively. The final VMS statement reads: *Find* $\mathbf{U}^h \in \boldsymbol{\mathcal{V}}^h$ *s.t.* $\forall \; \mathbf{W}^h \in \boldsymbol{\mathcal{V}}^h$

$$
\begin{aligned}
\mathcal{A}^{\mathrm{V}}\left(\mathbf{W}^h, \mathbf{U}^h\right) - \left(\nabla \mathbf{w}^h, \boldsymbol{\mathcal{N}}_C^{\mathrm{V}} + \boldsymbol{\mathcal{N}}_R^{\mathrm{V}}\right) - \left(\nabla \cdot \mathbf{w}^h, P'\right) \\
+ \left(\nabla^{\mathrm{s}} \mathbf{w}^h, 2\nu \nabla^{\mathrm{s}} \mathbf{u}'\right) - \left(\nabla q^h, \mathbf{u}'\right) \\
+ \mathcal{A}^{\mathrm{I}}\left(\mathbf{W}^h, \mathbf{U}^h\right) - \left(\nabla \mathbf{c}^h, \boldsymbol{\mathcal{N}}_C^{\mathrm{I}} + \boldsymbol{\mathcal{N}}_R^{\mathrm{I}}\right) - \left(\nabla \cdot \mathbf{c}^h, r'\right) \\
+ \left(\nabla^{\mathrm{a}} \mathbf{c}^h, 2\lambda \nabla^{\mathrm{a}} \mathbf{B}'\right) - \left(\nabla s^h, \mathbf{B}'\right) \\
= \left(\mathbf{w}^h, \mathbf{f}^{\mathrm{V}}\right) + \left(\mathbf{c}^h, \mathbf{f}^{\mathrm{I}}\right)
\end{aligned}
\tag{4.46}
$$

with $\mathbf{u}'$, P', $\mathbf{B}'$, and r' given by (4.40) and the stabilization parameter given by relations (4.43)- (4.45). In the following two subsections, this statement is specialized to the particular numerical methods that are used to test the models.

4.2.1 Specialization to Fourier-Spectral Method

As previously noted, the Fourier-spectral basis consists of an orthogonal set of basis functions. Further, the projection operator that is used to split the solution into resolved and unresolved scales is selected so that the space of unresolved solutions is orthogonal to the space of resolved solutions. Endowed with this property, all inner products of linear terms between resolved and unresolved quantities vanish. Thus, the VMS statement for the Fourier-spectral method is: *Find* $\mathbf{U}^h \in \boldsymbol{\mathcal{V}}^h$ *s.t.* $\forall$ $\mathbf{W}^h \in \boldsymbol{\mathcal{V}}^h$

$$
\begin{aligned}
\mathcal{A}^{\mathrm{V}}\left(\mathbf{W}^h, \mathbf{U}^h\right) - \left(\nabla \mathbf{w}^h, \boldsymbol{\mathcal{N}}_C^{\mathrm{V}} + \boldsymbol{\mathcal{N}}_R^{\mathrm{V}}\right) \\
+ \mathcal{A}^{\mathrm{I}}\left(\mathbf{W}^h, \mathbf{U}^h\right) - \left(\nabla \mathbf{c}^h, \boldsymbol{\mathcal{N}}_C^{\mathrm{I}} + \boldsymbol{\mathcal{N}}_R^{\mathrm{I}}\right) \\
= \left(\mathbf{w}^h, \mathbf{f}^{\mathrm{V}}\right) + \left(\mathbf{c}^h, \mathbf{f}^{\mathrm{I}}\right).
\end{aligned}
\tag{4.47}
$$

After introducing the Fourier-basis functions, the resulting system of equations is

$$
\begin{aligned}
\frac{\partial \widehat{\mathbf{u}}_{\mathbf{k}}(t)}{\partial t} + \nu |\mathbf{k}|^2 \widehat{\mathbf{u}}_{\mathbf{k}} &= \mathcal{Q}\widehat{\mathbf{f}^{\mathrm{V}}}_{\mathbf{k}} - \mathcal{P}\left(\widehat{\boldsymbol{\mathcal{N}}^{\mathrm{V}}} + \widehat{\boldsymbol{\mathcal{N}}^{\mathrm{V}}_{\mathrm{C}}} + \widehat{\boldsymbol{\mathcal{N}}^{\mathrm{V}}_{\mathrm{R}}}\right) \\[2mm]
\frac{\partial \widehat{\mathbf{B}}_{\mathbf{k}}(t)}{\partial t} + \lambda |\mathbf{k}|^2 \widehat{\mathbf{B}}_{\mathbf{k}} &= \mathcal{Q}\widehat{\mathbf{f}^{\mathrm{I}}}_{\mathbf{k}} - \left(\widehat{\boldsymbol{\mathcal{N}}^{\mathrm{I}}} + \widehat{\boldsymbol{\mathcal{N}}^{\mathrm{I}}_{C}} + \widehat{\boldsymbol{\mathcal{N}}^{\mathrm{I}}_{R}}\right) \cdot \mathbf{k}.
\end{aligned}
\tag{4.48}
$$

Recall that $\mathcal{P}$ and $\mathcal{Q}$ were defined by (2.213) and (2.214), respectively. The root-mean-square velocity and magnetic inductions are used in the definition of the stabilization operator for the spectral case.

$$
\tau^{\mathrm{V}} = \frac{1}{\sqrt{\left(\frac{2}{h}\right)^2 \left((u_{\mathrm{rms}}^h)^2 + (B_{\mathrm{rms}}^h)^2\right) + 3\pi \left(\frac{4\nu}{h^2}\right)^2}}
\tag{4.49}
$$

$$
\tau^{\mathrm{I}} = \frac{1}{\sqrt{\left(\frac{2}{h} B_{\mathrm{rms}}^h\right)^2 + 3\pi \left(\frac{4\lambda}{h^2}\right)^2}}.
\tag{4.50}
$$

Remarks:

- The contributions of the time terms in the stabilization matrix have been ignored.

- Expressions for the stabilization parameters for the continuity equations are not provided as these equations are not solved in the spectral case.

4.2.1.1 Subgrid Dynamo

An exciting phenomenon in numerical work in MHD is the subgrid dynamo. The MHD dynamo phenomenon occurs when the turbulent velocity fluctuations transfer energy to the large scale magnetic field. The subgrid dynamo is the numerical counterpart to this phenomenon. The question becomes: Are the subgrid turbulent velocity fluctuations able to transfer energy to the resolved magnetic field? The VMS decomposition leads to a natural setting for this analysis in part due to the solution decomposition that is used and in part due to the fact that the formulation permits local inverse cascades of energy. To begin the analysis the energy equation for the induction equation in the spectral setting is developed. This permits a more straightforward analysis of the subgrid dynamo terms since the linear VMS terms

vanish. It is found that the VMS formulation is indeed able to capture the subgrid dynamo effect. However, under question are the conditions under which the VMS formulation is able to do so. These conditions are analyzed for physical fidelity. It is found that the VMS formulation is able to capture the subgrid dynamo effect under physically realistic conditions. The magnetic induction is in Alfvén velocity units in the following discussion.

Setting $\mathbf{W}^h = [\mathbf{0}, 0, \mathbf{B}^h, 0]^T$ in (4.47) results in the energy equation for the magnetic induction.

$$\frac{\mathrm{d}K^{\mathrm{I}}}{\mathrm{d}t} = \int_\Omega \mathbf{B}^h \cdot \mathbf{f}^{\mathrm{I}} \, \mathrm{d}\Omega - \lambda \int_\Omega |\nabla \mathbf{B}^h|^2 \, \mathrm{d}\Omega + \mathcal{T}_{\mathrm{I}}^{\mathrm{K}} + \mathcal{T}_{\mathrm{I}}^{\mathrm{C}} + \mathcal{T}_{\mathrm{I}}^{\mathrm{R}}. \qquad (4.51)$$

The energy transfers between the resolved and unresolved scales are given by

$$\mathcal{T}_{\mathrm{I}}^{\mathrm{K}} = \int_\Omega \nabla \mathbf{B}^h : \left[\mathbf{B}^h \otimes \mathbf{u}^h - \mathbf{u}^h \otimes \mathbf{B}^h \right] \, \mathrm{d}\Omega$$

$$\mathcal{T}_{\mathrm{I}}^{\mathrm{C}} = - \int_\Omega \nabla \mathbf{B}^h : \left[\mathbf{B}^h \otimes \mathbf{u}' + \mathbf{B}' \otimes \mathbf{u}^h - \mathbf{u}^h \otimes \mathbf{B}' - \mathbf{u}' \otimes \mathbf{B}^h \right] \, \mathrm{d}\Omega$$

$$\mathcal{T}_{\mathrm{I}}^{\mathrm{R}} = \int_\Omega \nabla \mathbf{B}^h : \left[\mathbf{B}' \otimes \mathbf{u}' - \mathbf{u}' \otimes \mathbf{B}' \right] \, \mathrm{d}\Omega.$$

In Equation (4.51) the energy transfer terms on the right hand side are described as follows:

- $\mathcal{T}_{\mathrm{I}}^{\mathrm{K}}$ represents the transfer of energy between $\mathbf{u}^h$ and $\mathbf{B}^h$.

- $\mathcal{T}_{\mathrm{I}}^{\mathrm{C}}$ represents the transfer of energy between resolved and unresolved scales.

- $\mathcal{T}_{\mathrm{I}}^{\mathrm{R}}$ represents the transfer of energy due to Reynolds stress terms.

An important observation is that if any of the terms on the right hand side is negative then the energy of the magnetic induction is decreasing in time. For example, the dissipation term takes energy away as expected. With this observation, (4.51) is analyzed with the subgrid dynamo in mind.

The idea behind the subgrid dynamo is that the unresolved velocity field passes energy to the resolved magnetic field thereby increasing the energy of the resolved magnetic induction. Another way of thinking about this is that the turbulent fluctuations give energy to the large scale magnetic field. From (4.51) we see that $\mathcal{T}_{\mathrm{I}}^{\mathrm{C}}$

and $\mathcal{T}_\text{I}^\text{R}$ include correlations between the unresolved velocity field and the resolved magnetic field. However, it is well-known that the VMS formulation with the first order approximation to $\mathbf{u}'$ is not able to represent terms of the form of $\mathcal{T}_\text{I}^\text{R}$ with any effectiveness. With this in mind, the consideration of the Reynolds stress terms are placed on the shelf for the time-being. It is entirely possible that the Reynolds stress terms may contribute significantly to the subgrid dynamo effect. It may even be possible that the subgrid dynamo effect cannot be fully captured without the contributions from the Reynolds stresses. If this is indeed the case, then a modification to the VMS formulation will be required to take these important effects into account. Either way, at this point it is taken to be sufficient to analyze $\mathcal{T}_\text{I}^\text{C}$ with the goal of determining if it has a role to play in the subgrid dynamo effect.

The subgrid dynamo can come from two terms in $\mathcal{T}_\text{I}^\text{C}$. These are

$$\mathcal{T}_D^{(1)} = -\int_\Omega \nabla \mathbf{B}^h : \left(\mathbf{B}^h \otimes \mathbf{u}' \right) \ \mathrm{d}\Omega$$

and

$$\mathcal{T}_D^{(2)} = \int_\Omega \nabla \mathbf{B}^h : \left(\mathbf{u}' \otimes \mathbf{B}^h \right) \ \mathrm{d}\Omega.$$

However, it can be shown that $\mathcal{T}_D^{(2)} = 0$ so in fact the subgrid dynamo only comes from $\mathcal{T}_D^{(1)}$.

$$\begin{aligned}
\mathcal{T}_D^{(2)} &= \int_\Omega \nabla \mathbf{B}^h : \left(\mathbf{u}' \otimes \mathbf{B}^h \right) \ \mathrm{d}\Omega \\
&= \int_\Omega B_{i,j}^h u_j' B_i^h \ \mathrm{d}\Omega \\
&= -\int_\Omega B_i^h \left(u_j' B_i^h \right)_{,j} \ \mathrm{d}\Omega \\
&= -\int_\Omega B_u^h u_j' B_{i,j}^h \ \mathrm{d}\Omega \\
&= -\int_\Omega B_{i,j}^j u_j' B_i^h \ \mathrm{d}\Omega \\
&= -\int_\Omega \nabla \mathbf{B}^h : \left(\mathbf{u}' \otimes \mathbf{B}^h \right) \ \mathrm{d}\Omega \\
&= -\mathcal{T}_D^{(2)}.
\end{aligned}$$

Thus $\mathcal{T}_D^{(2)} = -\mathcal{T}_D^{(2)}$ which is only true if $\mathcal{T}_D^{(2)} = 0$. So, the subgrid dynamo (if it exists) emanates from the term $\mathcal{T}_I^C$ in the form of

$$\mathcal{T}_D = -\int_\Omega \nabla \mathbf{B}^h : \left(\mathbf{B}^h \otimes \mathbf{u}'\right) \, d\Omega. \tag{4.52}$$

The next step is to determine when $\mathcal{T}_D$ is positive. As a reminder, the reason it should be positive is so that $\mathcal{T}_I^C$ is positive which then ensures that energy is being pumped back into the resolved magnetic induction. Another way of writing this is

$$\mathcal{T}_D > 0 \Rightarrow \mathcal{T}_I^C > 0$$

$$\mathcal{T}_I^C > 0 \Rightarrow \text{Positive term on right hand side (RHS) of (4.51)}$$

$$\text{Positive term on RHS of (4.51)} \Rightarrow K^I \text{ has energy source!}$$

The approximation for the unresolved velocity field is introduced into $\mathcal{T}_D$. That is

$$\mathbf{u}' \approx -\boldsymbol{\tau}^{VV} \mathbb{P}' \left[\nabla \cdot \left(\mathbf{u}^h \otimes \mathbf{u}^h\right) - \nabla \cdot \left(\mathbf{B}^h \otimes \mathbf{B}^h\right)\right].$$

So

$$\mathcal{T}_D = \tau^{VV} \int_\Omega \left[\mathbf{B}^h \cdot \nabla \mathbf{B}^h\right] \cdot \mathbb{P}' \left[\nabla \cdot \left(\mathbf{u}^h \otimes \mathbf{u}^h\right) - \nabla \cdot \left(\mathbf{B}^h \otimes \mathbf{B}^h\right)\right] \, d\Omega \tag{4.53}$$

$$= \tau^{VV} \int_\Omega \left[\nabla \cdot \left(\mathbf{B}^h \otimes \mathbf{B}^h\right)\right] \cdot \mathbb{P}' \left[\mathbf{u}^h \otimes \mathbf{u}^h\right] \, d\Omega$$

$$- \tau^{VV} \int_\Omega \left[\nabla \cdot \left(\mathbf{B}^h \otimes \mathbf{B}^h\right)\right] \cdot \mathbb{P}' \left[\mathbf{u}^h \otimes \mathbf{u}^h\right] \, d\Omega \tag{4.54}$$

$$= \tau^{VV} \int_\Omega \mathbb{P}' \left[\nabla \cdot \left(\mathbf{B}^h \otimes \mathbf{B}^h\right)\right] \cdot \mathbb{P}' \left[\mathbf{u}^h \otimes \mathbf{u}^h\right] \, d\Omega$$

$$- \tau^{VV} \int_\Omega \mathbb{P}' \left[\nabla \cdot \left(\mathbf{B}^h \otimes \mathbf{B}^h\right)\right] \cdot \mathbb{P}' \left[\mathbf{u}^h \otimes \mathbf{u}^h\right] \, d\Omega. \tag{4.55}$$

The last step is possible because the term $\nabla \cdot \left(\mathbf{B}^h \otimes \mathbf{B}^h\right)$ can have resolved and unresolved components. This is because in spectral methods the trigonometric basis functions are added in wavenumber space thereby providing some instances when the wavenumber is, for example, two times larger than the cutoff wavenumber. However, since the inner products involve a term on the unresolved scales the only way the

inner product will be nonzero is if the first term in the product is projected to the fine scales. Another way of thinking about this is that even if the first term was not projected to the fine scales and the inner product was taken then the resolved scales part would be zero and one would only be left with a multiplication of the unresolved scales. This leads to

$$
\mathcal{T}_D = \tau^{\text{VV}} \underbrace{\int_\Omega \mathbb{P}' \left(\nabla \cdot \left[\mathbf{B}^h \otimes \mathbf{B}^h \right] \right) \cdot \mathbb{P}' \left(\nabla \cdot \left[\mathbf{u}^h \otimes \mathbf{u}^h \right] \right) \ \mathrm{d}\Omega}_{\geqslant 0}
$$
$$
- \tau^{\text{VV}} \underbrace{\int_\Omega \left| \mathbb{P}' \left(\nabla \cdot \left[\mathbf{B}^h \otimes \mathbf{B}^h \right] \right) \right|^2 \ \mathrm{d}\Omega}_{>0}.
$$

In order for $\mathcal{T}_D$ to be positive, something must be said about the first term in the above expression. First of all, if this term is less than zero then there is no hope for $\mathcal{T}_D$ to be positive. Secondly, even if the first term *is* positive something more must happen in order to ensure that $\mathcal{T}_D$ is positive. Thus, not only should the first term be positive but it should also be larger than the second term (which is always positive). Clearly, if the velocity field is aligned with the magnetic induction then the first term is positive. Recall from Section 2.2.7 that in MHD the fields tend to align. Hence,

$$
\mathbf{u}^h = \beta \mathbf{B}^h.
$$

Using this relation in the expression for the subgrid energy transfer term yields,

$$
\mathcal{T}_D = \tau^{\text{VV}} \int_\Omega \beta^2 \left| \mathbb{P}' \left(\nabla \cdot \left[\mathbf{B}^h \otimes \mathbf{B}^h \right] \right) \right|^2 \ \mathrm{d}\Omega - \tau^{\text{VV}} \int_\Omega \left| \mathbb{P}' \left(\nabla \cdot \left[\mathbf{B}^h \otimes \mathbf{B}^h \right] \right) \right|^2 \ \mathrm{d}\Omega
$$
$$
= \tau^{\text{VV}} \int_\Omega \left(\beta^2 - 1 \right) \left| \mathbb{P}' \left(\nabla \cdot \left[\mathbf{B}^h \otimes \mathbf{B}^h \right] \right) \right|^2 \ \mathrm{d}\Omega.
$$

It is immediately apparent that if $|\beta| > 1$ then the first term is positive and greater than the second term. This condition also means that the velocity field must dominate the magnetic field (i.e. the velocity field is stronger than the magnetic field). The question now becomes whether or not this is physical or if it is only a mathematical artifact from the VMS formulation.

The assessment of if the VMS conditions are physical or not is initiated by considering a paper on the growth of correlations in MHD. In (Pouquet, Meneguzzi, and Frisch 1986) the growth correlation is defined as

$$\theta = \frac{H^C}{K^{\mathrm{T}}}$$

and is shown to always increase. That is, the velocity field and magnetic induction try to align themselves. This tendency toward field alignment was demonstrated in Section 2.2.7. If $\mathbf{u} = \beta \mathbf{B}$ then

$$\theta = \frac{2\beta}{(\beta^2 + 1)}.$$
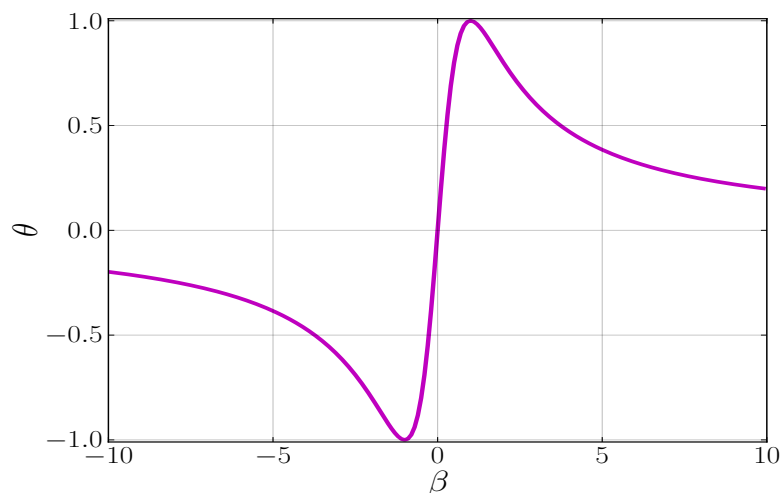
Figure 4.1: Plot of growth correlation as a function of the alignment parameter β.

Figure 4.1 shows how the growth correlation changes with β. To gain an understanding of what is going on, we only consider $\beta > 0$. Note that as θ approaches its maximum value from the left this corresponds to the situation of $\beta < 1$ since $\max\left(\theta\left(\beta = [0, \infty]\right)\right) = 1$ when $\beta = 1$. When $\beta < 1$ the situation is such that the magnetic induction dominates the velocity field. Thus, in this case, the magnetic induction transfers energy to the velocity field which precludes the subgrid dynamo. However, when θ approaches its maximum value from the right the situation is such

that $\beta > 1$. This means that the velocity field dominates the magnetic induction and that energy is transferred from the velocity field to the magnetic field. This is exactly what happens with the subgrid dynamo. The same reasoning applies for $\beta < 0$. It is therefore concluded that conditions imposed by the VMS formulation to capture the subgrid dynamo effect are not simply mathematical artifacts. They are in fact consistent with the theory. Note, however, that this explanation is contingent upon the growth correlation always increasing in strength.

4.2.2   Specialization to Finite Element Method

Using a polynomial basis will typically result in the same variational statement as (4.46). However, for simplicity of implementation we neglect gradients of the subgrid scales. Note that if the fine scale space is orthogonal to the finite element space then these terms vanish identically (see Codina 2002). The resulting variational statement is: *Find* $\mathbf{U}^h \in \mathcal{V}^h$ *s.t.* $\forall\, \mathbf{W}^h \in \mathcal{V}^h$

$$
\begin{aligned}
&\mathcal{A}^{\mathrm{V}}\left(\mathbf{W}^h, \mathbf{U}^h\right) - \left(\nabla \mathbf{w}^h, \mathcal{N}_C^{\mathrm{V}} + \mathcal{N}_R^{\mathrm{V}}\right) - \left(\nabla \cdot \mathbf{w}^h, P'\right) - \left(\nabla q^h, \mathbf{u}'\right) \\
&+\mathcal{A}^{\mathrm{I}}\left(\mathbf{W}^h, \mathbf{U}^h\right) - \left(\nabla \mathbf{c}^h, \mathcal{N}_C^{\mathrm{I}} + \mathcal{N}_R^{\mathrm{I}}\right) - \left(\nabla \cdot \mathbf{c}^h, r'\right) - \left(\nabla s^h, \mathbf{B}'\right) \\
&= \left(\mathbf{w}^h, \mathbf{f}^{\mathrm{V}}\right) + \left(\mathbf{c}^h, \mathbf{f}^{\mathrm{I}}\right).
\end{aligned}
\tag{4.56}
$$

The stabilization matrices in the unresolved scales in (4.56) are given by

$$
\tau^{\mathrm{V}} = \frac{1}{\sqrt{\left(\frac{2C_t^{\mathrm{V}}\rho}{\Delta t}\right)^2 + \rho^2 \mathbf{u} \cdot \mathbf{G}\mathbf{u} + C_\mu \mu^2 \|\mathbf{G}\|^2 + \frac{C_B \rho}{\mu_0} |\mathbf{B}|^2 \|\mathbf{G}\|}}
\tag{4.57}
$$

$$
\tau^{\mathrm{I}} = \frac{1}{\sqrt{\left(\frac{2C_t^{\mathrm{I}}}{\Delta t}\right)^2 + \mathbf{u} \cdot \mathbf{G}\mathbf{u} + \mathbf{B} \cdot \mathbf{G}\mathbf{B} + C_\lambda \lambda^2 \|\mathbf{G}\|^2}}
\tag{4.58}
$$

$$
\tau_c^{\mathrm{V}} = \frac{1}{8C_t^{\mathrm{V}} \mathrm{tr}\left(\mathbf{G}\right)}
\tag{4.59}
$$

$$
\tau_c^{\mathrm{I}} = \frac{1}{8C_t^{\mathrm{I}} \mathrm{tr}\left(\mathbf{G}\right)}
\tag{4.60}
$$

where

$$\|\mathbf{G}\| = \sqrt{\mathbf{G} : \mathbf{G}} \tag{4.61}$$

and the components of **G** are

$$\mathsf{G}_{ij} = \frac{\partial \xi_k}{\partial x_i} \frac{\partial \xi_k}{\partial x_j}. \tag{4.62}$$

Also note that $\mathrm{tr}(\mathbf{G})$ denotes the trace of the matrix **G**,

$$\mathrm{tr}\,(\mathbf{G}) = \sum_{i=1}^{n_{\mathrm{sd}}} \mathsf{G}_{ii}. \tag{4.63}$$

4.3   Residual-based Eddy Viscosity Model

This section will return to the eddy viscosity concept introduced in Section 4.1. A new type of eddy viscosity model for MHD based on the VMS formulation is introduced. The model builds upon and generalizes a hydrodynamic analog introduced in (Oberai et al. n.d.). The new residual-based eddy diffusivities are

$$\mu_T = \overline{C}\rho h \sqrt{|\mathbf{u}'|^2 + \frac{1}{\mu_0 \rho} |\mathbf{B}'|^2} \tag{4.64}$$

$$\lambda_T = \overline{C} h \sqrt{|\mathbf{u}'|^2 + \frac{1}{\mu_0 \rho} |\mathbf{B}'|^2} \tag{4.65}$$

where

$$\overline{C} = \left(\frac{4}{27}\right)^{1/2} \frac{1}{C_K^{3/2}\pi} \tag{4.66}$$

and $C_K = 2.2$ is the Kolmogorov constant for MHD turbulence as suggested in (Beresnyak 2011). This results in a numerical value for $\overline{C}$ of 0.0375. These eddy diffusivities are motivated by the expressions:

$$\mu_T = \overline{C}_0 \rho h |\mathbf{u}'| \tag{4.67}$$

$$\lambda_T = \overline{C}_0 h |\mathbf{u}'| \tag{4.68}$$

which have analogs in the molecular diffusivity and resistivity, respectively. A universal constant, $\overline{C}$, can be obtained in place of $\overline{C_0}$ by selecting

$$\overline{C_0} = \sqrt{\frac{K'^{\mathrm{T}}}{K'^{\mathrm{V}}}} \tag{4.69}$$

where K'^{T} is the total energy of the subgrid scales and K'^{V} is the kinetic energy of the subgrid scales. Using (4.64) and (4.65), the RBEV model is

$$\begin{aligned}
\mathcal{M}\left(\mathbf{W}^h, \mathbf{U}^h; h, \mathbf{c}_P\right) &= \mathcal{M}_{\mathrm{V}}\left(\mathbf{w}^h, \mathbf{U}^h; h, \mathbf{c}_P^{\mathrm{V}}\right) + \mathcal{M}_{\mathrm{I}}\left(\mathbf{c}^h, \mathbf{U}^h; h, \mathbf{c}_P^{\mathrm{I}}\right) \\
&= \left(\nabla^{\mathrm{s}}\mathbf{w}^h, 2\overline{C}h\sqrt{|\mathbf{u}'|^2 + \frac{1}{\mu_0\rho}|\mathbf{B}'|^2}\,\nabla^{\mathrm{s}}\mathbf{u}^h\right) \\
&\quad + \left(\nabla^{\mathrm{a}}\mathbf{c}^h, 2\overline{C}h\sqrt{|\mathbf{u}'|^2 + \frac{1}{\mu_0\rho}|\mathbf{B}'|^2}\,\nabla^{\mathrm{a}}\mathbf{B}^h\right). \tag{4.70}
\end{aligned}$$

<u>Remarks:</u>

- The eddy viscosity is analogous to the molecular viscosity where the element size h plays the role of mean free path and the subgrid velocity plays the role of average velocity between collisions.

- The turbulent magnetic diffusivity has its roots in the Drude model which provides a classical description of the magnetic resistivity, η. The Drude model motivation is presented in Section 4.3.1.

- The coefficient $\overline{C}$ is understood to be a constant rather than a coefficient that depends on the flow field. This model is said to be inherently dynamic since it automatically adjusts to the character of the flow field.

- A derivation of the expression for $\overline{C}$, (4.66), is postponed until a more mathematical discussion on homogeneous, isotropic turbulence is presented in Section 5.1.

- The reason for (4.69) is presented in the derivation of $\overline{C}$.

The Drude model is introduced next to give credence to the form of the magnetic eddy diffusivity. A broader discussion on the character of the new eddy viscosity model is initiated at the end of this section.

4.3.1 Drude Model

The Drude model begins with an expression for the current density of

$$\mathbf{j} = Nq\mathbf{v}_f$$

where N is the number of particles passing through an area, q is the charge of those particles, and $\mathbf{v}_f$ is the terminal velocity of the particles. The goal is to relate the current density to the electric field. To do this, an expression for the terminal velocity in terms of the electric field is needed. The classical forces acting on the charged particle are given by Newton's law,

$$\mathbf{F} = m\mathbf{a}. \tag{4.71}$$

The force that the charged particles experience in an electric field is

$$\mathbf{F}_E = q\mathbf{E} \tag{4.72}$$

where q is the charge of a particle and $\mathbf{E}$ is the electric field. The force the charged particles feel from collisions with particles of opposite charge is due to their velocity,

$$\mathbf{F}_C = \gamma m\mathbf{v}$$

where γ is a proportionality constant, m is the mass of the particle and $\mathbf{v}$ is its velocity. The force is assumed to act in the direction opposite to the one that the particle is moving in within the electric field. Thus,

$$q\mathbf{E} - \gamma m\mathbf{v} = m\frac{d\mathbf{v}}{dt}.$$

Once the terminal velocity is reached, the particles are no longer accelerating. Thus,

$$\Rightarrow \mathbf{v}_f = \frac{q}{\gamma m}\mathbf{E}.$$

So the current density becomes,

$$\begin{aligned}
\mathbf{j} &= Nq\mathbf{v}_f \\
&= Nq\frac{q}{\gamma m}\mathbf{E} \\
&= \frac{Nq^2}{\gamma m}\mathbf{E} \\
&= \sigma\mathbf{E}
\end{aligned}$$

where σ is called the electrical conductivity.

This derivation provided a relationship between the current density and the electromotive force (electric field). The induction equation, when written in curl form, yields a turbulent electromotive force,

$$\mathbf{E}_T = \left(\mathbf{u}' \times \mathbf{B}'\right).$$

The claim is that this turbulent electromotive force is proportional to the current density through an effective resistivity, η_T.

$$\mathbf{E}_T = \eta_T\mathbf{j}.$$

Therefore,

$$\eta_T = \frac{\gamma m}{Nq^2}.$$

In order for the analogy in the RBEV model to make sense, η_T should depend upon a fluctuating velocity and a mean-free path. This dependence is realized through the coefficient γ which is classically called the drag coefficient. It is well-known that γ depends on the mean-free path and the thermal velocities of the particles. In (4.73) the mean-free path dependence of the drag coefficient corresponds to the mesh size h while the thermal velocities correspond to the subgrid solutions $\mathbf{u}'$. Finally, note that the turbulent magnetic diffusivity is proportional to the turbulent resistivity

through the permeability of the medium,

$$\lambda_T = \frac{\eta_T}{\mu_0}. \tag{4.73}$$

With this, the RBEV analogy for the induction equation is complete.

4.3.2 Discussion on the RBEV Model

The RBEV model is appealing for several reasons. First of all, it is an inherently dynamic model. The reason for this stems from the fact that the eddy viscosity in the model is proportional to the subgrid fields which are defined within the VMS formulation. These subgrid fields are proportional to the residual of the coarse scales. Hence, whenever and wherever the numerical solution captures all of the turbulent fluctuations in a flow field, the model automatically vanishes. This is to be contrasted with the classical eddy viscosity model wherein the model is always active. This is true even for times and spatial pockets where the flow field is laminar. The classical eddy viscosity model is made dynamic by introducing the Germano identity which leads to a dynamic Smagorinsky coefficient. However, this coefficient, when determined in this manner, is only dynamic in time and therefore still remains uniform in space. Thus, there could be regions of the flow field that are laminar in which the dynamic model is still active. Due to the inherent dynamic nature of the new eddy viscosity model, it is conjectured that the calibration constant in the model is truly constant and need not be tuned during the simulation. It is important to note that this constant was calibrated using arguments from homogeneous, isotropic turbulence theory (to be presented in Chapter 5). In other situations this argument for determination of the constant may not be applicable and therefore the true value may be different than that presented in this work. In the context of MHD, the derivation of the value for the constant hinged on the assumption of a Kolmogorov spectrum for the total energy. It must be said that due to the universality conversation in MHD there is no guarantee that this assumption is correct. However, using different power law spectra leads to problem-dependent constants which necessitate the need for a dynamic procedure. In the present work, the Kolmogorov spectrum is assumed since one of the main benefits of this new

model is that it circumvents the need for a dynamic procedure. Finally, the RBEV model is consistent with the VMS approach. Therefore, the new models developed to this point are all closed with a single theory for the subgrid scales.

4.4   Mixed Model

Despite all the promise of using the VMS formulation for developing LES models for turbulence, there are still some shortcomings. In (Wang and Oberai 2010b) it was shown that LES models developed with the VMS formulation represent the cross stress terms well while the Reynolds stress terms are represented poorly. This observation led to the proposal of a mixed model for incompressible hydrodynamics in (Wang and Oberai 2010a). The idea behind this model is that the VMS framework is able to capture the cross stresses while an eddy viscosity model is augmented to the VMS formulation to capture the Reynolds stress terms. Indeed, EV models were initially designed to represent the contributions from the Reynolds stresses. Interestingly, they also contribute to the cross stresses. In (R. Kraichnan 1976) it was shown that the Reynolds stresses contribute about 1/3 of the total subgrid energy.

The situation is the same for incompressible MHD turbulence. The essential limitation of the VMS formulation stems for the approximate solution to $\mathbf{U}'$. Better approximations for the subgrid solutions may yield VMS methods that are able to capture higher-order terms. In the present work, the first order approximation to the subgrid solutions is used and the effects of the higher order terms are modeled with an eddy viscosity. The problem statement for the mixed model is: *Find* $\mathbf{U}^h \in \boldsymbol{\mathcal{V}}^h$ *s.t.* $\forall\ \mathbf{W}^h \in \boldsymbol{\mathcal{V}}^h$

$$
\begin{aligned}
\mathcal{A}\left(\mathbf{W}^h, \mathbf{U}^h + \mathbf{U}'\right) + \mathcal{M}_{\mathrm{V}}\left(\mathbf{w}^h, \mathbf{U}^h; h, \mathbf{c}_P^{\mathrm{V}}\right) \\
+ \mathcal{M}_{\mathrm{I}}\left(\mathbf{c}^h, \mathbf{U}^h; h, \mathbf{c}_P^{\mathrm{I}}\right) = \left(\mathbf{w}^h, \mathbf{f}^{\mathrm{V}}\right) + \left(\mathbf{c}^h, \mathbf{f}^{\mathrm{I}}\right).
\end{aligned}
\tag{4.74}
$$

This is expanded to show the individual terms: *Find* $\mathbf{U}^h \in \boldsymbol{\mathcal{V}}^h$ *s.t.* $\forall \mathbf{W}^h \in \boldsymbol{\mathcal{V}}^h$

$$\mathcal{A}^{\mathrm{V}}\left(\mathbf{W}^h, \mathbf{U}^h\right) - \left(\nabla \mathbf{w}^h, \boldsymbol{\mathcal{N}}_C^{\mathrm{V}}\right) - \left(\nabla \cdot \mathbf{w}^h, P'\right)$$

$$- \left(\nabla q^h, \mathbf{u}'\right) + \left(\nabla^{\mathrm{s}} \mathbf{w}^h, 2\overline{C}h\sqrt{|\mathbf{u}'|^2 + \frac{1}{\mu_0 \rho}|\mathbf{B}|^2}\,\nabla^{\mathrm{s}} \mathbf{u}^h\right)$$

$$+ \mathcal{A}^{\mathrm{I}}\left(\mathbf{W}^h, \mathbf{U}^h\right) - \left(\nabla \mathbf{c}^h, \boldsymbol{\mathcal{N}}_C^{\mathrm{I}}\right) - \left(\nabla \cdot \mathbf{c}^h, r'\right)$$

$$- \left(\nabla s^h, \mathbf{B}'\right) + \left(\nabla^{\mathrm{a}} \mathbf{c}^h, 2\overline{C}h\sqrt{|\mathbf{u}'|^2 + \frac{1}{\mu_0 \rho}|\mathbf{B}|^2}\,\nabla^{\mathrm{a}} \mathbf{B}^h\right)$$

$$= \left(\mathbf{w}^h, \mathbf{f}^{\mathrm{V}}\right) + \left(\mathbf{c}^h, \mathbf{f}^{\mathrm{I}}\right). \tag{4.75}$$

In (4.75) terms with gradients of subgrid scales have been dropped. Note also that the Reynolds stress terms have also been neglected since these are now accounted for with the eddy viscosity model.

Remarks:

- The mixed model contains both the VMS formulation and the RBEV model.

- The mixed model is a fully residual-based, inherently dynamic model.

- The calibration constants are assumed to be truly constant.

4.5   General Expression for the Models

The final form of the problem inclusive of the new models is: *Find* $\mathbf{U}^h \in \boldsymbol{\mathcal{V}}^h$ *s.t.* $\forall \mathbf{W}^h \in \boldsymbol{\mathcal{V}}^h$

$$\mathcal{A}^{\mathrm{V}}\left(\mathbf{W}^h, \mathbf{U}^h\right) - b_{\mathrm{VMS}}^{\mathrm{V}}\left[\left(\nabla \mathbf{w}^h, \boldsymbol{\mathcal{N}}_C^{\mathrm{V}}\right) + \left(\nabla \cdot \mathbf{w}^h, P'\right)\right] + c_{\mathrm{VMS}}^{\mathrm{V}}\left(\nabla q^h, \mathbf{u}'\right)$$

$$+ b_{\mathrm{EVM}}^{\mathrm{V}}\left(\nabla^{\mathrm{s}} \mathbf{w}^h, 2\overline{C}h\sqrt{|\mathbf{u}'|^2 + \frac{1}{\mu_0 \rho}|\mathbf{B}'|^2}\,\nabla^{\mathrm{s}} \mathbf{u}^h\right)$$

$$+ \mathcal{A}^{\mathrm{I}}\left(\mathbf{W}^h, \mathbf{U}^h\right) - b_{\mathrm{VMS}}^{\mathrm{I}}\left[\left(\nabla \mathbf{c}^h, \boldsymbol{\mathcal{N}}_C^{\mathrm{I}}\right) + \left(\nabla \cdot \mathbf{c}^h, r'\right)\right] + c_{\mathrm{VMS}}^{\mathrm{I}}\left(\nabla s^h, \mathbf{B}'\right)$$

$$+ b_{\mathrm{EVM}}^{\mathrm{I}}\left(\nabla^{\mathrm{a}} \mathbf{c}^h, 2\overline{C}h\sqrt{|\mathbf{u}'|^2 + \frac{1}{\mu_0 \rho}|\mathbf{B}'|^2}\,\nabla^{\mathrm{a}} \mathbf{B}^h\right)$$

$$= \left(\mathbf{w}^h, \mathbf{f}^{\mathrm{V}}\right) + \left(\mathbf{c}^h, \mathbf{f}^{\mathrm{I}}\right) \tag{4.76}$$

Table 4.1: A summary of the values of the parameters b_i and c and corresponding models.

Model	$b_{\text{VMS}}^{\text{V,I}}$	$b_{\text{EVM}}^{\text{V,I}}$	$c_{\text{VMS}}^{\text{V,I}}$	
VMS	1	0	1	
MM	1	1/3	1	
RBEV	0	1	1	equal order elements
			0	any other time

where the subgrid solutions are given by (4.40) and the parameters b_i determine what type of model is being used. The parameter c_{VMS} is a special parameter that must be on when using equal-order elements in the RBEV model. This term is required in order for the LBB condition to be circumvented when using equal order elements. For the VMS and mixed models we have $c_{\text{VMS}}^{\text{V,I}} = b_{\text{VMS}}^{\text{V,I}}$. In Table 4.1 specific values of the parameters are provided that result in the particular models developed.

CHAPTER 5
Assessment of Model Performance

The aim of this chapter is to present results on the the performance of the models developed in previous chapters. The models are tested on two types of problems: 1.) a decaying, homogeneous, isotropic turbulent flow field and 2.) a turbulent MHD channel flow problem.

5.1 Decaying, Homogeneous, Isotropic Turbulence

This section is divided into two parts. The first part, Section 5.1.1 presents an overview of the theory of homogenous isotropic turbulence (HIT) for hydrodynamics and MHD. Following this, results from the new models are presented in Section 5.1.3 on the canonical test problem of the decaying Taylor-Green vortex generalized to MHD. This flow evolves into a homogenous turbulent flow field.

5.1.1 Theory of Homogeneous, Isotropic Turbulence

This section provides more mathematical detail on the theory of turbulence. We first focus on the Kolmogorov phenomenology of hydrodynamic turbulence (Kolmogorov 1941b, 1941a, 1941c). This phenomenology of turbulence asserts that, for a large enough Reynolds number, the small scales of the turbulence are statistically isotropic regardless of the behavior of the large, energy containing scales. Following this we give an overview of HIT in MHD.

The anatomy of turbulence is dissected into three primary regions:

1. the large eddy, energy containing scales

2. the small scales that are small enough so as to be unaware of the energy production mechanisms but not so small that they are affected by viscosity
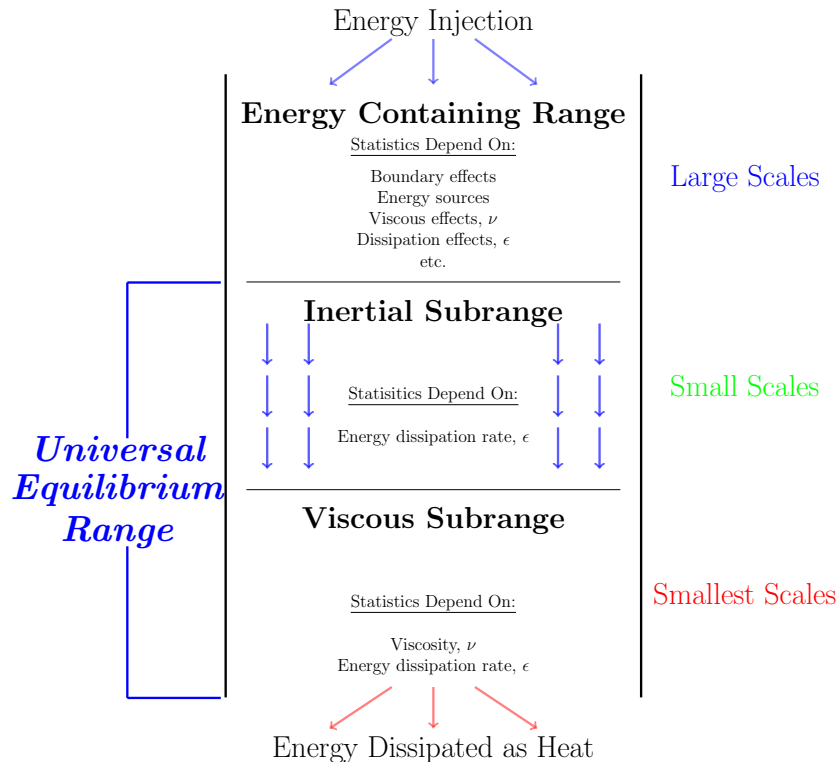
---

3. the very smallest scales that are not aware of the energy production mechanisms but are affected by viscous dissipation

This anatomy is depicted in Figure 5.1. The first region is termed the energy containing region, the second region is called the inertial subrange, and the third region is called the viscous dissipation region.

Figure 5.1: The simplest phenomenology of turbulence. The scales of turbulence are broken into three distinct regions.

With this terminology we are now able to introduce the Kolmogorov hypotheses. Although a cornerstone of modern turbulence theory, these hypotheses have a few shortcomings, some of which were acknowledged by Kolmogorov himself (Kolmogorov 1962). In the intervening years since his formulation of these hypotheses, modifications have been made to them to account for phenomena such as intermittency. However, the predictions on the behavior of the turbulence statistics that result from these hypotheses are still used as a starting point for the validation of new theories and turbulence models.

> **Kolmogorov Hypothesis 5.1.** *For a large enough Re the turbulence statistics in regions 2 and 3 depend only on the viscosity ν and the rate of energy transfer ϵ.*
>
> **Kolmogorov Hypothesis 5.2.** *For a large enough Re the turbulence statistics in the inertial subrange (region 2) are independent of the viscosity ν and only depend on the rate of energy transfer ϵ.*

We briefly introduce the Kolmogorov length, velocity, and time scales. These scales are the characteristic scales of the very smallest eddies in the system. They can be formed by combining the energy transfer rate ϵ and the viscosity ν which are the two parameters that play a role in affecting the smallest scales. Thus

$$\ell_K = \left(\frac{\nu^3}{\epsilon}\right)^{1/4} \tag{5.1}$$

$$u_{\ell_K} = \left(\epsilon\nu\right)^{1/4} \tag{5.2}$$

$$\tau_{\ell_K} = \left(\frac{\nu}{\epsilon}\right)^{1/2}. \tag{5.3}$$

Prior to discussing some consequences of this phenomenology, we introduce some useful turbulence statistics. In HIT most of the turbulence analysis is carried out in spectral space. The most common statistic when discussing HIT is the energy in wavenumber space,

$$E^{\mathrm{V}}\left(\mathbf{k}, t\right) = \frac{1}{2}\widehat{\mathbf{u}}^*\left(\mathbf{k}, t\right) \cdot \widehat{\mathbf{u}}\left(\mathbf{k}, t\right) \tag{5.4}$$

where $\mathbf{u}^*$ is the complex conjugate of $\mathbf{u}$. A particularly convenient representation of the energy spectrum is in terms of wavenumber bins,

$$E^{\mathrm{V}}\left(k, t\right) = \oint E^{\mathrm{V}}\left(\mathbf{k}, t\right) \, \mathrm{d}\mathbf{k} \tag{5.5}$$

where $k = |\mathbf{k}| = \sqrt{k_i k_i}$ is the magnitude of wavenumber $\mathbf{k}$. The integral in (5.5) is a surface integral taken over a spherical shell of radius k. This representation

removes directional information from the energy spectrum. It can be interpreted as the energy in a disc around k. In three dimensions this strip is a spherical shell. The concept is illustrated (with a two-dimensional example) in Figure 5.2.
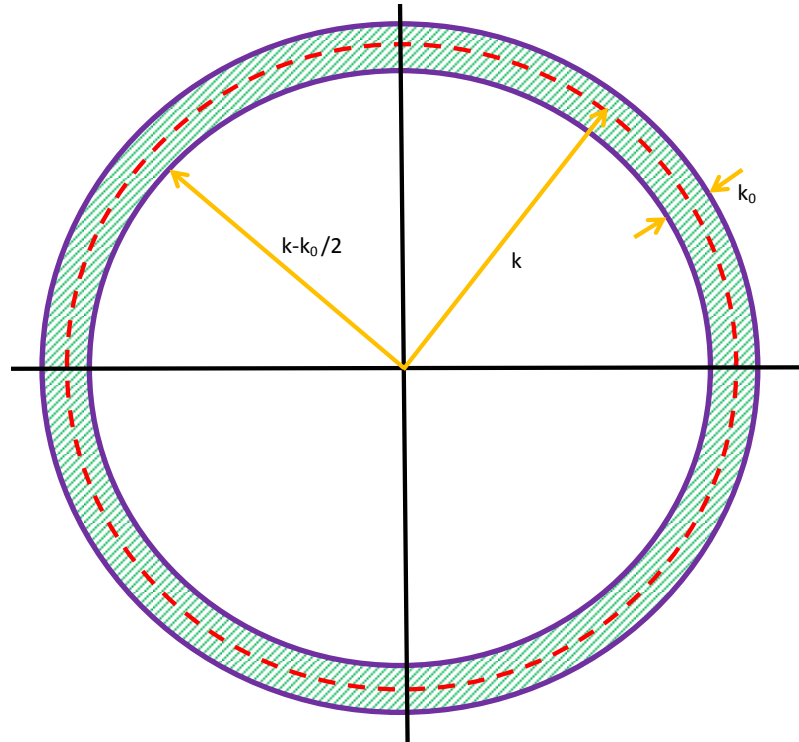
Figure 5.2: The energy spectrum indicates the amount of energy in the band of width k_0 around wavenumber k.

In order to obtain the total energy in the velocity field an integration over spherical shells is performed,

$$K^{\mathrm{V}}(t) = \int_0^\infty E^{\mathrm{V}}(k,t) \ \mathrm{d}k. \tag{5.6}$$

We are now prepared to introduce one of the triumphs of HIT theory based on the Kolmogorov phenomenology. The goal is to devise a dimensionless energy spectrum which we denote $E_s^{\mathrm{V}}(k\ell_K, t)$. Invoking Hypothesis 5.1 we note that the turbulence statistic being considered, namely $E^{\mathrm{V}}(k,t)$, is only dependent on the viscosity and dissipation rate (and k as well because we are in wavenumber space). We can devise a reference energy based on either ν and ϵ or from k and ϵ. We choose the latter as

it leads to a particularly famous result in HIT theory.

$$E_r^{\mathrm{V}}(k,t) = \epsilon^{2/3} k^{-5/3}. \tag{5.7}$$

Therefore,

$$E^{\mathrm{V}}(k,t) = \epsilon^{2/3} k^{-5/3} E_s^{\mathrm{V}}(k\ell_K,t). \tag{5.8}$$

Now invoking Hypothesis 5.2 we assert that $E_s^{\mathrm{V}}(k\ell_K,t)$ is independent of the viscosity *in the inertial subrange.* Therefore, in the inertial subrange the energy spectrum has the form,

$$E^{\mathrm{V}}(k,t) = C_K \epsilon^{2/3} k^{-5/3}. \tag{5.9}$$

This is the celebrated Kolmogorov energy spectrum and we refer to this result as the K41 spectrum. C_K is a presumably universal turbulence constant now called the Kolmogorov constant. In hydrodynamics, considerable experimental tests have determined $C_K \approx 1.4$ (Praskovsky and Oncley 1994). As a final note, we mention that the energy spectrum in (5.9) is a power law expression,

$$E^{\mathrm{V}} \sim k^{-n}. \tag{5.10}$$

We now turn to a discussion on HIT in MHD. For a detailed discussion, refer to (Biskamp 2003, chap. 5). The situation in MHD is less clear than in pure hydrodynamics. One of the primary difficulties is that it is not clear what the Kolmogorov length scales should be. Indeed, in addition to the hydrodynamic parameters of the problem, we now have additional parameters such as the magnetic diffusivity λ and the energy dissipation rate for the induction equation. Furthermore, the magnetic induction and velocity field often operate at different time and length scales. Finally, the fundamental assumption of local isotropy from the Kolmogorov theory may no longer apply. This is because anisotropy is inherent in MHD dynamics due to the magnetic field causing a preferred alignment direction, see (Müller and Biskamp 2003). Nevertheless, researchers have been inspired by the triumph of di-

mensional analysis in predicting the energy spectrum in the hydrodynamic case. An early proposition stemmed from dimensional arguments carried out by (Iroshnikov 1963) and (R. H. Kraichnan 1965) wherein a strong background magnetic field set a natural scale for the magnetic field. These researchers both predicted that the total energy spectrum in MHD is $E^{\mathrm{T}}(k) \sim k^{-3/2}$. This spectrum is known as the Iroshnikov-Kraichnan (IK) spectrum. The debate on the energy spectrum in MHD does not end here, however. A spectrum of $E^{\mathrm{T}}(k) \sim k_{\perp}^{-2}$ was discovered in the weak turbulence regime by (Galtier et al. 2000) where $k_{\perp}$ is the wavenumber in the direction perpendicular to the magnetic field.

Such difficulties have led to the proposition that MHD turbulence is not universal. That is, different flow fields may exhibit a different character in the inertial subrange. Interestingly, the predictions of the energy spectrum behavior have the power law exponent n lying somewhere between the IK prediction and the weak turbulence prediction, $3/2 < n < 2$. Another intriguing observation is that the K41 power law exponent is twice as close to the IK exponent than that of the weak turbulence exponent. For more details on the lack of universality of MHD turbulence refer to (Lee et al. 2010) and (Aluie and Eyink 2010).

The present work will consider the energy spectrum from the velocity field, already introduced as $E^{\mathrm{V}}(k)$, as well as the energy spectrum from the magnetic induction $E^{\mathrm{I}}(k, t)$ which is derived from $E^{\mathrm{I}}(\mathbf{k}, t)$ in the same way that $E^{\mathrm{V}}(k, t)$ was derived from $E^{\mathrm{V}}(\mathbf{k}, t)$. Note that

$$E^{\mathrm{I}}(\mathbf{k}, t) = \frac{1}{2\mu_o \rho} \widehat{\mathbf{B}}^*(\mathbf{k}, t) \cdot \widehat{\mathbf{B}}(\mathbf{k}, t). \tag{5.11}$$

The total energy spectrum is the sum of the kinetic and magnetic spectra,

$$E^{\mathrm{T}}(k, t) = E^{\mathrm{V}}(k, t) + E^{\mathrm{I}}(k, t). \tag{5.12}$$

We also have

$$K^{\mathrm{I}}(t) = \int_0^\infty E^{\mathrm{I}}(k,t) \ \mathrm{d}k \tag{5.13}$$

$$K^{\mathrm{T}}(t) = \int_0^\infty E^{\mathrm{T}}(k,t) \ \mathrm{d}k. \tag{5.14}$$

An alternative representation for the total energy is

$$K^{\mathrm{T}}(t) = K^{\mathrm{V}}(t) + K^{\mathrm{I}}(t). \tag{5.15}$$

We also introduce the energy dissipation,

$$\epsilon^{\mathrm{V}}(t) = 2\nu \left\langle \nabla^{\mathrm{s}}\mathbf{u} : \nabla^{\mathrm{s}}\mathbf{u} \right\rangle \tag{5.16}$$

$$\epsilon^{\mathrm{I}}(t) = 2\lambda \left\langle \nabla^{\mathrm{a}}\mathbf{B} : \nabla^{\mathrm{a}}\mathbf{B} \right\rangle. \tag{5.17}$$

We could also write

$$\epsilon^{\mathrm{V}}(t) = \int_0^\infty 2\nu k^2 E^{\mathrm{V}}(k) \ \mathrm{d}k \tag{5.18}$$

$$\epsilon^{\mathrm{I}}(t) = \int_0^\infty 2\lambda k^2 E^{\mathrm{I}}(k) \ \mathrm{d}k. \tag{5.19}$$

Finally note that the total MHD dissipation is

$$\epsilon^{\mathrm{T}}(t) = \epsilon^{\mathrm{V}} + \epsilon^{\mathrm{I}}. \tag{5.20}$$

With this background on HIT theory, we are now prepared to derive the RBEV constant $\overline{C}$ presented in Section 4.3.

5.1.2 The form of $\overline{C}$

The derivation of $\overline{C}$ begins with the turbulent dissipation of the total energy for MHD in the context of HIT. With the RBEV model the turbulent dissipation is

$$\epsilon^{\mathrm{T},\,h} = 2 \left\langle \nu_T \nabla^{\mathrm{s}}\mathbf{u}^h : \nabla^{\mathrm{s}}\mathbf{u}^h + \lambda_T \nabla^{\mathrm{a}}\mathbf{B}^h : \nabla^{\mathrm{a}}\mathbf{B}^h \right\rangle, \tag{5.21}$$

where the contributions from the molecular viscosity and magnetic diffusivity have been neglected and $\langle \cdot \rangle$ denotes an averaging operation. With $\mu_0/\rho = \nu_T = \lambda_T = \overline{C}_0 h |\mathbf{u}'|$,

$$\epsilon^{\mathrm{T},\,h} = 2\overline{C}_0 h \left\langle |\mathbf{u}'| \left(\nabla^{\mathrm{s}}\mathbf{u}^h : \nabla^{\mathrm{s}}\mathbf{u}^h + \nabla^{\mathrm{a}}\mathbf{B}^h : \nabla^{\mathrm{a}}\mathbf{B}^h \right) \right\rangle$$

$$\approx 2\overline{C}_0 h \left\langle |\mathbf{u}'|^2 \right\rangle^{1/2} \left\langle \nabla^{\mathrm{s}}\mathbf{u}^h : \nabla^{\mathrm{s}}\mathbf{u}^h + \nabla^{\mathrm{a}}\mathbf{B}^h : \nabla^{\mathrm{a}}\mathbf{B}^h \right\rangle. \tag{5.22}$$

To express each term on the right-hand-side of (5.22) in terms of the total energy spectrum the spectra for $\mathbf{u}$ and $\mathbf{B}$ are assumed to differ by a multiplicative constant. Thus, $|\mathbf{u}'|^2$ can be replaced with $\alpha \left(|\mathbf{u}'|^2 + \frac{1}{\mu_0\rho} |\mathbf{B}'|^2 \right)$ where

$$\alpha = \frac{|\mathbf{u}'|^2}{|\mathbf{u}'|^2 + \frac{1}{\mu_0\rho} |\mathbf{B}'|^2}. \tag{5.23}$$

It is assumed that the numerical method only solves for scales with wavenumber between 0 and the cutoff wavenumber k^h. Thus, discrete quantities such as $\mathbf{u}^h$ only contain information up to the cutoff wavenumber. Additionally, the subgrid scales are assumed to exist between the cutoff wavenumber and some maximum subgrid wavenumber, βk^h. In a pseudo-spectral numerical method $\beta > 1$ in order to account for the effects of aliasing. The magnitude of the fluctuating velocity components are related to the energy spectrum via

$$\left\langle |\mathbf{u}'|^2 \right\rangle = 2 \int_{k^h}^{\beta k^h} E^{\mathrm{V}}(k) \; \mathrm{d}k. \tag{5.24}$$

From (5.18), (5.19), and (5.20) we have

$$\left\langle \nabla^{\mathrm{s}}\mathbf{u}^h : \nabla^{\mathrm{s}}\mathbf{u}^h + \nabla^{\mathrm{a}}\mathbf{B}^h : \nabla^{\mathrm{a}}\mathbf{B}^h \right\rangle = \int_0^{k^h} k^2 E^{\mathrm{T}}(k) \; \mathrm{d}k. \tag{5.25}$$

Using these relationships in (5.22) yields,

$$\epsilon^h \approx 2\overline{C}_0 h \left(2\alpha \int_{k^h}^{\beta k^h} E^{\mathrm{T}}(k) \; \mathrm{d}k \right)^{1/2} \times$$
$$\left(\int_0^{k^h} k^2 E^{\mathrm{T}}(k) \; \mathrm{d}k \right). \tag{5.26}$$

A power law for the total energy spectrum is assumed,

$$E^{\mathrm{T}}(k) = C_K C' \epsilon^m k^n \tag{5.27}$$

where ϵ is the exact dissipation rate. The constant C' depends on the physics of the problem. For example, when $n = -2$, $C' = 1/v_A$, where v_A is the Alfvén velocity. Note that in general C' is not dimensionless. After some algebra,

$$\epsilon^h \approx \overline{C}_0 2\sqrt{2} h \sqrt{\alpha} \left(C_K C' \right)^{3/2} \frac{\left(k^h \right)^{3(n+1)/2}}{(n+3)(n+1)^{1/2}} \times$$
$$\left(\beta^{n+1} - 1 \right)^{1/2} \epsilon^{3m/2}. \tag{5.28}$$

Equating the modeled and exact dissipation rate, $\epsilon^h = \epsilon$, results in

$$\overline{C}_0 = \overline{C} \alpha^{-1/2} \tag{5.29}$$

with

$$\overline{C} = \frac{1}{2\sqrt{2} h \left(C_K C' \right)^{3/2} K \left(\beta^{n+1} - 1 \right)^{1/2} \epsilon^{(3m-2)/2}} \tag{5.30}$$

and

$$K = \frac{\left(k^h \right)^{3(n+1)/2}}{(n+3)(n+1)^{1/2}}. \tag{5.31}$$

Note that, in general, the calibration constant $\overline{C}$ will not be problem independent as it has a dependency on the dissipation rate. However, if a Kolmogorov spectrum

is assumed ($m = 2/3$, $n = -5/3$) then with a cutoff wavenumber of $k^h = \pi/h$ and $\beta \to \infty$ (to account for all of the subgrid scales)

$$\overline{C} = \left(\frac{4}{27}\right)^{1/2} \frac{1}{C_K^{3/2}\pi}. \tag{5.32}$$

Returning now to the expressions for the eddy viscosity and the magnetic diffusivity results in

$$\begin{aligned}
\nu_T = \lambda_T &= \overline{C}_0 h |\mathbf{u}'| \\
&= \overline{C}\alpha^{-1/2}h|\mathbf{u}'| \\
&= \overline{C}h\sqrt{|\mathbf{u}'|^2 + \frac{1}{\mu_0\rho}|\mathbf{B}'|^2}
\end{aligned} \tag{5.33}$$

which is the final result.

5.1.3 Taylor-Green Vortex and Results

The main problem that the new models were tested on was the insulating Taylor-Green vortex described in (Pouquet et al. 2010). The domain is a periodic box

$$\Omega = [-\pi, \pi]^3 \tag{5.34}$$

and is illustrated in Figure 5.3. The initial conditions were

$$\mathbf{u}_0 = u_0 \begin{bmatrix} \sin\left(\frac{x}{L}\right)\cos\left(\frac{y}{L}\right)\cos\left(\frac{z}{L}\right) \\ -\cos\left(\frac{x}{L}\right)\sin\left(\frac{y}{L}\right)\cos\left(\frac{z}{L}\right) \\ 0 \end{bmatrix} \tag{5.35}$$

for the velocity field and

$$\mathbf{B}_0 = B_0 \begin{bmatrix} \cos\left(\frac{x}{L}\right)\sin\left(\frac{y}{L}\right)\sin\left(\frac{z}{L}\right) \\ -\sin\left(\frac{x}{L}\right)\cos\left(\frac{y}{L}\right)\sin\left(\frac{z}{L}\right) \\ -2\sin\left(\frac{x}{L}\right)\sin\left(\frac{y}{L}\right)\cos\left(\frac{z}{L}\right) \end{bmatrix} \tag{5.36}$$

for the magnetic induction.
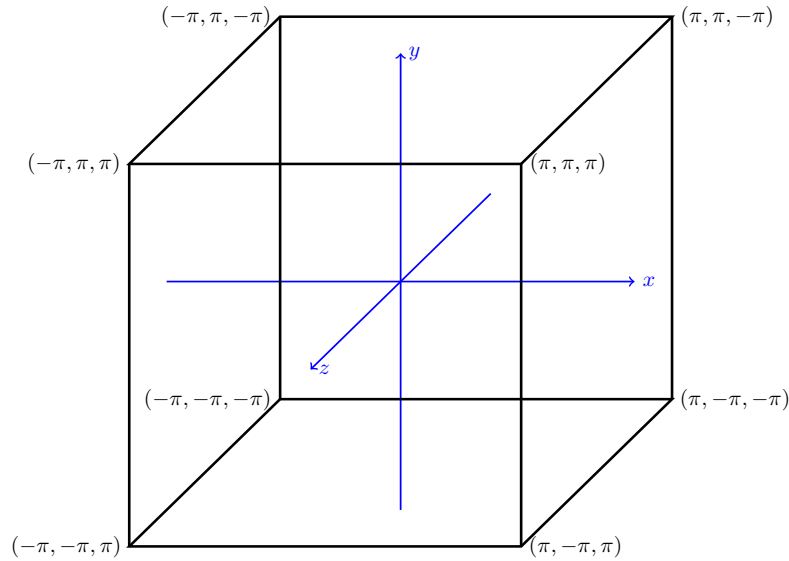
**Figure 5.3: The simulation domain for the insulating Taylor-Green vortex.**

This particular problem solved for the magnetic induction in Alfvén velocity units. The coefficients u_0 and B_0 were set so that the initial total energy had a value of 1/4. This flow field has been termed insulating in (Pouquet et al. 2010) because the current density is everywhere parallel to the artificial walls of the box. This is readily demonstrated by taking the curl of the initial magnetic field,

$$\mathbf{j} = \nabla \times \mathbf{B}_0 = 3 \begin{bmatrix} -\frac{\partial \mathbf{B}_y}{\partial z} \\ \frac{\partial \mathbf{B}_x}{\partial z} \\ 0 \end{bmatrix}. \tag{5.37}$$

Thus, the current density is only ever in the $x - y$ plane. By virtue of the form of the magnetic induction (5.36) it is easily seen that on surfaces of constant y the current density only points in the x-direction. Likewise, on surfaces of constant x the current density only points in the y-direction.

The DNS simulations of this problem were run with 512 Fourier modes in each direction. To account for aliasing effects in the pseudospectral code on the 2nd order nonlinearities a 2/3 dealiasing rule was used. Thus, the total number of modes was $M = 3N/2 = 768$. The total number of processors used was 384. Note also that

the code was set up so that modes in the $x - y$ direction were handled with one processor. Different processors handled different z values. Therefore, the processor decomposition was done via slabs. See Figure 5.4 for an illustration.
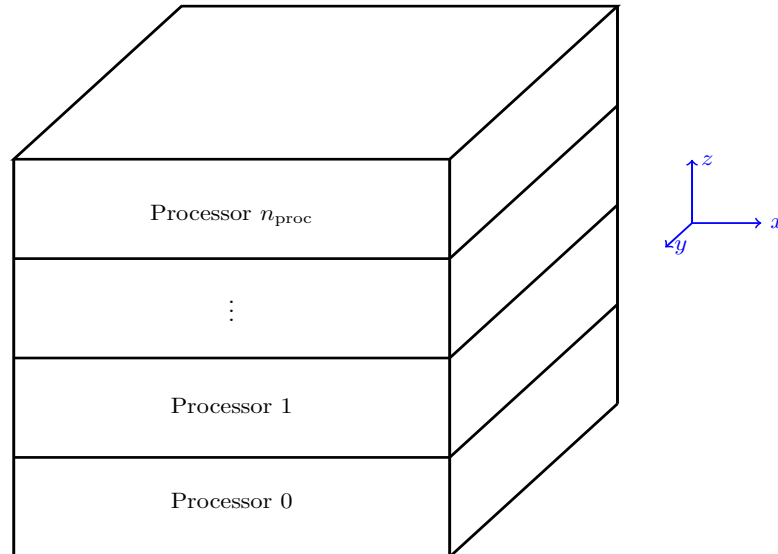
Figure 5.4: The processor decomposition for the Fourier-spectral code.

The LES simulations were run with 32, 64, and 128 modes in each direction, using a 2/3 dealiasing rule for each simulation. The LES code was set up in the same way as the DNS code. The DNS simulations had 4096 more modes than the LES simulations performed with 32^3 modes. This corresponds to the LES simulations having 99.9% less information than the DNS simulations.

Most of the runs were carried out with Re $= 5300$ and $Pr_m = 1$. The Reynolds numbers were defined as

$$\text{Re} = \frac{u^{\text{rms}} L^{\text{V}}}{\nu} \tag{5.38}$$

$$\text{Rm} = \frac{u^{\text{rms}} L^{\text{I}}}{\lambda} \tag{5.39}$$

where u^{rms} is the root mean square value of the velocity field and $L^{\text{V,I}}$ are integral length scales defined as

$$L^{\text{V,I}} = 2\pi \frac{\int \frac{1}{k} E^{\text{V,I}}(k) \ \mathrm{d}k}{\int E^{\text{V,I}}(k) \ \mathrm{d}k}. \tag{5.40}$$

The basic dynamics of the flow field are described by Figure 5.5 where the energies are plotted as a function of a dimensionless time scale, $t = t_s / (u_0/L)$ with $L = 1$ and t_s the simulation time.
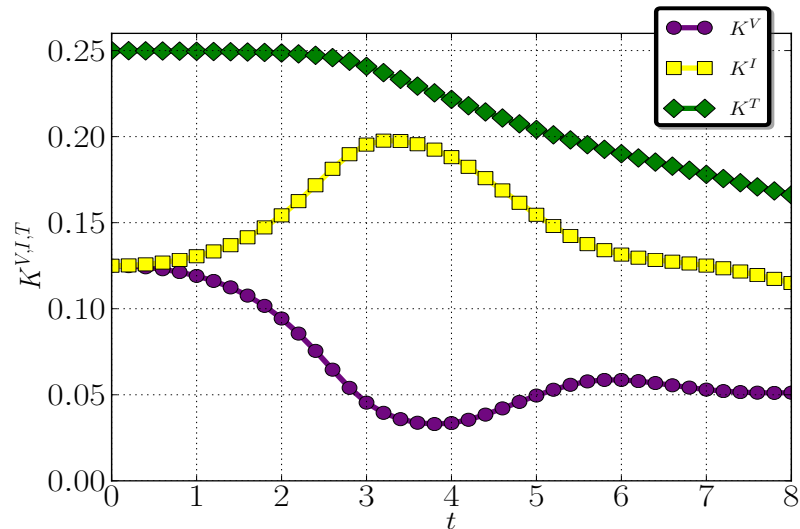
**Figure 5.5: Energy transfer between velocity and magnetic fields for the Taylor-Green vortex.**

The system is dissipative overall due to viscous and resistive effects and the lack of energy sources. However, there is an interesting interplay between the velocity and magnetic induction. In this particular problem, the magnetic induction gains energy at the expense of the velocity field. A comparison between the VMS, mixed, and dynamic Smagorinsky LES models and the DNS is made in Figure 5.6 . Note that all of the models are overly dissipative but that the dynamic Smagorinsky is the most dissipative of all by far. All of the models have difficulty in achieving the peak of the magnetic energy at around $t = 4$.

(a)

(b)

(c)
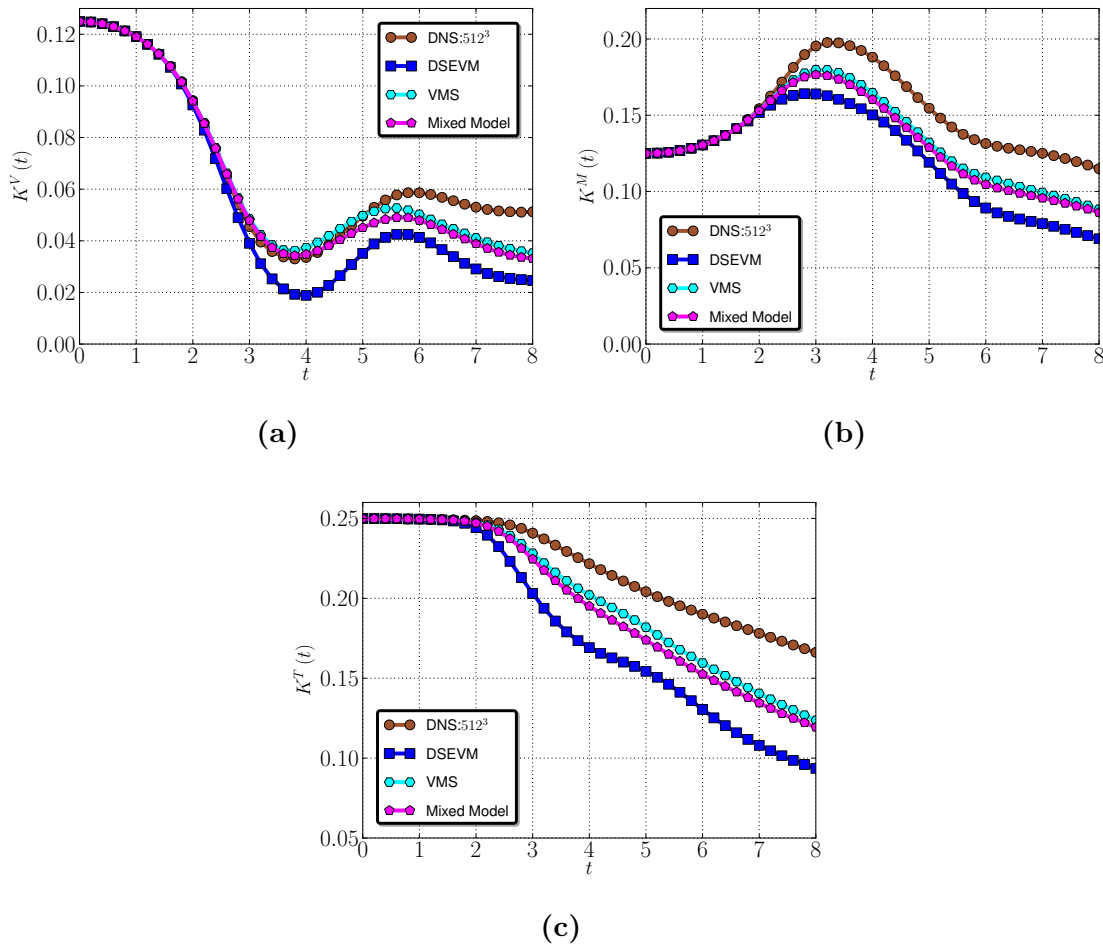
Figure 5.6: A comparison between the DNS solution and the VMS, MM, and dynamic Smagorinsky models.

5.1.3.1   Energy Spectra

Further insight into the nature of the models is gained by exploring plots of the energy spectra. The following figures present energy spectra plots at $t = 8$. Figure 5.7 compares all of the models to each other. Although somewhat crowded, some key observations can be made from this plot. First of all, the VMS and mixed models perform quite well especially in the mid-wavenumber range. They both also provide enough dissipation in the high-wavenumber range to match the DNS simulation satisfactorily.
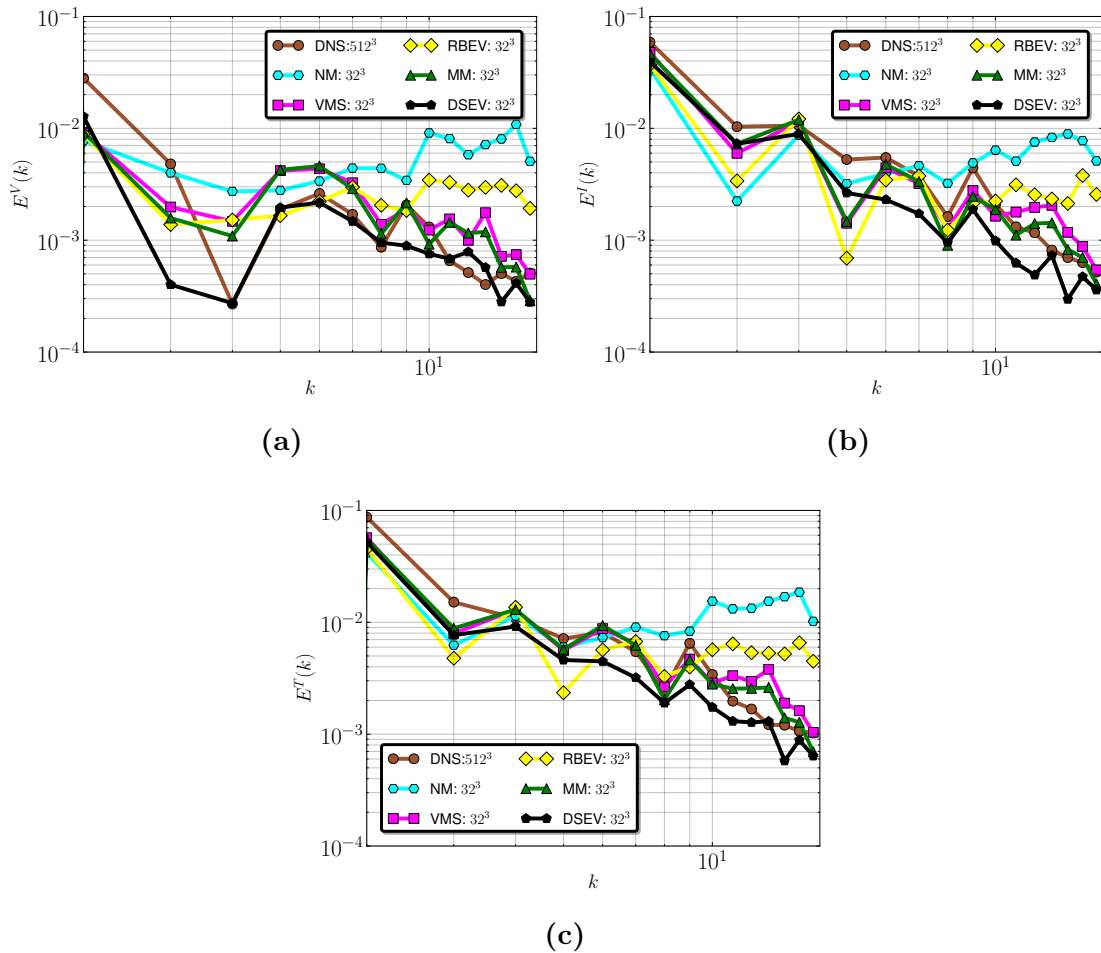
Figure 5.7: Comparison of kinetic, magnetic, and total energy spectra from each model to DNS. Results were obtained from a simulation with 32 **modes in each direction.**

We also note that the dynamic Smagorinsky model does not perform as well as the VMS and mixed models in the mid-wavenumber range but that it performs slightly better in the high-wavenumber range. The dynamic Smagorinsky model is excessively dissipative whereas the VMS and mixed models are slightly under diffuse. Turning to the RBEV model, we note that this model, by itself, does not perform particularly well. In the high wavenumber range it does out-perform the case with no model at all, but it clearly does not provide nearly enough dissipation to match the accepted DNS results. We will return to the effect of the RBEV on the mixed model later when considering other spectra plots.

We mention here a point about the amount of simulation time required for the above simulations. The goal of LES is to produce high-fidelity results with low computational cost. Such a simulation would be quick and therefore amenable to high throughput physics and design studies. It is critical that the LES models developed do not contribute much computation time. Figure 5.8 quantifies simulation times for the models presented in Figure 5.7.
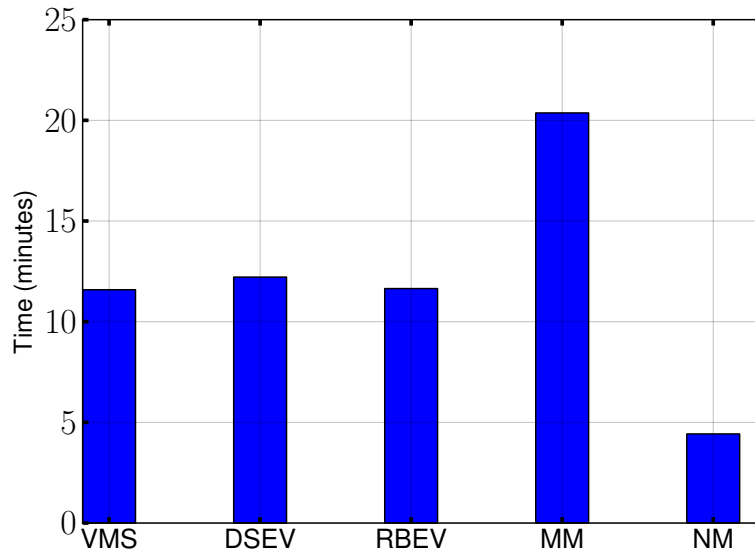

Figure 5.8: Duration in minutes of LES simulations as compared to a simulation of the same resolution with no model.

All of the simulations are completed quite quickly with the mixed model taking the longest amount of time. The 512^3 DNS simulations, on the other hand, took about 24 hours to complete. Therefore, given the initial performance of the new models, it is clear that they are promising and should be tested on many other problems.

We now return to the energy spectra. It is useful to compare fewer models on a plot in order to gain further insight. Figure 5.9 does this by comparing the VMS and mixed models to the dynamic Smagorinsky model. The main point that can be made from observations of this plot, that was not already observed from Figure 5.7 is that the VMS and mixed models perform comparably. The true benefit of the

mixed model becomes apparent when considering higher values of Re and Rm as will be seen in later sections.

(a)

(b)

(c)
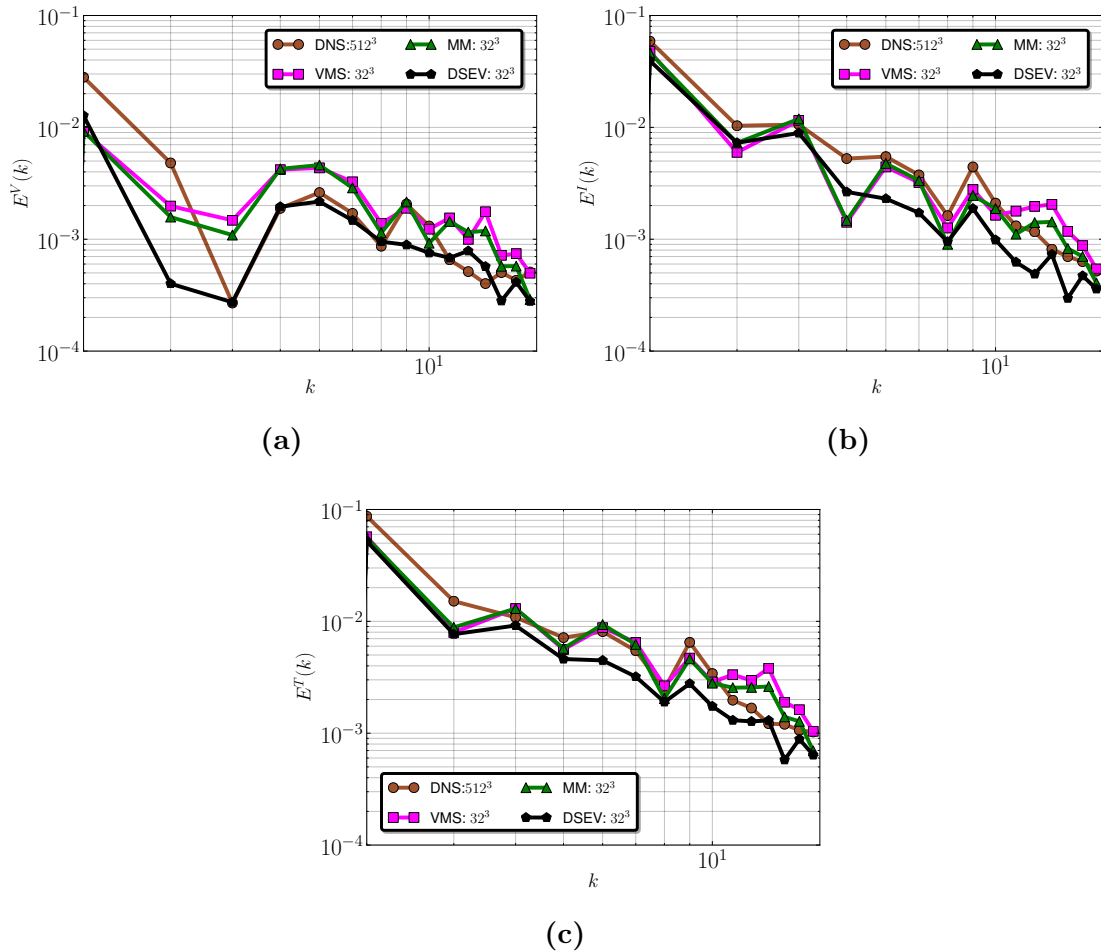
Figure 5.9: Comparison of kinetic, magnetic, and total energy spectra from the VMS and mixed models to the dynamic Smagorinsky model and a DNS simulation. Results were obtained from a simulation with 32 **modes in each direction.**

It is also instructive to compare the RBEV to the case with no model whatsoever as is done in Figure 5.10. Although the RBEV model does not perform well, it does provide some dissipation. Interestingly, this observation may be the key to the performance of the mixed model; the RBEV provides some much needed aid to the VMS method but not so much as to make the system excessively diffuse.
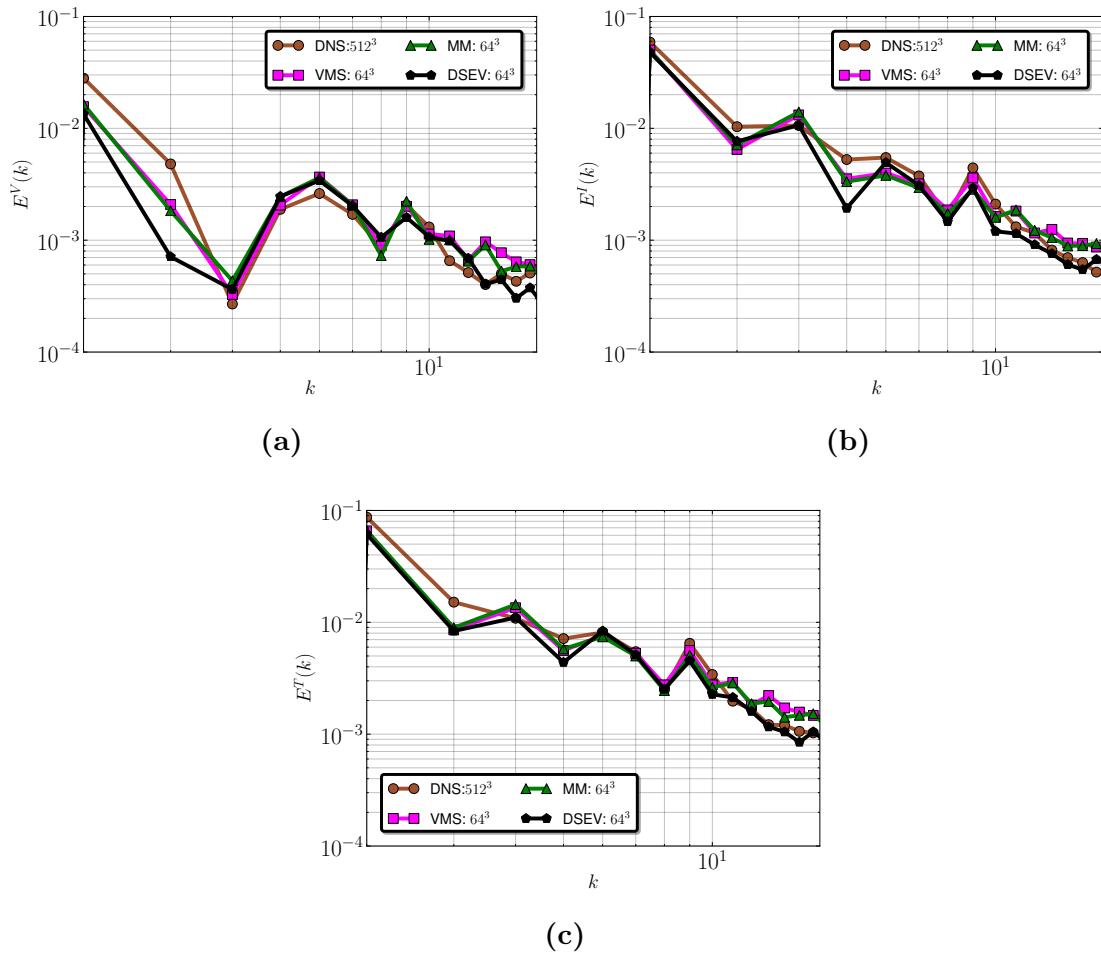
(a)

(b)

(c)
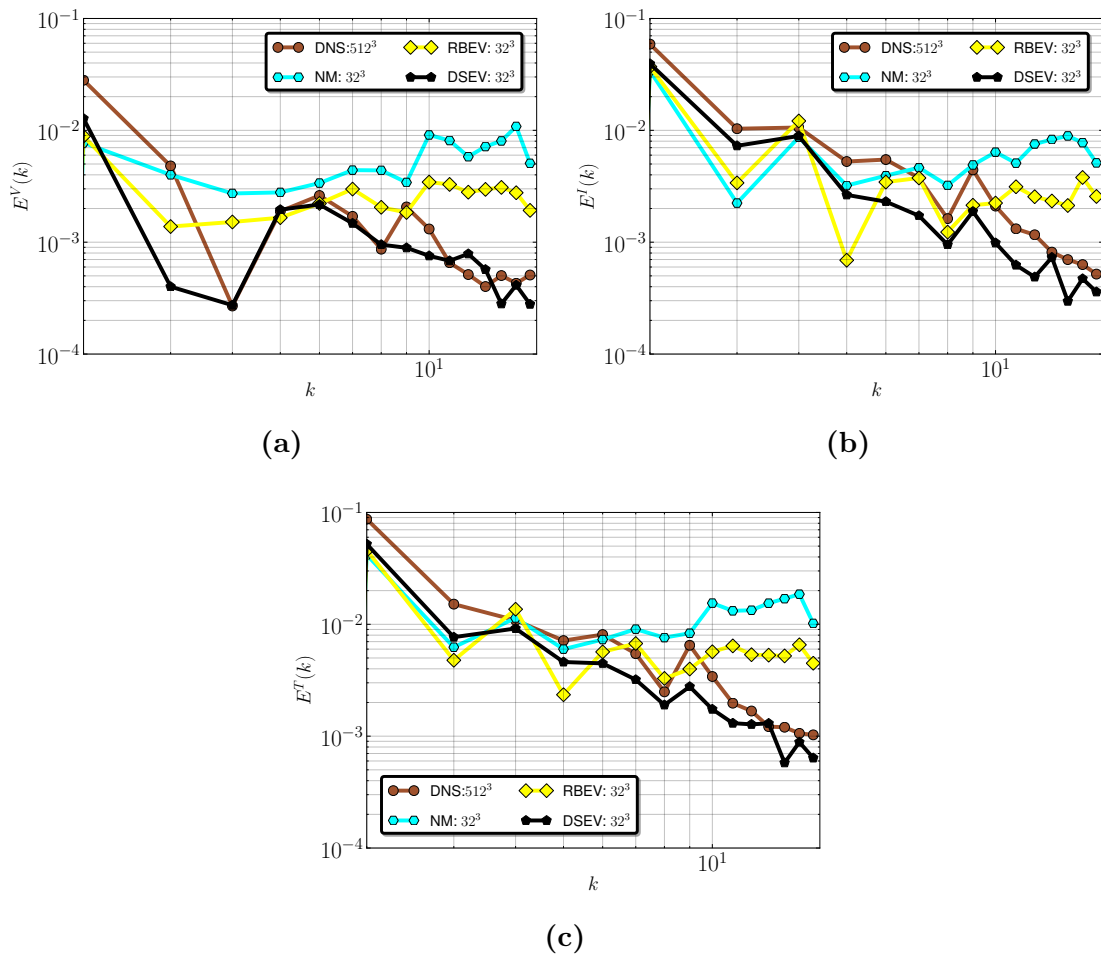
Figure 5.10: Comparison of kinetic, magnetic, and total energy spectra from the RBEV model and the case with no model to the dynamic Smagorinsky model and a DNS simulation. Results were obtained from a simulation with 32 modes in each direction.

5.1.3.2 Convergence with Mesh Refinement

In this section, we demonstrate that with mesh refinement the models converge to the DNS solution. Figure 5.11 shows results from a simulation with 64 modes in each direction. We note that the solution has improved considerably over the results from the 32^3 simulation.

(a)

(b)

(c)

Figure 5.11: Comparison of kinetic, magnetic, and total energy spectra from the VMS and mixed models to the dynamic Smagorinsky model and a DNS simulation. Results were obtained from a simulation with 64 modes in each direction.

Figure 5.12 shows convergence over successively finer meshes for the mixed model.

(a)

(b)

(c)
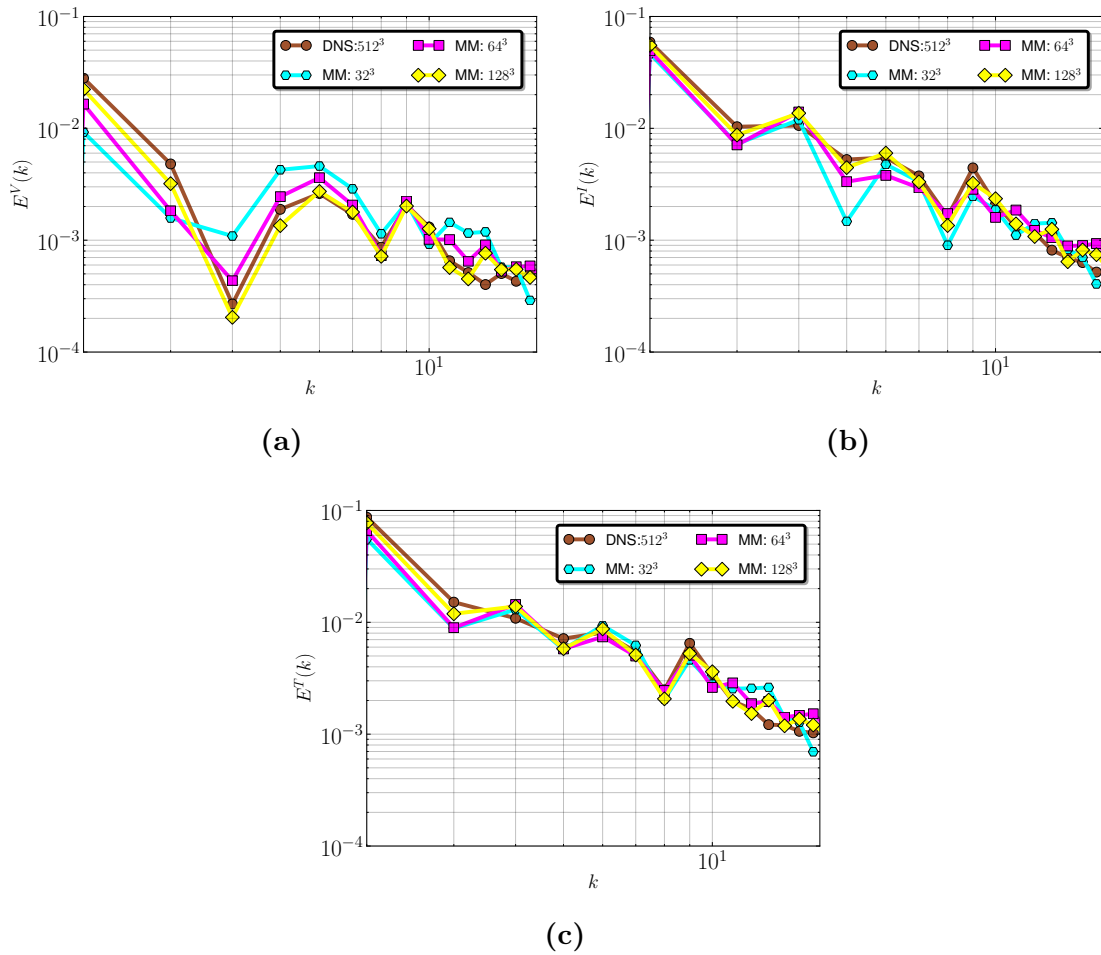
Figure 5.12: A convergence study for the mixed model on meshes of 32^3, 64^3, and 128^3.

5.1.3.3 Comparison to DSEVA Model

The DSEV model was designed to permit inverse cascades of magnetic energy which are known to occur in MHD. We compare the performance of this model to the VMS based model in Figure 5.13. This model does not appear to offer any benefit over the traditional DSEV model and even underperforms in representing certain regions of the spectra such as the mid-wavenumber range. As a result, the same conclusions with regard to the performance of the VMS-based models in comparison to the DSEV model holds.
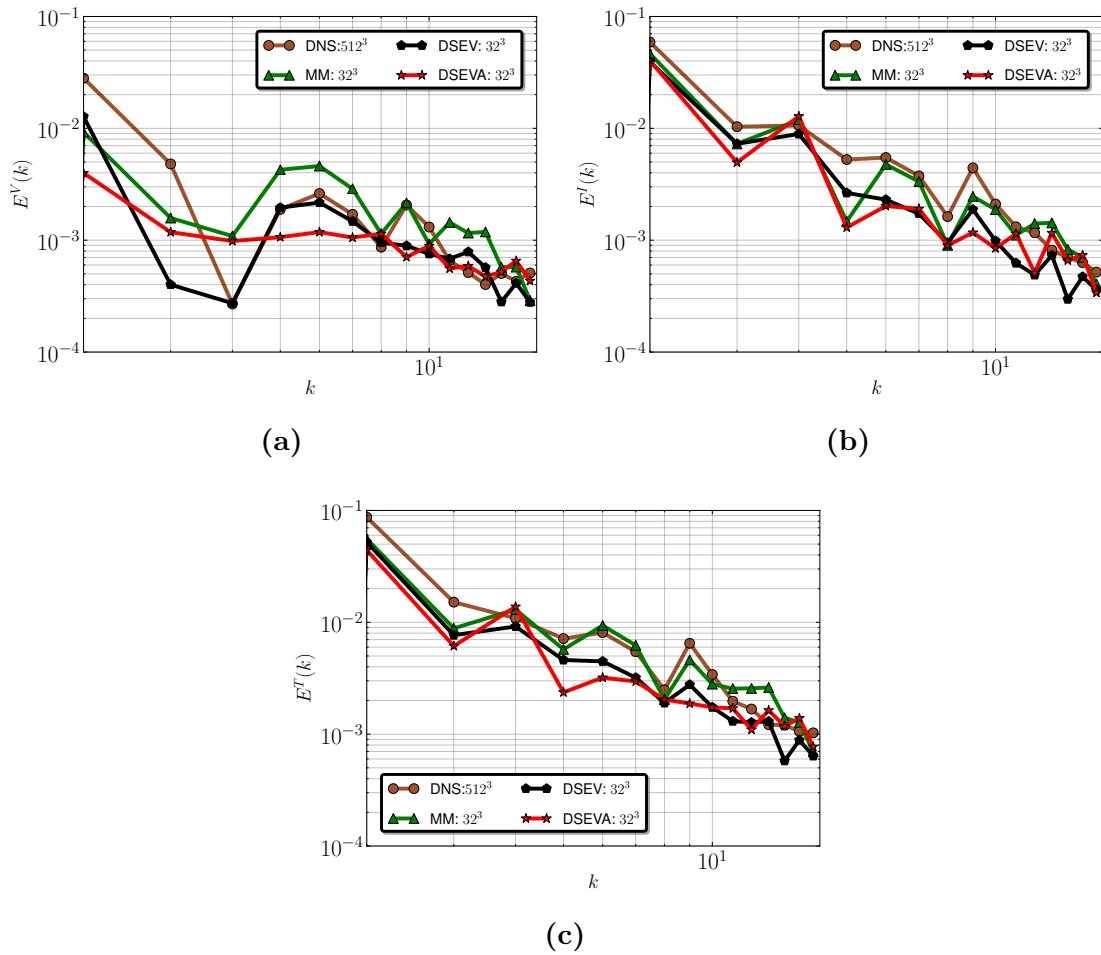
Figure 5.13: Comparison of kinetic, magnetic, and total energy spectra from the mixed model and the alignment-based dynamic Smagorinsky model to a DNS simulation. Results were obtained from a simulation with 32 modes in each direction.

5.1.3.4 Eddy Diffusivities

Studying the behavior of the eddy diffusivities (ν_T and λ_T) provides valuable information about the performance of the models. Figure 5.14 compares the average eddy viscosities from the mixed and RBEV models to the dynamic Smagorinsky model. Also included is the eddy viscosity from the alignment-based dynamic Smagorinsky model.

A significant observation is that the eddy viscosities from all of the models are nearly zero until $t \sim 1$. At this point, the eddy viscosities begin to take on

finite values because they are adjusting for the turbulence that has developed in the flow field. The dynamic Smagorinsky models make this adjustment through the dynamic determination of the Smagorinksy coefficients. However, the RBEV and mixed models use a universal constant in the models and yet automatically adjust as the simulation requires. Hence, the claim that these new VMS-based models are inherently dynamic is justified.
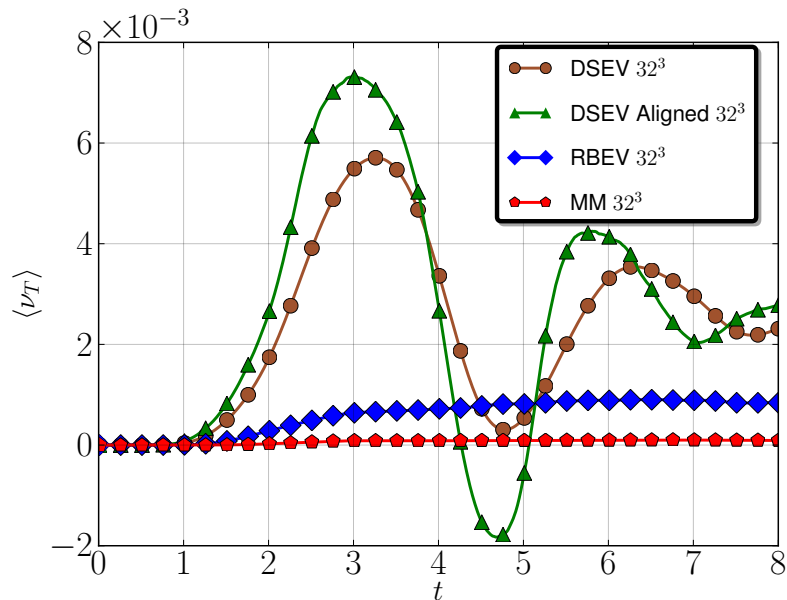
Figure 5.14: Plots of average eddy viscosities from the mixed, RBEV, and two versions of the dynamic Smagorinsky models. Results are from a 32^3 simulation.

Notice that the Smagorinsky models are much more variable than the VMS-based models. This is due to the fundamentally different natures of the models; the Smagorinsky eddy diffusivities are proportional to the rate of strain whereas the VMS-based eddy diffusivities are proportional to the subgrid solutions themselves. The dynamic nature of the Smagorinsky models derives from the variability of the Smagorinsky coefficient rather than the direct effect of the subgrid scales. One striking difference is that the Smagorinsky eddy viscosities are largest near $t = 4$ which corresponds to the peak of dissipation for this flow field. In this sense then, the Smagorinsky eddy viscosities reflect the dynamics of the flow field as they try to account for times that have more or less dissipation. We also observe that the eddy

viscosity for the alignment-based Smagorinsky model takes on negative values when the simulation is performed with 32 modes. This behavior is no longer present for $N = 64$. Figure 5.15 shows the eddy viscosities on a finer mesh and it is observed that their contribution is smaller. This is expected as the finer mesh represents more of the velocity field and therefore the modeling efforts required are not as significant.
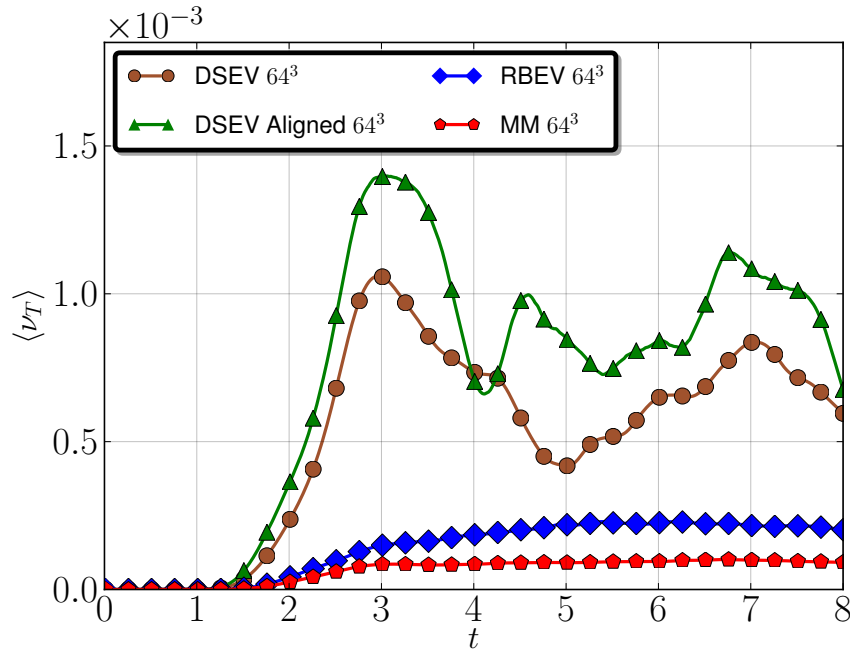
Figure 5.15: **Plots of average eddy viscosities from the mixed, RBEV, and two versions of the dynamic Smagorinsky models. Results are from a 64^3 simulation.**

The same analysis is performed in Figures 5.16 and 5.17 for the magnetic eddy diffusivities with similar conclusions. One stark difference between the magnetic diffusivities and the eddy viscosities is that the magnetic diffusivity for the alignment-based dynamic Smagorinsky model does not become negative.
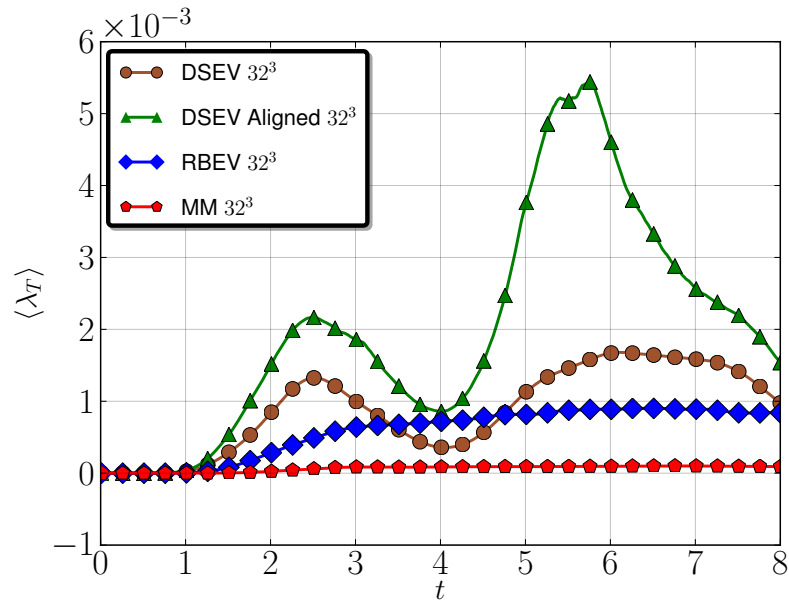
Figure 5.16: Plots of average magnetic diffusivities from the mixed, RBEV, and two versions of the dynamic Smagorinsky models. Results are from a 32^3 simulation.
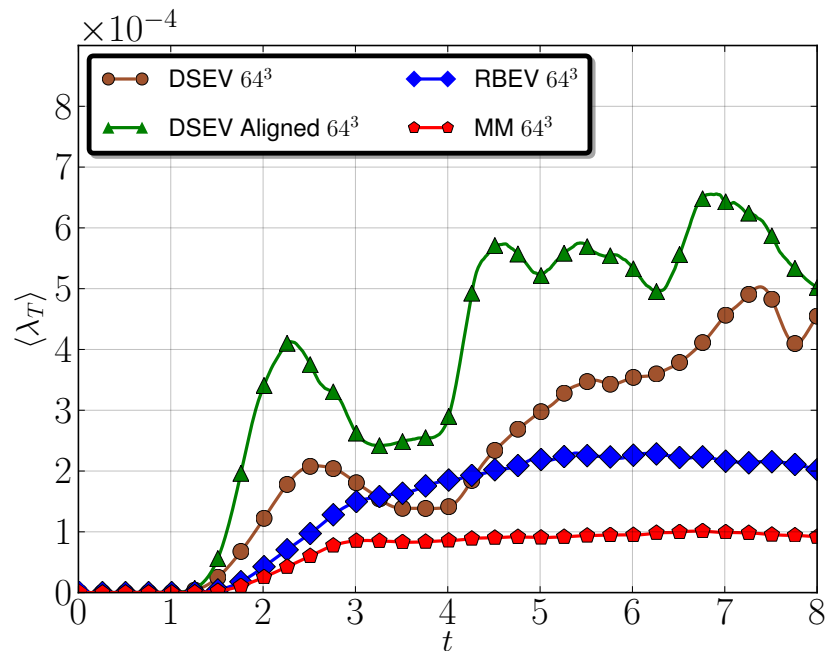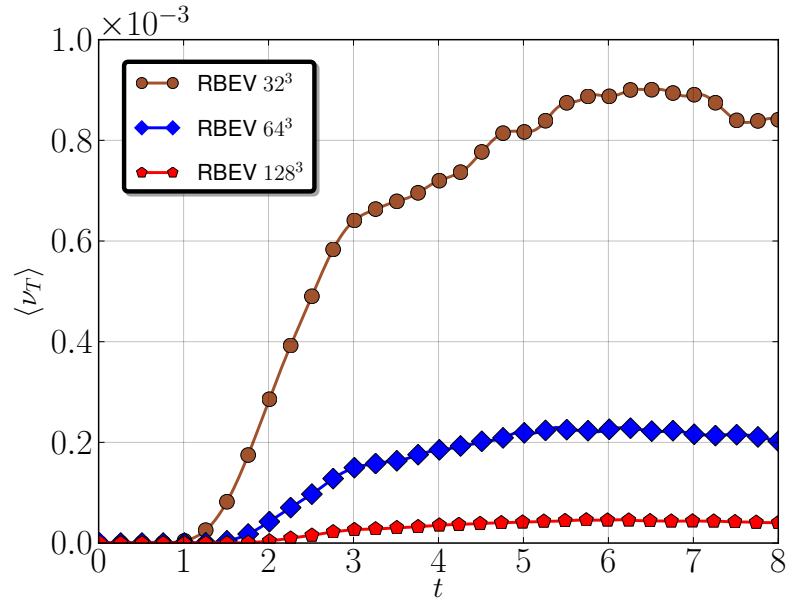

Figure 5.17: Plots of average magnetic diffusivities from the mixed, RBEV, and two versions of the dynamic Smagorinsky models. Results are from a 64^3 simulation.

With mesh refinement, the contribution from the eddy viscosities becomes noticeably smaller. This can be seen in Figure 5.18 for the eddy viscosities from the RBEV model.

Figure 5.18: The average eddy viscosity from the RBEV model. Results are presented on meshes of 32^3, 64^3, and 128^3.

5.1.3.5 Performance at High Re and Rm

The Reynolds numbers in the previous simulations were not particularly high. It was not easy to draw convincing conclusions on the performance of the mixed and VMS models as they appeared to behave comparably. A simulation at Re = 20000, again with $Pr_m = 1$, was performed in an effort to gain a deeper understanding of the differences in the mixed and VMS models. At such a high Re the subgrid stress terms should be more active than in the previous simulation. Figure 5.19 shows the results of a 32^3 LES simulation compared to a 2048^3 DNS carried out by (Pouquet et al. 2010). The plot is of the total energy spectrum compensated by k^2 and averaged around the peak of dissipation at $t = 4$. The averaging time was $t \in [3.5, 5]$. The performance of the models on such a coarse grid is striking. Furthermore, the mixed model outperforms the VMS model in the high-wavenumber range. This is attributed to the activity of the RBEV model. Although the RBEV

does not perform well in isolation, it is able to provide just enough dissipation in addition to that already present in the VMS model to give very good results. We also note that the dynamic Smagorinsky model yields far too much dissipation.
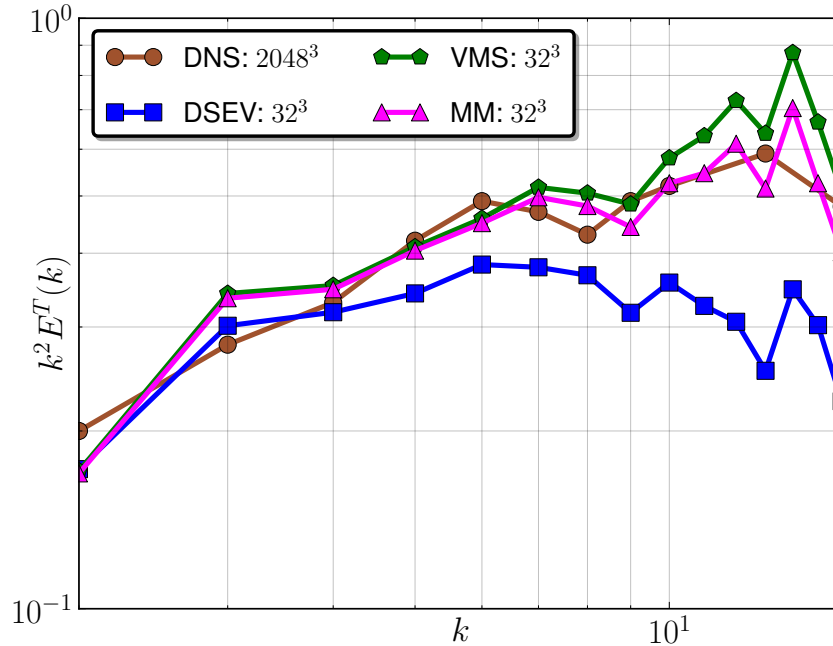
Figure 5.19: **Compensated energy spectra from the mixed, dynamic Smagorinsky, and VMS models. Results are from a 32^3 mesh. DNS data are from (Pouquet et al. 2010).**

Another interesting study involves the comparison of results obtained with the alignment-based DSEV model for this Re. These results are presented in Figure 5.20. It is apparent that the alignment-based model makes a valiant attempt to reach the proper dissipation in the high wavenumber range. However, this comes at a steep price because the compensated spectrum no longer exhibits the correct behavior or any semblance thereof.
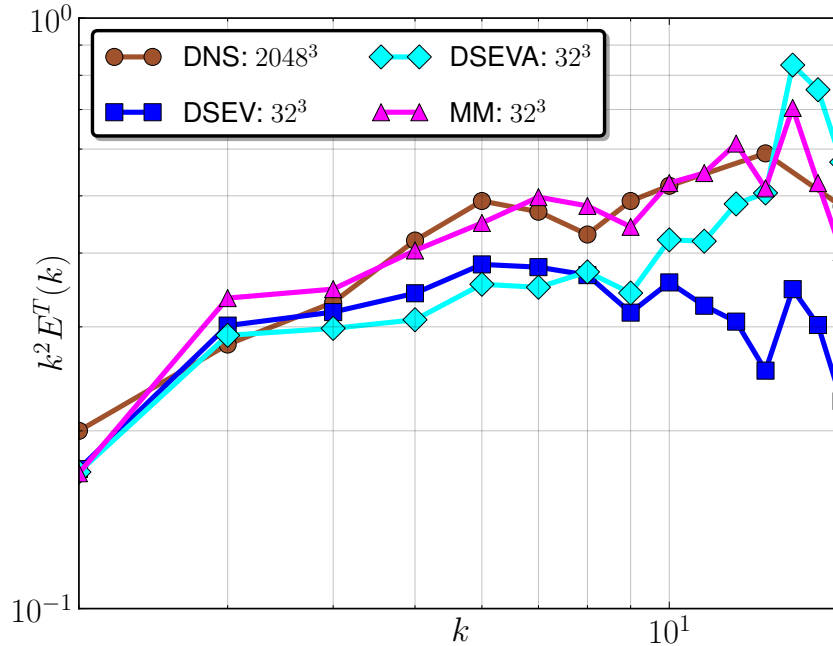
Figure 5.20: Compensated energy spectra from the mixed, dynamic Smagorinsky, and alignment-based dynamic Smagorinsky models. Results are from a 32^3 mesh. DNS data are from (Pouquet et al. 2010).

5.1.3.6 Finite Element Simulations of the Taylor-Green Vortex

The new VMS-based models were implemented into the finite element code Drekar. The VMS formulation with nonorthogonal basis functions, such as linear finite elements, is different from the spectral formulation in that the linear terms become active. In this section we present results from the Taylor-Green vortex simulation that has been discussed extensively in this section. The problem setup for the finite element and spectral simulations are the same. We use linear finite elements to perform these simulations. Note that one would not expect linear finite elements to perform as well as spectral basis functions. The following figures demonstrate, however, that the finite element method performs quite well. This is true even for a coarse grid of 32^3 elements. Figure 5.21 shows a comparison of the VMS model performance from spectral simulations and finite element simulations.

(a)

(b)

(c)
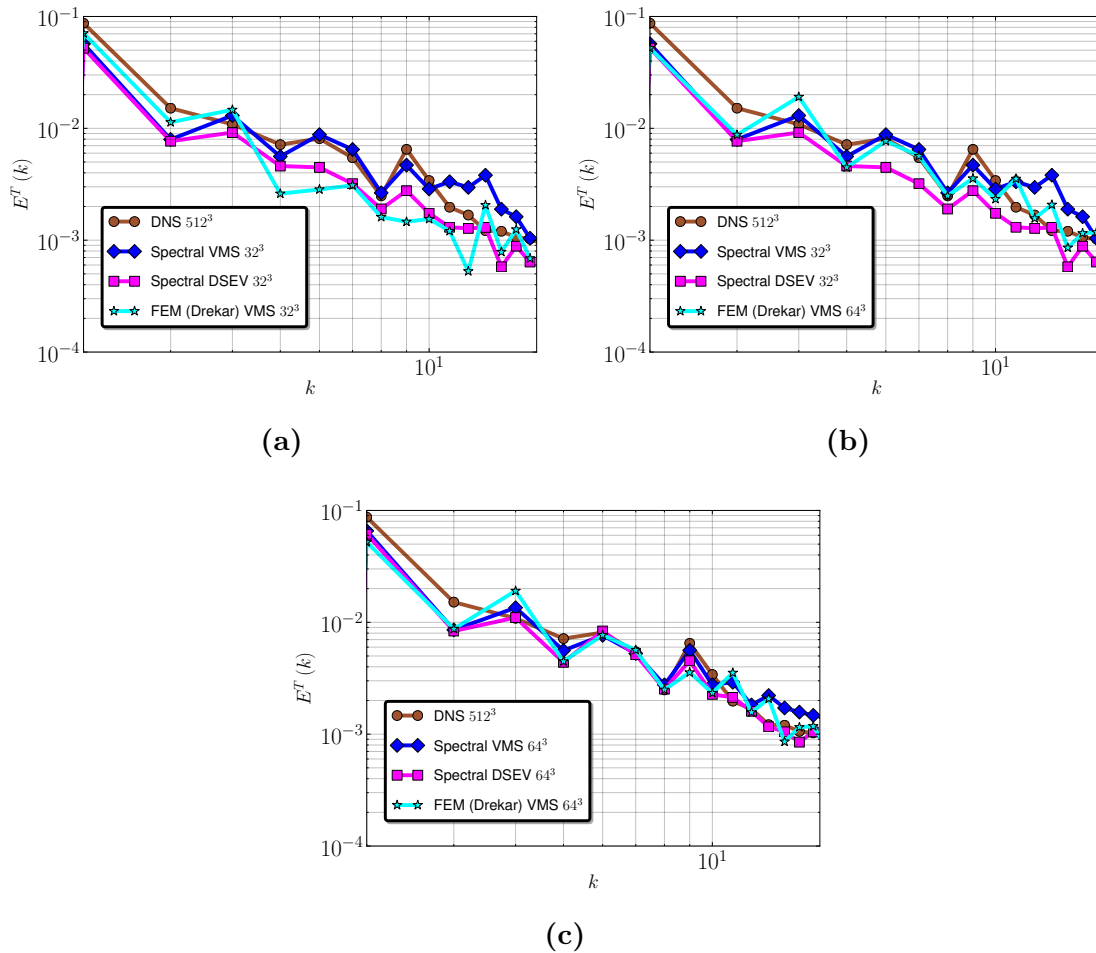
Figure 5.21: The total energy spectrum at $t = 8$. Figure 5.21a compares the finite element performance with 32^3 linear elements to the spectral results with 32^3 modes. Figure 5.21b compares the finite element performance with 64^3 linear elements to spectral results with 32^3 modes. Figure 5.21c compares the finite element performance with 64^3 linear elements to spectral results with 64^3 modes.

We observe that, as expected, the finite element implementation does not perform quite as well as the spectral formulation for 32^3 elements. However, the results are encouraging and simulations with 64^3 elements yield very good results. A convergence test was performed for the finite element simulations to test the numerical performance of the models. In particular, it is crucial that the models

converge to the DNS results as the mesh is refined. Figure 5.22 confirms that this is indeed the case.

(a)

(b)

(c)
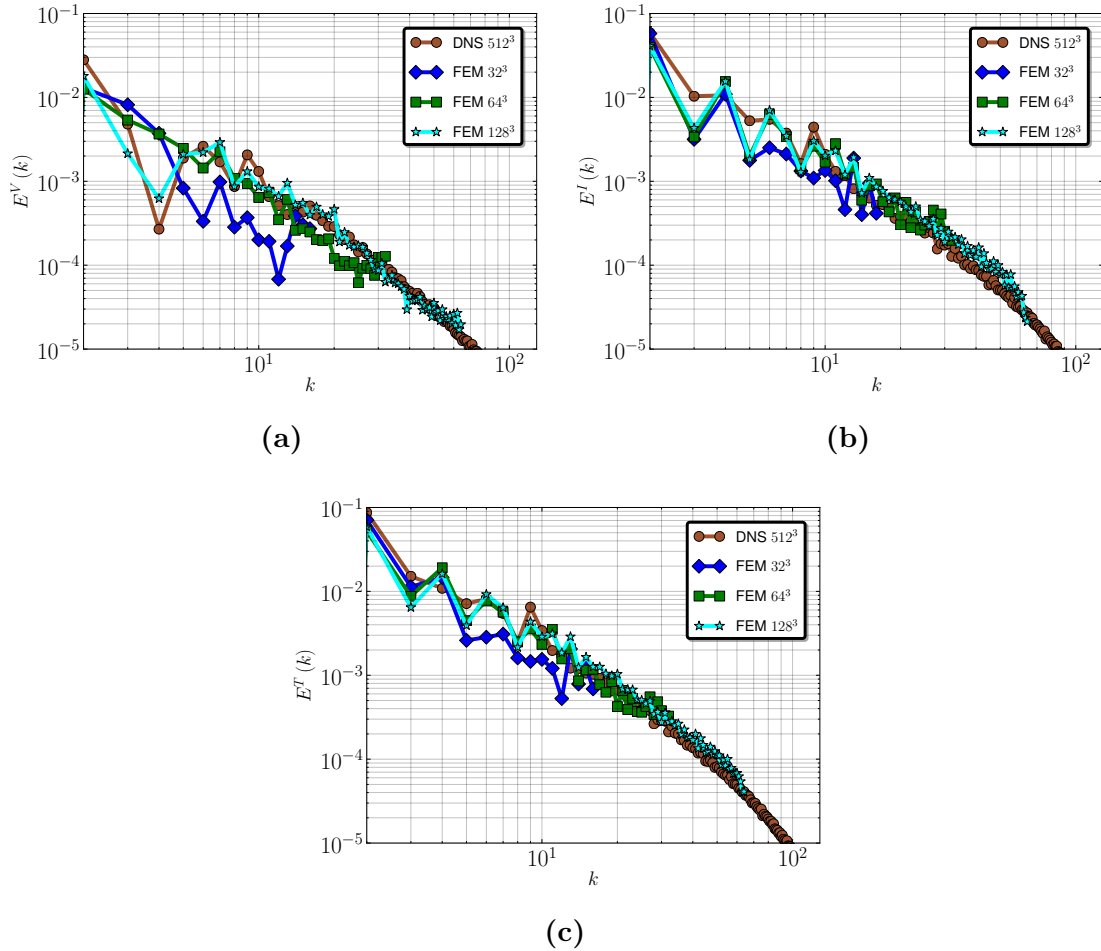
Figure 5.22: **Convergence of the total, kinetic, and magnetic energy spectra to corresponding DNS spectra for the finite element implementation of the models.**

A final test that tests the performance of the FEM with linear elements and the convergence properties of the method involves normalizing the spectra to the DNS spectrum. The results of this analysis are displayed in Figure 5.23.

(a)

(b)

(c)
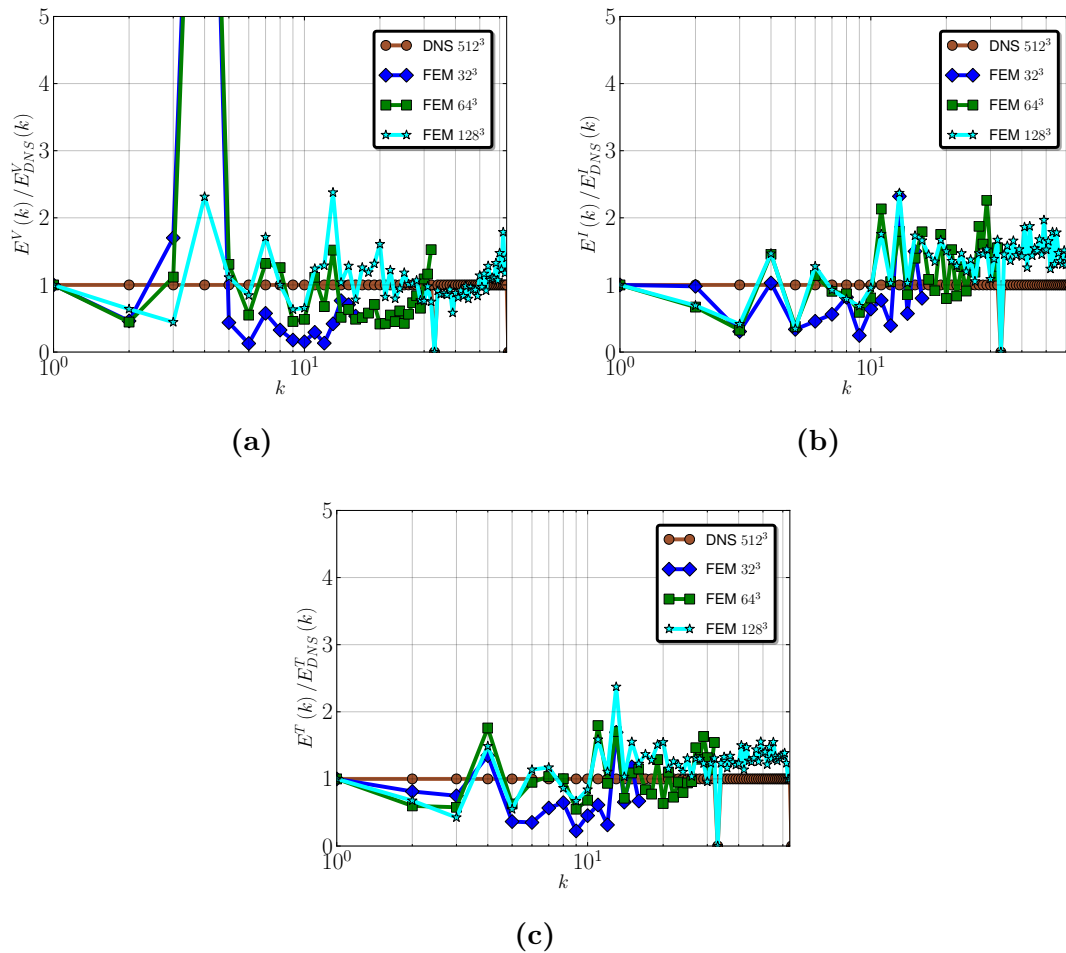
Figure 5.23: Semi-log plots of the normalized energy spectra demonstrating model performance and numerical convergence for the finite element implementation.

We conclude this section with some remarks. This section presented an overview of homogenous, isotropic turbulence theory for hydrodynamics and MHD. The new models from Chapter 4 were tested on the Taylor-Green flow for MHD. Results were reported primarily in terms of the kinetic, magnetic, and total energy spectra and compared to a DNS simulation and the standard dynamic Smagorinsky model. For this flow field, it was found that the mixed model performed the best but that all models, except for the RBEV, provided very good results. The RBEV model, when used in isolation, did not provide nearly enough dissipation to give acceptable comparisons to the DNS energy spectra. The new models were also compared to a

Smagorinsky model that was designed specifically for MHD which we referred to as the aligned-based dynamic Smagorinsky (DSEVA) model. This model uses the local physics of the cross helicity to account for an inverse cascade of magnetic energy. The VMS models take care of this physics process inherently as was demonstrated mathematically in Section 4.2.1.1. The DSEVA model did not offer any benefit over the VMS-based models or the classical DSEV model for this flow field. It is possible, however, that for other flow fields, such as those with finite global cross helicity, the DSEVA model would offer advantages over the DSEV model. Further tests on this must be done. A high Reynolds number simulation was performed to demonstrate the real strengths of the mixed model. The mixed model performed phenomenally well on a 32^3 grid when compared to a DNS simulation performed on a 2048^3 grid. The RBEV contribution to the mixed model was just enough to ensure a very good solution.

Further insight into the physical performance of the models was gained by analyzing the eddy viscosity contributions. The VMS-based models that employ an eddy viscosity (the mixed model and the RBEV model) were shown to be inherently dynamic. The magnitude of the eddy viscosities induced by these models was less than that from the dynamic Smagorinsky models which explains why the DSEV models were overly dissipative.

Numerical performance of the models was assessed by performing convergence tests on each of the models. The LES simulations were performed with $N = 32$, 64, 128 and with each refinement the models got progressively closer to the DNS result. This confirms that the models have an internal numerical consistency. The VMS-based models have the additional interpretation that with mesh refinement the numerical solution improves and the subgrid contributions to the grid solution becomes smaller. This effect was demonstrated by considering eddy viscosity contributions from the RBEV model with successively finer grids.

The finite element implementation was also tested on the Taylor-Green vortex problem. It was found that even with 32^3 linear elements the finite element solution was comparable to the 32^3 spectral simulation. Mesh convergence studies were performed to demonstrate the essential characteristics of the VMS subgrid models.

Such encouraging results provide motivation to test the FEM with the VMS-based models on a wall-bounded flow field as is done in the following section.

5.2   Turbulent MHD Channel Flow

Wall-bounded turbulent flows do not fit within the framework of HIT theory. The robustness of the new models is further tested by considering turbulent MHD channel flow. In this section we review some of the theory of turbulent hydrodynamic channel flows and turbulent MHD channel flows. Following this, results from performance tests of the new models on a turbulent MHD channel flow with perfectly electrically conducting walls are presented.

5.2.1   Theory of Channel Flow Turbulence

In this section, we provide a brief review of turbulent hydrodynamic channel flow and describe some aspects of turbulent MHD channel flow. For a nice treatment of turbulent channel flows in incompressible hydrodynamics see (Pope 2000, chap. 7). The present discussion focuses on fully developed turbulent channel flow driven by a streamwise pressure gradient. Such a situation requires that there is no mean streamwise acceleration. It is further assumed that the velocity statistics are independent of the spanwise direction. One final requirement is that the flow in the wall-normal direction be negligible compared to the streamwise component of velocity. Because of these assumptions and requirements on the flow field, we consider a force balance of the average quantities in the streamwise direction of the channel. An average quantity is denoted by angular brackets $\langle \cdot \rangle$. The force balance in the streamwise direction is

$$\left\langle F_x^b \right\rangle = 2 \left\langle F_x^w \right\rangle \tag{5.41}$$

where $\left\langle F_x^b \right\rangle$ is the average force in the channel driving the flow in the positive streamwise direction and $\left\langle F_x^w \right\rangle$ is the average surface force on one of the channel

walls. Introducing volumetric f_x^b and surface f_x^w forces gives

$$L_x L_y L_z f_x^b = 2 L_x L_z f_x^w. \tag{5.42}$$

We call the average surface force the wall shear stress τ_w. Thus

$$f_x^b = \frac{2}{L_y} \tau_w. \tag{5.43}$$

The body force in the streamwise direction is the pressure gradient $-\mathrm{d}\langle p\rangle/\mathrm{d}x$. Therefore, in a fully developed channel flow, the average pressure gradient is balanced by the wall shear stress,

$$-\frac{\mathrm{d}\langle p\rangle}{\mathrm{d}x} = \frac{2}{L_y} \tau_w. \tag{5.44}$$

A velocity and length scale can be defined in terms of the wall shear stress. These are called the friction velocity u_τ and the viscous length scale δ_ν. They are defined as:

$$u_\tau = \sqrt{\frac{u_\tau}{\rho}} \tag{5.45}$$

$$\delta_\nu = \frac{\nu}{u_\tau}. \tag{5.46}$$

Finally, two important dimensionless numbers based on these scales are the friction Reynolds number Re_τ and the wall unit y^+. These are given as:

$$\mathrm{Re}_\tau = \frac{u_\tau h}{\nu} \tag{5.47}$$

$$y^+ = \frac{u_\tau y}{\nu}. \tag{5.48}$$

We close the discussion on hydrodynamic channel flow with a quick overview of the anatomy of the velocity profile. There are two main regions in a channel flow, aptly referred to as the inner layer and the outer layer. The inner layer corresponds to $y/h < 0.1$ where h is the half-channel width, and is the region in which viscosity plays an important role. LES of turbulent channel flow, in its basic form, seeks to

resolve turbulent motions within the channel. However, for large Re a boundary layer near the wall develops. Many LES models are not designed to capture the effects of this boundary layer. As a result of this, and because boundary layer meshes are easily generated, most numerical simulations employ mesh refinement near the boundaries of the channel in order to capture this boundary layer. The amount of refinement that is necessary near the wall depends on Re_τ and is guided by the the theory of channel flow turbulence near the wall. This theory breaks the inner layer into three regions: 1.) the viscous sublayer, 2.) the buffer layer, and 3.) the log-law region. We will not delve into the details of each of these regions here. The important point in resolving the boundary layer near the wall is to be within the viscous sublayer. This is ensured by choosing a mesh refinement near the wall so that the first grid point away from the wall occurs at $y^+ \lesssim 5$ (see Pope 2000).

Much of the anatomy for the turbulent MHD channel flow is the same as that for the pure hydrodynamic case. See (Branover 1978, chap. 7), (Moreau 1990; Müller and Bühler 2001) for an introduction to turbulent MHD channel flow. The prototypical MHD channel flow problem is the Hartmann flow problem. This problem is an excellent way of introducing MHD channel flow effects. The problem involves a two-dimensional channel in which the velocity flows in the streamwise direction and a wall normal magnetic field of strength B_0 is applied uniformly throughout the channel. For such a flow field it is possible to show that the total average Lorentz force in the channel vanishes. With this result the same force balance for the momentum equation applies. Thus, the streamwise momentum is balanced by the pressure gradient and the wall shear stress. The Hartmann flow problem is characterized by the role of the Hartmann number Ha. For very large Ha the velocity profile becomes flat at the core of the channel and thin boundary layers develop along the channel walls. These boundary layers are also named after Hartmann and are called Hartmann layers. The Hartmann layer thickness is

$$\delta_{\mathrm{Ha}} = \frac{h}{\mathrm{Ha}}. \tag{5.49}$$

Thus, in MHD channel flows, there are two boundary layer considerations. The usual fluid boundary layer and the Hartmann layer. When creating the mesh it is

therefore necessary to make sure that the first mesh point is such that the smallest boundary layer will be resolved. We consider the ratio of distance from the wall to the Hartmann layer thickness,

$$\frac{y}{\delta_{\mathrm{Ha}}} = \frac{\mathrm{Ha}}{\mathrm{Re}_\tau} y^+ \tag{5.50}$$
$$\Rightarrow y = \frac{\mathrm{Ha}}{\mathrm{Re}_\tau} \delta_{\mathrm{Ha}} y^+.$$

From hydrodynamic turbulence theory we require the first mesh point y_1 to be such that $y^+ < 5$ so that y_1 is in the viscous sublayer. This gives us an idea of when it is important to consider the Hartmann layer thickness over the fluid boundary layer when creating the mesh.

$$y_1 < \frac{5\mathrm{Ha}}{\mathrm{Re}_\tau} \delta_{\mathrm{Ha}}. \tag{5.51}$$

This expression says that for $5\mathrm{Ha} < \mathrm{Re}$ the fluid boundary layer is smaller than the Hartmann layer thickness. In fluid turbulence this is typically the case and therefore the fluid boundary layer is smaller than the Hartmann layer thickness.

5.2.2 Turbulent MHD Channel

The new models were tested on a turbulent MHD channel flow. The simulation domain is $\Omega_x \times \Omega_y \times \Omega_z$ with

$$\Omega_x = [0, \ 2\pi] \tag{5.52}$$
$$\Omega_y = [-1, \ 1] \tag{5.53}$$
$$\Omega_z = [0, 3\pi/2]. \tag{5.54}$$

The problem configuration is illustrated in Figure 5.24. The mesh that was used for the simulation is presented in Figure 5.25.
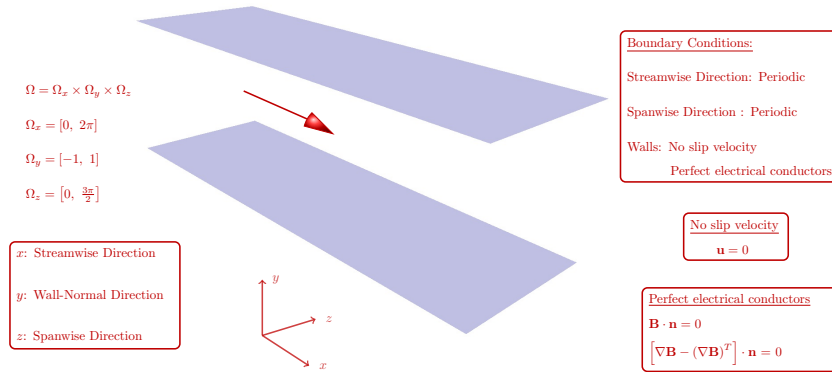
Figure 5.24: Configuration of the channel flow problem.
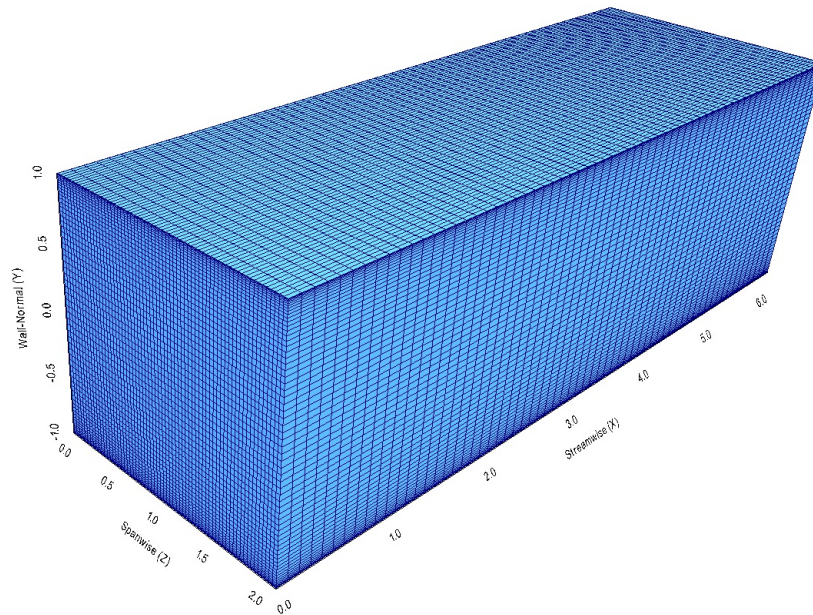
Figure 5.25: The finite element mesh for the turbulent MHD channel flow problem.

This mesh has 32 linear finite elements in each direction. In the streamwise and spanwise directions the elements are of uniform size, $h_x = L_x/n_{\mathrm{el},x}$ and $h_z = L_z/n_{\mathrm{el},z}$. The mesh in the wall-normal direction is nonuniform and is prescribed by

$$y_j = \cos\left(\pi\left(\frac{j}{n_{\mathrm{el},y}} + 1\right)\right), \quad 0 < j \leq n_{\mathrm{el},y}. \tag{5.55}$$

The boundary conditions are no slip velocity conditions at the walls and no fluid flow through the walls. The walls are perfect conductors of electricity. In the streamwise

and spanwise directions the flow is periodic. The finite element function spaces for this configuration were presented in Section 2.5.2. Initial conditions for the momentum equation were taken from a simulation of fully developed hydrodynamic turbulent channel flow. A random seed magnetic field with zero mean was used as the initial condition for the induction equation. The initial conditions for this simulation are shown in Figure 5.26. The flow parameters are $\mathrm{Re}_\tau = \mathrm{Rm}_\tau = 395$. There is initially no scale for the magnetic field and as a result Ha and S do not have clearly identifiable values.

(a) Initial condition of the velocity field.

(b) Initial condition of the magnetic field.
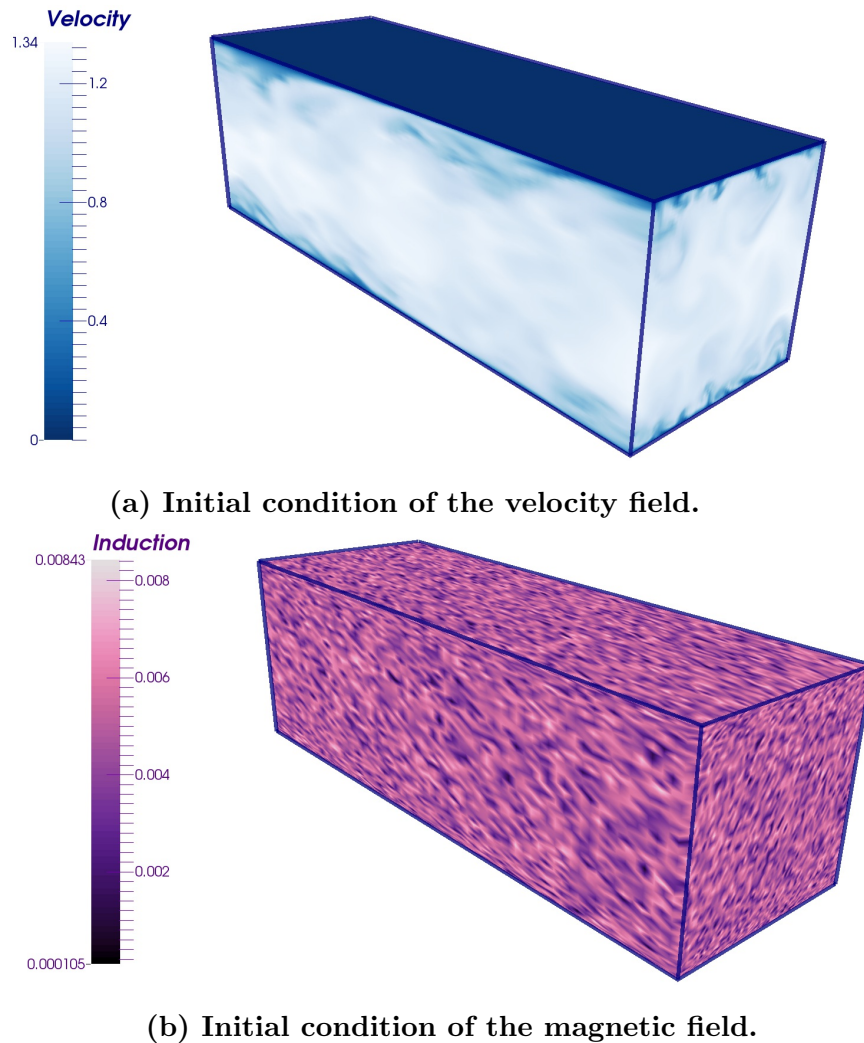
Figure 5.26: Initial conditions for the turbulent MHD channel flow.

It is expected that, due to the velocity fluctuations and the cross-helicity effect, the magnetic field will be amplified. A mean magnetic field will develop and

after considerable time both fields will reach a fully developed turbulent state. The evolution of the fields is monitored with the volume average of the fields at each time,

$$\langle \mathbf{u} \rangle_V (t) = \frac{1}{L_y} \int_{-1}^{1} \langle \mathbf{u} \rangle_{xz} (y, t) \ \mathrm{d}y \tag{5.56}$$

where

$$\langle \mathbf{u} \rangle_{xz} (y, t) = \frac{1}{L_z} \frac{1}{L_x} \int_0^{3\pi/2} \int_0^{2\pi} \mathbf{u} (x, y, z, t) \ \mathrm{d}x \mathrm{d}z \tag{5.57}$$

is the planar average in the x-z plane. In addition to these quantities, other turbulence statistics are of interest. In particular, root mean square values of a field and Reynolds stresses are often studied. We consider x-z planar averages of each of these quantities averaged over time. Such a quantity is denoted by $\langle \cdot \rangle_{xzt}$. This operation is:

$$\langle u \rangle_{xzt} = \int_0^T \left[\frac{1}{L_x L_z} \int_0^{2\pi} \int_0^{3\pi/2} u (x, y, z, t) \ \mathrm{d}z \mathrm{d}x \right] \ \mathrm{d}t. \tag{5.58}$$

The rms values are computed with:

$$u^{\mathrm{rms}} = \left\langle u'^2 \right\rangle = \frac{1}{T} \int_0^T \left[\frac{1}{L_x L_z} \int_0^{2\pi} \int_0^{3\pi/2} \left(u^h - \left\langle u^h \right\rangle_{xzt} \right)^2 \ \mathrm{d}z \mathrm{d}x \right] \ \mathrm{d}t. \tag{5.59}$$

The Reynolds stresses are computed similarly:

$$\langle uv \rangle = \frac{1}{T} \int_0^T \left[\int_0^{2\pi} \int_0^{3\pi/2} \left(u^h - \left\langle u^h \right\rangle_{xzt} \right) \left(v^h - \left\langle v^h \right\rangle_{xzt} \right) \ \mathrm{d}z \mathrm{d}x \right] \ \mathrm{d}t. \tag{5.60}$$

We make a final note on implementation of such calculations. Given an averaging operation $\langle \cdot \rangle$, the most efficient way to implement computations of second order

statistics is to rearrange the terms. This is demonstrated presently.

$$\begin{aligned}
\langle u'^2 \rangle &= \left\langle \left(u^h - \langle u^h \rangle \right)^2 \right\rangle \\
&= \langle u^h u^h - 2u^h \langle u^h \rangle + \langle u^h \rangle \langle u^h \rangle \rangle \\
&= \langle u^h u^h \rangle - 2 \langle u^h \rangle \langle u^h \rangle + \langle u^h \rangle \langle u^h \rangle \\
&= \langle u^h u^h \rangle - \langle u^h \rangle \langle u^h \rangle .
\end{aligned}$$

Existing Sandia post-processing tools were modified and extended to be able to perform such computations.

The finite element code, Drekar, did not have full VMS capabilities and before testing the new models Drekar was given these new features. The models were implemented in a flexible and general way so that HD and MHD problems can be run easily. Thus, the models were implemented so that they know the difference between a HD run and an MHD run. Moreover, the unresolved fields are now explicitly computed in the code so that the readability of the implementation of the models is seamless.

Before performing the full MHD simulation, the new models were tested on a HD channel flow problem and compared to DNS data from (Moser, Kim, and Mansour 1999) and LES data from (Liu 2012). The HD simulation was also performed with $\mathrm{Re}_\tau = 395$ and the fluids part of the problem configuration described in Figure 5.24 was identical. Figures 5.27- 5.28 present results from the Drekar finite element simulation. Figure 5.27 presents the planar-averaged streamwise velocity component. Figure 5.29 presents planar-averaged rms values of the velocity components and Figure 5.28 presents planar-averaged Reynolds stresses. Very good agreement between the LES results from the two different LES codes is found. Moreover, good agreement with the accepted DNS simulation was also attained.
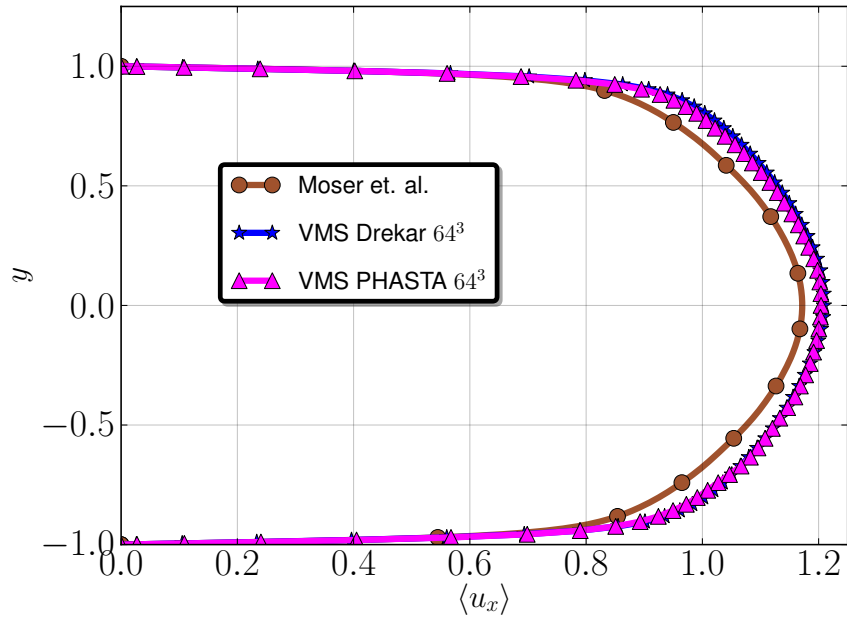
Figure 5.27: Planar-averaged streamwise velocity component for a HD simulation. Comparison of Drekar results to accepted DNS and LES simulations is made.
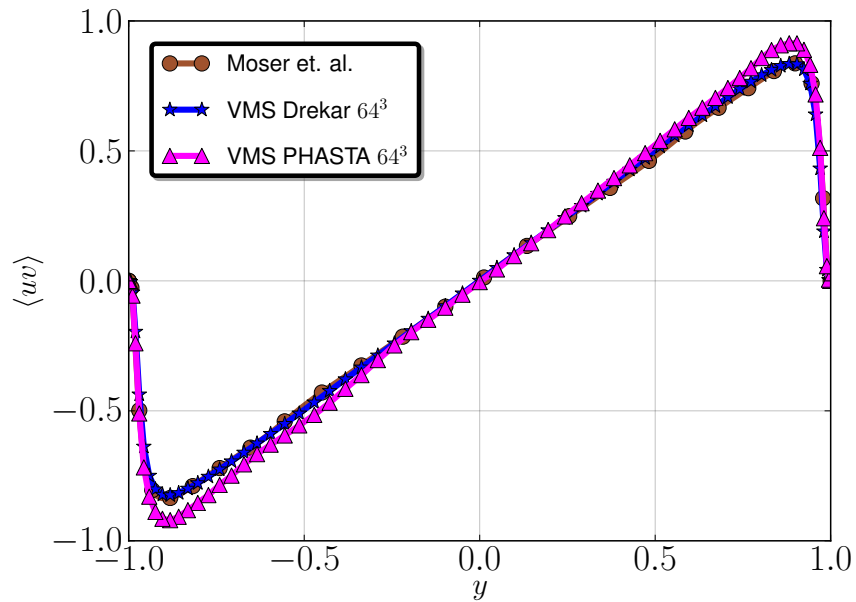
Figure 5.28: Planar-averaged Reynolds stresses for a HD simulation. Comparison of Drekar results to accepted DNS and LES simulations is made.
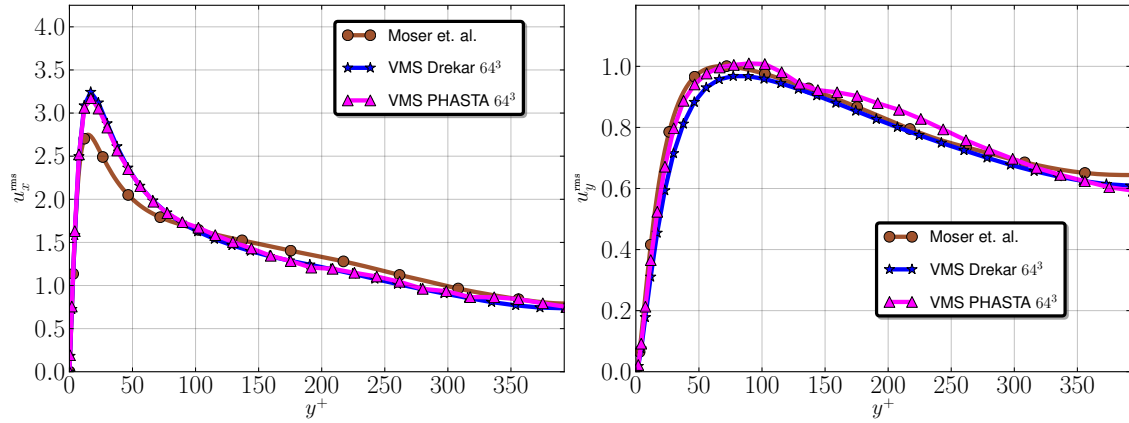
(a) Root mean square values of steam-wise velocity for HD simulation.

(b) Root mean square values of wall-normal velocity for HD simulation.
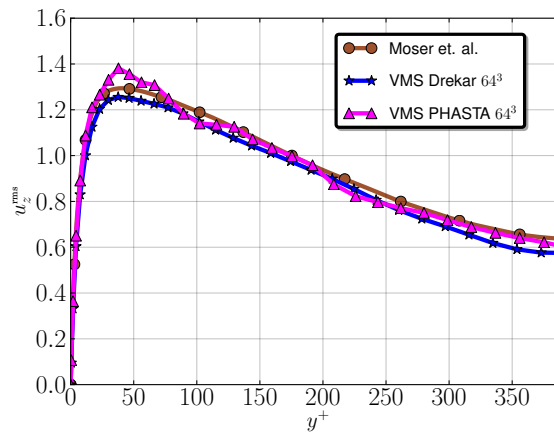
(c) Root mean square values of span-wise velocity for a HD simulation.

Figure 5.29: Root mean square values of velocity components for a HD simulation. Comparison of Drekar results to accepted DNS and LES simulations is made.

Alas, at the present time, the LES simulations of the MHD channel flow are not complete. This is due to two primary difficulties:

1. Significant effort was expended on simulation of a Hartmann flow problem with electrically insulating walls. However, the computation involved $\mathrm{Pr_m} \ll 1$ which required an unreasonably small time-step when simulating the full MHD equations to achieve reasonable results. By reasonable, we mean results that are in good agreement with a DNS simulation performed with the quasi-static

MHD approximation (Boeck, Krasnov, and Zienicke 2007).

2. Even for flows with $\mathrm{Pr_m} = 1$, the simulation time required for the flow to become fully developed is inordinate. We initially attempted a simulation with perfectly insulating walls. After ~ 400 flow-through times, the simulation had still not reached a steady state. We believe that a steady state should be reached based on previous LES simulations that have been published (Hamba and Tsuchiya 2010). In that work, the authors mention the extreme amount of time required for a fully developed profile to be realized.

There are still a few options to pursue in light of these difficulties. Concerning the first point, the new LES models could be adapted to the quasi-static system of equations. However, to change the format of Drekar would have led us rather far astray of our original intention of developing novel LES models for the full MHD equations. We hope to perform our own DNS simulation in the future and to compare LES simulations to the DNS simulation of the full MHD equations. However, considerable computing effort will be required for such an endeavor.

Concerning the second point, it is possible that our implementation of the insulating boundary conditions influenced the simulation time and ultimately the results. The procedure discussed in Section 2.4.4 for perfectly insulating boundary conditions is particularly difficult to implement in a finite element code such as Drekar. However, a simulation with perfectly conducting boundary conditions is reasonable to pursue. This simulation is running currently with results on their way soon.

CHAPTER 6
Discussion and Conclusions

6.1 Review

The field of incompressible MHD is a particularly rich subset of physics and applied mathematics. The challenges inherent in the equations provide a plethora of research opportunities. Aside from purely academic pursuits, MHD also plays an important role in the development of engineering technologies. Designing suitable engineering systems using electrically conducting fluids requires using computational techniques. Despite rapid advancement in computer power and technology, MHD DNS of most engineering systems will remain elusive for the foreseeable future. One of the most prominent reasons for this difficulty is the phenomenon of fluid turbulence which again rears its head in MHD. In addition to the velocity field displaying disordered behavior the EM quantities also display such behavior. This work sought to develop innovative turbulence models for incompressible MHD and to demonstrate their effectiveness using simulations of turbulent flow.

The models were built from the mathematical framework of the VMS formulation. This approach was used to develop LES models that differ from present LES models in several ways. First of all, the LES approach typically introduces the concept of a filter which decomposes the solution field into a smooth, resolved component and an unresolved component. The VMS approach decomposes the solution field into a discrete component and a continuous subgrid component. The goal in the traditional LES approach is to numerically approximate the smooth, resolved component whereas the goal in the VMS formulation is to numerically solve for the discrete component of the solution. Closure of the LES models is typically obtained via the introduction of a subgrid model which accounts for the subgrid effects. The most popular closure model is the dynamic Smagorinsky model which enhances the viscous dissipation of the fluid field. This dynamic model has been modified for incompressible MHD to account for energy transfer between the velocity and magnetic fields (see Müller and Carati 2002). In principle, the VMS approach is exact and

therefore, up to the model for the subgrid scales, it is exact. Thus, a dynamic model is not required and there are no undetermined coefficients. However, this ideal is not realized in practice. The work presented in this document sought to extend the VMS formulation to incompressible MHD.

This work focused on the development of the VMS formulation for turbulence modeling of incompressible MHD. The turbulence models were developed within the context of Fourier-spectral methods and the FEM. There is a connection between stabilized finite element methods and the VMS formulation. In particular, application of the VMS formulation results in classical stabilized FEMs; in this sense then, a stabilized FEM can be thought of as an incomplete turbulence model. An important parameter in models developed with the VMS formulation is referred to as the stabilization parameter. This parameter is typically a matrix and is used to approximately invert the differential equations for the subgrid scales and therefore approximately solve for the subgrid fields that influence the resolved solution. In MHD there is evidence that a non-diagonal stabilization matrix could enhance the approximation to the subgrid scales. A new non-diagonal stabilization parameter was designed specifically for this purpose first using Elsässer variables and then deriving a new set of transformation variables. The stabilization parameter built upon Elsässer variables was tested on one- and two-dimensional problems. Very promising results were obtained for the one-dimensional case as compared to the pure diagonal stabilization parameter. However, there did not appear to be a distinct advantage to a non-diagonal stabilization parameter in the multi-dimensional case. Possible explanations for this involve the type of problems that were tested; it may be that the non-diagonal stabilization parameter finds its utility for turbulent flow fields with very large or small magnetic Prandtl numbers. This idea remains to be tested numerically.

The primary contribution of this thesis was the derivation of turbulence models for incompressible MHD from the VMS formulation. The mathematical structure of the resulting equations is similar to that of the incompressible hydrodynamics equations in that the equations are quadratically nonlinear. These quadratic nonlinearities induce cross stresses and pure subgrid stresses once the VMS decomposition is

applied. The pure subgrid stresses are not adequately represented through the classic closure models. As such, a VMS-motivated, residual-based eddy viscosity model was introduced for MHD and appended to the VMS models in the MHD equations. The performance of the models was tested on different flow problems including decaying homogeneous, isotropic turbulence and shear turbulence. In the former case various physical aspects of the models were studied including energy spectra for the velocity and magnetic fields. Significantly, the capability of the VMS models to reproduce the subgrid dynamo effect was demonstrated mathematically. Additionally, the VMS models were compared to state-of-the art LES models such as the alignment-based dynamic Smagorinsky model and were shown to perform quite well. For inhomogeneous turbulence, the models were implemented into a finite element code called Drekar at Sandia National Labs and tested on a turbulent MHD channel flow. The simulation consisted of an electrically conducting fluid moving between two parallel, perfectly conducting walls. The simulation was performed for $\mathrm{Pr_m} = 1$. Turbulence statistics for the velocity field were obtained. Numerical experiments on convergence of the methods were performed for both the Taylor-Green flow and the MHD channel flow.

6.2 Future Outlook and Prospects

Although considerable progress has been made in the development of VMS-based turbulence models for MHD with this work, there is still much exploration to be done. Different avenues of exploration are outlined here; several of which are already in progress.

A thorough, quantitative study of the ability of the VMS-based turbulence models to represent physical effects such as the subgrid dynamo represents an especially exciting area of research. The VMS method allows for the possibility of a local inverse energy cascade because it is not always locally dissipative. Such dynamics are known to occur in MHD. How well do the new models capture such physics? A key task in such a study is to find an appropriate problem on which to study the subgrid dynamo effect because the subgrid dynamo does not appear in all MHD flows. Long-term goals would be to perform LES simulations of realistic flows such as those

found in geophysical fluid dynamics and astrophysics and compare predictions to experimentally measured quantities such as the cross-helicity and magnetic-helicity.

Extensions to inhomogeneous turbulence studies include applications to channels and ducts with more complicated and realistic geometries. A fascinating application area involves liquid metal blankets for a fusion reactor. For such an application, a liquid metal flows along first wall of a tokamak reactor. Thus, it is influenced by the very strong magnetic fields in found in a tokamak. This problem has additional difficulties including a complicated wall-boundary condition and a free-surface for the other boundary condition.

Additional areas of interest are to extend the VMS formulation to compressible MHD, Hall-MHD, and plasma kinetic theories such as the Vlasov equation. Furthermore, interesting studies in uncertainty quantification and optimization of the turbulence models are also possibilities.

LITERATURE CITED

Alfvén, H. 1942. "Existence of Electromagnetic-Hydrodynamic Waves." *Nature* 150:405–406.

———. 1950. *Cosmical Electrodynamics.* Oxford: Clarendon Press.

Aluie, H., and G. L. Eyink. 2010. "Scale Locality of Magnetohydrodynamic Turbulence." *Physical review letters* 104:81101.

Baerenzung, J., H. Politano, Y. Ponty, and A. Pouquet. 2008a. "Spectral Modeling of Magnetohydrodynamic Turbulent flows." *Physical Review E* 78:026310.

———. 2008b. "Spectral Modeling of Turbulent Flows and the Role of Helicity." *Physical Review E* 77:046303.

Batchelor, G. K. 1982. *The Theory of Homogeneous Turbulence.* Cambridge: Cambridge University Press.

Bazilevs, Y., V.M. Calo, J.A. Cottrell, T.J.R. Hughes, A. Reali, and G. Scovazzi. 2007. "Variational Multiscale Residual-Based Turbulence Modeling for Large Eddy Simulation of Incompressible Flows." *Computer Methods in Applied Mechanics and Engineering* 197:173–201.

Beresnyak, A. 2011. "Spectral Slope and Kolmogorov Constant of MHD Turbulence." *Physical Review Letters* 106:75001.

Biskamp, D. 2003. *Magnetohydrodynamic Turbulence.* Cambridge: Cambridge University Press.

Boeck, T., D. Krasnov, and E. Zienicke. 2007. "Numerical Study of Turbulent Magnetohydrodynamic Channel Flow." *Journal of Fluid Mechanics* 572:179–188.

Boldyrev, S. 2006. "Spectrum of Magnetohydrodynamic Turbulence." *Physical review letters* 96:115002.

Braginskii, S.I. 1965. "Transport Processes in a Plasma." *Reviews of Plasma Physics* 1:205.

Branover, H. 1978. *Magnetohydrodynamic Flow in Ducts.* New York: Halsted Press.

Brun, A. S., M.S. Miesch, and J. Toomre. 2004. "Global-Scale Turbulent Convection and Magnetic Dynamo Action in the Solar Envelope." *The Astrophysical Journal* 614:1073.

Chaudhary, R., S.P. Vanka, and B.G. Thomas. 2010. "Direct Numerical Simulations of Magnetic Field Effects on Turbulent Flow in a Square Duct." *Physics of Fluids* 22:075102.

Codina, R. 2002. "Stabilized Finite Element Approximation of Transient Incompressible Flows Using Orthogonal Subscales." *Computer Methods in Applied Mechanics and Engineering* 191 (39-40): 4295–4321.

Codina, R., and N. Hernández-Silva. 2006. "Stabilized Finite Element Approximation of the Stationary Magneto-Hydrodynamics Equations." *Computational Mechanics* 38 (4): 344–355.

Codina, R., J. Principe, O. Guasch, and S. Badia. 2007. "Time Dependent Subscales in the Stabilized Finite Element Approximation of Incompressible Flow problems." *Computer Methods in Applied Mechanics and Engineering* 196 (21): 2413–2430.

Cyr, E. C., J. N. Shadid, and R. S. Tuminaro. 2012. "Stabilization and Scalable Block Preconditioning for the Navier–Stokes Equations." *Journal of Computational Physics* 231:345–363.

Darrigol, O. 2002. "Between Hydrodynamics and Elasticity Theory: The First Five Births of the Navier-Stokes Equation." *Archive for History of Exact Sciences* 56 (2): 95–150.

Davidson, P.A. 2001. *An Introduction to Magnetohydrodynamics.* New York: Cambridge University Press.

Dobran, F. 2012. "Fusion Energy Conversion in Magnetically Confined Plasma Reactors." *Progress in Nuclear Energy* 60:89–116.

Ecke, R. 2005. "The Turbulence Problem: An Experimentalist's Perspective." *Los Alamos Science* 29:124–141.

Fox, P. A.., S. Sofia, and K. L. Chan. 1991. "Convective Flows Around Sunspot-Like Objects." *Solar Physics* 135:15–42.

Fox, P. A., M. L. Theobald, and S. Sofia. 1991. "Compressible Magnetic Convection-Formulation and Two-Dimensional Models." *The Astrophysical Journal* 383:860–881.

Frisch, U. 1996. *Turbulence: The Legacy of A. N. Kolmogorov.* Cambridge: Cambridge University Press.

Galperin, B. 1993. *Large Eddy Simulation of Complex Engineering and Geophysical Flows.* New York: Cambridge University Press.

Galtier, S., S.V. Nazarenko, A.C. Newell, and A. Pouquet. 2000. "A Weak Turbulence Theory for Incompressible Magnetohydrodynamics." *Journal of Plasma Physics* 63 (5): 447–488.

Germano, M., U. Piomelli, P. Moin, and W. H. Cabot. 1991. "A Dynamic Subgrid-Scale Eddy Viscosity Model." *Physics of Fluids A: Fluid Dynamics* 3:1760.

Glatzmaier, G.A. 2002. "Geodynamo Simulations-How Realistic Are They?" *Annual Review of Earth and Planetary Sciences* 30 (1): 237–257.

Goedbloed, H., R. Keppens, and S. Poedts. 2010. *Advanced Magnetohydrodynamics.* New York: Cambridge University Press.

Goedbloed, H., and S. Poedts. 2006. *Principles of Magnetohydrodynamics.* 74:462. New York: Cambridge University Press.

Gottlieb, D., and S. A. Orszag. 1987. *Numerical Analysis of Spectral Methods: Theory and Applications.* Philadelphia: Society for Industrial & Applied Mathematics.

Hamba, F., and M. Tsuchiya. 2010. "Cross-helicity Dynamo Effect in Magnetohydrodynamic Turbulent Channel Flow." *Physics of Plasmas* 17:012301.

Haugen, N.E., and A. Brandenburg. 2006. "Hydrodynamic and Hydromagnetic Energy Spectra from Large Eddy Simulations." *Physics of Fluids* 18:075106.

Holm, D. 1999. "Fluctuation Effects on 3D Lagrangian Mean and Eulerian Mean Fluid Motion." *Physica D: Nonlinear Phenomena* 133 (1): 215–269.

Holm, D.D. 2002. "Lagrangian Averages, Averaged Lagrangians, and the Mean Effects of Fluctuations in Fluid Dynamics." *Chaos: An Interdisciplinary Journal of Nonlinear Science* 12 (2): 518–530.

Holm, D.D., C. Jeffery, S. Kurien, D. Livescu, M. A. Taylor, and B. A. Wingate. 2005. "The LANS-α Model for Computing Turbulence." *Los Alamos Science* 29:152–171.

Hughes, T.J.R. 1995. "Multiscale Phenomena: Green's Functions, the Dirichlet-to-Neumann Formulation, Subgrid Scale Models, Bubbles and the Origins of Stabilized Methods." *Computer Methods in Applied Mechanics and Engineering* 127 (1-4): 387–401.

———. 2000. *The Finite Element Method: Linear Static and Dynamic Finite Element Analysis.* Mineola, New York: Dover Publications.

Hughes, T.J.R., G.R. Feijóo, L. Mazzei, and J.B. Quincy. 1998. "The Variational Multiscale Method–A Paradigm for Computational Mechanics." *Computer Methods in Applied Mechanics and Engineering* 166 (1-2): 3–24.

Hughes, T.J.R., L. P. Franca, and M. Balestra. 1986. "A New Finite Element Formulation for Computational Fluid Dynamics: V. Circumventing the Babuška-Brezzi Condition: A Stable Petrov-Galerkin Formulation of the Stokes Problem Accommodating Equal-Order Interpolations." *Computer Methods in Applied Mechanics and Engineering* 59 (1): 85–99.

Hughes, T.J.R., L.P. Franca, F. Chalot, and Z. Johan. 1994. *Stabilized Finite Element Methods in Fluid Dynamics.* Standford: Stanford Custom Publishing.

Hughes, T.J.R., L.P. Franca, and G.M. Hulbert. 1989. "A New Finite Element Formulation for Computational Fluid Dynamics: VIII. The Galerkin/Least-Squares Method for Advective-Diffusive Equations." *Computer Methods in Applied Mechanics and Engineering* 73 (2): 173–189.

Hughes, T.J.R., and G. Sangalli. 2008. "Variational Multiscale Analysis: The Fine-Scale Green's Function, Projection, Optimization, Localization, and Stabilized Methods." *SIAM Journal on Numerical Analysis* 45 (2): 539–557.

Iroshnikov, P.S. 1963. "Turbulence of a Conducting Fluid in a Strong Magnetic Field." *Astronomicheskii Zhurnal* 40:742.

Jackson, J.D. 1999. *Classical Electrodynamics.* 3rd ed. Hoboken, New Jersey: John Wiley & Sons.

John, V., and A. Kindl. 2008. "Variants of Projection-Based Finite Element Variational Multiscale Methods for the Simulation of Turbulent Flows." *International Journal for Numerical Methods in Fluids* 56 (8): 1321–1328.

Knaepen, B., and P. Moin. 2004. "Large-Eddy Simulation of Conductive Flows at Low Magnetic Reynolds Number." *Physics of Fluids* 16:1255.

Kobayashi, H. 2006. "Large Eddy Simulation of Magnetohydrodynamic Turbulent Channel Flows with Local Subgrid-Scale Model Based on Coherent Structures." *Physics of Fluids* 18:045107.

Kolmogorov, A.N. 1941a. "Dissipation of Energy in Locally Isotropic Turbulence." In *Dokl. Akad. Nauk SSSR,* 32:16–18.

———. 1941b. "On the Degeneration of Isotropic Turbulence in an Incompressible Viscous Fluid." In *Dokl. Akad. Nauk SSSR,* 31:538–541.

———. 1941c. "The Local Structure of Turbulence in Incompressible Viscous Fluid for Very Large Reynolds Numbers." In *Dokl. Akad. Nauk SSSR,* 30:9–13.

Kolmogorov, A.N. 1962. "A Refinement of Previous Hypotheses Concerning the Local Structure of Turbulence in a Viscous Incompressible Fluid at High Reynolds Number." *Journal of Fluid Mechanics* 13:82–85.

Kono, M., and P.H. Roberts. 2002. "Recent Geodynamo Simulations and Observations of the Geomagnetic Field." *Reviews of Geophysics* 40 (4): 1–53.

Kraichnan, R. H. 1965. "Inertial-Range Spectrum of Hydromagnetic Turbulence." *Physics of Fluids* 8:1385.

Kraichnan, R.H. 1976. "Eddy Viscosity in Two and Three Dimensions." *Journal of Atmospheric Science* 33 (8): 1521–1536.

Krasnov, D., O. Zikanov, and T. Boeck. 2012. "Numerical Study of Magnetohydrodynamic Duct Flow at High Reynolds and Hartmann Numbers." *Journal of Fluid Mechanics* 704:421.

Krasnov, D.S., E. Zienicke, O. Zikanov, T. Boeck, and A. Thess. 2004. "Numerical Study of the Instability of the Hartmann Layer." *Journal of Fluid Mechanics* 504:183–211.

Lee, E., M.E. Brachet, A. Pouquet, P.D. Mininni, and D. Rosenberg. 2010. "Lack of Universality in Decaying Magnetohydrodynamic Turbulence." *Physical Review E* 81 (1): 016318.

Liu, Jianfeng. 2012. "Residual-Based Variational Multiscale Models for Large Eddy Simulation of Compressible and Incompressible Turbulent Flows." PhD diss., Rensselaer Polytechnic Institute.

Meek, J.L. 1996. "A Brief History of the Beginning of the Finite Element Method." *International Journal for Numerical Methods in Engineering* 39:3761–3774.

Mininni, P.D. 2010. "Scale Interactions in Magnetohydrodynamic Turbulence." *arXiv:1006.1817v1 [physics.flu-dyn]* 1:1–47.

Montgomery, D.C., and A. Pouquet. 2002. "An Alternative Interpretation for the Holm α Model." *Physics of Fluids* 14:3365.

Moreau, R. 1990. *Magnetohydrodynamics.* Translated by A.F.Wright. Dordrecht: Kluwer Academic Publishers.

Moser, R.D., J. Kim, and N.N. Mansour. 1999. "Direct Numerical Simulation of Turbulent Channel Flow Up To Re= 590." *Physics of Fluids* 11:943.

Müller, U., and L. Bühler. 2001. *Magnetofluiddynamics in Channels and Containers.* Verlag Berlin Heidelberg: Springer.

Müller, W.C., and D. Biskamp. 2000. "Scaling Properties of Three-Dimensional Magnetohydrodynamic Turbulence." *Physical Review Letters* 84:475–478.

Müller, W.C, and D. Biskamp. 2003. "Statistical Anisotropy of Magnetohydrodynamic Turbulence." *Physical Review E* 67:066302.

Müller, W.C.., and D. Carati. 2002. "Large-Eddy Simulation of Magnetohydrodynamic Turbulence." *Computer Physics Communications* 147 (1-2): 544–547.

Nelson, N.J., B.P. Brown, A.S. Brun, M.S. Miesch, and J. Toomre. 2011. "Buoyant Magnetic Loops in a Global Dynamo Simulation of a Young Sun." *The Astrophysical Journal Letters* 739 (2): L38.

———. 2013. "Magnetic Wreaths and Cycles in Convective Dynamos." *The Astrophysical Journal* 762 (2): 73.

Oberai, A.A., and J. Wanderer. 2005. "A Dynamic Approach for Evaluating Parameters in a Numerical Method." *International Journal for Numerical Methods in Engineering* 62:50–71.

Oberai, Assad A., Jianfeng Lui, David Sondak, and T.J.R. Hughes. n.d. "A Residual-Based Eddy Viscosity Model for the LES of Turbulent flows." Submitted to Computer Methods in Applied Mechanics and Engineering.

Oden, J. T. 1990. "Historical Comments on Finite Elements." In *A History of Scientific Computing,* 152–166. ACM.

Fluid Dynamics, Proceedings of the 1973 Les Houches Summer School. 1977.

Panton, R.L. 2006. *Incompressible Flow.* Hoboken, New Jersey: John Wiley & Sons.

Pawlowski, R.P., E. T. Phipps, A.G. Salinger, S.J. Owen, C.M. Siefert, and M.L. Staten. 2012. "Automating Embedded Analysis Capabilities and Managing Software Complexity in Multiphysics Simulation, Part II: Application to Partial Differential Equations." *Scientific Programming* 20 (3): 327–345.

Pawlowski, R.P.., E.T. Phipps, and A. G. Salinger. 2012. "Automating Embedded Analysis Capabilities and Managing Software Complexity in Multiphysics Simulation, Part I: Template-Based Generic Programming." *Scientific Programming* 20 (2): 197–219.

Perez, J.C., J. Mason, S. Boldyrev, and F. Cattaneo. 2012. "On the Energy Spectrum of Strong Magnetohydrodynamic Turbulence." *Physical Review X* 2 (4): 041005.

Podesta, J.J., and J.E. Borovsky. 2010. "Scale Invariance of Normalized Cross-Helicity Throughout the Inertial Range of Solar Wind Turbulence." *Physics of Plasmas* 17 (11): 112905.

Podesta, J.J., D.A. Roberts, and M.L. Goldstein. 2007. "Spectral Exponents of Kinetic and Magnetic Energy Spectra in Solar Wind Turbulence." *The Astrophysical Journal* 664 (1): 543–548.

Ponty, Y., P.D. Mininni, D.C. Montgomery, J.-F Pinton, H. Politano, and A. Pouquet. 2005. "Numerical Study of Dynamo Action at Low Magnetic Prandtl Numbers." *Physical Review Letters* 94 (16): 164502.

Ponty, Y., H. Politano, and J-F. P. Pinton. 2004. "Simulation of Induction at Low Magnetic Prandtl Number." *Physical Review Letters* 92 (14): 144503.

Pope, S. B. 2000. *Turbulent Flows.* New York: Cambridge University Press.

Pouquet, A. 2012. "A Review of the Possible Role of Constraints in MHD Turbulence." *arXiv:1211.0715v1 [physics.plasm-ph]* 1:1–17.

Pouquet, A., E. Lee, M.E. Brachet, P.D. Mininni, and D. Rosenberg. 2010. "The Dynamics of Unforced Turbulence at High Reynolds Number for Taylor–Green Vortices Generalized to MHD." *Geophysical and Astrophysical Fluid Dynamics* 104 (2-3): 115–134.

Pouquet, A., M. Meneguzzi, and U. Frisch. 1986. "Growth of Correlation in Magnetohydrodynamic Turbulence." *Physical Review A* 33 (6): 4266–4276.

Prandtl, L. 1925a. "Bemerkungen zur Theorie der freien Turbulenz." *ZAMM-Journal of Applied Mathematics and Mechanics/Zeitschrift für Angewandte Mathematik und Mechanik* 22 (5): 241–243.

———. 1925b. "Bericht über Untersuchungen zur ausgebildeten Turbulenz." *Z. Angew. Math. Mech* 5 (2): 136–139.

Praskovsky, A., and S. Oncley. 1994. "Measurements of the Kolmogorov Constant and Intermittency Exponent at Very High Reynolds Numbers." *Physics of Fluids* 6 (9): 2886.

Reynolds, O. 1883. "An Experimental Investigation of the Circumstances Which Determine Whether the Motion of Water Shall be Direct or Sinuous, and of the Law of Resistance in Parallel Channels." *Proceedings of the Royal Society of London* 35 (224-226): 84–99.

———. 1895. "On the Dynamical Theory of Incompressible Viscous Fluids and the Determination of the Criterion." *Philosophical Transactions of the Royal Society of London. A* 186:123–164.

Richardson, L.F. 2007. *Weather Prediction by Numerical Process.* Cambridge: Cambridge University Press.

Satake, S., T. Kunugi, N. Naito, and A. Sagara. 2006. "Direct Numerical Simulation of MHD Flow with Electrically Conducting Wall." *Fusion Engineering and Design* 81:367–374.

Satake, S.i, T. Kunugi, K. Takase, and Y. Ose. 2006. "Direct Numerical Simulation of Turbulent Channel Flow Under a Uniform Magnetic Field for Large-Scale Structures at High Reynolds Number." *Physics of Fluids* 18:125106.

Schmitt, F.F. 2007. "About Boussinesq's Turbulent Viscosity Hypothesis: Historical Remarks and a Direct Evaluation of its Validity." *Comptes Rendus Mécanique* 335:617–627.

Shadid, J. N., E. C. Cyr, R. P. Pawlowski, R.S. Tuminaro, L. Chacón, and P. T. Lin. 2010. "Initial Performance of Fully-Coupled AMG and Approximate Block Factorization Preconditioners for Solution of Implicit FE Resistive MHD." In *Proceedings of ECCOMAS-CFD.*

Shadid, J.N., R.P. Pawlowski, J.W. Banks, L. Chacon, P.T. Lin, and R.S. Tuminaro. 2010. "Towards a Scalable Fully-Implicit Fully-Coupled Resistive MHD Formulation with Stabilized FE Methods." *Journal of Computational Physics* 229 (20): 7649–7671.

Shakib, F., T.J.R. Hughes, and Z. Johan. 1991. "A New Finite Element Formulation for Computational Fluid Dynamics: X. The Compressible Euler and Navier-Stokes Equations." *Computer Methods in Applied Mechanics and Engineering* 89 (1-3): 141–219.

Shimomura, Y. 1991. "Large Eddy Simulation of Magnetohydrodynamic Turbulent Channel Flows Under a Uniform Magnetic Field." *Physics of Fluids A* 3:3098.

Smagorinsky, J. 1963. "General Circulation Experiments with the Primitive Equations." *Monthly Weather Review* 91 (3): 99–164.

Smolarkiewicz, P.K., and P. Charbonneau. 2013. "EULAG, a Computational Model for Multiscale Flows: an MHD Extension." *Journal of Computational Physics* 236:608–623.

Sondak, D., and A.A. Oberai. 2012. "Large Eddy Simulation Models for Incompressible Magnetohydrodynamics Derived from the Variational Multiscale Formulation." *Physics of Plasmas* 19:102308.

Sovinec, C.R., T.A. Gianakon, E.D. Held, S.E. Kruger, D.D. Schnack, and NIMROD Team. 2003. "NIMROD: A Computational Laboratory for Studying Nonlinear Fusion Magnetohydrodynamics." *Physics of Plasmas* 10:1727.

Strauss, H.R. 1976. "Nonlinear, Three-Dimensional Magnetohydrodynamics of Noncircular Tokamaks." *Physics of Fluids* 19:134.

Takahashi, M., S. Nitta, Y. Tatematsu, and A. Tomimatsu. 1990. "Magnetohydro-dynamic Flows in Kerr Geometry-Energy Extraction from Black Holes." *The Astrophysical Journal* 363:206–217.

Tang, W.M. 2008. "Scientific and Computational Challenges of the Fusion Simu-lation Project (FSP)." In *Journal of Physics: Conference Series,* 125:012047. IOP Publishing.

Tennekes, H., and J. L. Lumley. 1972. *First Course in Turbulence.* Cambridge: MIT Press.

Theobald, M.L., P.A. Fox, and S. Sofia. 1994. "A Subgrid-Scale Resistivity for Mag-netohydrodynamics." *Physics of Plasmas* 1:3016.

Thomas, J.W. 1995. *Numerical Partial Differential Equations: Finite Difference Methods.* Verlag New York: Springer.

Tietjens, O.K.G. 1934. *Applied Hydro-and Aeromechanics: Based on Lectures of L. Prandtl.* Translated by J.P.Den Hartog. New York: Dover Publications.

Trefethen, L.N., and D. Bau III. 1997. *Numerical Linear Algebra.* Philadelphia: Society for Industrial & Applied Mathematics.

Vreman, A.W. 2004. "An Eddy-Viscosity Subgrid-Scale Model for Turbulent Shear Flow: Algebraic Theory and Applications." *Physics of Fluids* 16 (10): 3670–3681.

Waleffe, F. 1997. "On a Self-Sustaining Process in Shear Flows." *Physics of Fluids* 9:883.

Wang, Z., and A.A. Oberai. 2010a. "A Mixed Large Eddy Simulation Model Based on the Residual-Based Variational Multiscale Formulation." *Physics of Fluids* 22:075107.

———. 2010b. "Spectral Analysis of the Dissipation of the Residual-Based Varia-tional Multiscale Method." *Computer Methods in Applied Mechanics and En-gineering* 199:810–818.

Yoshizawa, A. 1990. "Self-Consistent Turbulent Dynamo Modeling of Reversed Field Pinches and Planetary Magnetic Fields." *Physics of Fluids B: Plasma Physics* 2 (7): 1589–1600.

Zweibel, E.G. 1999. "Magnetohydrodynamics Problems in the Interstellar Medium." *Physics of Plasmas* 6:1725.

Zweibel, E.G., and M Yamada. 2009. "Magnetic Reconnection in Astrophysical and Laboratory Plasmas." *Annual Review of Astronomy and Astrophysics* 47:291–332.

Zwillinger, D. 2003. *CRC Standard Mathematical Tables and Formulae.* New York: Chapman & Hall/CRC.

APPENDIX A
Derivation of Incompressible Momentum Equation

The compressible momentum equation is,

$$\frac{\partial \mathbf{m}}{\partial t} + \nabla \cdot \left(\frac{\mathbf{m} \otimes \mathbf{m}}{\rho} \right) = \nabla \cdot \mathbf{T} + \mathbf{F}$$

where $\mathbf{m} = \rho \mathbf{u}$ is the momentum. The stress tensor $\mathbf{T}$ is assumed to be linearly related to the rate of strain $\mathbf{S}$,

$$\mathsf{T}_{ij} = \mathsf{A}_{ij} + \mathsf{C}_{ijkl}\mathsf{S}_{kl}.$$

The matrix A_{ij} represents the normal forces acting on the fluid element. We traditionally refer to this as the fluid pressure p. Thus,

$$\mathsf{A}_{ij} = -p\delta_{ij}$$

where δ_{ij} is the Kronecker-delta. We will work with fluids that are isotropic. In the MHD case this precludes ferromagnetic fluids. Thus, the 4th order, isotropic tensor C_{ijkl} is generally represented as

$$\mathsf{C}_{ijkl} = \lambda\delta_{ij}\delta_{kl} + \mu\left(\delta_{ik}\delta_{jl} + \delta_{il}\delta_{jk}\right)$$

which preserves the desired symmetry of the stress tensor. This symmetry stems from the conservation of angular momentum. After some manipulation of these quantities we find

$$\mathsf{T}_{ij} = -p\delta_{ij} + \lambda u_{k,k}\delta_{ij} + 2\mu\mathsf{S}_{ij}.$$

Thus, the compressible Navier-Stokes equations become

$$\frac{\partial \mathbf{m}}{\partial t} + \nabla \cdot \left(\frac{\mathbf{m} \otimes \mathbf{m}}{\rho} \right) = \nabla \cdot \left(-p\mathbf{I} + \lambda \nabla \cdot \mathbf{u}\mathbf{I} + 2\mu \mathbf{S} \right) + \mathbf{F}.$$

This is written as

$$\frac{\partial \mathbf{m}}{\partial t} + \nabla \cdot \left(\frac{\mathbf{m} \otimes \mathbf{m}}{\rho} \right) = -\nabla p + \nabla \left(\lambda \nabla \cdot \mathbf{u} \right) + \nabla \cdot \left(2\mu \mathbf{S} \right) + \mathbf{F}.$$

The equation stating conservation of mass reads

$$\frac{\partial \rho}{\partial t} + \nabla \cdot (\rho \mathbf{u}) = 0.$$

We will be considering only incompressible flows. Therefore density variations in space and time are assumed to be negligible. This leads to

$$\nabla \cdot \mathbf{u} = 0.$$

Moreover, material properties such as the fluid molecular viscosity are also assumed to be constant in space and time. This facilitates a simplification to the momentum equation. We can write

$$\rho \frac{\partial \mathbf{u}}{\partial t} + \rho \nabla \cdot (\mathbf{u} \otimes \mathbf{u}) = -\nabla p + \mu \nabla^2 \mathbf{u} + \mathbf{f}.$$

APPENDIX B

Details on Filtered Equations

In this chapter we will filter the momentum and induction equations to arrive at an expression for the subgrid stress tensors for MHD. We only focus on the nonlinear term since the subgrid stress tensors are the result of the filtering operation applied to the nonlinear term. For the momentum equation we have

$$\overline{\boldsymbol{\mathcal{N}}^{\mathrm{V}}} = \overline{\mathbf{u} \otimes \mathbf{u}} - \frac{1}{\mu_0 \rho} \overline{\mathbf{B} \otimes \mathbf{B}}$$

$$= \overline{\mathbf{u} \otimes \mathbf{u}} - \frac{1}{\mu_0 \rho} \overline{\mathbf{B}} \otimes \overline{\mathbf{B}}$$

$$+ \overline{\mathbf{u}} \otimes \overline{\mathbf{u}} - \overline{\mathbf{u}} \otimes \overline{\mathbf{u}} - \frac{1}{\mu_0 \rho} \overline{\mathbf{B}} \otimes \overline{\mathbf{B}} + \frac{1}{\mu_0 \rho} \overline{\mathbf{B}} \otimes \overline{\mathbf{B}}$$

$$= = \overline{\mathbf{u}} \otimes \overline{\mathbf{u}} - \frac{1}{\mu_0 \rho} \overline{\mathbf{B}} \otimes \overline{\mathbf{B}}$$

$$+ \overline{\mathbf{u} \otimes \mathbf{u}} - \overline{\mathbf{u}} \otimes \overline{\mathbf{u}}$$

$$- \frac{1}{\mu_0 \rho} \left(\overline{\mathbf{B} \otimes \mathbf{B}} - \overline{\mathbf{B}} \otimes \overline{\mathbf{B}} \right)$$

$$= \boldsymbol{\mathcal{N}}^{\mathrm{V}}_F + \boldsymbol{\mathcal{T}}^{\mathrm{V}}$$

where

$$\boldsymbol{\mathcal{N}}^{\mathrm{V}}_F = \overline{\mathbf{u}} \otimes \overline{\mathbf{u}} - \frac{1}{\mu_0 \rho} \overline{\mathbf{B}} \otimes \overline{\mathbf{B}}$$

$$\boldsymbol{\mathcal{T}}^{\mathrm{V}} = \overline{\mathbf{u} \otimes \mathbf{u}} - \overline{\mathbf{u}} \otimes \overline{\mathbf{u}} - \frac{1}{\mu_0 \rho} \left(\overline{\mathbf{B} \otimes \mathbf{B}} - \overline{\mathbf{B}} \otimes \overline{\mathbf{B}} \right).$$

The filtered nonlinear term in the induction equation is

$$
\begin{aligned}
\overline{\mathcal{N}^{\mathrm{I}}} &= -\overline{\mathbf{u} \otimes \mathbf{B}} + \overline{\mathbf{B} \otimes \mathbf{u}} \\
&= -\left(\overline{\mathbf{u}} \otimes \overline{\mathbf{B}} - \overline{\mathbf{u}} \otimes \overline{\mathbf{B}} + \overline{\mathbf{u} \otimes \mathbf{B}} \right) \\
&\quad + \left(\overline{\mathbf{B}} \otimes \overline{\mathbf{u}} - \overline{\mathbf{B}} \otimes \overline{\mathbf{u}} + \overline{\mathbf{B} \otimes \mathbf{u}} \right) \\
&= -\overline{\mathbf{u}} \otimes \overline{\mathbf{B}} + \overline{\mathbf{B}} \otimes \overline{\mathbf{u}} \\
&\quad - \left(\overline{\mathbf{u} \otimes \mathbf{B}} - \overline{\mathbf{u}} \otimes \overline{\mathbf{B}} \right) \\
&\quad + \left(\overline{\mathbf{B} \otimes \mathbf{u}} - \overline{\mathbf{B}} \otimes \overline{\mathbf{u}} \right) \\
&= \mathcal{N}^{\mathrm{I}}_{F} + \mathcal{T}^{\mathrm{I}}
\end{aligned}
$$

where

$$
\begin{aligned}
\mathcal{N}^{\mathrm{I}}_{F} &= -\overline{\mathbf{u}} \otimes \overline{\mathbf{B}} + \overline{\mathbf{B}} \otimes \overline{\mathbf{u}} \\
\mathcal{T}^{\mathrm{I}} &= -\left(\overline{\mathbf{u} \otimes \mathbf{B}} - \overline{\mathbf{u}} \otimes \overline{\mathbf{B}} \right) + \left(\overline{\mathbf{B} \otimes \mathbf{u}} - \overline{\mathbf{B}} \otimes \overline{\mathbf{u}} \right).
\end{aligned}
$$

The filtered momentum and induction equations are therefore

$$
\begin{aligned}
\frac{\partial \overline{\mathbf{u}}}{\partial \mathrm{t}} + \nabla \cdot \left(\mathcal{N}^{\mathrm{V}}_{F} + \mathcal{T}^{\mathrm{V}} \right) + \nabla \overline{P} - \nu \nabla^2 \overline{\mathbf{u}} &= \overline{\mathbf{f}^{\mathrm{V}}} \\
\frac{\partial \overline{\mathbf{B}}}{\partial \mathrm{t}} + \nabla \cdot \left(\mathcal{N}^{\mathrm{I}}_{F} + \mathcal{T}^{\mathrm{I}} \right) + \nabla \overline{r} - \lambda \nabla^2 \overline{\mathbf{B}} &= \overline{\mathbf{f}^{\mathrm{I}}}.
\end{aligned}
$$

APPENDIX C
Index Notation

Index notation, also commonly referred to as the Einstein summation convention, is a shorthand for writing out summations. The rules for index notation are outlined below.

1. Summation occurs when two numbers with the same subscript are multiplied. As an example we consider the dot product of two vectors.

$$\mathbf{u} \cdot \mathbf{v} = \sum_{i=1}^{n} u_i v_i.$$

   In index notation this becomes,

$$\mathbf{u} \cdot \mathbf{v} = u_i v_i.$$

   The summation is simply dropped and the summation limit is implied by the context of the problem. Such indices are called repeated indices.

2. A free index is an index that is not involved in a summation.

$$u_i = \mathsf{T}_{ij} v_j \tag{C.1}$$

3. A free index can be changed only if it is changed on both sides of the equation. So (C.1) can be changed to

$$u_k = \mathsf{T}_{kj} v_j.$$

4. It makes no sense to have more than than two repeated indices. For example, the meaning of the following expression is not clear

$$t_i = u_i v_i w_i.$$

Two very useful symbols written in index notation are the Kronecker delta and the Cevi-Levita symbol. Both of these symbols are defined in (Panton 2006) and we follow the notation therein in what follows. The Kronecker delta acts as the identity matrix. It is defined as

$$\delta_{ij} = \begin{cases} 1 & \text{if} \quad i = j \\ 0 & \text{if} \quad i \neq j. \end{cases}$$

The Cevi-Levi symbol, also known as the alternating symbol, is defined as

$$\epsilon_{ijk} = \begin{cases} 1 & \text{if} \quad ijk = 123, \ 231, \ 312 \\ 0 & \text{if} \quad i = j, \ i = k, \ j = k \\ -1 & \text{if} \quad ijk = 321, \ 213, \ 132 \end{cases}$$

The following relationship is very useful and is used extensively.

$$\epsilon_{ijk}\epsilon_{ilm} = \delta_{jl}\delta_{km} - \delta_{jm}\delta_{kl}.$$

APPENDIX D
Properties of Integral Forms

We now demonstrate some simple properties of integral forms. In this section we will consider functions u, v, and w in a region Ω. In general we will have $u \neq v \neq w$. The following results hold for u, v, $w \in \mathbb{C}^n$ however we only consider $n = 1$ for demonstration purposes here. Furthermore, a, $b \in \mathbb{C}$ are constants.

D.1 Linearity and Bilinearity

Linearity in a slot means the following.

$$\mathcal{A}\left(\cdot, av + bw\right) = a\mathcal{A}\left(\cdot, u\right) + b\mathcal{A}\left(\cdot, v\right).$$

To demonstrate this we will consider two examples. First consider the integral form

$$\mathcal{A}_1\left(u, v\right) = \left(u, v\right) = \int_\Omega uv \ \mathrm{d}\Omega.$$

Then

$$\mathcal{A}_1\left(u, av + bw\right) = \left(u, av + bw\right)$$
$$= \int_\Omega u\left(av + bw\right) \ \mathrm{d}\Omega$$
$$= \int_\Omega auv \ \mathrm{d}\Omega + \int_\Omega buw \ \mathrm{d}\Omega$$
$$= a\int_\Omega uv \ \mathrm{d}\Omega + b\int_\Omega uw \ \mathrm{d}\Omega$$
$$= a\left(u, v\right) + b\left(u, w\right)$$
$$= a\mathcal{A}_1\left(u, v\right) + b\mathcal{A}_1\left(u, w\right).$$

Therefore $\mathcal{A}_1 (u, v)$ is linear in its second slot. We could also test the linearity of $\mathcal{A}_1 (u, v)$ in the first slot. We would find,

$$
\begin{aligned}
\mathcal{A}_1 (au + bv, w) &= (au + bv, w) \\
&= a (u, w) + b (v, w) \\
&= a\mathcal{A}_1 (u, w) + b\mathcal{A}_1 (v, w).
\end{aligned}
$$

With this we see that $\mathcal{A}_1 (u, v)$ is also linear in its first slot. When an integral form is linear in both slots it is called a bilinear form.

As a second example, we consider the form,

$$
\begin{aligned}
\mathcal{A}_2 (u, v) &= \left(u^2, v^2\right) \\
&= \int_\Omega u^2 v^2 \ \mathrm{d}\Omega.
\end{aligned}
$$

This gives

$$
\begin{aligned}
\mathcal{A}_2 (u, av + bw) &= \left(u^2, (av + bw)^2\right) \\
&= \int_\Omega u^2 (av + bw)^2 \ \mathrm{d}\Omega \\
&= \int_\Omega u^2 \left(a^2 v^2 + 2abvw + b^2 w^2\right) \ \mathrm{d}\Omega \\
&= a^2 \left(u^2, v^2\right) + 2ab \left(u^2, vw\right) + b^2 \left(u^2, w^2\right) \\
&\neq a\mathcal{A}_2 (u, v) + b\mathcal{A}_2 (u, w).
\end{aligned}
$$

It is therefore clear that $\mathcal{A}_2 (u, v)$ is not linear in the second slot. The same argument holds for the first slot of $\mathcal{A}_2 (u, v)$.

As a final note, it is possible that a form may be linear in one slot and not in another. Such a form is called a semilinear form. An example of such a form would be

$$
\mathcal{A}_3 (u, v) = \left(u, v^2\right).
$$

$\mathcal{A}_3 (u, v)$ is linear in its first slot and quadratic in its second slot.

D.2 Sesquilinearity

We briefly discuss the property of sesquilinearity. Sesquilinearity is similar to bilinearity except for one difference. This is illustrated with an example. A form $\mathcal{A}(u, v)$ is said to be sesquilinear if

$$\mathcal{A}(\cdot, av + bw) = a^*\mathcal{A}(\cdot, v) + b^*\mathcal{A}(\cdot, w)$$
$$\mathcal{A}(au + bv, \cdot) = a^*\mathcal{A}(u, \cdot) + b^*\mathcal{A}(v, \cdot)$$

where the $*$ denotes a complex conjugate. Note that this is bilinearity except that the coefficients in one slot become their complex conjugate.

D.3 Symmetry

A symmetric form is one such that

$$\mathcal{A}(u, v) = \mathcal{A}(v, u).$$

The form

$$\mathcal{A}(u, v) = (u, v) = \int_\Omega uv \ d\Omega$$

is very much symmetric. Clearly

$$\begin{aligned}
\mathcal{A}(u, v) &= \int_\Omega uv \ d\Omega \\
&= \int_\Omega vu \ d\Omega \\
&= \mathcal{A}(v, u).
\end{aligned}$$

The form

$$
\begin{aligned}
\mathcal{A}\left(u, v\right) &= \left(u, v\right) + \left(u, v^{3}\right) \\
&= \int_{\Omega} uv \ \mathrm{d}\Omega + \int_{\Omega} uv^{3} \ \mathrm{d}\Omega \\
&\neq \int_{\Omega} vu \ \mathrm{d}\Omega + \int_{\Omega} vu^{3} \ \mathrm{d}\Omega \\
&= \mathcal{A}\left(v, u\right)
\end{aligned}
$$

and is therefore not symmetric.

APPENDIX E
Sundry Vector Derivations

E.1 Derivation of Divergence Form of Induction Equation

The electromotive force term becomes,

$$
\begin{aligned}
-\nabla \times (\mathbf{u} \times \mathbf{B}) &= -\epsilon_{ijk} \left(\epsilon_{klm} u_l B_m\right)_{,j} \\
&= -\epsilon_{kij}\epsilon_{klm} \left(u_l B_m\right)_{,j} \\
&= -\left[\delta_{il}\delta_{jm} - \delta_{im}\delta_{jl}\right] \left(u_l B_m\right)_{,j} \\
&= -\left[u_i B_j - u_j B_i\right]_{,j} \\
&= \left[-u_i B_j + u_j B_i\right]_{,j} \\
&= \nabla \cdot (-\mathbf{u} \otimes \mathbf{B} + \mathbf{B} \otimes \mathbf{u})
\end{aligned}
$$

while the diffusion term is

$$
\begin{aligned}
-\nabla \times \left(\frac{\eta}{\mu_0}\nabla \times \mathbf{B}\right) &= -\epsilon_{ijk} \left(\frac{\eta}{\mu_0}\epsilon_{klm} B_{m,l}\right)_{,j} \\
&= -\epsilon_{ijk}\epsilon_{klm} \left(\frac{\eta}{\mu_0} B_{m,l}\right)_{,j} \\
&= -\epsilon_{kij}\epsilon_{klm} \left(\frac{\eta}{\mu_0} B_{m,l}\right)_{,j} \\
&= -\left[\delta_{il}\delta_{jm} - \delta_{im}\delta_{jl}\right] \left(\frac{\eta}{\mu_0} B_{m,l}\right)_{,j} \\
&= -\left[\frac{\eta}{\mu_0} \left(B_{j,i} - B_{i,j}\right)\right]_{,j} \\
&= \left[\frac{\eta}{\mu_0} \left(B_{i,j} - B_{j,i}\right)\right]_{,j} \\
&= \nabla \cdot \left[\frac{\eta}{\mu_0} \left(\nabla\mathbf{B} - (\nabla\mathbf{B})^T\right)\right].
\end{aligned}
$$

Thus,

$$-\nabla \times (\mathbf{u} \times \mathbf{B}) - \nabla \times \left(\frac{\eta}{\mu_0}\nabla \times \mathbf{B}\right)$$

$$= \nabla \cdot (-\mathbf{u} \otimes \mathbf{B} + \mathbf{B} \otimes \mathbf{u}) + \nabla \cdot \left[\frac{\eta}{\mu_0}\left(\nabla\mathbf{B} - (\nabla\mathbf{B})^T\right)\right].$$

E.2   Integral Relationships

E.2.1 $\int_\Omega (\nabla \times \mathbf{A}) \cdot (\mathbf{u} \times \mathbf{B}) \ \mathrm{d}\Omega$

$$\int_\Omega (\nabla \times \mathbf{A}) \cdot (\mathbf{u} \times \mathbf{B}) \ \mathrm{d}\Omega = -\int_\Omega \mathbf{A} \cdot \nabla \times (\mathbf{u} \times \mathbf{B}) \ \mathrm{d}\Omega.$$

This identity will be proved using index notation. Thus,

$$\int_\Omega (\nabla \times \mathbf{A}) \cdot (\mathbf{u} \times \mathbf{B}) \ \mathrm{d}\Omega = \int_\Omega \epsilon_{ijk}A_{k,j}\epsilon_{ilm}u_l B_m \ \mathrm{d}\Omega$$

$$= \underbrace{\int_\Gamma \epsilon_{ijk}n_j A_k \epsilon_{ilm}u_l B_m \ \mathrm{d}\Gamma}_{0}$$

$$-\int_\Omega \epsilon_{ijk}\epsilon_{ilm}A_k \left(u_l B_m\right)_{,j} \ \mathrm{d}\Omega$$

$$= -\int_\Omega A_k \epsilon_{kij}\left(\epsilon_{ilm}u_l B_m\right)_{,j} \ \mathrm{d}\Omega$$

$$= -\int_\Omega \mathbf{A} \cdot \nabla \times (\mathbf{u} \times \mathbf{B}) \ \mathrm{d}\Omega.$$

E.2.2 $\int_\Omega \mathbf{v} \cdot (\nabla \cdot (\mathbf{v} \otimes \mathbf{w})) \ \mathrm{d}\Omega = 0$

$$\int_\Omega \mathbf{v} \cdot (\nabla \cdot (\mathbf{v} \otimes \mathbf{w})) \ \mathrm{d}\Omega = \int_\Omega v_i \left(v_i w_j\right)_{,j} \ \mathrm{d}\Omega$$

$$= -\int_\Omega v_{i,j}v_i w_j \ \mathrm{d}\Omega \qquad \longrightarrow \text{ No boundary effects}$$

$$= -\int_\Omega \left(v_i w_j\right)_{,j} v_i \ \mathrm{d}\Omega \qquad \longrightarrow \nabla \cdot \mathbf{w} = 0.$$

Therefore since $A = -A \Rightarrow A = 0$ the identity is satisfied. Selecting $\mathbf{w} = \mathbf{v}$ is a special case of this identity. Therefore

$$\int_\Omega \mathbf{v} \cdot (\nabla \cdot (\mathbf{v} \otimes \mathbf{v})) \ \mathrm{d}\Omega = 0.$$

E.2.3 $\int_\Omega \mathbf{v} \cdot \nabla f \ \mathrm{d}\Omega = 0$

$$
\begin{aligned}
\int_\Omega \mathbf{v} \cdot \nabla f \ \mathrm{d}\Omega &= \int_\Omega v_i f_{,i} \ \mathrm{d}\Omega \\
&= -\int_\Omega v_{i,i} f \ \mathrm{d}\Omega \quad \longrightarrow \ \text{No boundary effects} \\
&= 0 \quad \longrightarrow \ \nabla \cdot \mathbf{v} = 0
\end{aligned}
$$

E.3   Vector Identities

E.3.1 $\mathbf{j} \times \mathbf{B}$

The electromagnetic forcing term in the momentum equation is

$$
\begin{aligned}
\mathbf{j} \times \mathbf{B} &= \left(\frac{1}{\mu_0} \nabla \times \mathbf{B} \right) \times \mathbf{B} \\
&= \frac{1}{\mu_0} \epsilon_{ijk} \left(\epsilon_{jlm} B_{m,l} \right) B_k \\
&= \frac{1}{\mu_0} \epsilon_{jki} \epsilon_{jlm} B_{m,l} B_k \\
&= \frac{1}{\mu_0} \left(\delta_{kl} \delta_{im} - \delta_{km} \delta_{il} \right) B_{m,l} B_k \\
&= \frac{1}{\mu_0} \left(B_{i,k} B_k - B_{k,i} B_k \right) \\
&= \frac{1}{\mu_0} \left(B_i B_k \right)_{,k} - \frac{1}{\mu_0} \left(\frac{1}{2} B_k B_k \right)_{,i} \\
&= \frac{1}{\mu_0} \nabla \cdot (\mathbf{B} \otimes \mathbf{B}) - \frac{1}{\mu_0} \nabla \left(\frac{1}{2} \mathbf{B} \cdot \mathbf{B} \right).
\end{aligned}
$$

E.3.2 $-\mathbf{n} \times (\mathbf{u}_1 \times \mathbf{B}_1)$

$$
\begin{aligned}
-\mathbf{n} \times (\mathbf{u}_1 \times \mathbf{B}_1) &= -\epsilon_{ijk} n_j \epsilon_{klm} u_l B_m \\
&= -\epsilon_{klm} \epsilon_{klm} n_j u_k B_m \\
&= - \left[\delta_{il}\delta_{jm} - \delta_{im}\delta_{jm} \right] n_j u_k B_m \\
&= - \left[n_j u_i B_j - n_j u_j B_i \right] \\
&= - \left[u_i B_j - u_j B_i \right] n_j \\
&= \left[u_j B_i - u_i B_j \right] n_j \\
&= \left[-\mathbf{u}_1 \otimes \mathbf{B}_1 + \mathbf{B}_1 \otimes \mathbf{u}_1 \right] \cdot \mathbf{n}.
\end{aligned}
$$

E.3.3 $\mathbf{v} \times (\nabla \times \mathbf{w})$

Given two vectors $\mathbf{v}$ and $\mathbf{w}$ we have

$$
\begin{aligned}
\mathbf{v} \times (\nabla \times \mathbf{w}) &= \epsilon_{ijk} v_j \left(\epsilon_{klm} \partial_l w_m \right) \\
&= \epsilon_{kij} \epsilon_{klm} v_j \partial_l w_m \\
&= \left[\delta_{il}\delta_{jm} - \delta_{im}\delta_{jl} \right] v_j \partial_l w_m \\
&= -v_j \left[\partial_j w_i - \partial_i w_j \right] \\
&= -2 \left[\nabla \mathbf{w} - (\nabla \mathbf{w})^{\mathrm{T}} \right] \cdot \mathbf{v}.
\end{aligned}
$$

APPENDIX F

Spectral Equations from the Variational Statement

The variational form of the MHD equations is written using a concise notation in this section. The reason for this is that the momentum and inductions equations take on a similar form when written in the divergence form. Thus, the variational form for both the momentum and induction equations are written as

$$\mathcal{A}\left(\mathbf{W},\mathbf{U}\right) = \left(\mathbf{v}, \frac{d\mathbf{a}}{dt}\right) + \left(\mathbf{w}, \nabla \cdot \left(\mathbf{a} \otimes \mathbf{b} + \mathbf{c} \otimes \mathbf{d}\right)\right) + \left(\mathbf{w}, \nabla P\right) + \left(\nabla \mathbf{w}, D \nabla \mathbf{v}\right) \quad \text{(F.1)}$$

where $\mathbf{a}$, $\mathbf{b}$, $\mathbf{c}$, $\mathbf{d}$ are vector fields and D is a diffusion coefficient. Note also that $\mathbf{v}$ is either $\mathbf{u}$ or $\mathbf{B}$ depending on the equation being considered. Table F.1 shows the specific variables that the nonlinear form takes for each equation.

Table F.1: Coefficient mappings corresponding to the nonlinear term in (F.1).

	Momentum	Induction
$\mathbf{a}$	$\mathbf{u}$	$-\mathbf{u}$
$\mathbf{b}$	$\mathbf{u}$	$\mathbf{B}$
$\mathbf{c}$	$-\frac{1}{\mu_0 \rho}\mathbf{B}$	$\mathbf{B}$
$\mathbf{d}$	$\mathbf{B}$	$\mathbf{u}$

For reference we present the basis functions for the fields,

$$\mathbf{W} = \sum_{\mathbf{q}} \widehat{\mathbf{W}}\left(\mathbf{q}\right) e^{-\imath \mathbf{q} \cdot \mathbf{x}}$$

$$\mathbf{U} = \sum_{\mathbf{k}} \widehat{\mathbf{U}}\left(\mathbf{k}\right) e^{-\imath \mathbf{k} \cdot \mathbf{x}}.$$

For algebraic simplicity we will consider the linear and nonlinear terms in turn. We

begin with the linear terms. Thus,

$$
\left(\sum_{\mathbf{q}} \widehat{\mathbf{w}}\left(\mathbf{q}\right) e^{-\imath \mathbf{q}\cdot\mathbf{x}}, \frac{\mathrm{d}}{\mathrm{dt}} \sum_{\mathbf{k}} \widehat{\mathbf{v}}\left(\mathbf{k}\right) e^{\imath \mathbf{k}\cdot\mathbf{x}} \right) + \left(\sum_{\mathbf{q}} \widehat{\mathbf{w}}\left(\mathbf{q}\right) e^{-\imath \mathbf{q}\cdot\mathbf{x}}, \nabla \sum_{\mathbf{k}} \widehat{\mathsf{P}} e^{\imath \mathbf{k}\cdot\mathbf{x}} \right) +
$$

$$
\mathsf{D} \left(\nabla \sum_{\mathbf{q}} \widehat{\mathbf{w}}\left(\mathbf{q}\right) e^{-\imath \mathbf{q}\cdot\mathbf{x}}, \nabla \sum_{\mathbf{k}} \widehat{\mathbf{v}}\left(\mathbf{k}\right) e^{\imath \mathbf{k}\cdot\mathbf{x}} \right)
$$

$$
= \sum_{\mathbf{k}}\sum_{\mathbf{q}} \widehat{\mathbf{w}}\left(\mathbf{q}\right) \cdot \frac{\mathrm{d}\widehat{\mathbf{v}}\left(\mathbf{k}\right)}{\mathrm{dt}} \left(e^{-\imath \mathbf{q}\cdot\mathbf{x}}, e^{\imath \mathbf{k}\cdot\mathbf{x}} \right) + \sum_{\mathbf{k}}\sum_{\mathbf{q}} \widehat{\mathbf{w}}\left(\mathbf{q}\right) \cdot \imath \mathbf{k}\widehat{\mathsf{P}}\left(\mathbf{k}\right) \left(e^{-\imath \mathbf{q}\cdot\mathbf{x}}, e^{\imath \mathbf{k}\cdot\mathbf{x}} \right) +
$$

$$
\mathsf{D} \sum_{\mathbf{k}}\sum_{\mathbf{q}} \widehat{\mathbf{w}}\left(\mathbf{q}\right) \cdot \widehat{\mathbf{v}}\left(\mathbf{k}\right) \left(-\imath \mathbf{q}\cdot\imath \mathbf{k} \right) \left(e^{-\imath \mathbf{q}\cdot\mathbf{x}}, e^{\imath \mathbf{k}\cdot\mathbf{x}} \right)
$$

$$
= (2\pi)^3 \sum_{\mathbf{k}} \widehat{\mathbf{w}}\left(\mathbf{k}\right) \cdot \left(\frac{\mathrm{d}\widehat{\mathbf{v}}\left(\mathbf{k}\right)}{\mathrm{dt}} + \imath \mathbf{k}\widehat{\mathsf{P}}\left(\mathbf{k}\right) + \mathsf{D}\left|\mathbf{k}\right|^2 \widehat{\mathbf{v}}\left(\mathbf{k}\right) \right).
$$

The final step results from the following relationship

$$
\left(e^{-\imath \mathbf{q}\cdot\mathbf{x}}, e^{\imath \mathbf{k}\cdot\mathbf{x}} \right) = \begin{cases} (2\pi)^3, & \mathbf{q} = \mathbf{k} \\ 0 & \mathbf{q} \neq \mathbf{k} \end{cases}.
$$

The nonlinear term is

$$
\left(\sum_{\mathbf{q}} \widehat{\mathbf{w}}\left(\mathbf{q}\right) e^{-\imath \mathbf{q}\cdot\mathbf{x}}, \nabla \cdot \left(\sum_{\mathbf{l}} \widehat{\mathbf{a}}\left(\mathbf{l}\right) e^{\imath \mathbf{l}\cdot\mathbf{x}} \otimes \sum_{\mathbf{m}} \widehat{\mathbf{b}}\left(\mathbf{m}\right) e^{\imath \mathbf{m}\cdot\mathbf{x}} + \sum_{\mathbf{l}} \widehat{\mathbf{c}}\left(\mathbf{l}\right) e^{\imath \mathbf{l}\cdot\mathbf{x}} \otimes \sum_{\mathbf{m}} \widehat{\mathbf{d}}\left(\mathbf{m}\right) e^{\imath \mathbf{m}\cdot\mathbf{x}} \right) \right)
$$

$$
= \sum_{\mathbf{q}}\sum_{\mathbf{l}}\sum_{\mathbf{m}} \widehat{\mathbf{w}}\left(\mathbf{q}\right) \cdot \left[\widehat{\mathbf{a}}\left(\mathbf{l}\right) \otimes \widehat{\mathbf{b}}\left(\mathbf{m}\right) + \widehat{\mathbf{c}}\left(\mathbf{l}\right) \otimes \widehat{\mathbf{d}}\left(\mathbf{m}\right) \right] \cdot \left(\mathbf{l} + \mathbf{m}\right) \left(e^{-\imath \mathbf{q}\cdot\mathbf{x}}, e^{\imath \mathbf{l}+\mathbf{m}\cdot\mathbf{x}} \right)
$$

$$
= \sum_{\mathbf{q}}\sum_{\mathbf{l}} \widehat{\mathbf{w}}\left(\mathbf{q}\right) \cdot \left[\widehat{\mathbf{a}}\left(\mathbf{l}\right) \otimes \widehat{\mathbf{b}}\left(\mathbf{k}-\mathbf{l}\right) + \widehat{\mathbf{c}}\left(\mathbf{l}\right) \otimes \widehat{\mathbf{d}}\left(\mathbf{k}-\mathbf{l}\right) \right] \cdot \mathbf{k} \left(e^{-\imath \mathbf{q}\cdot\mathbf{x}}, e^{\imath \mathbf{k}\cdot\mathbf{x}} \right)
$$

$$
= (2\pi)^3 \sum_{\mathbf{k}}\sum_{\mathbf{l}} \widehat{\mathbf{w}}\left(\mathbf{k}\right) \cdot \left[\widehat{\mathbf{a}}\left(\mathbf{l}\right) \otimes \widehat{\mathbf{b}}\left(\mathbf{k}-\mathbf{l}\right) + \widehat{\mathbf{c}}\left(\mathbf{l}\right) \otimes \widehat{\mathbf{d}}\left(\mathbf{k}-\mathbf{l}\right) \right] \cdot \mathbf{k}.
$$

The forcing term becomes

$$
\left(\mathbf{w}, \mathbf{f}\right) = (2\pi)^3 \sum_{\mathbf{k}} \widehat{\mathbf{w}}\left(\mathbf{k}\right) \widehat{\mathbf{f}}\left(\mathbf{k}\right).
$$

Putting it all together results in

$$\sum_{\mathbf{k}} \widehat{\mathbf{w}}(\mathbf{k}) \cdot \left[\frac{d\widehat{\mathbf{v}}(\mathbf{k})}{dt} + \imath \mathbf{k} \widehat{\mathsf{P}}(\mathbf{k}) + \mathsf{D} |\mathbf{k}|^2 \widehat{\mathbf{v}}(\mathbf{k}) \right.$$

$$\left. + \sum_{\mathbf{l}} \widehat{\mathbf{w}}(\mathbf{k}) \cdot \left[\widehat{\mathbf{a}}(\mathbf{l}) \otimes \widehat{\mathbf{b}}(\mathbf{k}-\mathbf{l}) + \widehat{\mathbf{c}}(\mathbf{l}) \otimes \widehat{\mathbf{d}}(\mathbf{k}-\mathbf{l}) \right] \cdot \mathbf{k} \right] = \sum_{\mathbf{k}} \widehat{\mathbf{w}}(\mathbf{k}) \cdot \widehat{\mathbf{f}}(\mathbf{k}).$$

This is true for all weighting functions and therefore we arrive at an equation for each wavenumber,

$$\frac{d\widehat{\mathbf{v}}(\mathbf{k})}{dt} + \imath \mathbf{k} \widehat{\mathsf{P}}(\mathbf{k}) + \mathsf{D} |\mathbf{k}|^2 \widehat{\mathbf{v}}(\mathbf{k}) + \widehat{\mathcal{N}}(\mathbf{k}) \cdot \mathbf{k} = \widehat{\mathbf{f}}(\mathbf{k})$$

where

$$\widehat{\mathcal{N}}(\mathbf{k}) = \sum_{\mathbf{l}} \widehat{\mathbf{a}}(\mathbf{l}) \otimes \widehat{\mathbf{b}}(\mathbf{k}-\mathbf{l}) + \widehat{\mathbf{c}}(\mathbf{l}) \otimes \widehat{\mathbf{d}}(\mathbf{k}-\mathbf{l}).$$